UNIVERSITY OF LJUBLJANA
BIOTECHNICAL FACULTY

Tjaša POTOČNIK

EFFICIENCY AND MECHANISMS OF GENE TRANSFECTION BY ELECTROPORATION IN MAMMALIAN CELLS *IN VITRO*

DOCTORAL DISSERTATION

Ljubljana, 2023

UNIVERSITY OF LJUBLJANA
BIOTECHNICAL FACULTY

Tjaša POTOČNIK

EFFICIENCY AND MECHANISMS OF GENE TRANSFECTION BY ELECTROPORATION IN MAMMALIAN CELLS *IN VITRO*

DOCTORAL DISSERTATION

UČINKOVITOST IN MEHANIZMI GENSKE TRANSFEKCIJE Z ELEKTROPORACIJO V SESALSKIH CELICAH *IN VITRO*

DOKTORSKA DISERTACIJA

Ljubljana, 2023

Based on the Statute of the University of Ljubljana and the decision of the Biotechnical Faculty senate, as well as the decision of the Commission for Doctoral Studies of the University of Ljubljana adopted on 24th September 2019 it has been confirmed that the candidate meets the requirements for pursuing a PhD in the interdisciplinary doctoral programme in Biosciences, Scientific Field Cell Sciences. Doc. Dr. Alenka Maček Lebar is appointed as supervisor.

Doctoral dissertation was conducted at the Laboratory of Biocybernetics, Faculty of Electrical Engineering, University of Ljubljana.

Commission for assessment and defense:

President: Prof. Dr. Marko KREFT
University of Ljubljana, Biotechnical Faculty, Department of Biology

Member: Prof. Dr. Tadej KOTNIK
University of Ljubljana, Faculty of Electrical Engineering, Department of Biomedical Engineering

Member: Prof. Dr. Marie-Pierre ROLS
CNRS, Institute of Pharmacology and Structural Biology,
Department of Cellular Biophysics

Date of the defense: 19th January 2023

Tjaša Potočnik

KEY WORDS DOCUMENTATION

DN   Dd

DC   UDC 602.621(043.3)

CX   Gene electrotransfer, electroporation, pH, high-frequency bipoar pulses, nanosecond pulses

AU   POTOČNIK, Tjaša

AA   MAČEK LEBAR, Alenka (supervisor)

PP   SI-1000, Ljubljana, Jamnikarjeva 101

PB   University of Ljubljana, Biotechnical Faculty, Interdisciplinary Doctoral Programme in Biosciences, Scientific Field Cell Sciences

PY   2023

TI   EFFICIENCY AND MECHANISMS OF GENE TRANSFECTION BY ELECTROPORATION IN MAMMALIAN CELLS *IN VITRO*

DT   Doctoral dissertation

NO   X, 186 p.,1 fig., 2 ann., 192 ref.

LA   en

AL   en/sl

AB   With the aim of better understanding and optimizing gene transfection by electroporation (GET) we tested the effect of different biological and electrical parameters on GET efficiency *in vitro*. Due to possibility that microenvironment in applications of *in vivo* is slightly acidic, we studied the effects of slightly acidic electroporation and recovery medium on cell membrane permeabilization, cell survival and GET. Slightly acidic (pH 6.5) electroporation medium did not affect permeabilization threshold, but the survival of cells was better if slightly acidic electroporation and recovery medium were used. However, slightly acidic electroporation and recovery medium decreased GET. Further, to avoid or to mitigate pain and muscle contractions associated with the application of high-voltage electrical pulses *in vivo* we showed that with short bipolar pulses with a repetition rate on the order of tens or hundreds of kHz delivered in bursts of low frequency (HF-BP) and nanosecond pulses we can achieve comparable GET *in vitro* as with longer monopolar pulses, but only with high concentrations of plasmid DNA (pDNA). Although we were able to achieve similar percent of transfected cells, the number of transgenes produced was higher with longer monopolar pulses. We showed that GET efficiency depends on pulse parameters, pDNA concentration and differs between cell lines. Time dynamics of transgene expression were comparable between different pulse protocols but differed greatly between cell lines. Finally, a review, of current understanding of the mechanisms by which electric field can aid pDNA in overcoming the barriers encountered on the way to the cell nucleus was performed with the hope that gathered knowledge will enable further and faster development of GET *in vitro* as well as in *in vivo* across various cell lines, tissues, and species.

KLJUČNA DOKUMENTACIJSKA INFORMACIJA

AI   V doktorskem delu smo raziskali vpliv parametrov elektroporacije na učinkovitost genske elektrotransfekcije (GET) in vitro, z namenom boljšega razumevanja in izboljšanja učinkovitosti GET. Ker je mikrookolje pri aplikacijah in vivo lahko rahlo kislo, smo preučili tudi učinke rahlo kislega medija (pH 6,5) na permeabilizacijo celične membrane, celično preživetje in GET. Po elektroporaciji in okrevanju celic v rahlo kislem mediju nismo opazili razlik v permeabilizaciji celične membrane, preživetje celic pa je bilo boljše, kot pri celicah, ki so bile elektroporirane in so okrevale v rastnem mediju. Nasprotno sta elektroporacija in okrevanje v rahlo kislem mediju zmanjšala učinkovitost GET. Da bi se izognili ali ublažili bolečine in mišične kontrakcije, ki spremljajo dovajanje visokonapetostnih električnih pulzov za GET *in vivo* smo pokazali, da lahko z nizkofrekvenčnimi vlaki kratkih bipolarnih pulzov, ki si sledijo s frekvencami nekaj deset ali sto kHz (HF-BP), in nanosekundnimi pulzi dosežemo GET in vitro primerljivo z GET z daljšimi monopolarnimi pulzi, vendar le z višanjem koncentracije plazmidne DNK (pDNK). Kljub temu, da smo dosegli primerljiv odstotek transfeciranih celic, je bila količina nastalega transgena večja z daljšimi monopolarnimi pulzi. Učinkovitost GET je odvisna od parametrov pulzov, koncentracije pDNK in se razlikuje pri različnih celičnih linijah. Časovna dinamika izražanja transgena je primerljiva med milisekundami, mikrosekundami, HF-BP in nanosekundnimi pulzi, se pa močno razlikuje med celičnimi linijami. Naredili smo tudi pregled trenutnega razumevanja mehanizmov GET, z namenom, da bo zbrano znanje o mehanizmih in identifikacija obstoječih vrzeli v znanju, omogočilo hitrejše izboljšanje učinkovitosti GET *in vitro* kot tudi *in vivo* v različnih celicah, tkivih in bioloških vrstah.

TABLE OF CONTENTS

LIST OF SCIENTIFIC PAPERS

Potočnik T., Miklavčič D., Maček Lebar A. 2019. Effect of electroporation and recovery medium pH on cell membrane permeabilization, cell survival and gene transfer efficiency *in vitro*. Bioelectrochemistry, 130: 107342, doi.org/10.1016/j.bioelechem.2019.107342: 11 p.

Potočnik T., Miklavčič D., Maček Lebar A. 2021. Gene transfer by electroporation with high frequency bipolar pulses *in vitro*. Bioelectrochemistry, 140: 107803, doi.org/10.1016/j.bioelechem.2021.107803: 13 p.

Potočnik T., Sachdev S., Polajžer T., Maček Lebar A., Miklavčič D. 2022. Efficient gene transfection by electroporation - *in vitro* and *in silico* study of pulse parameters. Applied Sciences, 12, 16: 8237, doi.org/10.3390/app12168237: 50 p.

Sachdev S., **Potočnik T.**, Rems L., Miklavčič D. 2022. Revisiting the role of pulsed electric fields in overcoming the barriers to *in vivo* gene electrotransfer. Bioelectrochemistry, 144: 107994, doi.org/10.1016/j.bioelechem.2021.107994: 26 p.

LIST OF FIGURES

LIST OF ANNEXES

ANNEXES A: Permission by Elsevier to use accepted articles in printed and online version of dissertation for articles Potočnik et al. (2019), Potočnik et al. (2021), and Sachdev et al. (2022).

ANNEX B: Permission by MDPI to use published article in printed and online version of dissertation for article Potočnik et al. (2022).

ABBREVIATIONS

DNA	Deoxyribonucleic acid
ECT	Electrochemotherapy
GET	Gene electrotransfection
GFP	Green fluorescent protein
HF-BP	High frequency bipolar pulses
HFIRE	High frequency irreversible electroporation
IRE	Irreversible electroporation
pDNA	Plasmid deoxyribonucleic acid
pH_e	Extracellular pH
pH_i	Intracellular pH
PI	Propidium iodide
RNA	Ribonucleic acid

1   INTRODUCTION

1.1   ELECTROPORATION

Electroporation, also called electropermeabilization, is one of the most successful non-viral methods of introducing molecules into cells. When cells are exposed to an external electric field of sufficient amplitude and duration, transient permeabilization of the cell membrane is achieved (Rems et al., 2016; Kotnik et al., 2019), allowing various molecules that normally cannot cross the cell membrane, such as ions (Mir et al., 1988), dyes (Dinchuk et al., 1992) antibodies (Verspohl et al., 1997), oligonucleotides (Spiller et al., 1998), RNA (Sæbøe-Larssen et al., 2002), and DNA (Heller et al., 1996; Rols et al., 1998; Gehl and Mir, 1999) to enter into the cell. Electroporation is usually explained by the formation of aqueous pores in the cell membrane (Kotnik et al., 2019), which has been demonstrated using molecular dynamics simulations (Tarek, 2005). The strength of the external electric field, the duration, the number of applied electric pulses, and pulse repetition rate are key factors controlling cell membrane permeabilization. The external electric field is determined by the geometry of electrodes, target cells/tissues and applied voltage. When the amplitude of applied electric field is low, no molecular transport occurs. Higher or longer lasting electric fields result in reversible electroporation, which is characterized by transient increase in the cell membrane permeability. Irreversible electroporation (IRE) is observed at higher electric field amplitudes that lead to cell death. Finally, at even higher electric field amplitudes thermal damage causes cell death (Yarmush et al., 2014). Electroporation is used in medicine (Yarmush et al., 2014), as electrochemotherapy (ECT) for delivery of chemotherapeutic agents (Miklavcic et al., 2010; Mali et al., 2013; Campana et al., 2019), IRE as a method of tissue ablation (Davalos et al., 2005; Scheffer et al., 2014; Sugrue et al., 2018; Maor et al., 2019; Reddy et al., 2019), transdermal drug delivery (Zorec and Pavselj, 2013), gene transfection by electroporation (GET) as gene therapy (Heller L.C. and Heller R., 2010; Heller R. and Heller L.C, 2015) and DNA vaccination (Vasan et al., 2011; Lambricht et al., 2016), as well as in biotechnology (Meglic and Kotnik, 2017) and food and biomass processing (Mahnič-Kalamiza et al., 2014; Golberg et al., 2016).

1.2   TRANSFECTION

Transfection, a method in which foreign nucleic acids (DNA, RNA) are introduced into cells to produce transgenes or modify cells, is an indispensable method in basic genetic research, bioproduction, gene therapy, and cell therapies. Treatments based on cell and gene therapies have been approved for cancers such as head and neck squamous cell carcinoma, acute lymphoblastic leukaemia, B-cell lymphoma, and unresectable metastatic melanoma, as well as for inherited diseases such as lipoprotein lipase deficiency, adenosine deaminase deficiency - severe combined immunodeficiency, and retinal dystrophy (Ginn et al., 2018; Sachdev et al., 2022). The approval of these therapies, particulary with the advent of chimeric antigen receptor T-Cell therapy,

represents a milestone in medicine as it allows for the highest remission rates in hard-to-treat cancers (Singh and McGuirk, 2020). In addition, genetically engineered RNA vaccines were the first to be approved for vaccination against the corona virus pandemic (Topol, 2021).

Nucleic acids cannot easily pass through the cell membrane due to the electrostatic repulsion that occurs between the anionic nucleic acids and the negatively charged cell membrane at physiological pH values (Antipina and Gurtovenko, 2016). In addition, nucleic acids are highly susceptible to degradation by extracellular nucleases and therefore suffer from limited extracellular stability (Cervia and Yuan, 2018). Great efforts have been made to develop approaches and tools to improve the efficiency of transferring nucleic acids into target cells (Chong et al., 2021). These are generally divided into viral and non-viral based methods. Non-viral based methods are subdived into physical methods of gene delivery, such as electroporation, sonoporation, magnetofection, optoporation, gene gun, and microinjection, and chemical-mediated methods which can be lipid based or non-lipid based. In lipid based methods positively charged lipid aggregates are formed which can merge with the phospholipid bilayer of the target cell and allow the entry of the foreign genetic materials. Non-lipid based methods are calcium phosphate, dendrimers, polymers, nanoparticles or non-liposomal lipids based (Chong et al., 2021; Sayed et al., 2022).

Viral based methods are among the earliest described for gene delivery and have shown high efficiency (Zhao et al., 2022). However, viral vectors have some alarming drawbacks: pre-existing immunity and immune response activation following viral vector injections can reduce the efficacy of therapy and cause immunotoxicity - preventing the use of certain viruses in certain geographic locations and patients (Wilson and Flotte, 2020). Viral vectors, although effective also for genetic engineering of human primary cells, have serious limitations such as high manufacturing cost, long production timelines and genotoxic risks derived from their semi-random chromosomal integration profiles (Mingozzi and High, 2011). Therefore, the development of non-viral delivery methods has become an important area of research (Yin et al., 2014). Chemical-mediated delivery methods are often toxic to cells and limited to particular molecules and cell types, whereas physical methods have shown high local transfection efficiency and are less limited on gene size compared to viral based methods, but often require specific instruments. The biggest advantage of non-viral vectors is that they are in principle free of immune response activation and mutagenesis but, *in vivo* they do not yet achieve the same efficiency as viral vectors (Ginn et al., 2018).

1.3 GENE ELECTROTRANSFECTION
Forty years ago, in 1982, Neumann et al. showed that naked nucleic acids can be successfully transferred into cells using high-voltage electric pulses (Neumann et al.,

1982). A non-viral method for introducing nucleic acids into cells through the application of electric pulses is now known as gene transfection by electroporation, (gene) electrotransfection or gene electrotransfer (GET). GET increases plasmid DNA (pDNA) transfection rates by 100-2000-fold and improves transfection reproducibility compared to injecting pDNA without the application of electric pulses (Sachdev et al., 2022). Compared to other methods of gene delivery, GET has important advantages. It is relatively inexpensive, flexible, and safe for clinical use, and it delivers naked pDNA into cells without the use of additional chemicals or viruses (Young and Dean, 2015).

In clinical setting GET is also considered a promising method for delivery of CRISPR/Cas9 gene editing complexes (Fajrial et al., 2020). Additionally, GET can be used for vaccination against infectious diseases (Lambricht et al., 2016). DNA vaccine against COVID-19 is currently being developed (Morrow et al., 2016; Folegatti et al., 2020; Topol, 2021). In oncology GET is used for treatment of and vaccination against various cancers with different treatments against cancers based on the *ex vivo* genetic engineering (Heller R. and Heller L.C, 2015; Algazi et al., 2020; Bhatia et al., 2020; Geboers et al., 2020). GET can also be used for *ex vivo* genetic engineering of T cells to express chimeric antigen receptors which bind tumor antigens or tumor-associated antigens in a human leukocyte antigen independent manner (Alzubi et al., 2021). In recent years, GET has become the simplest and most appealing non-viral deliver technology with the ability to introduce diverse biomolecules to millions of cells per treatment (Sayed et al., 2022). Low transfection efficiency in some cell types and cell death following transfection however represent major limitations of GET in cell therapies (Stewart et al., 2016). The fact that the mechanisms of GET are still unclear represents additional limitation to wider use of GET in clinical medicine (Cervia and Yuan, 2018; Sachdev et al., 2022).

1.3.1   Mechanisms of gene electrotransfection

GET is achieved when nucleic acids enter the cell and produce a protein or knock down a defective or overexpressed gene. Based on the existing knowledge, GET is a multistep process. Depending on the type and size of the nucleic acids introduced into the cells, they have to overcome several barriers before they reach the cytoplasm of the cell (in the case of RNA) or the cell nucleus (in the case of DNA) in order to exert their therapeutic effect (Sachdev et al., 2022). In the case of pDNA GET involves interaction of pDNA with the cell membrane, its translocation across the cell membrane, migration through the cytoplasm, import across the nuclear envelope, and gene expression (Rosazza et al., 2016b). During GET electric filed applied to cells enables cell membrane permeabilization and electrophoresis of negatively charged pDNA molecules from the cathode towards the anode, bringing them closer and into contact with the cell membrane (Golzio et al., 2002a; Faurie et al., 2010). Small nucleic acid molecules (up to 25 bp) enter the cell primarily by electrophoresis during pulse delivery through permeable sites in the

cell membrane. It was shown that as the size of nucleic acid increases, the proportion of nucleic acids that enter the cell by electrophoresis decreases (Sachdev et al., 2020). Larger pDNA molecules (larger than 1 kbp) interact with the cell membrane and form aggregates on the cell membrane during and/or shortly after pulse delivery (Golzio et al., 2002a). To allow transgene expression these aggregates must then be transferred into the cell, transported intracellularly through the cytoplasm, and imported through the nuclear envelope into the nucleus (Golzio et al., 2002b; Satkauskas et al., 2002; Rosazza et al., 2016b).

Endocytosis is suggested as a possible mechanism for pDNA translocation based on the observations that pDNA molecules form large aggregates on the cell membrane, which are protected from degradation by extracellular nucleases, and appear on the intracellular side few minutes after pulse delivery (Golzio et al., 2002b). Endocytosis is a fundamental cellular process occurring in all cells with different endocytic transport pathways that coexist and can be active simultaneously in the same cell type (Kumari et al., 2010). However, since there are no known cellular receptors for pDNA, endocytosis was initially not considered as a possible mechanism by which pDNA could cross the cell membrane (Rosazza et al., 2016b). Nevertheless, there are several ways in which endocytosis could be involved in pDNA uptake following the delivery of electric pulses.

Initially, it was proposed that electric pulses could trigger "electroendocytosis" - an electric field induced endocytic-like process observed first when DNA was internalized into large unilamellar vesicles by forming endosome-like vesicles after exposure to electric pulses (Chernomordik et al., 1990). Later, "electroendocytosis" was also observed in various cells *in vitro* (Antov et al., 2005; Ben-Dov et al., 2012). However, it remains unclear whether "electroendocytosis" is specific to the delivery of electric pulses or whether it is simply a native cellular response to membrane damage (Tsong, 1991). Indeed, endocytosis is involved in cell membrane repair mechanisms that are activated in response to cell membrane damage (Cooper and McNeil, 2015). Within 30 s of injury, the resulting cell membrane damage causes an influx of calcium ions from the extracellular space into the cytoplasm and triggers exocytosis of lysosomes, followed by massive endocytosis (Zhen et al., 2021). In this way, pDNA aggregates at the cell membrane could be internalized into the cell with cell membrane repair mechanisms after the delivery of electric pulses, when damaged segments of the cell membrane and proteins are internalized into vesicles for recycling (Sachdev et al., 2022).

Desaturated cell membrane proteins or mechanical damage to the cell membrane by the electric field leads to activation of repair mechanisms, consisting of patching in which cytoplasmic vesicles fuse together and form a patch to fill the wound; clogging with annexins and other proteins, followed by membrane shedding; exocytosis, followed by endocytosis; and membrane shedding via ESCRT proteins (Batista Napotnik et al., 2021).

Endocytosis and wound removal are triggered by the extracellular activity of the lysosomal enzyme acidic sphingomyelinase (Reddy et al., 2001; Castro-Gomes et al., 2016). Glunde et al. (2003) showed that in human mammary epithelial cells and breast cancer cells of different malignancy grade slightly acidic extracellular pH (pH_e) values of 6.8 and 6.4 caused a significant relocation of lysosomes from the perinuclear region to the cell periphery. They also observed a higher number of lysosomes in cells exposed to extracellular acidity (Glunde et al., 2003). The relocation of lysosomes from the perinuclear region to the cell periphery triggered by extracellular acidosis, could increase the exocytosis of lysosomes, allowing faster and more efficient cell membrane repair (Potočnik et al., 2019).

Further, endocytosis could be caused by the disruption and remodeling of the cytoskeleton after the application of electric pulses (Sachdev et al., 2022). The cytoskeleton, particularly actin filaments and microtubules, are involved in all stages of endocytosis and post endocytic intracellular transport (Qualmann and Kessels, 2002). Cytoskeleton mediates endocytic vesicle formation and early stages of endosomal transport, transport of vesicles between different cell organelles, and their transport into the perinuclear space (Murray and Wolkoff, 2003). Shortly after the application of electric pulses, actin polymerization was observed on the side of the cell where pDNA aggregates formed, but only if pDNA was present during the application of electric pulses (Rosazza et al., 2011).

Another possibility is that formation of endocytic vesicles could be triggered by electrophoretically driven negatively charged pDNA aggregates on the cell membrane which could led to membrane curvature large enough to initiate membrane invagination (Klenchin et al., 1991; Sukharev et al., 1992). Negatively charged pDNA aggregates on the cell membrane could also trigger similar effects as negatively charged PIP_2 molecules (Rosazza et al., 2016b; Sachdev et al., 2022). PIP_2 is an important regulator of endocytosis and the cytoskeleton (Williams, 2007). Prior to endocytosis, PIP_2 molecules are present in patches in the cell membrane, where they are involved in the regulation and recruitment of endocytic proteins to the cell membrane (Farrer and Rossotti, 1964; Mandal, 2020). A high concentration of PIP_2 molecules in the cell membrane triggers actin polymerization by recruiting dynamin proteins that polymerize in areas of strong membrane curvature (Schafer, 2004; Roux et al., 2010). Negatively charged pDNA aggregates on the cell membrane could trigger a similar response leading to actin polymerization followed by the formation of endocytic vesicles (Rosazza et al., 2016a). In addition, PIP_2 molecules also interact with many transmembrane proteins, for example bin-amphiphysin-rvs domain proteins, which are curvature-sensitive and play an important role in regulating membrane shape transitions during endocytosis (Sorre et al., 2009).

Several studies have reported that translocation of pDNA molecules across the cell membrane during GET is mediated by endocytosis (Wu and Yuan, 2011; Chang et al., 2014; Rosazza et al., 2016a; Wang et al., 2018). Several endocytic pathways have been identified to participate in GET: Caveolae- and clathrin-mediated endocytosis, macropinocytosis, and clathrin- independent carrier/GPI-enriched early endosomal compartment (CLIC/GEEC) pathway, both *in vitro* (Rosazza et al., 2011, 2016a; Wu and Yuan, 2011; Wang et al., 2018) and *in vivo* (Šatkauskas et al., 2001; Markelc et al., 2015). However, the contribution of each endocytic pathway or a dominant endocytic pathway during GET is not yet clear (Sachdev et al., 2022). To determine which endocytic pathway is involved in pDNA internalization during GET, most of the studies have used endocytic inhibitors or measured co-localization of pDNA and endocytic markers. However, endocytic inhibitors are not fully specific and may disrupt multiple endocytic mechanisms simultaneously (Rennick et al., 2021). Even endocytic markers are not fully specific and thus may mark several endocytic pathways (Shearer and Petersen, 2019). Moreover, endocytic pathways are complex and diverse. There are many fundamental questions that remain unanswered, such as whether the key components of a particular endocytic pathway are conserved in different cell lines and whether there is overlap in the functions of molecules known to be involved in a particular endocytic pathway (Kumari et al., 2010). Further, pDNA aggregates od different sizes (100-500 nm) formed on the cell membrane during GET could trigger different endocytic pathways simultaneously (Golzio et al., 2002a; Faurie et al., 2004; Sachdev et al., 2020).

Once internalized, pDNA molecules encounter another barrier regardless of the translocation pathway i.e., endocytosis or diffusion through permeable sites in cell membrane. pDNA molecules must travel through the cytoplasm, which consist primarily of the dense network of the cytoskeleton. pDNA aggregates that have been endocytosed are encapsulated in endocytic vesicles and are protected from degradation by intracellular nucleases (Rosazza et al., 2016a). pDNA molecules in endosomes rely on endosomal transport mediated by the actin and microtubule network and associated molecular motors (myosin and dynein) to reach the nucleus (Vaughan and Dean, 2006; Rosazza et al., 2013). However, the endosomal membrane presents an additional barrier, as pDNA molecules must escape from endosomes to pass through the nuclear envelope to be expressed (El Ouahabi et al., 1997). On the other side, pDNA molecules that entered through permeable sites in cell membrane and have direct access to the cytoplasm rely primarily on hindered diffusion to reach the nucleus. Diffusion of molecules within the cytoplasm is size-dependent and is hindered by the actin network (Lukacs et al., 2000; Dauty and Verkman, 2005). Large DNA molecules, such as pDNA of about 5 kb, have an extremely low diffusion coefficient and are virtually immobile (Lukacs et al., 2000). They are therefore highly susceptible to degradation by intracellular nucleases (Lechardeur et al., 1999; Cervia et al., 2018). However, it has been shown that naked pDNA molecules form complexes with intra-cellular proteins as early as 15 mins post

their introduction into the cytoplasm (Badding et al., 2013). The protein-DNA complexes can protect pDNA from degradation by intracellular nucleases. Further, protein-DNA complexes can facilitate active trafficking inside the cytoplasm and nuclear import of pDNA, thus providing a possible pathway for pDNA molecules that diffused through permeable sites in cell membrane to reach the nucleus (Badding et al., 2013).

Irrespective of the cell internalization pathway, the final barrier for pDNA is the nuclear envelope. The nuclear envelope is temporarily disrupted during cell division, and synchronization of GET with the mitotic phase of cell cycle has been shown to increase GET efficiency (Brunner et al., 2002). pDNA molecules can also enter the nucleus of nondividing, slowly dividing, and terminally differentiated cells by using specific DNA sequences known as DNA nuclear targeting sequences that can bind to proteins in the cytoplasm which facilitate the entry of pDNA molecules into the nucleus (Badding et al., 2013). However, GET has also been achieved with pDNA molecules lacking these specific sequences (Utvik et al., 1999).

At least two possible mechanisms of nuclear import have also been proposed for pDNA molecules enclosed in endosomes. For example, endosomes containing pDNA aggregates could fuse with the endoplasmic reticulum and release pDNA molecules to the lumen of endoplasmic reticulum. pDNA molecules could then use the network between the endoplasmic reticulum and nuclear membrane to enter the nucleus (Elouahabi and Ruysschaert, 2005). Additionally, early endosomes that were observed to localize in the perinuclear space and fuse with the nuclear envelope – nuclear envelope associated endosomes, could transport pDNA into the nucleus by fusing with the nuclear envelope (Chaumet et al., 2015). The two nuclear import mechanisms could be involved as a separate or could be involved simultaneously.

1.4 FACTORS AFFECTING GENE ELECTROTRANSFECTION

GET efficiency *in vitro* and *in vivo* depends on several factors which can be categorized as parameters of electric pulses (Šatkauskas et al., 2005; Haberl et al., 2013; Rosazza et al., 2016a), pDNA characteristics (Kandušer et al., 2009), biological characteristics of cells/tissue and extracellular environment (Rosazza et al., 2012, 2016b; Maglietti et al., 2013; Olaiz et al., 2014).

1.4.1 Parameters of electric pulses

In GET applications, pulse parameters (amplitude, duration, pulse repetition rate, and pulse number) are usually varied to achieve permeabilization of the cell membrane while preventing excessive cell damage (Gehl and Mir, 1999). Determining the parameters of electric pulses is one of the most important steps in GET. The amplitude, duration, and number of electric pulses determine electrophoresis enabling electrophoretic mobility of

negatively charged pDNA molecules towards cell membrane and/or through cell membrane (Kandušer et al., 2009).

In general, smaller cells require a higher electric field to permeabilize their cell membrane. Therefore, the thresholds to permeabilize cell membrane in different cells may vary (Čemažar et al., 1998; Young and Dean, 2015).

GET protocols have been established for decades and recommend the use of long monopolar millisecond pulses which provide electrophoresis that brings sufficient number of pDNA molecules in contact with the cell membrane (Rosazza et al., 2016b; Potočnik et al., 2022). The main disadvantages of treating tissues with long monopolar pulses are discomfort and even pain, requiring the use of muscle relaxants and anesthesia, as well as the need to synchronize the delivery of the pulses with the electrocardiogram (Yao et al., 2017). In addition, long monopolar pulses can also lead to electrode oxidation, pH changes near the electrodes, bubble formation, and Joule heating (Turjanski et al., 2011; Faroja et al., 2013; Klein et al., 2019; Mahnič-Kalamiza and Miklavčič, 2020) all of which are undesired in GET applications. Since electric pulses have a dual function in GET: they permeabilize the cell membrane and cause electrophoresis of pDNA. The lack of pDNA electrophoresis is considered a limiting factor for the use of short pulses in GET (Faurie et al., 2010).

The results of recent studies have shown that high-frequency bipolar pulses (HF-BP), initially used for IRE (HF-IRE), can achieve a similar degree of cell membrane permeabilization as monopolar pulses of micro-millisecond duration at low pulse repetition rate (Sweeney et al., 2016), which form the basis of the existing IRE, ECT, and GET protocols. In HF-BP protocols long (100 µs–5 ms) monopolar pulses are replaced by bursts of short (0.25–5 µs) bipolar pulses. Bipolar pulses in one burst are delivered with high pulse repetition rate (on the order of tens or hundreds of kHz), while burst repetition rate is usually low (in order of Hz) (Yao et al., 2017; Sano et al., 2018) (Figure 1). In the dissertation, we will use the term HF-BP to refer to these types of pulses, as the term is already established. Monopolar pulses cause pDNA accumulation only on the side of the cell facing the cathode, whereas bipolar pulses cause pDNA accumulation on both sides of the cell facing the electrodes (Tekle et al., 1991; Faurie et al., 2010). With HF-BP pulses, we can also achieve more symmetrical permeabilization, which means a more predictable cellular response, that can be used to improve clinical precision of IRE, ECT and GET (Arena et al., 2011; Sano et al., 2015). During HF-BP pulse delivery, also fewer metal ions are released from the electrodes and electrochemical reactions are less compared to longer pulses (Mahnič-Kalamiza and Miklavčič, 2020; Vižintin et al., 2020). Further, HF-BP pulses trigger fewer muscle contractions and reduce pain during pulse delivery (Mercadal et al., 2017; Yao et al., 2017; Aycock et al., 2021; Cvetkoska et al., 2022).
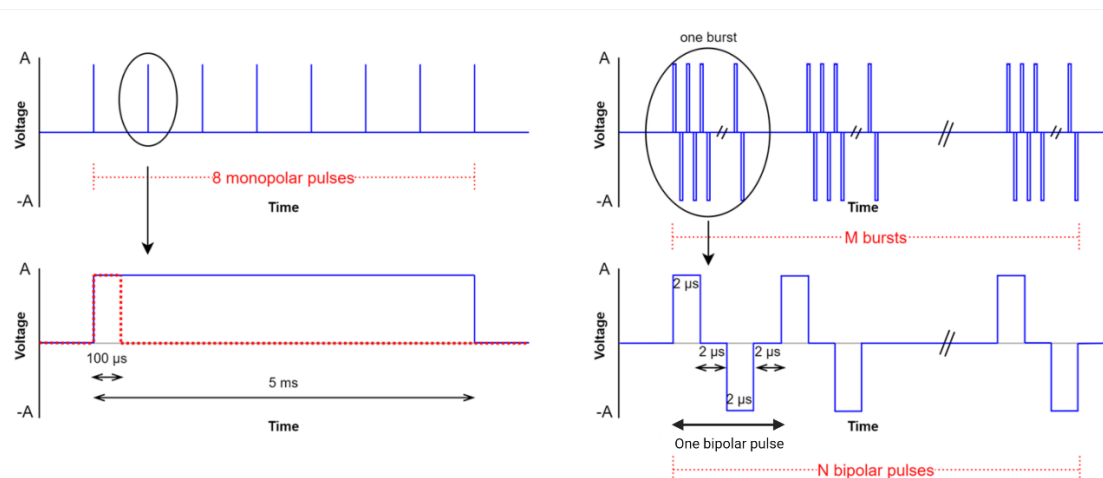
Figure 1: Comparison of monopolar (left) and HF-BP pulse protocols (right). M: number of bursts – 20, 50 or 100; N: number of bipolar pulses in one burst – 32, 50 or 216.

Even shorter, nanosecond pulses have been already used for GET, but only with high pulse repetition rates in the range of 100 kHz. When 200 ns pulses in bursts of ten were applied it was shown that as the pulse repetition rate was increased, also GET efficiency increased (Ruzgys et al., 2018). It was recently shown that up to 40% GET can be achieved with 300 ns pulses delivered at a 1 MHz pulse repetition rate, which is comparable to the efficiency of microsecond pulses (Novickij et al., 2020).

It has been suggested that nanosecond pulses disrupt the nuclear envelope, which could facilitate the transport of pDNA into the nucleus and thus increase GET (Batista Napotnik et al., 2016; Thompson et al., 2016; Chang et al., 2020). In several papers authors describe the use of different combinations of nanosecond and millisecond or microsecond pulses in an attempt to improve GET. Electroporation approaches using a combination of nanosecond and millisecond pulses increased transgene expression when nanosecond pulses were applied first followed by millisecond pulses but not in reverse order (Chopinet et al., 2013; Guo et al., 2014; Chang et al., 2020).

Similar to HF-BP pulses, nanosecond pulses can also potentially mitigate limitations present in GET with longer millisecond and microsecond pulses. Some cells exposed to GET with long monopolar pulses may lose viability due to excessive local heating, pH changes, and ionic imbalance (Ford et al., 2010). Nanosecond pulses reduce electrochemical reactions and heating during pulse delivery and can provide more patient friendly treatment in the *in vivo* setting with reduced muscle contractions (Ruzgys et al., 2018; Vižintin et al., 2021; Novickij et al., 2022). However, to date, successful GET with shorter (i.e., less than 10 µs) pulses *in vitro* has mostly been achieved with high pDNA

concentrations that are difficult to reach *in vivo*, at least in a larger volume (Sokołowska and Błachnio-Zabielska, 2019; Novickij et al., 2020).

1.4.2   pDNA characteristics

GET efficiency also depends on pDNA characteristics such as topology, size, concentration, and mobility. It has been shown that supercoiled pDNA leads to 100-fold higher transfection rates compared to open circular or linearized pDNA (Maucksch et al., 2009). Also, smaller pDNA molecules, presumably due to easier mobility, yield better GET efficiency (Novickij et al., 2020). Additionally, specific DNA sequences known as DNA nuclear targeting sequences can bind to proteins in the cytoplasm and facilitate entry of pDNA molecules into the nucleus (Badding et al., 2013).

Also, pDNA concentration affects GET efficiency. Increasing pDNA concentration leads to increased GET efficiency, but could, at least in some cell lines, lead to reduced cell survival (Chopra et al., 2020; Potočnik et al., 2021, 2022). pDNA concentration in solution can also be viewed as the distance between pDNA molecule and the cell membrane. With increasing pDNA concentration the probability of pDNA molecule being close enough to the cell membrane so that during pulse delivery with electrophoresis it reaches the cell membrane increases (Chopra et al., 2020; Potočnik et al., 2022). But increasing pDNA concentration above 100 µg/ml *in vitro* results in pDNA entanglement, which further reduces the mobility of pDNA molecules, especially if they are larger than 6 kb *in vitro* (Robertson and Smith, 2007).

1.4.3   Biological characteristics of cells/tissue and extracellular environment

Biological characteristics of cells/tissue and extracellular environment such as composition of cell membrane, tissue structure and conductivity, interstitial composition and extracellular pH can also affect GET efficiency (Maglietti et al., 2013; Olaiz et al., 2014; Rosazza et al., 2016b; Potočnik et al., 2019).

In vitro GET of tumor cells is efficient, but gene expression in tumors *in vivo* is weak. GET efficiency *in vivo* is highly dependent on tissue type, as different tissues have different structure that affect pDNA mobility in an extracellular environment. GET in muscle can achieve a high percentage of transfected cells (Mir et al., 1999), whereas tumors are extremely difficult to transfect (Rols et al., 1998). GET in tumors *in vivo* usually results in only a few percent of transfected cells (Cemazar et al., 2009; Chopinet et al., 2012). *In vivo*, tissue structure impedes pDNA movement and distribution, resulting in low GET efficiency in tumors (Cemazar et al., 2009). GET efficiency with the same protocols (pDNA concentration and pulse parameters) is different in tumors with different cell/tissue density (Cemazar et al., 2009). When tumors were exposed to enzymes that degrade the extracellular matrix, such as hyaluronidase, increased efficiency of GET in tumors *in vivo* was observed (Cemazar et al., 2012). However, hyaluronidase added prior

to the application of pulses increases tissue conductivity and thus the electric current, resulting in more heating and significant pH changes near the electrodes, which can lead to sever tissue damage (Lacković et al., 2009; Olaiz et al., 2014). These results suggest that also the extracellular environment of tumor cells may influence the efficiency of GET.

Local pH changes during pulse delivery can affect pDNA stability (Maglietti et al., 2013), and cell membrane recovery (Potočnik et al., 2019), both affecting GET efficiency. Normally, cells are exposed to a slightly acidic pH_e during hypoxic periods in normal tissues during wound healing (Crowther et al., 2001) or in the pathophysiological microenvironment of tumors (Stubbs et al., 2000). One of the main differences between tumor cells and their surrounding normal cells is the nutritional and metabolic environment. The microenvironment in tumors tends to be slightly acidic (pH_e: 6.2-6.9) due to the overproduction of lactate, whereas the intracellular pH (pH_i: 7.1-7.6) can remain neutral or become alkaline due to compensation mechanisms. In contrast, the pH_e of normal cells tends to be slightly or strongly alkaline (7.3-7.7) and the pH_i (6.9-7.2) slightly more acidic (Sharma et al., 2015).

Reversal of the pH gradient across the cell membrane is present in many tumors due to acidified pH_e and alkalinized pH_i and is becoming one of the most important and selective hallmarks of cancer (Sharma et al., 2015; Zheng et al., 2020; Pérez-Herrero and Fernández-Medarde, 2021). pH_e can affect numerous biological functions, such as endocytosis (Ben-Dov and Korenstein, 2012, 2013), lysosomal trafficking (Glunde et al., 2003), gene expression (Bumke et al., 2003; Duggan et al., 2006), proliferation, and viability (Bohloli et al., 2016). In addition, extracellular acidity has been shown to have immunosuppressive effects, thereby promoting tumorigenesis and metastasis (Zheng et al., 2020).

There are very few publications examining the effects of pH changes on GET. It has been shown that the processes triggered by electric pulses in cells depend on the properties of the electroporation medium and can affect the response of cells to the applied electric field (Dermol et al., 2016). During electroporation, ions conduct the current, leading to electrochemical reactions occurring at the electrode – electrolyte interface that led to pH changes. The pH gradient between the anode and cathode occurs as a result of the acidic pH on the anode side and the alkaline pH on the cathode side, potentially causing cell death near the electrodes (Maglietti et al., 2013; Olaiz et al., 2014; Phillips et al., 2015; Klein et al., 2019). The time in which the pH changes between electrodes are neutralized after treatments with electroporation-based methods is very short for ECT and IRE and much longer for GET. The difference arises from different pulse parameters used; for ECT and IRE generally shorter pulses with higher amplitude are delivered, while for GET, longer pulses of lower amplitude are applied. Changes in pH increase the risk of

pDNA denaturation and cell damage near the electrodes leading to a decrease in the efficiency of GET (Maglietti et al., 2013). Understanding and regulating pH changes in treatments based on electroporation can significantly contribute to increasing efficiency and to better understanding of the overall phenomenon of electropermeabilization. Electrochemical reactions, including pH changes, that occur during the application of electric pulses can be mitigated by the adjusted composition of the electroporation medium (Li et al., 2015), the choice of electrode material, platinum, stainless steel or conductive polymers instead of aluminum (Saulis et al., 2005), and by the choice of pulse parameters (Chafai et al., 2015).

1.5   RESEARCH AIMS

In the dissertation we mostly focused on understanding and optimization of GET *in vitro* with the long-term aim of improving GET applications, gene therapy and DNA vaccination. In this respect following research aims were tested:

Gene therapies *in vivo,* especially in tumors, still fail to reach high efficiency. One of the reasons is the difference in extracellular environment present in tumors. The effect of pH on many processes in the cell has been demonstrated (Glunde et al., 2003; Duggan et al., 2006; Ben-Dov and Korenstein, 2012, 2013; Bohloli et al., 2016). Applications of electroporation, such as ECT and GET, are mainly targeting tumor cells in which the pH gradient reversal across cell membrane is formed by a decrease in pH_e (Sharma et al., 2015). Acidic pH_e leads to the movement of lysosomes, which are crucial in the repairing of cell membrane damage, from the perinuclear region to the vicinity of the cell membrane (Glunde et al., 2003). Our aim was to determine the effect of slightly acidic pH_e on cell membrane permeabilization and cell survival. We expect that slightly acidic pH_e can affect the process of electroporation, especially cell membrane resealing. After electroporation and cell recovery in slightly acidic medium we expect no differences in the permeabilization rate, but we expect improved survival of cells after electroporation compared to cells electroporated and recovered in neutral medium.

GET in tumors is less efficient than in other tissues (Mir et al., 1999; Cemazar et al., 2009). By degrading the compact extracellular matrix of tumor cells, we can improve the efficacy of GET (Cemazar et al., 2012). In addition to the compact extracellular matrix that causes lower pDNA mobility, lower pH_e is also present in tumors (Sharma et al., 2015). Our aim was to determine if slightly acidic pH_e is a factor affecting the efficacy of GET. In the slightly acid medium *in vitro*, we expect less efficient GET.

DNA vaccination, besides efficient should also be patient friendly with minimal muscle contractions and pain and should not cause cell damage at the site of application. This can all be achieved by using appropriate pulse parameters. According to the findings of Sweeney et al. (2016) that high-frequency bipolar pulses can achieve similar percentage of cellular permeabilization, which is also more symmetrical, and recently successfully achieved GET by changing the repetition frequency of nanosecond pulses (Ruzgys et al., 2018) our aim was to achieve successful GET with shorter micro and nano-second pulses, which would potentially allow GET with less pain and muscle contractions.

2   SCIENTIFIC PAPERS

2.1   EFFECT OF ELECTROPORATION AND RECOVERY MEDIUM pH ON CELL MEMBRANE PERMEABILIZATION, CELL SURVIVAL AND GENE TRANSFER EFFICIENCY *IN VITRO*

Electroporation is a method in which an adequate number of electric pulses of sufficient amplitude, and duration applied to cells, thus inducing transient permeabilization of the cell membrane. Due to possibility that microenvironment in applications of *in vivo* electroporation is slightly acidic, we studied the effects of slightly acidic electroporation and recovery medium. We observed no difference in the permeabilization threshold, detected by propidium iodide, of cells which were electroporated and allowed to recover in growth (pH 7.8) or acidic (pH 6.5) medium. In contrast, statistically significant difference was observed in survival of cells that were exposed to pulse amplitudes greater than permeabilization threshold. Survival of cells was improved if acidic electroporation and recovery medium were used, however in contrast to our expectations acidic extracellular pH decreased gene electrotransfer efficiency. We also observed differences in morphology between cells that were electroporated and left to recover in growth medium and cells that were electroporated and left to recover in acidic medium. Our results imply that slightly acidic extracellular pH allows more efficient repair of damage that is induced on cell membrane during electroporation with high pulse amplitudes.

Effect of electroporation and recovery medium pH on cell membrane permeabilization, cell survival and gene transfer efficiency *in vitro*

Tjaša Potočnik, Damijan Miklavčič, Alenka Maček Lebar *

University of Ljubljana, Faculty of Electrical Engineering, Tržaška 25, 1000 Ljubljana, Slovenia

ABSTRACT

Electroporation is a method which uses an adequate number of electric pulses of enough amplitude, duration and number applied to cells, thus inducing transient permeabilization of the cell membrane. Due to possibility that microenvironment in applications of *in vivo* electroporation is slightly acidic, we studied the effects of slightly acidic electroporation and recovery medium. We observed no difference in the permeabilization threshold, detected by propidium iodide, of cells which were electroporated and allowed to recover in growth (pH 7.8) or acidic (pH 6.5) medium. In contrast, statistically significant difference was observed in survival of cells that were exposed to pulse amplitudes greater than permeabilization threshold. Survival of cells was greater if acidic electroporation and recovery medium were used, but acidic extracellular pH decreased gene electrotransfer efficiency. We also observed differences in morphology between cells that were electroporated and left to recover in growth medium and cells that were electroporated and left to recover in acidic medium. Our results imply that slightly acidic extracellular pH allows more efficient repair of damage that is induced on cell membrane during electroporation with high pulse amplitudes.

© 2019 Published by Elsevier B.V.

1. Introduction

Electroporation also named electropermeabilization is a method in which the application of an appropriate number of electric pulses of sufficient amplitude and duration causes transient permeabilization of the cell membrane, allowing ions and molecules to enter and/or leave the cell. Electroporation can be used for treatment of tumors, since increased membrane permeability due to electroporation enables entering of chemotherapeutic drugs into tumor cells, as a method named electrochemotherapy (ECT) [1,2]. It can also be used as delivery method for a large variety of molecules such as ions [3], dyes [4], tracers [5], antibodies [6], and also oligonucleotides [7], RNA [8] and DNA [9–11]. Electroporation is used in medicine [12], as ECT [13], irreversible electroporation (IRE) as a method of tissue ablation [14–16], gene electrotransfer (GET) as gene therapy [17,18] and DNA vaccination [19,20], transdermal drug delivery [21,22], as well as in biotechnology [23] and food and biomass processing [24,25].

ECT is an extremely effective, physical technique for elimination of cutaneous and subcutaneous solid tumors and also deep-seated tumors [26]. Commonly used drugs for ECT are bleomycin and cisplatin. Low rate of side effects and low systemic toxicity are the advantage of ECT. Response rates of 77–87% have been reported with bleomycin [1]. The efficacy of ECT depends on a variety of factors, mostly of physical

quantities, which should be chosen with care. Among those factors are electric field intensity, pulse duration and the number of pulses [27].

GET is a method of DNA delivery into cell nucleus in order to achieve therapeutic effect. For effective DNA delivery and expression several steps must be overcome, among which are membrane electroporation, DNA-membrane interaction, transfer of DNA into the cell, intracellular trafficking of DNA through cytosol and nuclear import of DNA [28]. With electrotransfered DNA there is a possibility of correction of a defective gene by silencing it or with its functional replacement, electrotransfered DNA can encode a therapeutic protein or a protein that induces cell death [29]. GET efficiency depends on several factors such as electrophoretic movement of the plasmid [28,30,31], plasmid concentration [32] and pH changes [33] since medium pH can affect plasmid stability [34]. GET efficiency also highly depends on tissue type. GET in muscle can achieve high percentage of transfected cells [10] while tumors are extremely hard to transfect [11]. *In vitro* GET of tumor cells is efficient, however gene expression in tumor cells *in vivo* is weak. GET in tumors *in vivo* usually results in only a few percent of transfected cells [11,35].

One of major differences between tumor cells and surrounding normal cells is the nutritional and metabolic environment. Microenvironment in tumors tend to be acidic (pHe: 6.2–6.9) due to the overproduction of lactate, while the intracellular pH (pHi: 7.1–7.6) may remain neutral or become alkaline due to compensation mechanisms. In contrast, normal cells pHe tends to be slightly or highly alkaline (7.3–7.7) and while pHi is a little bit lower (6.9–7.2) [36].

* Corresponding author.
E-mail address: alenka.maceklebar@fe.uni-lj.si (A. Maček Lebar).

Regulation of pHi is one of the most important physiological functions of homeostasis, because activity of most chemical reactions *via* enzyme proteins is dependent on pH. Membrane proton pumps and transporters whose activity is controlled by intra-cytoplasmic pH sensors maintain pHi within narrow range. Intra-cytoplasmic pH sensors recognize changes in pHi and induce cellular responses to maintain the pHi, often at the expense of acidifying the pHe. On the other hand, pHe acidification impacts cells *via* specific acid-sensing ion channels and proton-sensing G-protein coupled receptors [37]. During electroporation, increase in plasma membrane permeability leads to equilibration of pH between pHe and pHi [38].

Due to acidified pHe and alkalinized pHi the reversal of pH gradients across plasma membrane is present in many tumors and is becoming one of the most significant and selective hallmarks of cancer [39]. The extracellular pH can affect numerous biological functions, such as endocytosis [40,41], lysosomal trafficking [42], gene expression [43–45], proliferation and viability [46].

Most *in vitro* electroporation and GET experiments are done in electroporation medium or growth medium with pH 7.4, while extracellular pH at least in tumors *in vivo* is acidic. In this study we investigated if acidic electroporation and recovery medium have any effect on cell processes during electroporation and GET and consequently could have an impact on effectiveness of ECT and GET. We performed electroporation and GET experiments *in vitro* in electroporation buffers of different acidity to test the effects of acidic conditions in *in vitro* experiments which however differs from extracellular composition in *in vivo* treatments. Electroporation and GET were performed in growth medium which is an approximation of the *in vivo* extracellular fluid. However, there are many more factors *in vivo* that cannot be taken in account *in vitro* such as, blood supply, immune system, electric field shielding, cell crowding. In this study we focused on effects of electroporation and recovery medium pH on membrane permeabilization, cell viability and recovery after electroporation, and GET efficiency.

2. Materials and methods

2.1. Cells

Chinese hamster ovary cell line (CHO-K1; European Collection of Cell Cultures, Great Britain) was used in our experiments. Cells were grown in 150 mm^2 culture flasks (TPP, Switzerland) for 2–4 days in an incubator (Kambič, Slovenia) at 37 °C, in a humid atmosphere of 5% CO$_2$ in air. CHO cells were cultured in HAM-F12 growth medium (PAA, Austria) supplemented with 10% fetal bovine serum (Sigma Aldrich, Germany), L-glutamine (StemCell, Canada) and antibiotics penicillin/streptomycin (PAA, Austria), and gentamycin (Sigma Aldrich, Germany).

Cell suspension for experiments was prepared from cells in exponential growth phase by trypsinization using trypsin – EDTA (5 g trypsin/2 g EDTA in 0.9% NaCl; SigmaAldrich) 10 x diluted in Hanks' Balanced Salt solution (Sigma-Aldrich). From the obtained cell suspension, trypsin and growth medium were removed by centrifugation at 270 RCF for 5 min at 4 °C (Sigma 3–15 K, UK). The cell pellet was resuspended in cell growth medium to obtain a final cell density of 2×10^7 cells/ml.

2.2. Medium pH

The pH of cell growth medium was lowered using acetic acid or HCl. HAM-F12 growth medium (G) at room temperature had the pH of 7.8. pH was lowered to 6.72, 6.38, 6.13 and 5.47 by adding 0.021%, 0.033%, 0.042% and 0.066% weight of acetic acid respectively and to pH 7.3, 7.0, 6.5 and 5.9 by adding 0.0004%, 0.0008%, 0.0016% and 0.0032% weight of HCl respectively. The interim pH values were calculated with cross calculation, since pH in this range was dropping in a linear way. pH was measured using SevenGo-SG2 (Mettler-Toledo) pH

meter and measuring electrode Inlab Routine Pro (Mettler-Toledo). Medium with the pH of 6.5 was used as an acidic medium (A) as pH 6.5 is an approximation of tumor pHe.

Conductivity of acidic medium was measured with conductometer (MA 5950, Metrel). Conductivity of acidic (pH 6.5) medium was 14.52 mS/cm and conductivity of growth medium (pH 7.8) was 14.24 mS/cm.

2.3. Cytotoxicity

We exposed CHO cells to medium with different pH values (lowered either with acetic acid or HCl) for 24 h. Cell survival was determined with the MTS-based Cell Titer 96 AQueous One Solution Cell Proliferation Assay (Promega, USA). Absorption at 490 nm wavelength (A490) was measured with a Tecan Infinite M200 spectrophotometer (Tecan, Switzerland). An average absorption obtained in the samples containing only growth medium was subtracted from the absorption measured in cell samples. To calculate the percentage of viable cells the absorption of each sample was divided by an average absorption of the control samples.

2.4. Electroporation

Four combinations of electroporation and recovery medium were tested: cells were electroporated in growth medium and recovered in growth medium (GG), cells were electroporated in growth medium however recovered in acidic medium (GA), cells were electroporated in acidic medium and recovered in growth medium (AG) and cells were electroporated in acidic medium and recovered in acidic medium (AA).

30 μl of cell suspension was mixed with 30 μl of double concentrated acidic medium or 30 μl of growth medium. A drop of prepared cell suspension (50 μl) was pipetted between two parallel stainless steel electrodes with the distance between them being 2 mm. The cell sample-electrodes contact surface was not measured. It can be estimated from the equation for the volume of the cylinder with height 2 mm (the distance between electrodes) to be 25 mm^2; *i.e.* surface = 50 μl (*i.e.* volume of the sample)/(2 mm) = 25 mm^2. The total electrode surface is 200 mm^2 = 10 mm × 20 mm. Therefore the ratio of the contact surface in relation to the total electrode surface is 1:8. All the cells were thus exposed to approximately the same electric field, which was estimated as the voltage applied divided by the distance between the electrodes. Cells were exposed to a train of eight rectangular electric pulses with 100 μs duration and 1 Hz pulse repetition frequency, generated by Betatech electroporator (Electro cell B10; Betatech, France) for permeabilization experiments where lower voltages were applied, and a laboratory prototype pulse generator [47] for applying higher voltages for cell survival experiments. The amplitude of the pulses and consequently the applied electric field was varied from 0 to 3 kV/cm. During each experiment voltage and current applied to sample were measured with differential probe (ADP305, LeCroy, USA) and current probe (CP030, LeCroy, USA) and monitored on oscilloscope (Wavesurfer 422, 200 MHz, LeCroy, USA). At the same applied voltage, measured current did not differ between samples in acidic and growth medium. Also, the pulse generators produced the same current at the same applied voltage. The electrodes were washed with sterile 0.9% NaCl and dried with sterile gauze between electroporated samples. After electroporation cells were left for 10 min to recover either in growth or in acidic medium at room temperature.

2.5. Cell viability

After pulse application as previously described, 40 μl of cell suspension was transferred into a 1.5 ml microcentrifuge tube containing 40 μl of growth medium or double concentrated acidic medium and left for 10 min at room temperature to allow for cell membrane resealing. Then, 20 μl of cell suspension (10^5 cells) was transferred in 80 μl of growth medium prepared previously in each well of 96-well plates

3

(TPP, Switzerland). Three samples were taken from each electroporated droplet. Cells were placed in the incubator (37 °C, 5% CO_2) for 24 h. Cell viability was measured using the MTS-based Cell Titer 96 AQueous One Solution Cell Proliferation Assay (Promega, USA) as described above. To calculate the percentage of viable cells after electroporation the absorption of each sample was divided by an average absorption of the control samples, *i.e.* the samples that were exposed to electric field of 0 V/cm.

2.6. Fluorescence microscopy

Cell recovery after electroporation was followed by adding propidium iodide (PI; 5 μl of 1.5 mM) immediately before pulse application or 5 min after it. Again four combinations of electroporation and recovery medium were tested: GG, GA, AG and AA. Cells were electroporated according to above described protocol. Cell suspension of CHO cells between the electrodes was exposed to electric field of 2.4 kV/cm. After pulse application, 40 μl of cell suspension was transferred into a small petri dish where 320 μl of recovery medium was prepared. If PI was added before application of electric pulses, the sample was left for 10 min at room temperature prior to the capture of images. If PI was not added before application of electric pulses, the sample was left for 5 min, then PI was added and the images were captured after additional 10 min. The phase contrast and fluorescent images (Ex 562/40, Em 624/40) of the treated cells were captured using cooled CCD camera (Visicam 1280, Visitron, Puchheim, Germany) mounted on a fluorescence microscope (Zeiss AxioVert 200, objective 20×, Zeiss, Oberkochen, Germany) using MetaMorph 7.0 software (Molecular Devices Corporation, Sunnyvale, CA, USA), exposure time 100 ms. For each sample, three phase contrast and corresponding fluorescent images of a distinct area were acquired. The number of electroporated cells was determined by manually counting the cells in fluorescence and phase contrast images. The percentage of electroporated cells in a given sample was determined as the ratio between the average number of fluorescent cells counted in the fluorescence images and the average number of all cells counted in the corresponding phase contrast images.

2.7. Light microscopy

Using light microscopy cell morphology changes were observed after electroporation with electric field of 1.8 kV/cm, under 100 x oil immersion objective (Zeiss AxioVert 200, 100 x oil immersion objective, Zeiss, Oberkochen, Germany). Cells electroporated and recovered in AA and GG combinations were observed during recovery (6 min after electroporation) and after recovery (11 min after electroporation). Images were acquired using the VisiCam 1280 camera (Visitron, Germany) and the MetaMorph PC software (Molecular Devices, USA).

2.8. Flow cytometry

Cells were electroporated as described above in four combinations of growth and acidic medium (pH 6.5); AA, AG, GA and GG. Immediately before electroporation 5 μl of PI was added to cell suspension. After electroporation cells were left to recover for 10 min in 100 μl of growth or acidic medium. Incorporation of PI in cells was detected using flow cytometer (Attune® NxT, Life Technologies, Carlsbad, CA, USA). Cells were excited with a blue laser at 488 nm, and the emitted fluorescence was detected through a 574/26 nm band-pass filter. The measurement ended when 10,000 events were recorded. Obtained data was analyzed using the Attune NxT software.

2.9. Gene electrotransfer

5×10^4 cells were seeded in 24-well plates as a monolayer culture at 37 °C in a humidified atmosphere in a 5% CO_2 incubator 24 h before GET. Prior to electric pulses delivery growth medium was removed and 150 μl of growth or acidic medium with plasmid pEGFP-N1 (10

μg/ml) (Clontech Laboratories Inc., MountainView, CA, USA) encoding green fluorescent protein (GFP) was added to cells. Cells were incubated with plasmid for 2 min, then electric pulses were applied using two parallel stainless steel wire (diameter of 1 mm) electrodes with a length of 10 mm which were 4 mm apart. Three different pulse protocols were tested; Protocol 1: 8 pulses, 100 μs, 1 Hz and 1.3 kV/cm; Protocol 2: 4 pulses, 200 μs, 1 Hz and 1.2 kV/cm, and Protocol 3: 4 pulses, 1 ms, 1 Hz and 0.8 kV/cm. Pulses were generated by Betatech electroporator (Electro cell B10, France). Immediately after electric pulses delivery 150 μl of medium with pEGFP-N1 was removed and replaced with 150 μl of growth or acidic medium with 25% of fetal bovine serum (Sigma-Aldrich Chemie GmbH, Deisenhofen, Germany). Cells were incubated for 10 min at 37 °C in a humidified atmosphere in a 5% CO_2 incubator. Then 1 ml of growth medium was added and cells were incubated for 24 h at 37 °C in a humidified atmosphere in a 5% CO_2 incubator. Three images per well on an area between electrodes were recorded using a fluorescent microscope (Zeiss 200; Axiovert) with excitation wavelength 488 nm, emitted fluorescence through a bandpass filter 525/50 nm, and counted by ImageJ program for image analysis. Transfection rate was determined as a number of GFP positive cells divided by all cells in each image, expressed in %.

2.10. Statistical analysis

All results are reported as a mean value of 3 to 5 experiments. The spread of the data is given by standard deviation. The significance between the experimental groups was analyzed in SigmaPlot 11.0 (Systat Software Inc., Chicago, IL, USA), and determined using Two way ANOVA test. The statistically significant difference was indicated by $p < .05$.

3. Results

3.1. Cytotoxicity of acidic medium

According to MTS assay, exposure of CHO cells to medium with pH values of 7.3, 7.0, 6.5 and 5.9, lowered with adding acetic acid or HCl, affects cell viability. After 24 h incubation in the medium with pH of 5.9, lowered with adding HCl, $86.5 \pm 5.9\%$ of cells are viable, using shorter incubation times or medium with higher pH the survival of the cells is even better. With lowering medium pH with acetic acid we obtained similar results (data not shown). We tested HCl and acetic acid to see if there is any difference in cytotoxicity of acidic medium depending on the acid used for acidification. We observed no difference in cell survival between the two acids used.

3.2. Cell viability after electroporation

The viability of CHO cells following electroporation with different combinations of electroporation and recovery medium is presented in Fig. 1. We observed statistically significant correlation between applied electric field and electroporation and recovery medium pH. CHO cells survival after electroporation at 1.2 kV/cm, 1.8 kV/cm and 2.4 kV/cm was better when cells were electroporated and recovered in acidic medium (AA) compared to survival of cells that were electroporated and recovered in growth medium (GG). The biggest difference was observed after electroporation at 1.8 kV/cm. Survival of cells that were treated with AA combination was 34% better than survival of cells that were treated with GG combination. Following electroporation with AA combination $73.4 \pm 7.9\%$ cells is viable in contrast to only $39.1 \pm 23.4\%$ of cells treated with GG combination ($p = .047$). Cell viability of GA treatment ($48.1 \pm 5.7\%$) is also lower compared to AA treatment ($p = .011$). When electric pulses with 2.4 kV/cm are applied, different pH of electroporation and recovery medium used caused smaller variations in cell viability. Again the highest survival was observed with AA combination ($31.8 \pm 5.2\%$)
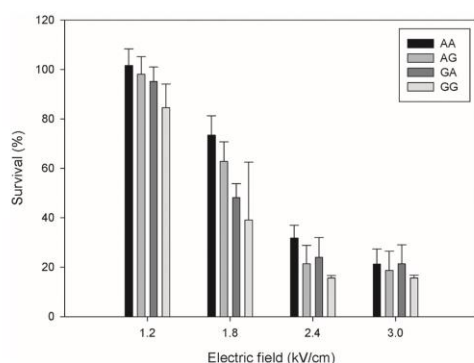
Fig. 1. Viability of CHO cells after electroporation with growth or acidic electroporation and recovery medium. Vertical bars represent standard deviation.

followed by GA, AG and GG combination (24.0 ± 8.0%, 21.4 ± 7.4% and 15.6 ± 1.0%, respectively). Survival of CHO cells at 3 kV/cm is low – around 20% - regardless of electroporation and recovery medium pH. With all four tested electric field strengths cell viability was always the highest with AA and the lowest with GG combination used. Results also show that values of applied electric field >1.8 kV/cm, especially 2.4 kV/cm and 3.0 kV/cm seem to approach IRE.

3.3. Light microscopy

When cells were exposed to growth or acidic medium without electroporation we did not observe any differences in cell morphology. There was no morphological differences between cells in growth or acidic medium after 6 or 11 min of observation. Small membrane blebs can be seen on the cell surface in either growth or acidic medium (Fig. 2). Membrane blebs are rounded membrane protrusions caused by the detachment of the lipid bilayer from the underlying cytoskeleton. Typically membrane blebs are viewed as a sign of apoptosis, but they are often observed also during the life cycle of intact cells [48], during cytokinesis [49], migration [50], and during cell detachment and spreading [51]. Short-lived membrane blebs were also observed when cells underwent spin/wash cycles and media changes [52]. Membrane blebs as can be seen in Fig. 2 are familiar features of the initial spreading process [53]. In contrast cells that were electroporated show extensive bleb formation (Fig. 3). Blebs can grow several seconds or minutes, while remaining attached to the cell [52]. Cells electroporated with GG combination had more membrane blebs that formed faster, had larger diameter and were more stable (Fig. 3; marked with arrows) than membrane blebs formed after electroporation with AA protocol. Many blebs that formed after electroporation with AA protocol already retracted in first 6 min after electroporation.

3.4. Permeabilization

Using flow cytometry we measured permeabilization level (PI uptake) of cells exposed to various electric field strengths. Again we used
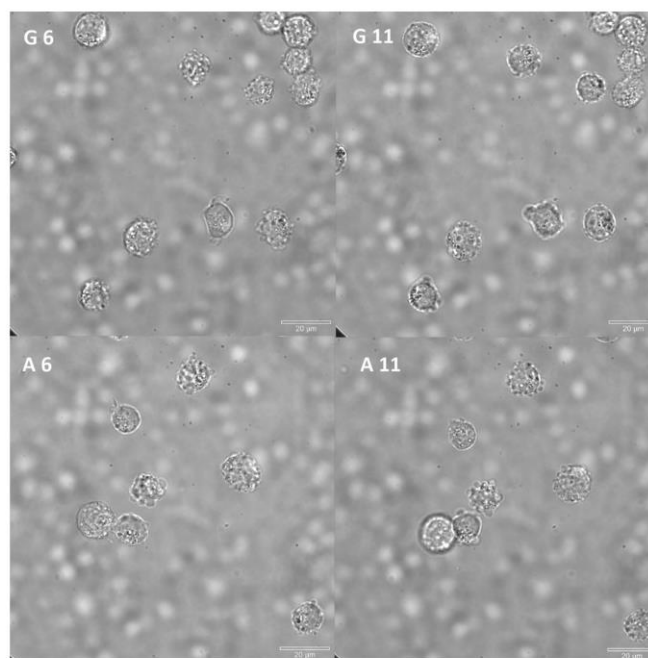

Fig. 2. CHO cells under light microscope, 100× oil immersion objective. G 6 – cells in growth medium after 6 min of observation, G 11 – cells in growth medium after 11 min of observation, A 6 – cells in acidic medium after 6 min of observation, A 11 – cells in acidic medium after 11 min of observation.
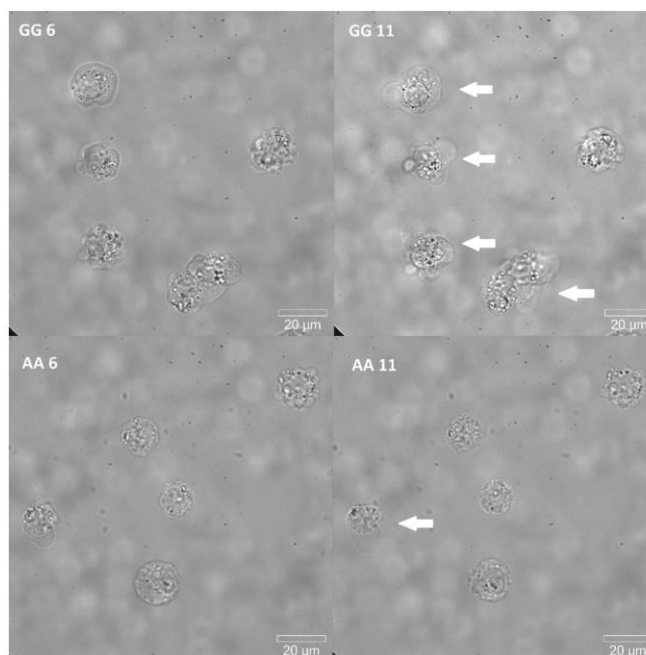
Fig. 3. CHO cells under light microscope, 100× oil immersion objective. Cells were electroporated with 1.8 kV/cm. GG 6 – cells electroporated with GG combination 6 min after electroporation, GG 11 – cells electroporated with GG combination 11 min after electroporation, AA 6– cells electroporated with AA combination 6 min after electroporation, AA 11 – cells electroporated with AA combination 11 min after electroporation.

AA, AG, GA and GG combinations of electroporation and recovery medium pH values. Percent of PI containing cells is presented in Fig. 4. Results show that electroporation and recovery medium pH value had no effect on percent of permeabilized CHO cells nor on their fluorescence intensity (data not shown). We observed no difference in permeabilization at any electric field strength applied (0–1.4 kV/cm) and at any combination of electroporation and recovery medium pH used.
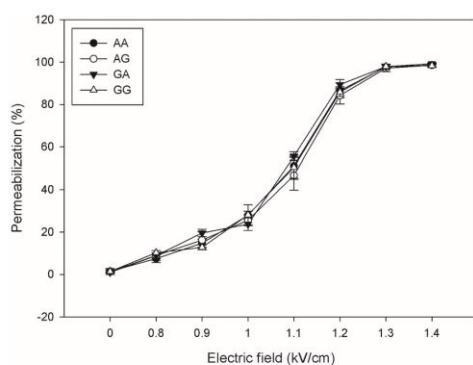
3.5. Recovery of cells after electroporation

In these experiments, PI was added immediately before (0) exposure to electric pulses or 5 min after it. Since we wanted to test cell membrane repair capacity of cells we choose electric field strength at which all the cells were permeabilized *i.e.* > 1.4 kV/cm (Fig. 4) and also decreased cell survival was observed (Fig. 1). In cell viability experiments we observed a slight difference, although not significant, in survival of cells after electroporation at 2.4 kV/cm. Based on this results we choose electric field of 2.4 kV/cm for our cell recovery experiments. The percentages of CHO cells, which were exposed to electric field of 2.4 kV/cm in growth or acidic cell medium, with incorporated PI are shown in Fig. 5. If PI was added before exposure to electric pulses, the acidity of electroporation medium and acidity of recovery medium did not affect the percentage of fluorescent cells significantly which is consistent with permeabilization assay (Fig. 4). If exposure of the cells to electric pulses and recovery were done in growth medium, the cells did not recover within 5 min time interval after electroporation. Namely the percentage of fluorescent cells remained 66.6 ± 19.1% also if PI was added 5 min after exposure to electric pulses. The graph in Fig. 5 shows that recovery after exposure to electric pulses is much better in acidic medium than in growth medium, independent of whether electroporation is done in growth or acidic medium. This can be seen in cells in which PI was added 5 min after exposure to electric pulses and later recovered in acidic medium. Here, only 4.8 ± 2.3% of cells electroporated in growth and 4.7 ± 3.1% of cells electroporated in acidic medium, incorporated PI. If cells were exposed to electric pulses in acidic medium and recovery was proceeded in growth medium, 39.0 ± 6.1% of cells were still

Fig. 4. PI uptake in CHO cell line after electroporation with growth or acidic electroporation and recovery medium. Vertical bars represent standard deviation.
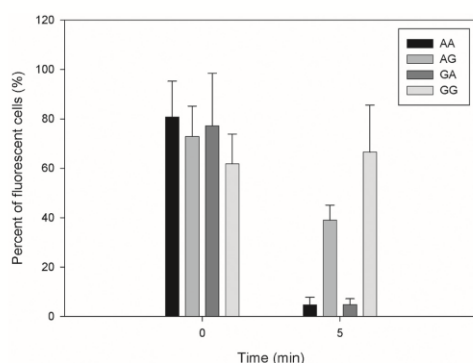
Fig. 5. Percentage of flourescent CHO cells after electroporation at 2.4 kV/cm and recovery in growth or acidic medium. Vertical bars represent standard deviation.

unrecovered 5 min after exposure to electric pulses. When comparing percentage of fluorescent cells with PI added 5 min after electroporation statistically significant differences are observed between all pairs except GA-AA pair (AA-GG: $p < .001$; GG-GA: $p < .001$; GG-AG: $p = .023$; AG-AA: $p = .002$; AG-GA: $p = .002$).

3.6. Gene electrotransfer (GET)

Same as electroporation experiments, also GET was performed in AA, AG, GA and GG combinations of electroporation and recovery medium. We tested three different pulse protocols; protocol 1 (8 pulses, 100 µs, 1 Hz and 1.3 kV/cm) for comparison with electroporation experiments and two pulse protocols with longer pulses, which are reported in the literature to be used for GET; protocol 2 (4 pulses, 200 µs, 1 Hz and 1.2 kV/cm) and protocol 3 (4 pulses, 1 ms, 1 Hz and 0.8 kV/cm) (Fig. 6).

With all three pulse protocols the lowest percentage of transfected cells was obtained when electroporation and recovery were done in acidic medium (AA) (Protocol 1: 9.5 ± 1.3%; Protocol 2: 7.3 ± 2.7%; Protocol 3: 11.1 ± 5.9%) (Figs. 7 and 8). The highest percentage of transfected cells was obtained when electroporation and recovery were done in growth medium (GG) (Protocol 1: 33.7 ± 5.2%; Protocol
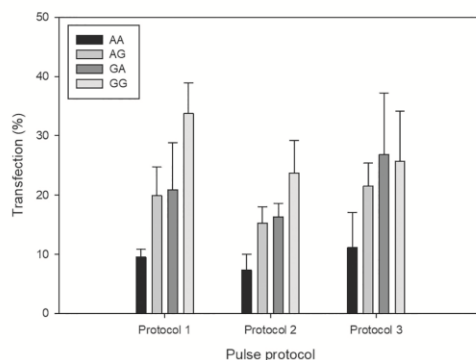

Fig. 6. Percentage of transfected CHO cells after GET with different pulse protocols (Protocol 1: 8 pulses, 100 µs, 1 Hz and 1.3 kV/cm; Protocol 2: 4 pulses, 200 µs, 1 Hz and 1.2 kV/cm, and Protocol 3: 4 pulses, 1 ms, 1 Hz and 0.8 kV/cm) and recovery in growth or acidic medium. Vertical bars represent standard deviation.

2: 23.7 ± 5.6%) except for pulse protocol 3 where the highest percentage of transfected cells was obtained with GA combination (26.8 ± 10.5%), however not statistically significant. When comparing different electroporation and recovery medium combinations statistically significantly higher transfection was achieved with GG combination compared to AA for pulse protocols 1 ($p < .001$) and 2 ($p = .001$). In these two pulse protocols transfection was also statistically significantly higher with AG (Protocol 1: $p = .007$; Protocol 2: $p = .049$) and GA (Protocol 1: $p = .003$; Protocol 2: $p = .021$) combinations compared with AA combination. Pulse protocol 3 gave statistically significant different result only between GG and AA combinations ($p = .014$), again GG being higher than AA. We observed no statistically significant difference in GET efficiency among the same electroporation and recovery medium combinations between three tested pulse protocols. In agreement with results presented in Fig. 1 no statistical differences in cell survival after GET with all three pulse protocols (electric field: 0.8, 1.2 and 1.3 kV/cm) among different electroporation and recovery medium combinations were observed (data not shown).

4. Discussion

In vitro electroporation and GET experiments are most often performed in medium with neutral or slightly alkaline pH. Since extracellular environment of most tumors is acidic, applications of electroporation *in vivo* are thus done in acidic conditions. With the goal of most effective transfer of findings *in vitro* to *in vivo* treatments, we investigated if acidic electroporation and recovery medium have any effect on cell membrane permeabilization, cell survival after electroporation and on GET efficiency.

Our results show that electroporation and recovery medium pH had no effect on CHO cell membrane permeabilization threshold. The similarity of PI uptake curves implies that induced transmembrane voltage and accompanying process of pore formation are not affected by acidity of electroporation or recovery media. However, we observed differences in cell viability depending on the pH of electroporation and recovery medium. Cells electroporated and recovered in acidic medium had significantly higher percentage of survival compared to cells electroporated and recovered in growth medium. When electroporation was done in medium with different pH than the pH of the medium in which cells recovered (GA and AG combinations), the differences in survival were less pronounced, although cells exposed to AG combination had higher survival, which might suggest that electroporation in acidic medium allows better survival. Medium pH had small influence on cell viability if low or very high electric fields were applied (Fig. 1). With fluorescence microscopy we observed that in growth medium less cells completely recovered within 5 min than in acidic medium. (Fig. 5), which implies that in cells recovering in growth medium cell membrane resealing is slower. Electroporation and recovery medium pH also has effect in GET efficiency. Acidic electroporation and recovery medium (AA combination) significantly decreased GET efficiency compared to growth electroporation and recovery medium (GG combination). When GET was performed in medium with different pH than the pH of the medium in which cells recovered (GA and AG combinations) GET efficiency was lower than with GG combination and higher than with AA combination. No differences in GET efficiency between GA and AG combinations were observed.

Electric pulses trigger different processes in cells and on their membranes. Apparently these processes depend on characteristics of electroporation and recovery medium and can influence the response of cells to applied electric field. Pulse parameters for efficient electroporation treatments are determined on the basis of results obtained in *in vitro* experiments which are mostly performed in selected electroporation buffers. Electroporation medium composition can have a profound effect on electroporation effectiveness [54]. There are contradictory reports of medium composition and conductivity effects on cell membrane permeabilization
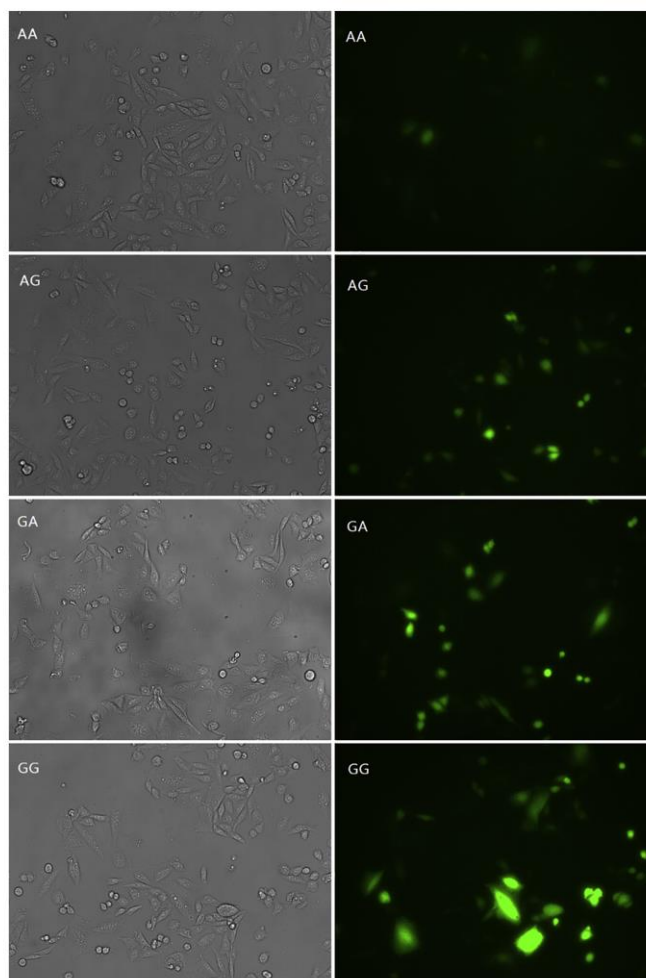
Fig. 7. Bright field images (left) and fluorescence images (right) of CHO cells 24 h after GET with pulse protocol 1 (8 pulses, 100 μs, 1 Hz and 1.3 kV/cm) with electroporation and recovery in growth or acidic medium.

and resealing. In some studies, increasing the ionic strength of the medium caused cell membrane electroporation at lower electric field intensities [55] in others, at the unchanged medium conductivity, ionic composition and strength of the medium had almost no effect on electroporation but, when medium conductivity was decreased, increased electroporation efficiency was observed [56]. On the contrary, the resealing of the membrane was independent of medium ionic composition or conductivity [57]. Electroporation medium osmolarity also has an effect on electroporation. In a hypertonic medium, cells are permeabilized at a lower voltage than cells in isotonic medium. In contrast, increasing the osmotic pressure of the recovery medium (hypertonic) facilitates the resealing of electroporated cells [58].

Higher survival of cells electroporated and recovered in acidic medium can be a consequence of more efficient pore resealing in acidic environment. Membrane repair process is started with Ca2+ influx through plasma membrane within <30 s after injury. Resealing involves exocytosis of lysosomes followed by massive endocytosis. Endocytosis and injury removal are triggered by extracellular activity of the lysosomal enzyme acidic sphingomyelinase [59,60]. Glunde et al. (2003) showed that in human mammary epithelial cells (HMECs) and breast cancer cells of different degrees of malignancy acidic pHe values of pH 6.8 and pH 6.4 cause a significant displacement of lysosomes from the perinuclear region to the cell periphery. They also observed higher number of lysosomes in cells exposed to extracellular acidity [42]. It was demonstrated that exposure of the
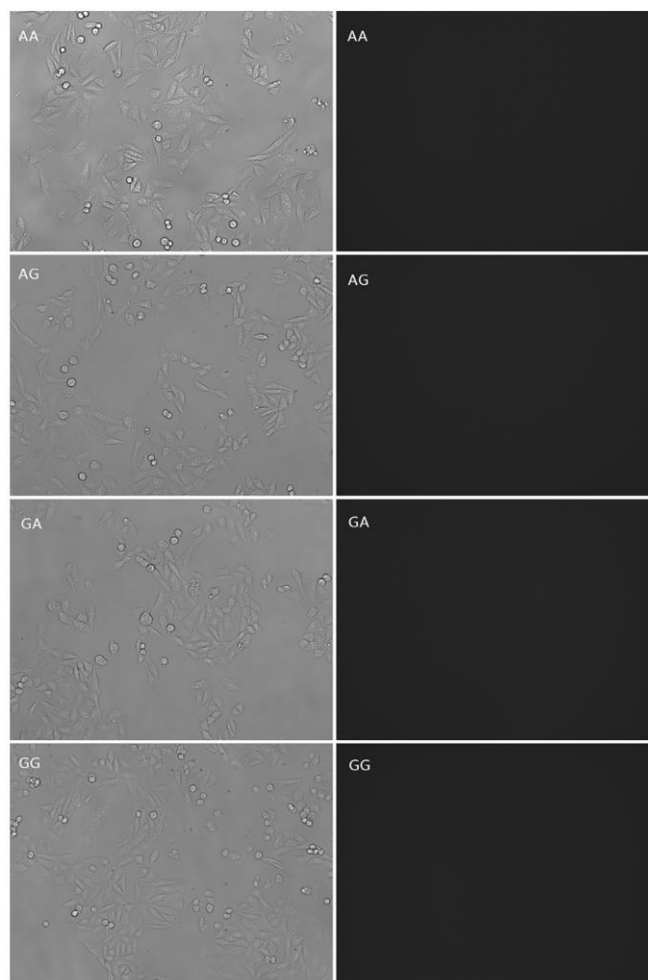
Fig. 8. Bright field images (left) and fluorescence images (right) of control CHO cells 24 h after exposure to growth or acidic electroporation and recovery medium without pulse application.

cell surface to a high concentration of protons stimulates the formation of inward membrane invaginations and vesicles, accompanied by an enhanced uptake of macromolecules [40,41]. Membrane invaginations and displacement of lysosomes from the perinuclear region to the cell periphery, driven by extracellular acidosis, could increase exocytosis of lysosomes and thus facilitate faster and more efficient plasma membrane damage repair which enables better cell survival in acidic environment. [61] showed that cells which are adapted to grow in acidic conditions express higher number of lysosomal proteins. The most upregulated protein was LAMP2 which protects lysosomal membranes from acid proteolysis. Interestingly more LAMP2 protein was found in cell plasma membrane compared to lysosomal membranes, which is in contrast with cells

that grow in neutral pH. Higher expression of LAMP2 protein in cell plasma membrane triggered by acidosis was confirmed *in vitro*, *in vivo* and in patient samples. Increased number of LAMP 2 proteins in plasma membrane could thus present an advantage in cell membrane repair after electroporation in acidic environment [61].

We can observe characteristic changes in cell appearance after electroporation with 1.8 kV/cm as seen in images of cells under light microscope. Cells exposed to electric pulses show signs of granulation, loss of cell membrane integrity and long lasting membrane blebs, which could be regarded as signs of cell death. Described changes appear more often and are more pronounced in cells that were electroporated and recovered in growth medium (GG combination) compared to cells that were electroporated and left to recover in acidic medium (AA

combination) (Fig. 3). Primarily, cells electroporated in AA combination exhibit less long lasting huge membrane blebs.

It is proposed that blebbing is a by-product of electric field induced cell damage. Blebs can grow several seconds or minutes and they can reach sizes comparable to the size of the cell [52,62]. Blebs are initiated by a local disruption in the proteins that link the membrane to the cytoskeleton or local rupture of the cortex, a thin layer of the cytoskeleton directly beneath the membrane. Locally decreased pressure results in flow of the cytosol toward the area of detachment and local expansion of the cell membrane [63]. The hydrostatic pressure drops as the blebs expand. Therefore blebbing is possibly a primary self-protection process because it can rapidly releases the stress inside cells and prevents the immediate cell lysis. If the cortex gradually reassembles at the bleb membrane, the bleb retraction occurs [52]. Experimental observations were related to mathematical models of membrane blebs dynamics, but detailed mechanisms of bleb expansion and retraction are still unclear [49,64].

Sonoporation experiments performed on a site-specific basis *via* the synergized use of targeted microbubbles and single-shot ultrasound exposure showed that, membrane blebbing occurs at the sonoporation site after membrane initial resealing [65]. Although membrane integrity may be restored within tens of seconds, cytoskeleton disassembly may persist, and promotes bleb formation. Blebs were also observed at other places along the membrane periphery, because sonoporation-induced cytoskeleton disruption may not necessarily be a localized phenomenon and may propagate to the entire cell over time [66]. Moreover, it was proved that blebs physically serve as a buffer compartment to accommodate the high cytoplasmic Ca^{2+} level caused by an influx of extracellular Ca^{2+} due to cell membrane permeabilization [65]. If the cell membrane was permeabilized in Ca^{2+} depleted media, no blebs were formed on the cell membrane, substantiating the essential role of Ca^{2+} influx during cell membrane permeabilization in the membrane blebbing response.

According to our results less blebs were formed on the cells that were electroporated and left to recover in acidic medium (AA combination). It has been shown that higher number of lysosomes is present in cell periphery in acidic extracellular media and that lysosomes are recruited in the sites of injuries in a Ca^{2+}-dependent fashion. Based on this, lysosomes could be involved in the early stage of the blebbing processes by fusion with the cell membrane, inducing compensatory endocytosis and internalization of the injured membrane. These observations are in agreement with our results obtained with MTS assay, showing higher survival of cells that were electroporated and recovered in acidic medium (Fig. 1). It is also known that resealing of small membrane defects is faster, less energy demanding and has less negative effects on cell survival [54].

Our results show that for standard ECT pulse protocol (ESOPE pulse protocol; 8 pulses, 100 μs, 1 Hz) the effect of acidic pHe present in tumors is most likely irrelevant at lower electric field strengths. At 1.2 kV/cm we observed only small differences in cell survival between acidic and growth electroporation and recovery medium. However better survival of cells that were electroporated and recovered in acidic medium observed at 1.8 kV/cm and 2.4 kV/cm (Fig. 1) imply that acidic pHe should be considered when applying IRE. Our results show that tissueswhich have acidic pHe such as tumors, might need higher voltages applied during IRE to successfully achieve ablation.

According to our results of PI uptake measured with flow cytometry, electroporation and recovery medium pH had no effect on membrane permeabilization, since PI uptake was almost identical in all four combinations of electroporation and recovery medium pH used (Fig. 4).

In studies on effect of medium pH on process of electrofusion it was shown that the optimal pH for cell fusion is around pH 7.5. Fusion yield was higher at medium pH 7.5 and the average number of cells within a fusion chain was also larger compared to medium with lower pH. The fusion yield dropped by 40% when the pH was lowered from 7.5 to 6.0 [67]. There could be connection between lower fusion rates observed

in acidic medium and faster membrane resealing and less defects formed on cell membrane after electroporation in acidic medium observed in our experiments.

In literature only the effects of pH fronts that form between electrodes during GET were studied. It was shown that pH fronts are the main reason for tissue damage observed after GET near electrodes [33]. Therefore we excluded cells that were near electrodes and analyze only cells in the middle between the electrodes. In our experiments we primarily studied GET in acidic extracellular medium which is present in numerus tumors. We observed decreased GET efficiency in acidic electroporation and recovery medium (AA) with all three pulse protocols tested (Fig. 6). The level of permeabilization as shown in Fig. 4 is the same in all medium pH combinations for all three pulse protocols. It is possible that acidic pH reduces net DNA negative charge and decreases electrophoretic movement of DNA [68] which in tumors *in vivo* is already low due to dense extracellular matrix. This hypothesis is supported also by lower GET efficiency of AG combination compared to GG combination and higher GET efficiency of GA compared to AA combination. Acidic pH also reduces endocytosis [69] which is one of proposed mechanism of DNA entry into cells during GET [70]. We did not observe any significant difference in GET efficiency between GG and GA combinations, however GET efficiency was higher with AG compared to AA combination using protocols 1 and 2. Since no difference in GET efficiency between GA and AG combinations was observed, we assume that acidic pH effects are not limited to one, but may affect several of the steps involved in GET. Although pH changes depend on pulse parameters and may induce damage near the electrodes, our results show that away from the electrodes these effects are negligible, as no statistically significant difference in GET efficiency in the same pH combinations between three pulse protocols was observed. However, we tested only three pulse protocols out of a wide range of pulse protocols used in GET and only one plasmid size so more experiments with various pulse parameters and plasmids are needed to generalize our results.

The results, obtained in experiments done on CHO cell line, imply that there is a difference in cell membrane repair that depends on extracellular pH or that extracellular pH affects the characteristics of defects that form on plasma membrane during electroporation. It is possible that acidic extracellular pH allows more efficient repair of damage that is induced on cell membrane during electroporation with high pulse amplitudes. However further studies including various cell lines are needed to confirm if our observations are general.

5. Conclusions

To conclude, our results indicate that there is a difference in cell membrane repair that depends on extracellular pH or that extracellular pH affects the characteristics of defects that form on plasma membrane during electroporation. It is possible that acidic extracellular pH allows more efficient repair of damage that is induced on cell membrane during electroporation with high pulse amplitudes. Our results also show that acidic extracellular pH decreases GET efficiency.

Acknowledgments

References

[1] D. Miklavčič, B. Mali, B. Kos, R. Heller, G. Serša, Electrochemotherapy: from the drawing board into medical practice, Biomed. Eng. Online 13 (1) (2014) 29, https://doi.org/10.1186/1475-925X-13-29.

10   *T. Potočnik et al. / Bioelectrochemistry 130 (2019) 107342*

[2] G. Serša, čemažar, M., & Miklavčič, D., Antitumor effectiveness of electrochemotherapy with cis-diamminedichloroplatinum(II) in mice, Cancer Res. 55 (15) (1995) 3450–3455, https://doi.org/10.3389/fnsys.2011.00084.

[3] L.M. Mir, H. Banoun, C. Paoletti, Introduction of definite amounts of nonpermeant molecules into living cells after electropermeabilization: direct access to the cytosol, Exp. Cell Res. 175 (1988) 15–25, https://doi.org/10.1016/0014-4827(88)90251-0.

[4] J.E. Dinchuk, K.A. Kelley, G.N. Callahan, Flow cytometric analysis of transport activity in lymphocytes electroporated with a fluorescent organic anion dye, J. Immunol. Methods 155 (1992) 257–265, https://doi.org/10.1016/0022-1759(92)90293-3.

[5] P.E. Engström, B.R.R. Persson, L.G. Salford, Studies of in vivo electropermeabilization by gamma camera measurements of 99mTc-DTPA, Biochim. Biophys. Acta Gen. Subj. 1473 (1999) 321–328, https://doi.org/10.1016/S0304-4165(99)00199-3.

[6] E.J. Verspohl, I. Kaiserling-Buddemeier, A. Wienecke, Introducing specific antibodies into electropermeabilized cells is a valuable tool for eliminating specific cell functions, Cell Biochem. Funct. 15 (1997) 127–134, https://doi.org/10.1002/(SICI)1099-0844(19970601)15:2<127::AID-CBF732>3.0.CO;2-E.

[7] D.G. Spiller, R.V. Giles, J. Grzybowski, D.M. Tidd, R.E. Clark, Improving the intracellular delivery and molecular efficacy of antisense oligonucleotides in chronic myeloid leukemia cells: a comparison of streptolysin-O permeabilization, electroporation, and lipophilic conjugation, Blood. 91 (1998) 4738–4746.

[8] S. Sæbøe-Larssen, E. Fossberg, G. Gaudernack, mRNA-based electrotransfection of human dendritic cells and induction of cytotoxic T lymphocyte responses against the telomerase catalytic subunit (hTERT), J. Immunol. Methods 259 (2002) 191–203, https://doi.org/10.1016/S0022-1759(01)00506-3.

[9] R. Heller, M. Jaroszeski, A. Atkin, D. Moradpour, R. Gilbert, J. Wands, C. Nicolau, In vivo gene electroinjection and expression in rat liver, FEBS Lett. 389 (1996) 225–228.

[10] L.M. Mir, M.F. Bureau, J. Gehl, R. Rangara, D. Rouy, J.-M. Caillaud, ... D. Scherman, High-efficiency gene transfer into skeletal muscle mediated by electric pulses, Proc. Natl. Acad. Sci. 96 (1999) 4262–4267, https://doi.org/10.1073/pnas.96.8.4262.

[11] M.P. Rols, C. Delteil, M. Golzio, P. Dumond, S. Gros, J. Teissie, In vivo electrically mediated protein and gene transfer in murine melanoma, Nat. Biotechnol. 16 (1998) 168–171, https://doi.org/10.1038/nbt0298-168.

[12] M.L. Yarmush, A. Golberg, G. Serša, T. Kotnik, D. Miklavčič, Electroporation-based technologies for medicine: principles, applications, and challenges, Annu. Rev. Biomed. Eng. 16 (1) (2014) 295–320, https://doi.org/10.1146/annurev-bioeng-071813-104622.

[13] B. Mali, T. Jarm, M. Snoj, G. Sersa, D. Miklavcic, Antitumor effectiveness of electrochemotherapy: a systematic review and meta-analysis, Eur. J. Surg. Oncol. 39 (2013) 4–16, https://doi.org/10.1016/j.ejso.2012.08.016.

[14] R.V. Davalos, S. Bhonsle, R.E. Neal, Implications and considerations of thermal effects when applying irreversible electroporation tissue ablation therapy, Prostate. 75 (10) (2015) 1114–1118, https://doi.org/10.1002/pros.22986.

[15] H.J. Scheffer, K. Nielsen, M.C. De Jong, A.A.J.M. Van Tilborg, J.M. Vieveen, A. Bouwman, M.R. Meijerink, Irreversible electroporation for nonthermal tumor ablation in the clinical setting: a systematic review of safety and efficacy, J. Vasc. Interv. Radiol. 25 (7) (2014) 997–1011, https://doi.org/10.1016/j.jvir.2014.01.028.

[16] A. Sugrue, E. Maor, A. Ivorra, V. Vaidya, C. Witt, S. Kapa, S. Asirvatham, Irreversible electroporation for the treatment of cardiac arrhythmias, Expert. Rev. Cardiovasc. Ther. 16 (5) (2018) 349–360, https://doi.org/10.1080/14779072.2018.1459185.

[17] R. Heller, L.C. Heller, Chapter eight – gene electrotransfer clinical trials, In Nonviral Vectors for Gene Therapy. 89 (2015) 235–262, https://doi.org/10.1016/bs.adgen.2014.10.006.

[18] J. Gehl, Electroporation: theory and methods, perspectives for drug delivery, gene therapy and research, Acta Physiol. Scand. 177 (4) (2003) 437–447, https://doi.org/10.1046/j.1365-201X.2003.01093.x.

[19] L. Lambricht, A. Lopes, S. Kos, G. Sersa, V. Préat, G. Vandermeulen, Clinical potential of electroporation for gene therapy and DNA vaccine delivery, Expert Opin. Drug Deliv. 13 (2) (2016) 295–310, https://doi.org/10.1517/17425247.2016.1121990.

[20] S. Vasan, A. Hurley, S.J. Schlesinger, D. Hannaman, D.F. Gardiner, D.P. Dugin, ... D.D. Ho, In vivo electroporation enhances the immunogenicity of an HIV-1 DNA vaccine candidate in healthy volunteers, PLoS One 6 (5) (2011), e19252. https://doi.org/10.1371/journal.pone.0019252.

[21] B. Zorec, V. Preat, D. Miklavcic, N. Pavselj, Active enhancement methods for intra- and transdermal drug delivery: a review, Zdravniski Vestnik-Slovenian Medical Journal. 82 (5) (2013) 339–356.

[22] B. Zorec, S. Becker, M. Reberšek, N. Pavšelj, Skin electroporation for transdermal drug delivery: the influence of the order of different square wave electric pulses, Int. J. Pharm. 457 (2013) 214–223, https://doi.org/10.1016/j.ijpharm.2013.09.020.

[23] T. Kotnik, W. Frey, M. Sack, S. Haberl Meglič, M. Peterka, D. Miklavčič, Electroporation-based applications in biotechnology, Trends Biotechnol. 33 (2015) 480–488.

[24] S. Mahnič-Kalamiza, E. Vorobiev, D. Miklavčič, Electroporation in food processing and biorefinery, J. Membr. Biol. 247 (2014) 1279–1304, https://doi.org/10.1007/s00232-014-9737-x.

[25] A. Golberg, M. Sack, J. Teissie, G. Pataro, U. Pliquett, G. Saulis, ... W. Frey, Energy-efficient biomass processing with pulsed electric fields for bioeconomy and sustainable development, Biotechnol. Biofuels 9 (94) (2016) https://doi.org/10.1186/s13068-016-0508-z.

[26] D. Miklavcic, R.V. Davalos, Electrochemotherapy (ECT) and irreversible electroporation (IRE) -advanced techniques for treating deep-seated tumors based on electroporation, Biomed. Eng. Online 14 (3) (2015) https://doi.org/10.1186/1475-925X-14-S3-I1.

[27] R. Cadossi, M. Ronchetti, M. Cadossi, Locally enhanced chemotherapy by electroporation: clinical experiences and perspective of use of electrochemotherapy, Future Oncol. 10 (5) (2014) 877–890, https://doi.org/10.2217/fon.13.235.

[28] C. Rosazza, S. Haberl Meglic, A. Zumbusch, M.-P. Rols, D. Miklavcic, Gene electrotransfer: a mechanistic perspective, Curr. Gene Ther. 16 (2) (2016) 98–129, https://doi.org/10.2174/1566523216666160331130040.

[29] M.M. Cian, O.M. Helen, Cancer Gene Therapy – Key Biological Concepts in the Design of Multifunctional Non-viral Delivery Systems, 1, INTECH Open Access Publisher, 2013 213–249 (10.5772/54271).

[30] S. Haberl, M. Kandušer, K. Flisar, D. Hodžić, V.B. Bregar, D. Miklavčič, ... M. Pavlin, Effect of different parameters used for in vitro gene electrotransfer on gene expression efficiency, cell viability and visualization of plasmid DNA at the membrane level, J. Gene Med. 15 (2013) 169–181, https://doi.org/10.1002/jgm.2706.

[31] S. Šatkauskas, F. André, M.F. Bureau, D. Scherman, D. Miklavčič, L.M. Mir, Electrophoretic component of electric pulses determines the efficacy of in vivo DNA electrotransfer, Hum. Gene Ther. 16 (10) (2005) 1194–1201, https://doi.org/10.1089/hum.2005.16.ft-128.

[32] M. Kandušer, D. Miklavčič, M. Pavlin, Mechanisms involved in gene electrotransfer using high- and low-voltage pulses–an in vitro study, Bioelectrochemistry (Amsterdam, Netherlands) 74 (2) (2009) 265–271, https://doi.org/10.1016/j.bioelechem.2008.09.002.

[33] N. Olaiz, E. Signori, F. Maglietti, A. Soba, C. Suárez, P. Turjanski, ... G. Marshall, Tissue damage modeling in gene electrotransfer: the role of pH, Bioelectrochemistry. 100 (2014) 105–111, https://doi.org/10.1016/j.bioelechem.2014.05.001.

[34] F. Maglietti, S. Michinski, N. Olaiz, M. Castro, C. Suárez, G. Marshall, The role of Ph fronts in tissue electroporation based treatments, PLoS One 8 (2013), e80167. https://doi.org/10.1371/journal.pone.0080167.

[35] L. Chopinet, L. Wasungu, M.P. Rols, First explanations for differences in electrotransfection efficiency in vitro and in vivo using spheroid model, Int. J. Pharm. 423 (1) (2012) 7–15, https://doi.org/10.1016/j.ijpharm.2011.04.054.

[36] M. Sharma, M. Astekar, S. Soi, B. Manjunatha, D. Shetty, R. Radhakrishnan, pH gradient reversal: an emerging Hallmark of cancers, Recent Patents Anti-Cancer Drug Discov. 10 (3) (2015) 244–258, https://doi.org/10.2174/1574892810666150708110608.

[37] J.R. Casey, S. Grinstein, J. Orlowski, Sensors and regulators of intracellular pH, Nat. Rev. Mol. Cell Biol. 11 (1) (2010) 50–61, https://doi.org/10.1038/nrm2820.

[38] J. Vecer, A. Holoubek, P. Herman, Manipulation of intracellular pH by electroporation: an alternative method for fast calibration of pH in living cells, Anal. Biochem. 329 (2) (2004) 348–350, https://doi.org/10.1016/j.ab.2004.03.026.

[39] M. Damaghi, J.W. Wojtkowiak, R.J. Gillies, pH sensing and regulation in cancer, Front. Physiol. 17 (4) (2013) 370, https://doi.org/10.3389/fphys.2013.00370.

[40] N. Ben-Dov, R. Korenstein, Enhancement of cell membrane invaginations, vesiculation and uptake of macromolecules by protonation of the cell surface, PLoS One 7 (4) (2012), e35204. https://doi.org/10.1371/journal.pone.0035204.

[41] N. Ben-Dov, R. Korenstein, Proton-induced endocytosis is dependent on cell membrane fluidity, lipid-phase order and the membrane resting potential, Biochim. Biophys. Acta Biomembr. 1828 (11) (2013) 2672–2681, https://doi.org/10.1016/j.bbamem.2013.07.027.

[42] K. Glunde, S.E. Guggino, M. Solaiyappan, A.P. Pathak, Y. Ichikawa, Z.M. Bhujwalla, Extracellular acidification alters lysosomal trafficking in human breast cancer cells, Neoplasia. 5 (6) (2003) 533–545, https://doi.org/10.1016/S1476-5586(03)80037-4.

[43] M.A. Bumke, D. Neri, G. Elia, Modulation of gene expression by extracellular pH variations in human fibroblasts: a transcriptomic and proteomic study, Proteomics 3 (5) (2003) 675–688, https://doi.org/10.1002/pmic.200300395.

[44] S.P. Duggan, W.M. Gallagher, E.J.P. Fox, M.M. Abdel-Latif, J.V. Reynolds, D. Kelleher, Low pH induces co-ordinate regulation of gene expression in oesophageal cells, Carcinogenesis. 27 (2) (2006) 319–327, https://doi.org/10.1093/carcin/bgi211.

[45] B.S. Sørensen, M. Busk, J. Overgaard, M.R. Horsman, J. Alsner, Simultaneous hypoxia and low extracellular pH suppress overall metabolic rate and protein synthesis in vitro, PLoS One 10 (8) (2015), e0134955. https://doi.org/10.1371/journal.pone.0134955.

[46] M. Bohloli, A. Atashi, M. Soleimani, S. Kaviani, A. Anbarlou, Investigating effects of acidic pH on proliferation, invasion and drug-induced apoptosis in lymphoblastic Leukemia, Cancer Microenviron. 9 (2–3) (2016) 119–126, https://doi.org/10.1007/s12307-016-0187-0.

[47] V. Novickij, A. Grainys, P. Butkus, S. Tolvaišienė, J. Švedienė, A. Paškevičius, J. Novickij, High-frequency submicrosecond electroporator, Biotechnol. Biotechnol. Equip. 30 (3) (2016) 607–613, https://doi.org/10.1080/13102818.2016.1150792.

[48] H. Blaser, M. Reichman-Fried, I. Castanon, K. Dumstrei, F.L. Marlow, K. Kawakami, L. Solnica-Krezel, C.P. Heisenberg, E. Raz, Migration of zebrafish primordial germ cells: a role for myosin contraction and cytoplasmic flow, Dev. Cell 11 (5) (2006) 613–627, https://doi.org/10.1016/j.devcel.2006.09.023.

[49] J.Y. Tinevez, U. Schulze, G. Salbreux, J. Roensch, J.F. Joanny, E. Paluch, Role of cortical tension in bleb growth, PNAS 106 (44) (2009) 18581–18586, https://doi.org/10.1073/pnas.0903353106.

[50] E.K. Paluch, E. Raz, The role and regulation of blebs in cell migration, Curr. Opin. Cell Biol. 25 (5) (2013) 582–590, https://doi.org/10.1016/j.ceb.2013.05.005.

[51] L.L. Norman, J. Brugués, K. Sengupta, P. Sens, H. Aranda-Espinoza, Cell blebbing and membrane area homeostasis in spreading and retracting cells, Biophys. J. 99 (6) (2010) 1726–1733, https://doi.org/10.1016/j.bpj.2010.07.031 22.

[52] M.A. Rassokhin, A.G. Pakhomov, Electric field exposure triggers and guides formation of pseudopod-like blebs in U937 monocytes, J. Membr. Biol. 245 (9) (2012) 521–529, https://doi.org/10.1007/s00232-012-9433-7.

[53] L. Norman, K. Sengupta, H. Aranda-Espinoza, Blebbing dynamics during endothelial cell spreading, Eur. J. Cell Biol. 90 (1) (2011) 37–48, https://doi.org/10.1016/j.ejcb.2010.09.013.

11

[54] J. Dermol, O.N. Pakhomova, A.G. Pakhomov, D. Miklavčič, Cell electrosensitization exists only in certain electroporation buffers, PLoS One 11 (7) (2016), e0159434.

[55] M.P. Rols, J. Teissie, Ionic strenght modulation of electrically induced permeabilization and associated fusion of mammalian cells, Eur. J. Biochem. 179 (1989) 109–115, https://doi.org/10.1111/j.1432-1033.1989.tb14527.x.

[56] G. Pucihar, T. Kotnik, M. Kandušer, D. Miklavčič, The influence of medium conductivity on electropermeabilization and survival of cells in vitro, Bioelectrochemistry. 54 (2) (2001) 107–115, https://doi.org/10.1016/S1567-5394(01)00117-7.

[57] C.S. Djuzenova, U. Zimmermann, H. Frank, V.L. Sukhorukov, E. Richter, G. Fuhr, Effect of medium conductivity and composition on the uptake of propidium iodide into electropermeabilized myeloma cells, Biochim. Biophys. Acta Biomembr. 1284 (1996) 143–152, https://doi.org/10.1016/S0005-2736(96)00119-8.

[58] M.P. Rols, J. Teissié, Modulation of electrically induced Permeabilization and fusion of Chinese hamster ovary cells by osmotic pressure, Biochemistry. 29 (1990) 4561–4567, https://doi.org/10.1021/bi00471a009.

[59] A. Reddy, E.V. Caler, N.W. Andrews, Plasma membrane repair is mediated by Ca2+ —regulated exocytosis of lysosomes, Cell. 106 (2) (2001) 157–169, https://doi.org/10.1016/S0092-8674(01)00421-4.

[60] T. Castro-Gomes, M. Corrotte, C. Tam, N.W. Andrews, Plasma membrane repair is regulated extracellularly by proteases released from lysosomes, PLoS One 11 (3) (2016), e0152583. https://doi.org/10.1371/journal.pone.0152583.

[61] M. Damaghi, N.K. Tafreshi, M.C. Lloyd, R. Sprung, V. Estrella, J.W. Wojtkowiak, ... R.J. Gillies, Chronic acidosis in the tumour microenvironment selects for overexpression of LAMP2 in the plasma membrane, Nat. Commun. 6 (2015) 8752, https://doi.org/10.1038/ncomms9752.

[62] T. Tsong, Y., Electroporation of cell membranes, Biophys. J. 60 (2) (1991) 297–306, https://doi.org/10.1016/S0006-3495(91)82054-9.

[63] W. Strychalski, R. Guy, D., Intracellular pressure dynamics in Blebbing cells, Biophys. J. 110 (5) (2016) 1168–1179, https://doi.org/10.1016/j.bpj.2016.01.012.

[64] C. Fang, T.H. Hui, X. Wei, X. Shao, Y. Lin, A combined experimental and theoretical investigation on cellular blebbing, Sci. Rep. 7 (1) (2017) 16666, https://doi.org/10.1038/s41598-017-16825-0.

[65] R.S. Leow, J.M. Wan, A.C. Yu, Membrane blebbing as a recovery manoeuvre in site-specific sonoporation mediated by targeted microbubbles, J. Royal Soc. Interface 12 (105) (2015) https://doi.org/10.1098/rsif.2015.0029 pii: 20150029.

[66] X. Chen, R.S. Leow, Y. Hu, J.M. Wan, A.C. Yu, Single-site sonoporation disrupSts actin cytoskeleton organization, J. R. Soc. Interface 11 (95) (2014) 20140071, https://doi.org/10.1098/rsif.2014.0071.

[67] D.C. Chang, J.R. Hunt, P.Q. Gao, Effects of pH on cell fusion induced by electric fields, Cell Biophys. 14 (3) (1989) 231–243, https://doi.org/10.1007/BF02797270.

[68] V.A. Klenchin, S.I. Sukharev, S.M. Serov, L.V. Chernomordik, Yu.A. Chizmadzhev, Electrically induced DNA uptake by cells is a fast process involving DNA electrophoresis, Biophys. J. 60 (4) (1991) 804–811.

[69] J. Davoust, J. Gruenberg, K.E. Howell, Two threshold values of low pH block endocytosis at different stages, EMBO J. 6 (12) (1987) 3601–3609.

[70] L. Wang, S.E. Miller, F. Yuan, Ultrastructural analysis of vesicular transport in Electrotransfection, Microsc. Microanal. 24 (05) (2018) 553–563, https://doi.org/10.1017/S143192761801509X.

2.2 GENE TRANSFER BY ELECTROPORATION WITH HIGH FREQUENCY BIPOLAR PULSES *IN VITRO*

High-frequency bipolar pulses (HF-BP) have been demonstrated to be efficient for membrane permeabilization and irreversible electroporation. Since membrane permeabilization has been achieved by HF-BP pulses our aim was to also achieve gene electrotransfer (GET) with this type of pulses. Three variations of bursts of 2 μs bipolar pulses with 2 μs interphase delay were applied in HF-BP protocols. We compared transfection efficiency of monopolar micro and millisecond pulses and HF-BP protocols at various plasmid DNA (pDNA) concentrations on CHO – K1 cells. GET efficiency increased with increasing pDNA concentration. Overall GET obtained by HF-BP pulse protocols was comparable to overall GET obtained by longer monopolar pulse protocols. However, although we were able to achieve similar percent of transfected cells, the number of pDNA copies that were successfully transferred into cells was higher when longer monopolar pulses were used. Interestingly, we did not observe any direct correlation between fluorescence intensity of pDNA aggregates formed on cell membrane and transfection efficiency. The results of our study confirmed that we can achieve successful GET with bipolar microsecond i. e. HF-BP pulses, although at the expense of higher pDNA concentrations.
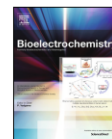
Gene transfer by electroporation with high frequency bipolar pulses *in vitro*

Tjaša Potočnik, Damijan Miklavčič, Alenka Maček Lebar *

University of Ljubljana, Faculty of Electrical Engineering, Tržaška 25, 1000 Ljubljana, Slovenia

ARTICLE INFO

ABSTRACT

High-frequency bipolar pulses (HF-BP) have been demonstrated to be efficient for membrane permeabilization and irreversible electroporation. Since membrane permeabilization has been achieved using HF-BP pulses we hypothesized that with these pulses we can also achieve successful gene electrotransfer (GET). Three variations of bursts of 2 μs bipolar pulses with 2 μs interphase delay were applied in HF-BP protocols. We compared transfection efficiency of monopolar micro and millisecond pulses and HF-BP protocols at various plasmid DNA (pDNA) concentrations on CHO – K1 cells. GET efficiency increased with increasing pDNA concentration. Overall GET obtained by HF-BP pulse protocols was comparable to overall GET obtained by longer monopolar pulse protocols. Our results, however, suggest that although we were able to achieve similar percent of transfected cells, the number of pDNA copies that were successfully transferred into cells seemed to be higher when longer monopolar pulses were used. Interestingly, we did not observe any direct correlation between fluorescence intensity of pDNA aggregates formed on cell membrane and transfection efficiency. The results of our study confirmed that we can achieve successful GET with bipolar microsecond i. e. HF-BP pulses, although at the expense of higher pDNA concentrations.

© 2021 Elsevier B.V. All rights reserved.

1. Introduction

When cells are exposed to external electric field of sufficient amplitude and duration transient destabilization of cell membrane is achieved [1,2]. This is called electroporation (also electropermeabilization) and is one of the universal methods used for introducing various molecules into cells *in vitro* and *in vivo*. The most commonly established theory states that during electroporation pores are formed on the cell membrane which allow ions and molecules to enter and/or leave the cell [2,3]. Electroporation is used in medicine [4,5], biotechnology [6] and in food [7] and biomass processing [8].

In medicine electroporation can be used as electrochemotherapy (ECT) for delivery of chemotherapeutic drugs [9,10], irreversible electroporation (IRE) for tissue ablation [11–15], administration of active substances into and through the skin [16,17] or for efficient delivery of DNA into cells and tissues as a method named gene electrotransfer (GET) [18,19]. Among the most promising GET applications in medicine are DNA vaccination and gene therapy. GET enables improved expression of therapeutic

or immunogenic proteins that are encoded by DNA or RNA which can be used for the prevention or treatment of many cancers, cardiovascular diseases, autoimmune diseases, organ specific disorders as well as infectious diseases [20–25].

GET is successful only if plasmid DNA (pDNA) is added before the application of the electric pulses [18,26], which according to current knowledge have a dual role in GET; they enable permeabilization of the cell membrane and cause electrophoresis of pDNA that brings pDNA in contact with the cell membrane. During electric field delivery heterogenous population of permeable sites is formed on cell membrane, with longer pulses leading to formation of larger permeable sites [27,28]. Negatively charged pDNA molecules in electric field move due to electrophoretic force and make contact with cell membrane in a larger number compared to free diffusion [29]. If permeable sites on cell membrane are large enough small DNA molecules (equal or smaller than 15 bp [30]) can enter the cell with electrophoresis. Large pDNA molecules form aggregates on cell membrane during electric pulses delivery and after electropermeabilization enter the cell via endocytosis [18,31–33]. Because electrophoresis is involved in pDNA aggregates formation on cell membrane during electric field delivery, the lack of electrophoresis is an important if not essential barrier for use of short pulses in GET *in vitro* and *in vivo* [29,34–36]. However, it was published before, that under optimized conditions the

transfection efficiency with 5 × 400 µs bipolar square wave pulses is better than with the same number of unipolar square wave pulses of same duration or single square pulse of the same cumulative duration [37]. The explanation is offered in symmetric permeabilization of cell membrane and formation of pDNA aggregates on both sides of the cell membrane facing the electrodes not only on one side as with monopolar pulses [29,38] which could lead to an increase in GET efficiency. The lack of electrophoretic force during delivery of short pulses can be partially compensated with higher pDNA concentration which enables that more pDNA molecules are near cell membrane [39]. But increasing pDNA concentration above 100 µg/ml *in vitro* presumably leads to pDNA entanglement which reduces the mobility of pDNA molecules, especially if they are larger than 6 kbp, probably resulting in lower GET efficiency [40].

Electroporation applications are accompanied by some undesirable effects like electrode oxidation, changes in pH and Joule heating [41–45]. While in applications *in vitro* these effects are not considered critical, they are much more relevant in applications *in vivo* and in food industry. Intense pH changes close to the electrodes [46] can be damaging to the cells and tissues and can result in changes in molecules, especially denaturation of pDNA in GET [43,46,47]. The time in which the pH changes between electrodes are neutralized after electroporation based treatments is short in ECT and IRE and much longer in GET [47] due to different pulse parameters used. For ECT and IRE usually shorter pulses with higher voltage are applied, while in GET, longer pulses of lower voltage are used [48].

Recently, the use of short bipolar electroporation pulses applied in bursts with repetition frequencies over 100 kHz, high-frequency bipolar pulses (HF-BP), was proposed [49]. In HF-BP long (100 µs– 5 ms) monopolar pulses are replaced with burst of short (0.25– 5 µs) bipolar pulses [50,51]. It was shown that with the use of HF-BP pulses similar levels of cell membrane permeabilization *in vitro* [52–54] can be achieved compared to long monopolar pulses which are dominant in current IRE, ECT and GET protocols. *In vivo* experiments have shown that HF-BP pulses are effective in ECT, IRE of tumors and in cardiac ablation [12–14,55–57]. HF-BP pulses are also suggested to provide more uniform distribution of electric field in inhomogeneous tissue, which results in more predictable cellular response and potentially leading to improved clinical precision of IRE, ECT and GET [49,58]. During HF-BP pulses delivery smaller amounts of metal ions are released from electrodes and electrochemical reactions are reduced [41,59]. However, in HF-BP higher electric fields are needed to achieve the same results as with longer monopolar pulses [52,60]. This can lead to increased Joule heating and consequently, thermal damage in the area around the electrodes [42,61]. Also, attention should be given to demonstration of cancelation effect originally observed in sub-microsecond pulses but recently also in range of microsecond pulses where the opposite polarity phase of the pulse cancels the effect of the first phase if the interphase delay is short enough, which might be one of the reasons for lower GET efficiency [53,59,62,63].

Muscle contractions that cause discomfort and electrical stimulation of sensory nerves [64–67] causing pain are the main disadvantages that accompany the electroporation based treatments with long monopolar pulses and dictates the use of muscle relaxants and anesthesia. Electric pulses delivery, if applied close or in the heart, must also be synchronized with electrocardiogram [68–73]. But the use of HF-BP pulses promises to mitigate muscle contractions and reduce pain during electroporation based treatments [67]. Namely, electrical stimulation studies proved that short bipolar pulses require higher amplitudes for stimulation of nerves and muscles compared to longer pulses [51,67,74,75] and bipolar pulses with long (80–100 µs) interphase delay further increase excitation thresholds [76].

Since membrane permeabilization is a prerequisite for successful GET [18,39] we hypothesize that with HF-BP pulse parameters successful GET can be achieved. HF-BP pulse parameters, used in our experiments, were determined according to previously published experimental and theoretical findings [49,77]. According to previous studies cancellation effect is considerable when delivering 1 µs HF-BP pulses of 1 µs interphase delay [53], while muscle contractions were observed at HF-BP pulses of 5 µs duration and longer [51]. Based on this we chose 2 µs as a duration of positive and negative phase of biphasic pulse and 2 µs interphase delay ensured complete charging and discharging of cell membrane in high-conductivity cell growth medium [53]. The same pulse waveform was shown to substantially decrease the intensity of muscle contractions compared with traditional monopolar pulses [49,50,77]. Because approximately 1 s was reported to be necessary for stable pDNA aggregates formation [29], we chose 1 Hz repetition frequency of bursts.

We first tested the number of pulses in each burst and the number of bursts in accordance with pulse protocols used in [49,77] and then adjusted them to achieve considerable GET efficiency with minimal effect on cell viability. Transfection efficiency obtained by HF-BP protocols at various pDNA concentrations was compared to that of "classical", monopolar micro (8 × 100 µs) and millisecond (8 × 5 ms) pulses.

2. Materials and methods

2.1. Cells

We used Chinese hamster ovary cell line (CHO-K1; European Collection of Cell Cultures, Great Britain). Cells were grown in 25 mm² culture flasks (TPP, Switzerland) for 2–4 days in an incubator (Kambič, Slovenia) at 37 °C, in a humidified atmosphere of 5% CO_2 in air. CHO cells were cultured in HAM-F12 growth medium (PAA, Austria) supplemented with 10% fetal bovine serum (Sigma Aldrich, Germany), L-glutamine (StemCell, Canada) and antibiotics penicillin/streptomycin (PAA, Austria), and gentamycin (Sigma Aldrich, Germany).

For experiments cells in exponential growth phase were trypsinized using trypsin – EDTA; 5 g trypsin/2 g EDTA in 0.9% NaCl (Sigma Aldrich, Germany) 10 × diluted in Hanks' Balanced Salt solution (Sigma Aldrich, Germany). From the obtained cell suspension, trypsin and growth medium were removed by centrifugation at 180 g for 5 min at room temperature (Sigma 3–15 K, UK). The cell pellet was then resuspended in HAM-F12 growth medium to obtain a final cell density of 6.6×10^5 cells/ml.

2.2. Plasmid

A 4.7 kb plasmid pEGFP-N1 (Clontech Laboratories Inc., USA) encoding green fluorescent protein (GFP) under the control of CMV promotor was used. Plasmid (pDNA) was amplified using Escherichia coli and isolated with HiSpeed Plasmid Maxi Kit (Qiagen, Germany). pDNA concentration was spectrophotometrically determined at 260 nm. We tested seven pDNA concentrations, namely 20, 40, 60, 80, 100, 250 and 500 µg/ml.

2.3. Electric pulses

Five different pulse protocols were used in our experiments, namely 8 × 100 µs: 8 pulses, 100 µs duration, 1 Hz repetition frequency; 8 × 5 ms: 8 pulses, 5 ms duration, 1 Hz repetition frequency and three HF-BP pulse protocols. In HF-BP pulse protocols bipolar pulses of 2 µs duration of positive and negative phase were applied. The pause between positive and negative

2

T. Potočnik, D. Miklavčič and A.M. Lebar

pulse phase and pause between bipolar pulses in all three pulse protocols were 2 µs. Number of pulses in each burst and number of bursts were varied, while burst repetition frequency was 1 Hz in all three HF-BP protocols. Pulse protocol HF-BP 1 consisted of 20 bursts and in each burst 216 pulses were applied. Pulse protocol HF-BP 2 consisted of 50 bursts; in each burst 50 pulses were applied. And pulse protocol HF-BP 3 consisted of 100 bursts; in each burst 32 pulses were applied. Electric field was estimated as the voltage applied divided by the distance between the electrodes. For all pulse protocols the range 0–2 kV/cm was tested for cell membrane permeabilization and cell viability. For each pulse protocol we determined GET efficiency on the interval of electric fields below and above the intersection of permeabilization and cell viability curves. Based on these results we decided on electric field used in our GET experiments. Pulse parameters of all five pulse protocols used in GET experiments are summarized in Tables 1 and 2 and Supplementary schematic 1.

For the application of pulses, a laboratory prototype pulse generator (University of Ljubljana) based on H-bridge digital amplifier with 1 kV MOSFETs (DE275-102N06A, IXYS, USA) was used [52]. During each experiment voltage and current applied to sample were measured with differential probe (ADP305, LeCroy, USA) and current probe (CP030, LeCroy, USA) and monitored on oscilloscope (Wavesurfer 422, 200 MHz, LeCroy, USA). Representative measurements of voltage and current in HF-BP pulse protocols are shown in Supplementary Fig. 1.

2.4. Permeabilization

For permeabilization detection 150 µl of cell suspension (1×10^5 cells) with 5 µl of propidium iodide, final concentration 33 µg/ml, (Life Technologies, USA) was pipetted into 4 mm cuvettes (VWR International, Belgium). After pulse application cells were incubated for 10 min at room temperature. Propidium iodide incorporation into cells was detected with flow cytometer (Attune® NxT, Life Technologies, USA) using a blue laser excitation at 488 nm and detecting the emitted fluorescence through a 574/26 nm band-pass filter. At every measurement 10,000 events were recorded. Data obtained were analyzed with the Attune NxT software. The voltage that was applied to the cuvette was varied in the 100–800 V range, corresponding to 0.25–2 kV/cm electric field.

2.5. Gene electrotransfer

150 µl of cell suspension (2×10^5 cells) were pipetted into 4 mm cuvette and various concentrations of pDNA were added. We tested final concentrations of 20, 40, 60, 80, 100, 250 or 500 µg/ml pDNA in cell suspension. Cells were incubated with pDNA for 2 min at room temperature then electric pulses were applied as described above. To increase cell viability 37.5 µl (25% of volume) of fetal bovine serum (Sigma Aldrich, Germany) was added immediately after pulse delivery and cells were incubated in cuvette for 5 min at 37 °C in a humidified atmosphere in a 5% CO₂ incubator [78,79]. After incubation cell suspension was transferred to 1 ml

of HAM-F12 growth medium in 24 well plate (TPP, Switzerland) and incubated for 24 h at 37 °C in a humidified atmosphere in a 5% CO₂ incubator. Afterwards, cells were trypsinized as described above and percent of GFP positive cells and median fluorescence of GFP positive cells were detected using flow cytometer (Attune® NxT, USA). Excitation wavelength was detected with a blue laser at 488 nm and emitted fluorescence was through a 530/30 nm band-pass filter. At every measurement 10,000 events were recorded. Obtained data were analyzed with the Attune NxT software.

2.6. Cell viability

After cells were exposed to pulse protocols at different electric fields (cell viability curve) or pulse protocols at fixed electric field with different pDNA concentrations (cell viability after GET) 2×10^4 cells were transferred to HAM-F12 growth medium prepared previously in wells of 96-well plate (TPP, Switzerland). Three samples were taken from each cuvette. Cells were placed in the incubator (37 °C, 5% CO₂) for 24 h. Cell viability was determined with the MTS-based Cell Titer 96 AQueous One Solution Cell Proliferation Assay (Promega, USA). After 24 h incubation 20 µl of MTS reagent were added to each well and cells were incubated for additional 2 h in the incubator (37 °C, 5% CO₂). Absorption at 490 nm wavelength was measured with a Tecan Infinite M200 spectrophotometer (Tecan, Switzerland). An average absorption obtained in the samples containing only growth medium was subtracted from the absorption measured in cell samples. To calculate the percentage of viable cells the absorption of each sample was divided by an average absorption of the control samples.

2.7. Visualization of pDNA interaction with cell membrane

To visualize pDNA interaction with cell membrane TOTO-1 (Molecular Probes — Invitrogen, USA) nucleic acid stain was used. The protocol of staining was the same as in [80,81]. Briefly, the plasmid pEGFP-N1 was labeled with 2.3×10^{-4} M TOTO-1 DNA intercalating dye with an average base pair to dye ratio of 5 for 60 min on ice and in the dark.

1×10^5 CHO cells were plated as a monolayer culture in Lab-Tek chambered coverglass (Nunc, TermoFisher Scientifc, USA) for 8 h in cell growth medium at 37 °C in a humidified 5% CO₂ atmosphere in the incubator. Immediately before electric pulse application, growth medium was removed and fresh growth medium with labeled pDNA was added to cells in 20 µg/ml or 500 µg/ml concentration. A pair of two parallel Pt/Ir wire electrodes, with 4 mm distance between inner edges, was positioned to the bottom of Lab-Tek chamber and samples were exposed to electric pulses. Only HF-BP 2, 8 × 100 µs and 8 × 5 ms protocols were tested.

To monitor the interaction of pDNA with the cell membrane fluorescent microscope (Zeiss 200, Axiovert, Germany) was used with 100 × oil immersion objective. The images were recorded using imaging system (MetaMorph imaging system, Visitron, Germany). Fluorescence emission along the cell membrane was analyzed (MetaMorph, Germany) and the fluoresce intensity along perime-

Table 1
Pulse parameters of all pulse protocols.

Protocol	Duration of positive phase (µs)	Duration of negative phase (µs)	Pause between positive and negative phase (µs)	Pause between pulses (µs)	Number of pulses in each burst	Number of bursts	Burst repetition frequency (Hz)	Electric field (kV/cm)
8 × 100 µs	100	0	0	0	1	8	1	1.6
8 × 5 ms	5000	0	0	0	1	8	1	0.5
HF-BP 1	2	2	2	2	216	20	1	1
HF-BP 2	2	2	2	2	50	50	1	1.25
HF-BP 3	2	2	2	2	32	100	1	1.25

3

Table 2
Cumulative parameters of all pulse protocols. Dose = voltage^2 × On-time per burst was calculated according to [77].

Protocol	On time per pulse (μs)	On-Time per Burst (μs)	On-Time per treatment (μs)	Pulse repetition frequency (1/s)	Duration of the treatment (s)	Dose (U^2 × On time per burst $[V^2 \times s]$)
8×100 μs	100	800	800	8	8	327.68
8×5 ms	5000	40000	40000	8	8	1600
HF-BP 12–2–2–2	4	864	17280	4320	20	2764.8
HF-BP 22–2–2–2	4	200	10000	2500	50	2500
HF-BP 32–2–2–2	4	128	12800	3200	100	3200

ter of cell membrane was obtained from recorded images. At least 3 images per pulse protocol were analyzed.

2.8. Measurements of pH changes after pulse delivery and temperature monitoring

For measurement of pH changes in 4 mm cuvette after pulse delivery SevenGo-SG2 pH meter and InLab Nano (Mettler-Toledo, Switzerland) measuring electrode were used. 150 µl of cell suspension (1x10^5 cells) were pipetted into 4 mm cuvette and pulses were applied. Immediately after pulse delivery 37.5 µl (25% of volume) of fetal bovine serum (FBS) were added and cell suspensions was mixed by pipetting. Cuvette with cell suspension was placed in water bath heated to 37 °C and pH probe was dipped in cell suspension. pH of cell suspension was measured every minute for 5 min after pulse delivery. Temperature of the cell suspension was monitored during pH measurements using the fiber optic sensor system (opSens, Canada), which consisted of ProSens signal conditioner and a fiber optic temperature sensor OTG-M170 in order to make sure that measured pH changes were not the consequence of temperature changes. Temperature of the sample was also measured during pulse delivery for all five pulse protocols.

2.9. Statistical analysis

All results are reported as a mean value of 3 to 5 experiments. The spread of the data is given by standard deviation. The significance between the experimental groups was analyzed in SigmaPlot 11.0 (Systat Software Inc., Chicago, IL, USA), and determined using One way ANOVA test followed by Tukey's multiple comparison test. The statistically significant difference was assumed at $p < 0.05$.

3. Results

3.1. Permeabilization and cell viability curves

Electroporation experiments resulting in membrane permeabilization and cell viability curves were performed for all five pulse protocols (Fig. 1). Electroporation with applying 8×5 ms lead to permeabilization at the lowest electric field; 95% of permeabilized cells were already obtained at 0.75 kV/cm. All three HF-BP pulse protocols and pulse protocol 8×100 μs lead to similar permeabilization; 73%–87% of cells were permeabilized at 1 kV/cm. Using pulse protocol 8×5 ms also a decrease in cell viability at lower electric fields was observed; less than 10% of cells were viable at 1 kV/cm, while using HF-BP pulse protocols or 8×100 μs pulse protocol viability of the cells was better than 80% at the same electric field. Pulse protocol HF-BP 1 and 3 lead to decrease in cell viability at lower electric fields compared to pulse protocol HF-BP 2 and pulse protocol 8×100 μs, which ensued similar viability of the cells at electric fields tested; more than 80% of cells were viable

at 1.25 kV/cm. The intersection of permeabilization and cell viability curve is where the greatest fraction of cells is permeabilized and cell viability is the highest. The intersection of permeabilization and cell viability curve was at electric fields 0.6, 1.25, 1, 1.20 and 1.05 kV/cm for pulse protocols 8×5 ms, 8×100 μs, HF-BP 1, HF-BP 2 and HF-BP 3, respectively. Since optimal permeabilization for PI is not necessary also optimal for pDNA uptake we screened the interval of electric fields below and above the intersection of permeabilization and cell viability curves for GET efficiency (data not shown) to choose the final electric field used in every GET pulse protocol. The final electric fields used in GET experiments were 0.5, 1.6, 1, 1.25, 1.25 for pulse protocols 8×5 ms, 8×100 μs, HF-BP 1, HF-BP 2 and HF-BP 3, respectively.

3.2. Gene electrotransfer

We tested seven different pDNA concentrations: 20, 40, 60, 80, 100, 250 or 500 μg/ml. In all five pulse protocols percent of GFP positive cells increased with increasing pDNA concentration (Fig. 2). Increasing pDNA concentration above 100 μg/ml if pulse protocols 8×100 μs or 8×5 ms were applied lead to almost no increase in GFP positive cells, contrary to HF-BP pulse protocols where the percent of GFP positive cells with highest pDNA concentrations (250 and 500 μg/ml) increased significantly. When applying HF-BP pulse protocols we were able to obtain around 40% of GFP positive cells.

Percent of GFP positive cells obtained with pulse protocol 8×100 μs and pulse protocol 8×5 ms was similar at same concentrations of pDNA. With the highest pDNA concentration we successfully transfected around 50% of cells. Also, the transfection efficiency obtained between pulse protocols HF-BP was similar at same concentrations of pDNA. With the lowest concentration of pDNA (20 μg/ml) around 5% of cells were successfully transfected and with the highest concentration (500 μg/ml) around 40%. Exact percent of GET with the highest concentration of pDNA for all five pulse protocols and accompanying viability results are summarized in Table 3.

At the lowest pDNA concentration (20 μg/ml) percent of GFP positive cells was statistically significant higher after GET with pulse protocol 8×100 μs and pulse protocol 8×5 ms compared to all three pulse protocols HF-BP. When the highest pDNA concentration (500 μg/ml) was used statistically significant difference in percent of GFP positive cells was observed only in GET with pulse protocol 8×100 μs and pulse protocol 8×5 ms compared to pulse protocol HF-BP 1 and pulse protocol HF-BP 3.

No GFP positive cells were observed in the absence of electric pulses or the absence of pDNA.

3.3. Cell viability after GET

In addition to cell viability measurement in 0–2 kV electric field range in order to get cell viability curves, MTS assay was also performed after every GET experiment at fixed electric field without or
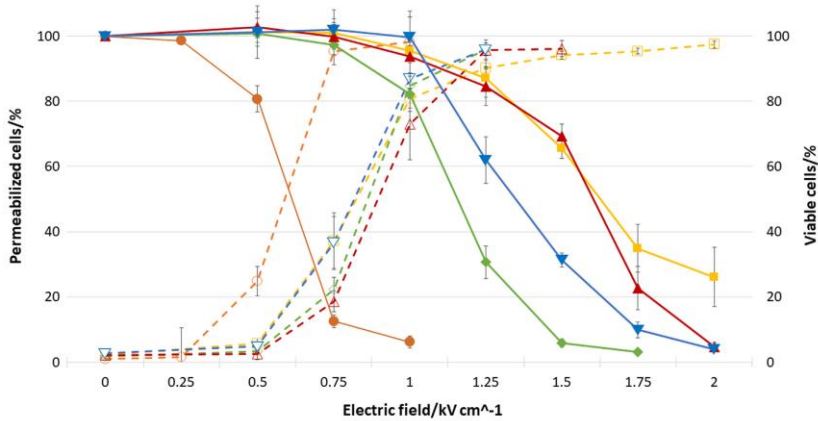
4

Fig. 1. Permeabilization dashed lines (empty symbols) and cell viability solid lines (filled symbols) for all five pulse protocols used. 8 × 100 μs (yellow □/■); 8 × 5 ms (orange ○/●); HF-BP 1(green ◇/◆); HF-BP 2 (red △/▲) and HF-BP 3 (blue ▽/▼). Vertical bars represent standard deviation.
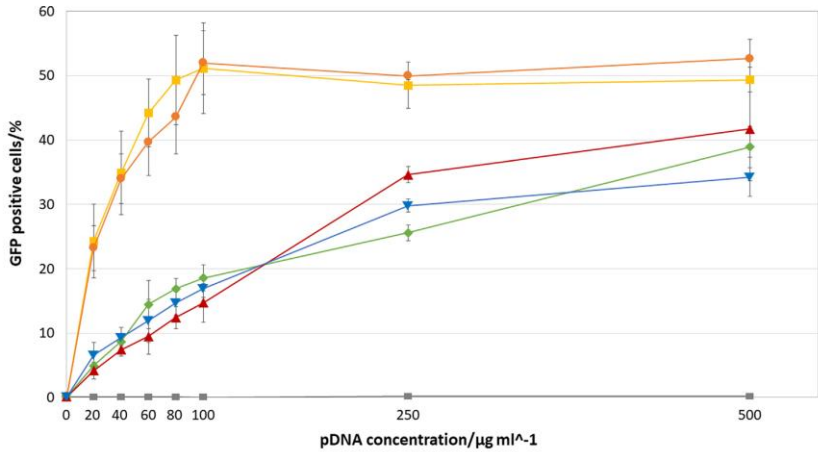
Fig. 2. GET efficiency for all five pulse protocols, 8 × 100 μs (yellow ■); 8 × 5 ms (orange ●); HF-BP 1(green ◆); HF-BP 2 (red ▲) and HF-BP 3 (blue ▼), without and with seven pDNA concentrations, 20, 40, 60, 80, 100, 250 and 500 μg/ml, 0 V – no applied pulses (gray ■). Bars represent standard deviation.

Table 3
Results of GET, viability and overall GET with the highest concentration (500 μg/ml) of pDNA using all five pulse protocols.

Pulse protocol	Electric field (kV/cm)	GET (%)	Viability (%)	Overall GET (%)
8 × 100 μs	1.6	49 ± 1.9	56 ± 5.6	28 ± 3.3
8 × 5 ms	0.5	53 ± 3	75 ± 16.7	40 ± 10.3
HF-BP 1	1	39 ± 3.2	82 ± 6	32 ± 1.6
HF-BP 2	1.25	42 ± 8.1	82 ± 11.8	34 ± 7
HF-BP 3	1.25	34 ± 3.1	72 ± 3.1	25 ± 2.2

with seven pDNA concentrations (Fig. 3). Viability of cells was different among five pulse protocols tested. The lowest cell viability was observed after application of pulse protocol 8 × 100 μs, around 50%. A bit higher viability, around 60%, was obtained when pulse protocol HF-BP 3 was applied. Pulse protocol 8 × 5 ms and pulse protocol HF-BP 1 led to approximately 80% of cell viability. The highest cell viability was observed with pulse protocol HF-BP 2 where nearly 90% of cells were viable 24 h after pulse delivery.
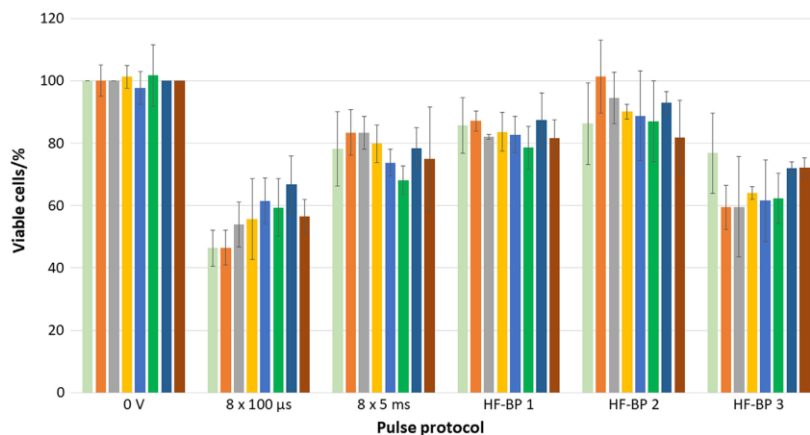
5

Fig. 3. Cell viability for all five pulse protocols, 8×100 µs, 8×5 ms, HF-BP 1, HF-BP 2 and HF-BP 3, without (light green) and with seven pDNA concentrations, 20 (orange), 40 (gray), 60 (yellow), 80 (light blue), 100 (dark green), 250 (dark blue) and 500 µg/ml (red), 0 V – no applied pulses. Vertical bars represent standard deviation.

Exact percent of cell viability with the highest concentration of pDNA (500 µg/ml) for all five pulse protocols are summarized in Table 3.

In control cells as well as in cells that were exposed to any of five pulse protocols tested there was no statistically significant difference in cell viability between group with no added pDNA and groups with various pDNA concentrations added in cell suspension. Even in groups in which the highest pDNA concentration (500 µg/ml) was used there was no significant decrease in cell viability observed which shows that pDNA concentration did not have any negative effect on cell viability as detected by MTS cell viability assay.

3.4. Overall gene electrotransfer

Overall GET in percent (Fig. 4) was calculated as % of GFP positive cells multiplied by % of viable cells divided by 100. We can observe that the highest overall gene electrotransfer (GET) (40 ± 10.3%) was achieved with pulse protocol 8×5 ms. At the lowest pDNA concentration (20 µg/ml) percent of viable GFP positive cells was statistically significant higher after GET with pulse protocol 8×100 µs and pulse protocol 8×5 ms compared to all three pulse protocols HF-BP. Percent of GFP positive cells was also significantly higher with pulse protocol 8×5 ms compared to pulse protocol 8×100 µs.

Overall GET with pulse protocol 8×100 µs and all three pulse protocols HF-BP with the highest pDNA concentration was not statistically significant different, it amounted approximately 25–34%. Exact percent of overall GET with the highest concentration of pDNA for all five pulse protocols are summarized in Table 3. When the highest pDNA concentration (500 µg/ml) was used statistically significant difference in percent of viable GFP positive cells was observed only between pulse protocol 8×5 ms and pulse protocol HF-BP 3.

3.5. Median fluorescence intensity

Measurements of median fluorescence intensity of GFP positive cells on flow cytometer were also collected for each experiment (Fig. 5). Median fluorescence was the highest when the highest

concentration of pDNA was used. In this case maximum median fluorescence of all three pulse protocols HF-BP was similar, while more than double median fluorescence was obtained with pulse protocol 8×100 µs and pulse protocol 8×5 ms. With pulse protocol 8×5 ms higher median fluorescence was measured at pDNA concentrations between 40 µg/ml and 100 µg/ml compared to pulse protocol 8×100 µs and pulse protocols HF-BP where more pronounced increase in median fluorescence was observed only with the highest pDNA concentrations, 250 and 500 µg/ml.

Median fluorescence intensity at the lowest (20 µg/ml) and at the highest (500 µg/ml) pDNA concentration was statistically significant higher after GET with pulse protocols 8×100 µs and 8×5 ms compared to all three pulse protocols HF-BP.

3.6. pDNA interaction with cell membrane

pDNA interaction with cell membrane was visualized following 8×100 µs, 8×5 ms and HF-BP 2 protocols each with the lowest and the highest pDNA concentrations, 20 µg/ml and 500 µg/ml, respectively. In the absence of pulse delivery no increase in fluorescence intensity alongside cell membrane was observed.

Analyzing fluorescence intensity along cell perimeter following 8×100 µs and 8×5 ms protocols increased fluorescence intensity was observed only on one side of cell membrane representing formation of pDNA aggregates on cell membrane facing the cathode (Figs. 6, B and 7, B). After 8×100 µs pulse protocol pDNA aggregates on cell membrane were visible after GET with both pDNA concentrations, 20 µg/ml (Fig. 6, A) and 500 µg/ml (Fig. 6, D). Peak in average fluorescence intensity after 8×100 µs protocol with 500 µg/ml of pDNA was significantly (10 times) higher than average peak in fluorescence intensity after 8×100 µs protocol with 20 µg/ml of pDNA (Fig. 6, C).

pDNA aggregates on cell membrane after 8×5 ms pulse protocol with both pDNA concentrations, 20 µg/ml and 500 µg/ml, are shown in Fig. 7, A and D respectively. Peak in fluorescence intensity after 8×5 ms protocol with 20 µg/ml of pDNA was almost the same as peak in fluorescence intensity after 8×100 µs protocol with 500 µg/ml of pDNA. Peak in fluorescence intensity after 8×5 ms protocol with 500 µg/ml of pDNA was significantly

6

34

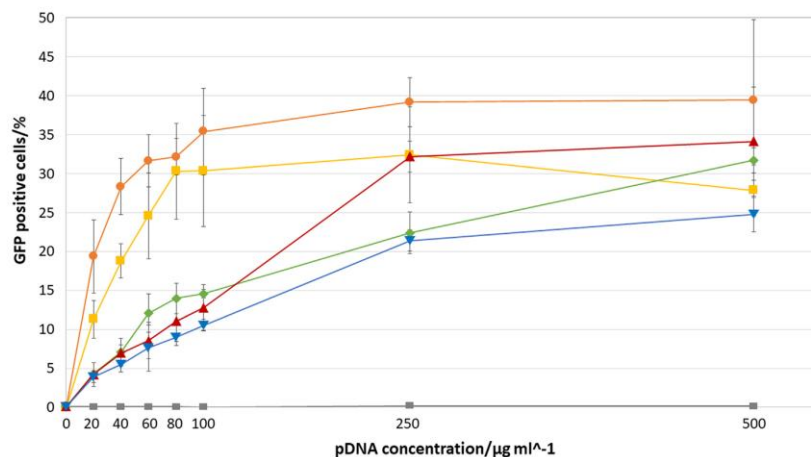**Fig. 4.** Overall GET efficiency for all five pulse protocols 8 × 100 µs (yellow ■); 8 × 5 ms (orange ●); HF-BP 1(green ◆); HF-BP 2 (red ▲) and HF-BP 3 (blue ▼), without and with seven pDNA concentrations, 20, 40, 60, 80, 100, 250 and 500 µg/ml, 0 V – no applied pulses (gray ■). Vertical bars represent standard deviation.

Fig. 5. Median fluorescence intensity for all 5 pulse protocols, 8 × 100 µs (yellow ■); 8 × 5 ms (orange ●); HF-BP 1(green ◆); HF-BP 2 (red ▲) and HF-BP 3 (blue ▼), without and with seven pDNA concentrations, 20, 40, 60, 80, 100, 250 and 500 µg/ml, 0 V – no applied pulses (gray ■). Vertical bars represent standard deviation.
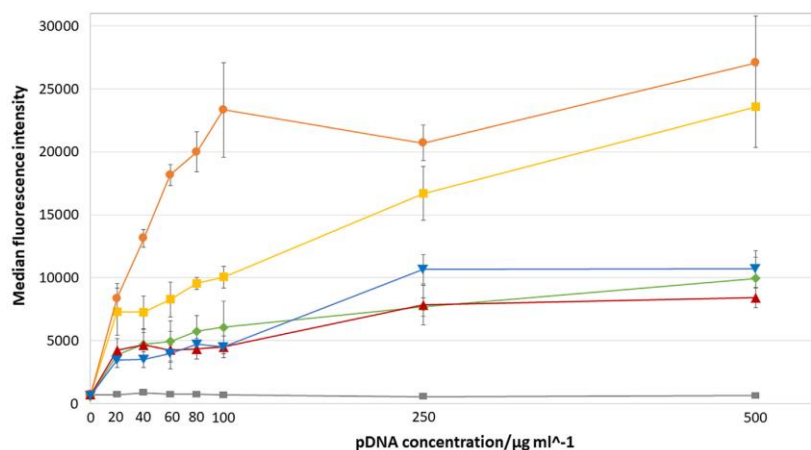
(almost 3 times) higher compared to the peak in fluorescence intensity with 20 µg/ml of pDNA (Fig. 7, C).

Analyzing fluorescence intensity alongside cell perimeter after HF-BP 2 protocol two peaks in fluorescence intensity were observed representing formation of pDNA aggregates on both sides of cell membrane facing the electrodes. The peaks were distinct when 500 µg/ml of pDNA was used and hard to notice after HF-BP 2 protocol with 20 µg/ml of pDNA (Fig. 8, B). Statistical analysis of peaks in fluorescence intensity showed significantly higher fluorescence in both peaks compared to background fluorescence at both pDNA concentrations. The two peaks in fluorescence intensity were not significantly different, however, slightly lower fluores-

cence was observed at peak 1 with both pDNA concentrations used (Fig. 8, C). Up to 7 times higher peak in fluorescence intensity was observed when 500 µg/ml of pDNA was added compared to when 20 µg/ml of pDNA was added. Peak fluorecence intensity after 8 × 100 µs pulse protocol with with 500 µg/ml of pDNA was also significantly higher compared to peak in fluorescence intensity after HF-BP 2 protocol with 20 µg/ml and 500 µg/ml of pDNA. Application of 8 × 100 µs protocol with 20 µg/ml of pDNA resulted in an average peak in fluorescence intensity only a little higher compared to peak in fluorescence intensity after HF-BP 2 protocol with 20 µg/ml of pDNA and lower compared to peak in fluorescence intensity after HF-BP 2 protocol with 500 µg/ml of pDNA.

7

Fig. 6. pDNA interaction with cell membrane after 8 × 100 μs pulse protocol. A) Images of brightfield and TOTO-1 fluorescence taken under the microscope, with 20 μg/ml or D) 500 μg/ml of pDNA. B) TOTO-1 fluorescence measured along perimeter of cell membrane of a single cell. 20 μg/ml of pDNA (blue); background 20 μg/ml (light gray); 500 μg/ml of pDNA (orange); background 500 μg/ml (dark gray). C) Average TOTO-1 fluorescence intensity at peaks measured on 5 cells. Vertical bars represent standard deviation.
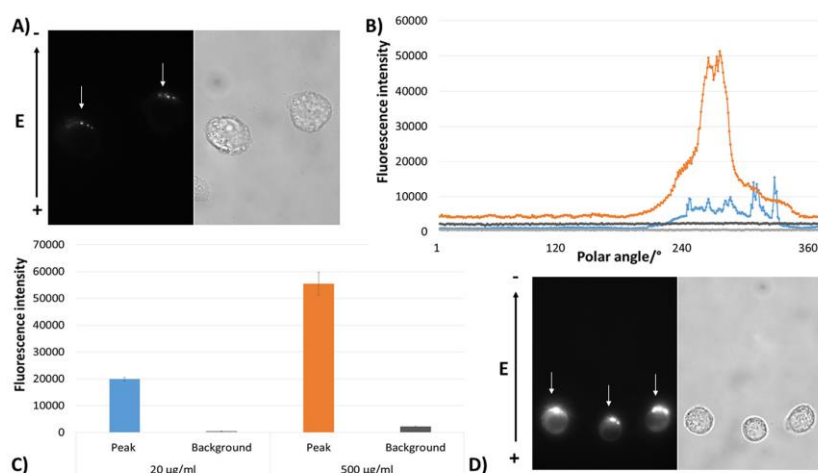
Fig. 7. pDNA interaction with cell membrane after 8 × 5 ms pulse protocol. A) Images of brightfield and TOTO-1 fluorescence taken under the microscope, with 20 μg/ml or D) 500 μg/ml of pDNA. B) TOTO-1 fluorescence measured along perimeter of cell membrane of a single cell. 20 μg/ml of pDNA (blue); background 20 μg/ml (light gray); 500 μg/ml of pDNA (orange); background 500 μg/ml (dark gray). C) Average TOTO-1 fluorescence intensity at peaks measured on 5 cells. Vertical bars represent standard deviation.

Following application of 8 × 5 ms protocol with 20 μg/ml of pDNA average peak in fluorescence intensity was significantly higher compared to the peaks in fluorescence intensity after HF-BP 2 protocol with both pDNA concentrations and 8 × 100 μs protocol with 20 μg/ml of pDNA.

3.7. pH and temperature measurements

We measured pH changes after pulse delivery in the middle of 4 mm cuvettes according to gene electrotransfer protocol; i.e. at fixed temperature of 37 °C for 5 min (Fig. 9). After pulse delivery
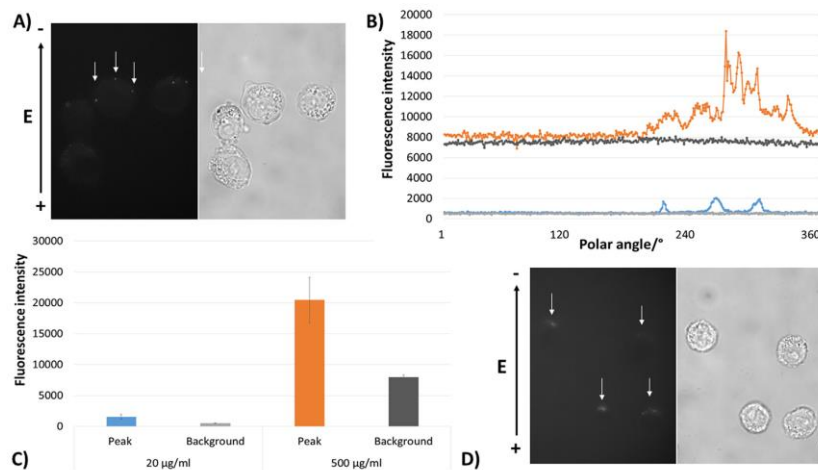
8

36
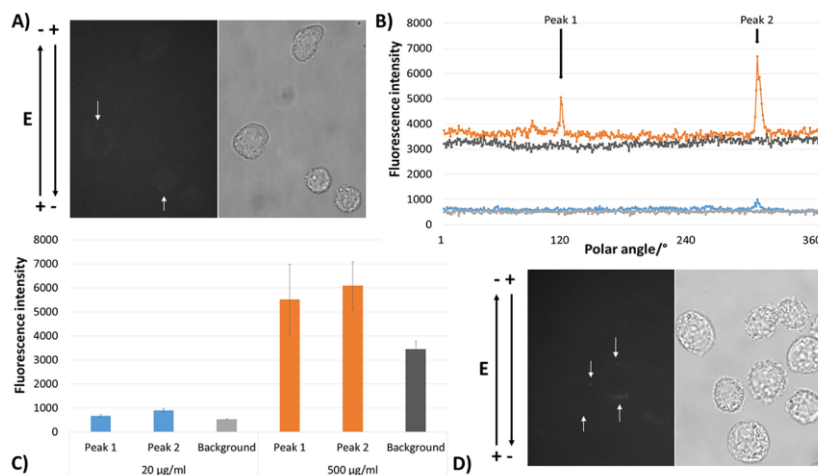
Fig. 8. pDNA interaction with cell membrane after HF-BP 2 pulse protocol. A) Images of brightfield and TOTO-1 fluorescence taken under the microscope, with 20 μg/ml or D) 500 μg/ml of pDNA. B) TOTO-1 fluorescence measured along perimeter of cell membrane of a single cell. 20 μg/ml of pDNA (blue); background 20 μg/ml (light gray); 500 μg/ml of pDNA (orange); background 500 μg/ml (dark gray). C) Average TOTO-1 fluorescence intensity at peaks measured on 5 cells. Vertical bars represent standard deviation.
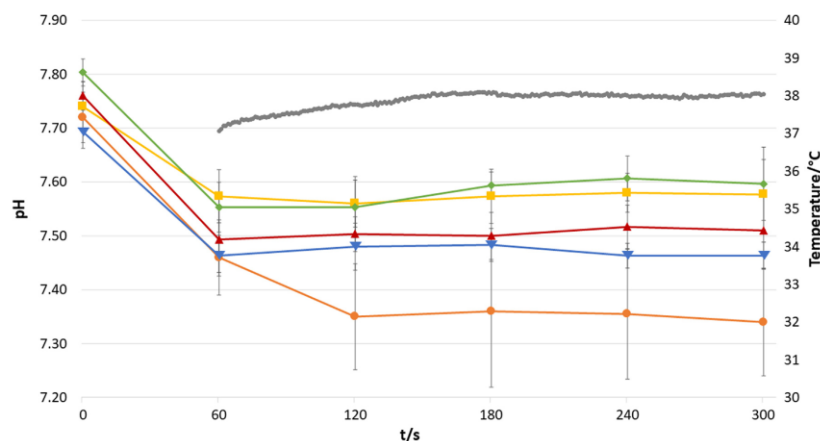
**Fig. 9.** Cell suspension pH changes for all five pulse protocols used, 8 × 100 μs (yellow ■); 8 × 5 ms (orange ●); HF-BP 1 (green ◆); HF-BP 2 (red ▲) and HF-BP 3 (blue ▼). Vertical bars represent standard deviation. Also shown is example of temperature (gray ●) monitoring during pH measurement.

we also added FBS and mixed cells by pipetting, following protocol for GET, therefore local pH changes in the cuvette were blurred.

Electroporation statistically significant decreased pH in average in overall suspension of cells. Decrease in pH of 0.17–0.27 was measured first minute after pulse delivery in all five pulse protocols tested. pH remained constantly lower all 5 min after pulse delivery in all pulse protocols tested except 8 × 5 ms pulse protocol. Using 8 × 5 ms pulse protocol pH additionally decreased for 0.11 in the second minute after pulse delivery and remained constant then after. When comparing pH changes following different pulse protocols in 5 min after pulse delivery statistically significant

difference was observed at 2, 3, 4 and 5 min after electroporation between pulse protocol 8 × 5 ms and pulse protocols 8 × 100 μs and HF-BP 1. At every time point pH after delivery of pulse protocol 8 × 5 ms was significantly lower compared to pH after delivery of pulse protocol 8 × 100 μs or pulse protocol HF-BP 1. However, although the decrease was statistically significant the observed drop in pH was not large. The lowest measured pH values were still above 7.2.

For each tested pulse parameter sample temperature increase during pulse delivery was measured. All experiments were done at room temperature that was approximately 25.5 °C. The highest

9

temperature of 30.6 °C was recorded after application of HF-BP 1 pulse parameters. Measured temperature increases after delivery of 8×100 μs, 8×5 ms, HF-BP 1, HF-BP 2 and HF-BP 3 pulse parameters were 0.8 °C, 2.4 °C, 5.1 °C, 3.1 °C and 3.6 °C, respectively (Supplementary Fig. 2).

4. Discussion

The results of our study confirm that with HF-BP pulses we can achieve successful GET with bipolar microsecond pulses *in vitro* with sufficiently high pDNA concentration. The electric field chosen for GET with pulse protocols HF-BP was in the range of electric fields used for GET with longer monopolar pulses. GET efficiency increased with increasing pDNA concentration. However, in attempt to achieve GET efficiency comparable to that of longer monopolar pulses (8×100 μs and 8×5 ms pulse protocols) 5 times higher pDNA concentration was needed for GET with HF-BP pulse protocols. Further optimization of HF-BP pulse protocols could lessen the need for high pDNA concentrations. Nevertheless, presented results potentially open completely new field of possible GET applications – less painful and widely accepted GET applications, like nucleic acid-based vaccination.

Electric field required for successful GET using protocols HF-BP (1.25 kV/cm) was lower than electric field required for GET with pulse protocol 8×100 μs (1.6 kV/cm) and 2.5 times higher than electric field required for GET with pulse protocol 8×5 ms (0.5 kV/cm). This is in contrast with previously published data [53,54,59] showing that higher electric fields are required when applying HF-BP pulses. However, previous studies were performed with HF-BP pulse protocols that had the same on-time per treatment as 8×100 μs. In our experiments we extended on-time per treatment in HF-BP pulse protocols (12–21x) compared to 8×100 μs and thus were able to achieve permeabilization and GET at lower electric filed. In HF-BP pulse protocols on-time per treatment was still more than 2x shorter as in 8×5 ms pulse protocol. On-time per treatment was prolonged with increased number of pulses in each burst of HF-BP pulse protocols. This might be the explanation for lower electric field required for GET with HF-BP pulse protocols as it was previously shown that with increased number of pulses, the electric field needed to obtain the same fraction of electroporated cells decreases [82].

In order to investigate if the lack of electrophoretic force during HF-BP pulse delivery can be compensated with higher pDNA concentration we tested the effect of increasing pDNA concentration on cell viability and GET efficiency. The addition of pDNA in cell suspension was not toxic regardless of the concentration used (Fig. 3). Moreover, even the highest pDNA concentration (500 μg/ml) did not decrease cell viability, alone or in combination with applying any of five pulse protocols tested as detected by MTS assay 24 h after GET. Our results are comparable to results obtained in [83] where it was shown that pDNA concentrations up to 1 mg/ml did not decrease survival of mesenchymal stem cells. However, some studies report that pDNA concentrations above 100 μg/ml already have reduced cell survival [84,85] as a consequence of cell defense mechanisms activation triggered by pDNA entrance leading to programmed cell death [86,87].

Our results show that percent of GFP positive cells was increasing with increasing pDNA concentration. Increase was more pronounced when HF-BP pulse protocols were applied. With the highest two pDNA concentrations (250 and 500 μg/ml) the increase in percent of GFP positive cells was significant in all three HF-BP pulse protocols. Contrary to pulse protocol 8×100 μs and pulse protocol 8×5 ms where no further increase in percent of GFP positive cells with pDNA concentrations above 60 μg/ml or 80 μg/ml

was observed (Fig. 2). Similar trend was observed for overall GET with the highest pDNA concentration (500 μg/ml). Overall GET obtained by HF-BP pulse protocols was comparable to overall GET obtained by "classical", long monopolar pulse protocols (Fig. 4). It was already shown that with higher pDNA concentration successful GET is possible also with shorter high voltage pulses where weaker electrophoretic forces are present [34,39,88]. This is in agreement with our results obtained with HF-BP pulse protocols where with higher pDNA concentration we were able to achieve comparable GET efficiency in the absence of net electrophoretic force on pDNA. According to findings of [40] the diffusion coefficient of circular 4.7 kbp large pDNA used in our study is similar at all tested concentrations (20 to 500 μg/ml).

Protein expression following transfection is regulated by a number of factors, including the promoter used, pDNA copy number within the cell and the availability of cellular machinery for transcription and translation. Fluorescence intensity of the cell is considered to be indicative of the number of pDNA copies inside the cell that have reached the cell nucleus and have been successfully transcribed and translated into fluorescent proteins [89,90]. Our results of median fluorescence intensity thus suggest that the lack of electrophoretic force can only partially be compensated with higher pDNA concentration. Median fluorescence intensity with the lowest (20 μg/ml) and the highest (500 μg/ml) pDNA concentration was significantly higher after GET with pulse protocols 8×100 μs and 8×5 ms compared to all three pulse protocols HF-BP (Fig. 5). Suggesting that although with the highest pDNA concentration (500 μg/ml) we were able to achieve similar percent of transfected cells, the number of pDNA copies that were successfully transfected into cells was higher when pulse protocols 8×100 μs and 8×5 ms were used. This indicates that electrophoretic force is also instrumental in pDNA translocation across cell membrane.

Recently in a study reported by [88] authors observed increase in GET with increasing pDNA concentration and that at some point GET efficiency no longer increases with higher pDNA concentration. They also reported that if pulse parameters are suboptimal this plateau in GET efficiency is not observed. However, contrary to our results, they observed decrease in cell survival with increasing pDNA concentration. Reason for this might be that different assays for cell survival were used. We used MTS assay which measures cell viability 24 h after experiments, and they did clonogenic assay which is a cell survival assay based on the ability of a single cell to grow into a colony.

Direct observation of pDNA aggregates formation on cell membrane showed that increasing pDNA concentration also increases the fluorescence intensity of pDNA aggregates labeled with TOTO-1 nucleic acid stain formed on cell membrane. Florescence intensity of pDNA aggregates depends also on duration of applied pulses. With the lowest pDNA concentration (20 μg/ml) the fluorescence intensity of pDNA aggregates formed on cell membrane following 8×5 ms pulse protocol (Fig. 7) was almost 4 times higher as fluorescence intensity of pDNA aggregates formed after HF-BP 2 pulse protocol (Fig. 8) with the highest pDNA concentration (500 μg/ml) and comparable to 8×100 μs pulse protocol (Fig. 6) with the highest pDNA concentration. However, we did not observe any direct correlation between fluorescence intensity of pDNA aggregates formed on cell membrane and transfection efficiency. With the highest pDNA concentration used, fluorescence intensity of pDNA aggregates formed after HF-BP 2 pulse protocol was almost 10 times lower compared to fluorescence intensity of pDNA aggregates formed after 8×5 ms protocol while no significant difference was observed in percent of GFP positive cells. Similar observations were reported previously [91]. The interaction of pDNA with cell membrane is only one of several steps and barriers that pDNA has to overcome in order to be expressed. Other factors

10

such as pDNA stability in cytoplasm, its transport to perinuclear region and successful crossing of nuclear envelope are also crucial and contribute to differences in transfection efficiency [18].

Since application of bipolar pulses also comes with decreased electrochemical reactions [92,93], and lower metal release from electrodes [59], we measured pH changes of overall cell suspension after pulse delivery. To mimic our experimental protocol with cells FBS was added after pulse delivery to increase cell survival [78] and cell suspension was mixed by pipetting. Cell suspension in cuvette was placed in water bath heated to 37 °C. We observed slight decrease in pH of cell suspension, but not large enough to affect cell membrane resealing dynamics [94]. This drop in pH was stable during 5 min following pulse delivery in all pulse protocols tested except pulse protocol 8×5 ms where pH additionally decreased in the second minute after pulse delivery and remained constant then after. Significant drop in pH was observed after pulse protocol 8×5 ms compared to pH after delivery of pulse protocol 8×100 µs and pulse protocol HF-BP 1 (Fig. 9). Our measurements are in agreement with [92], where it was shown that longer pulses lead to more electrochemical reactions which cause changes in the chemical composition of electroporation medium or pH. According to our results larger pH changes must be occurring at anode side since the overall pH decreased after pulse delivery. This is in agreement with [45] where larger extension of the anodic pH front relative to the cathodic one was observed. Another explanation for slight decrease in medium pH can be the repair mechanisms of cells which are activated in order to repair damage caused on cell membrane during electric field delivery. This mechanisms include exocytosis of lysosomes and the release of their acidic content in cell surroundings [95]. Cell lysis could also contribute to observed decrease in pH since intracellular pH is around 7.0–7.2 [96].

Temperature is reported to affect cell membrane fluidity, consequently permeabilization [97] and GET efficiency [98,99]. However, final temperature of the electroporated cell samples measured during delivery of different pulse protocols in our study was not higher than 37 °C which was the temperature of after pulse incubation. Therefore, we conclude that temperature increase during pulse delivery had no observable effect on GET efficiency.

We did not observe any difference in efficiency between all three HF-BP protocols tested. Changing number of bursts or number of pulses in each burst in the tested range of parameters did not lead to increased GET efficiency. Minor differences were observed in cell viability 24 h after pulse delivery where both increased number of bursts and increased number of pulses in burst lead to slightly lower cell viability, although not statistically significant.

5. Conclusions

Successful GET can be achieved with HF-BP bipolar microsecond pulses. The efficiency increases with increasing pDNA concentration however, number of transferred plasmid copies seems to be higher with longer monopolar pulses. Prolonged on-time per treatment with increased number of pulses in each burst or increased number of bursts enabled comparable overall GET with HF-BP pulse protocols at lower electric field compared to pulse protocol 8×100 µs. According to reports using similar HF-BP pulse protocols where even at double stimulating voltage eightfold reduction in muscle contraction intensity was observed [51,77], we can conclude that widely accepted GET applications, like nucleic acid-based vaccination, are feasible. However, achieving sufficiently high pDNA concentrations in tissue can be challenging.

References

[1] L. Rems, M. Tarek, M. Casciola, D. Miklavčič, Properties of lipid electropores II: Comparison of continuum-level modeling of pore conductance to molecular dynamics simulations, Bioelectrochemistry 112 (2016) 112–124, https://doi.org/10.1016/j.bioelechem.2016.03.005.

[2] T. Kotnik, L. Rems, M. Tarek, D. Miklavcic, Membrane Electroporation and Electropermeabilization: Mechanisms and Models, Annu. Rev. Biophys. 48 (2019) 63–91, https://doi.org/10.1146/annurev-biophys-052118-115451.

[3] J.C. Weaver, Y.A. Chizmadzhev, Theory of electroporation: A review, Bioelectrochem. Bioenerg. 41 (1996) 135–160, https://doi.org/10.1016/S0302-4598(96)05062-3.

[4] M.L. Yarmush, A. Golberg, G. Serša, T. Kotnik, D. Miklavčič, Electroporation-based technologies for medicine: Principles, applications, and challenges, Annu. Rev. Biomed. Eng. 16 (2014) 295–320, https://doi.org/10.1146/annurev-bioeng-071813-104622.

[5] B. Geboers, H.J. Scheffer, P.M. Graybill, A.H. Ruarus, S. Nieuwenhuizen, R.S. Puijk, P.M. Van Den Tol, R.V. Davalos, B. Rubinsky, T.D. De Gruijl, D. Miklavčič, M.R. Meijerink, High-voltage electrical pulses in oncology: Irreversible electroporation, electrochemotherapy, gene electrotransfer, electrofusion, and electroimmunotherapy, Radiol. Soc. North Am. (RSNA) (2020), https://doi.org/10.1148/radiol.2020192190.

[6] T. Kotnik, W. Frey, M. Sack, S. Haberl Meglič, M. Peterka, D. Miklavčič, Electroporation-based applications in biotechnology, Trends Biotechnol. 33 (2015) 480–488, https://doi.org/10.1016/j.tibtech.2015.06.002.

[7] S. Mahnič-Kalamiza, E. Vorobiev, D. Miklavčič, Electroporation in Food Processing and Biorefinery, J. Membr. Biol. 247 (2014) 1279–1304, https://doi.org/10.1007/s00232-014-9737-x.

[8] A. Golberg, M. Sack, J. Teissie, G. Pataro, U. Pliquett, G. Saulis, T. Stefan, D. Miklavcic, E. Vorobiev, W. Frey, Energy-efficient biomass processing with pulsed electric fields for bioeconomy and sustainable development, Biotechnol. Biofuels 9 (2016), https://doi.org/10.1186/s13068-016-0508-z.

[9] B. Mali, T. Jarm, M. Snoj, G. Sersa, D. Miklavcic, Antitumor effectiveness of electrochemotherapy: A systematic review and meta-analysis, Eur. J. Surg. Oncol. 39 (2013) 4–16, https://doi.org/10.1016/j.ejso.2012.08.016.

[10] L.G. Campana, I. Edhemovic, D. Soden, A.M. Perrone, M. Scarpa, L. Campanacci, M. Cemazar, S. Valpione, D. Miklavčič, S. Mocellin, E. Sieni, G. Sersa, Electrochemotherapy – Emerging applications technical advances, new indications, combined approaches, and multi-institutional collaboration, Eur. J. Surg. Oncol. 45 (2019) 92–102, https://doi.org/10.1016/j.ejso.2018.11.023.

[11] R.V. Davalos, L.M. Mir, B. Rubinsky, Tissue ablation with irreversible electroporation, Ann. Biomed. Eng. 33 (2005) 223–231, https://doi.org/10.1007/s10439-005-8981-8.

[12] A. Sugrue, V. Vaidya, C. Witt, C.V. DeSimone, O. Yasin, E. Maor, A.M. Killu, S. Kapa, C.J. McLeod, D. Miklavčič, S.J. Asirvatham, Irreversible electroporation for catheter-based cardiac ablation: a systematic review of the preclinical experience, J. Interv. Card. Electrophysiol. 55 (2019) 251–265, https://doi.org/10.1007/s10840-019-00574-3.

[13] E. Maor, A. Sugrue, C. Witt, V.R. Vaidya, C.V. DeSimone, S.J. Asirvatham, S. Kapa, Pulsed electric fields for cardiac ablation and beyond: A state-of-the-art review, Hear. Rhythm. 16 (2019) 1112–1120, https://doi.org/10.1016/j.hrthm.2019.01.012.

[14] H.J. Scheffer, K. Nielsen, M.C. De Jong, A.A.J.M. Van Tilborg, J.M. Vieveen, A. Bouwman, S. Meijer, C. Van Kuijk, P. Van Den Tol, M.R. Meijerink, Irreversible electroporation for nonthermal tumor ablation in the clinical setting: A

11

systematic review of safety and efficacy, J. Vasc. Interv. Radiol. 25 (2014) 997–1011, https://doi.org/10.1016/j.jvir.2014.01.028.

[15] V.Y. Reddy, A. Anic, J. Koruth, J. Petru, M. Funasako, K. Minami, T. Breskovic, I. Sikiric, S.R. Dukkipati, I. Kawamura, P. Neuzil, Pulsed Field Ablation in Patients With Persistent Atrial Fibrillation, J. Am. Coll. Cardiol. 76 (2020) 1068–1080, https://doi.org/10.1016/j.jacc.2020.07.007.

[16] A.R. Denet, R. Vanbever, V. Préat, Skin electroporation for transdermal and topical delivery, Adv. Drug Deliv. Rev. 56 (2004) 659–674, https://doi.org/10.1016/j.addr.2003.10.027.

[17] B. Zorec, V. Préat, D. Miklavčič, N. Pavšelj, Active enhancement methods for intra- and transdermal drug delivery: A review, Zdr. Vestn. 82 (2013) 339–356.

[18] C. Rosazza, S. Haberl Meglic, A. Zumbusch, M.-P. Rols, D. Miklavcic, Gene Electrotransfer: A Mechanistic Perspective, Curr. Gene Ther. 16 (2016) 98–129, https://doi.org/10.2174/1566523216666160331130040.

[19] L. Pasquet, S. Chabot, E. Bellard, B. Markelc, M.P. Rols, J.P. Reynes, G. Tiraby, F. Couillaud, J. Teissie, M. Golzio, Safe and efficient novel approach for non-invasive gene electrotransfer to skin, Sci. Rep. 8 (2018), https://doi.org/10.1038/s41598-018-34968-6.

[20] L. Lambricht, A. Lopes, S. Kos, G. Sersa, V. Préat, G. Vandermeulen, Clinical potential of electroporation for gene therapy and DNA vaccine delivery, Expert Opin. Drug Deliv. 13 (2016) 295–310, https://doi.org/10.1517/17425247.2016.1121990.

[21] L.C. Heller, R. Heller, Electroporation Gene Therapy Preclinical and Clinical Trials for Melanoma, Curr. Gene Ther. 10 (2010) 312–317, https://doi.org/10.2174/156652310791823489.

[22] N.Y. Sardesai, D.B. Weiner, Electroporation delivery of DNA vaccines: Prospects for success, Curr. Opin. Immunol. 23 (2011) 421–429, https://doi.org/10.1016/j.coi.2011.03.008.

[23] J.L. Young, D.A. Dean, Electroporation-Mediated Gene Delivery, Adv. Genet. 89 (2015) 49–88, https://doi.org/10.1016/bs.adgen.2014.10.003.

[24] J. Glasspool-Malone, S. Somiari, J.J. Drabick, R.W. Malone, Efficient nonviral cutaneous transfection, Mol. Ther. 2 (2000) 140–146, https://doi.org/10.1006/mthe.2000.0107.

[25] B. Ferraro, Y.L. Cruz, D. Coppola, R. Heller, Intradermal delivery of plasmid VEGF165 by electroporation promotes wound healing, Mol. Ther. 17 (2009) 651–657, https://doi.org/10.1038/mt.2009.12.

[26] L.M. Mir, M.F. Bureau, J. Gehl, R. Rangara, D. Rouy, J.M. Caillaud, P. Delaere, D. Branellec, B. Schwartz, D. Scherman, High-efficiency gene transfer into skeletal muscle mediated by electric pulses, Proc. Natl. Acad. Sci. U. S. A. 96 (1999) 4262–4267, https://doi.org/10.1073/pnas.96.8.4262.

[27] J. Teissie, M. Golzio, M.P. Rols, Mechanisms of cell membrane electropermeabilization: A minireview of our present (lack of ?) knowledge, Biochim. Biophys. Acta - Gen. Subj. 1724 (2005) 270–280, https://doi.org/10.1016/j.bbagen.2005.05.006.

[28] R.S. Son, K.C. Smith, T.R. Gowrishankar, P.T. Vernier, J.C. Weaver, Basic Features of a Cell Electroporation Model: Illustrative Behavior for Two Very Different Pulses, J. Membr. Biol. 247 (2014) 1209–1228, https://doi.org/10.1007/s00232-014-9699-z.

[29] C. Faurie, M. Rebersek, M. Golzio, M. Kanduser, J.M. Escoffre, D. Pavlin, J. Teissie, D. Miklavcic, M.P. Rols, Electro-mediated gene transfer and expression are controlled by the life-time of DNA/membrane complex formation, J. Gene Med. 12 (2010) 117–125, https://doi.org/10.1002/jgm.1414.

[30] S. Sachdev, S. Feijoo Moreira, Y. Keehnen, L. Rems, M.T.M.T. Kreutzer, P.E.P.E. Boukany, DNA-membrane complex formation during electroporation is DNA size-dependent, Biochim. Biophys. Acta - Biomembr. 1862 (2020), https://doi.org/10.1016/j.bbamem.2019.183089.

[31] M. Wu, F. Yuan, Membrane binding of plasmid DNA and endocytic pathways are involved in electrotransfection of mammalian cells, PLoS ONE 6 (2011), https://doi.org/10.1371/journal.pone.0020923.

[32] C.C. Chang, M. Wu, F. Yuan, Role of specific endocytic pathways in electrotransfection of cells, Mol. Ther. - Methods Clin. Dev. 1 (2014) 14058, https://doi.org/10.1038/mtm.2014.58.

[33] C. Rosazza, H. Deschout, A. Buntz, K. Braeckmans, M.P. Rols, A. Zumbusch, Endocytosis and Endosomal Trafficking of DNA After Gene Electrotransfer In Vitro, Mol. Ther. - Nucleic Acids. 5 (2016), https://doi.org/10.1038/mtna.2015.59 e286.

[34] M. Pavlin, K. Flisar, M. Kanduser, The role of electrophoresis in gene electrotransfer, J. Membr. Biol. 236 (2010) 75–79, https://doi.org/10.1007/s00232-010-9276-z.

[35] F.M. André, J. Gehl, G. Sersa, V. Préat, P. Hojman, J. Eriksen, M. Golzio, M. Cemazar, N. Pavselj, M.P. Rols, D. Miklavcic, E. Neumann, J. Teissié, L.M. Mir, Efficiency of high- and low-voltage pulse combinations for gene electrotransfer in muscle, liver, tumor, and skin, Hum. Gene Ther. 19 (2008) 1261–1271, https://doi.org/10.1089/hum.2008.060.

[36] S. Satkauskas, F. Andre, M.F. Bureau, D. Scherman, D. Miklavcic, L.M. Mir, Electrophoretic Component of Electric Pulses Determines the Efficacy of In Vivo DNA Electrotransfer, Hum. Gene Ther. 16 (2005), https://doi.org/10.1089/hum.2005.16.1194, 050926062340001.

[37] E. Tekle, R.D. Astumian, P.B. Chock, Electroporation by using bipolar oscillating electric field: An improved method for DNA transfection of NIH 3T3 cells, Proc. Natl. Acad. Sci. U. S. A. 88 (1991) 4230–4234, https://doi.org/10.1073/pnas.88.10.4230.

[38] M. Reberšek, C. Faurie, M. Kanduser, S. Korović, J. Teissié, M.P. Rols, D. Miklavčič, Electroporator with automatic change of electric field direction improves gene electrotransfer in-vitro, Biomed. Eng. Online 6 (2007), https://doi.org/10.1186/1475-925X-6-25.

[39] M. Kandušer, D. Miklavčič, M. Pavlin, Mechanisms involved in gene electrotransfer using high- and low-voltage pulses - An in vitro study, Bioelectrochemistry 74 (2009) 265–271, https://doi.org/10.1016/j.bioelechem.2008.09.002.

[40] R.M. Robertson, D.E. Smith, Self-diffusion of entangled linear and circular DNA molecules: Dependence on length and concentration, Macromolecules 40 (2007) 3373–3377, https://doi.org/10.1021/ma070051h.

[41] S. Mahnič-Kalamiza, D. Miklavčič, Scratching the electrode surface: Insights into a high-voltage pulsed-field application from in vitro & in silico studies in indifferent fluid, Electrochim. Acta 363 (2020), https://doi.org/10.1016/j.electacta.2020.137187.

[42] M. Faroja, M. Ahmed, L. Appelbaum, E. Ben-David, M. Moussa, J. Sosna, I. Nissenbaum, S. Nahum Goldberg, Irreversible electroporation ablation: Is all the damage nonthermal?, Radiology 266 (2013) 462–470, https://doi.org/10.1148/radiol.12120609.

[43] N. Klein, E. Guenther, F. Botea, M. Pautov, S. Dima, D. Tomescu, M. Popescu, A. Ivorra, M. Stehling, I. Popescu, The combination of electroporation and electrolysis (E2) employing different electrode arrays for ablation of large tissue volumes, PLoS ONE 14 (2019), https://doi.org/10.1371/journal.pone.0221393.

[44] M. Phillips, L. Rubinsky, A. Meir, N. Raju, B. Rubinsky, Combining electrolysis and electroporation for tissue ablation, Technol. Cancer Res. Treat. 14 (2015) 395–410, https://doi.org/10.1177/1533034614560102.

[45] P. Turjanski, N. Olaiz, F. Maglietti, S. Michinski, C. Suárez, F.V. Molina, G. Marshall, The role of pH fronts in reversible electroporation, PLoS ONE 6 (2011), https://doi.org/10.1371/journal.pone.0017303.

[46] N. Olaiz, E. Signori, F. Maglietti, A. Soba, C. Suárez, P. Turjanski, S. Michinski, G. Marshall, Tissue damage modeling in gene electrotransfer: The role of pH, Bioelectrochemistry 100 (2014) 105–111, https://doi.org/10.1016/j.bioelechem.2014.05.001.

[47] F. Maglietti, S. Michinski, N. Olaiz, M. Castro, C. Suárez, G. Marshall, The role of Ph fronts in tissue electroporation based treatments, PLoS ONE 8 (2013), https://doi.org/10.1371/journal.pone.0080167.

[48] J.C. Weaver, K.C. Smith, A.T. Esser, R.S. Son, T.R. Gowrishankar, A brief overview of electroporation pulse strength-duration space: A region where additional intracellular effects are expected, Bioelectrochemistry 87 (2012) 236–243, https://doi.org/10.1016/j.bioelechem.2012.02.007.

[49] C.B. Arena, M.B. Sano, J.L. Caldwell, P.A. Garcia, M.N. Rylander, R. V. Davalos, High-frequency irreversible electroporation (H-FIRE) for non-thermal ablation without muscle contraction, Biomed. Eng. Online 10 (2011), https://doi.org/10.1186/1475-925X-10-102.

[50] M.B. Sano, R.E. Fan, K. Cheng, Y. Saenz, G.A. Sonn, G.L. Hwang, L. Xing, Reduction of Muscle Contractions during Irreversible Electroporation Therapy Using High-Frequency Bursts of Alternating Polarity Pulses: A Laboratory Investigation in an Ex Vivo Swine Model, J. Vasc. Interv. Radiol. 29 (2018) 893–898.e4, https://doi.org/10.1016/j.jvir.2017.12.019.

[51] C. Yao, S. Dong, Y. Zhao, Y. Lv, H. Liu, L. Gong, J. Ma, H. Wang, Y. Sun, Bipolar Microsecond Pulses and Insulated Needle Electrodes for Reducing Muscle Contractions during Irreversible Electroporation, IEEE Trans. Biomed. Eng. 64 (2017) 2924–2937, https://doi.org/10.1109/TBME.2017.2690624.

[52] D.C. Sweeney, M. Reberšek, J. Dermol, L. Rems, D. Miklavčič, R.V. Davalos, Quantification of cell membrane permeability induced by monopolar and high-frequency bipolar bursts of electrical pulses, Biochim. Biophys. Acta - Biomembr. 2016 (1858) 2689–2698, https://doi.org/10.1016/j.bbamem.2016.06.024.

[53] T. Polajžer, J. Dermol-Černe, M. Reberšek, R. O'Connor, D. Miklavčič, Cancellation effect is present in high-frequency reversible and irreversible electroporation, Bioelectrochemistry 132 (2020), https://doi.org/10.1016/j.bioelechem.2019.107442.

[54] M. Scuderi, M. Rebersek, D. Miklavcic, J. Dermol-Cerne, The use of high-frequency short bipolar pulses in cisplatin electrochemotherapy in vitro, Radiol. Oncol. 53 (2019) 194–205, https://doi.org/10.2478/raon-2019-0025.

[55] A. Sugrue, E. Maor, A. Ivorra, V. Vaidya, C. Witt, S. Kapa, S. Asirvatham, Irreversible electroporation for the treatment of cardiac arrhythmias, Expert Rev. Cardiovasc. Ther. 16 (2018) 349–360, https://doi.org/10.1080/14779072.2018.1459185.

[56] D. Miklavčič, G. Pucihar, M. Pavlovec, S. Ribarič, M. Mali, A. MačEk-Lebar, M. Petkovšek, J. Nastran, S. Kranjc, M. Čemažar, G. SeršA, The effect of high frequency electric pulses on muscle contractions and antitumor efficiency in vivo for a potential use in clinical electrochemotherapy, Bioelectrochemistry 65 (2005) 121–128, https://doi.org/10.1016/j.bioelechem.2004.07.004.

[57] G. Sersa, S. Kranjc, J. Scancar, M. Krzan, M. Cemazar, Electrochemotherapy of mouse sarcoma tumors using electric pulse trains with repetition frequencies of 1 Hz and 5 kHz, J. Membr. Biol. 236 (2010) 155–162, https://doi.org/10.1007/s00232-010-9268-z.

[58] S. Jaichandran, S.T.B. Yap, A.B.M. Khoo, L.P. Ho, S.L. Tien, O.L. Kon, In vivo liver electroporation: Optimization and demonstration of therapeutic efficacy, Hum. Gene Ther. 17 (2006) 362–375, https://doi.org/10.1089/hum.2006.17.362.

[59] A. Vižintin, J. Vidmar, J. Ščančar, D. Miklavčič, Effect of interphase and interpulse delay in high-frequency irreversible electroporation pulses on cell survival, membrane permeabilization and electrode material release, Bioelectrochemistry 134 (2020), https://doi.org/10.1016/j.bioelechem.2020.107523.

[60] M.B. Sano, C.B. Arena, M.R. DeWitt, D. Saur, R.V. Davalos, In-vitro bipolar nano- and microsecond electro-pulse bursts for irreversible electroporation

therapies, Bioelectrochemistry 100 (2014) 69–79, https://doi.org/10.1016/j.bioelechem.2014.07.010.

[61] R.V. Davalos, B. Rubinsky, L.M. Mir, Theoretical analysis of the thermal effects during in vivo tissue electroporation, Bioelectrochemistry 61 (2003) 99–107, https://doi.org/10.1016/j.bioelechem.2003.07.001.

[62] B.L. Ibey, J.C. Ullery, O.N. Pakhomova, C.C. Roth, I. Semenov, H.T. Beier, M. Tarango, S. Xiao, K.H. Schoenbach, A.G. Pakhomov, Bipolar nanosecond electric pulses are less efficient at electropermeabilization and killing cells than monopolar pulses, Biochem. Biophys. Res. Commun. 443 (2014) 568–573, https://doi.org/10.1016/j.bbrc.2013.12.004.

[63] A.G. Pakhomov, S. Grigoryev, I. Semenov, M. Casciola, C. Jiang, S. Xiao, The second phase of bipolar, nanosecond-range electric pulses determines the electroporation efficiency, Bioelectrochemistry 122 (2018) 123–133, https://doi.org/10.1016/j.bioelechem.2018.03.014.

[64] C.B. Arena, R.V. Davalos, Advances in Therapeutic Electroporation to Mitigate Muscle Contractions, J. Membr. Sci. Technol. 02 (2012), https://doi.org/10.4172/2155-9589.1000e102.

[65] A. Županič, S. Ribarič, D. Miklavčič, Increasing the repetition frequency of electric pulse delivery reduces unpleasant sensations that occur in electrochemotherapy, Neoplasma 54 (2007) 246–250.

[66] M. Wallace, B. Evans, S. Woods, R. Mogg, L. Zhang, A.C. Finnefrock, D. Rabussay, M. Fons, J. Mallee, D. Mehrotra, F. Schödel, L. Musey, Tolerability of two sequential electroporation treatments using MedPulser DNA delivery system (DDS) in healthy adults, Mol. Ther. 17 (2009) 922–928, https://doi.org/10.1038/mt.2009.27.

[67] B. Mercadal, C.B. Arena, R.V. Davalos, A. Ivorra, Avoiding nerve stimulation in irreversible electroporation: A numerical modeling study, Phys. Med. Biol. 62 (2017) 8060–8079, https://doi.org/10.1088/1361-6560/aa8c53.

[68] B. Mali, V. Gorjup, I. Edhemovic, E. Brecelj, M. Cemazar, G. Sersa, B. Strazisar, D. Miklavcic, T. Jarm, Electrochemotherapy of colorectal liver metastases - An observational study of its effects on the electrocardiogram, Biomed. Eng. Online 14 (2015), https://doi.org/10.1186/1475-925X-14-S3-S5.

[69] R. Van Es, M.K. Konings, B.C. Du Pré, K. Neven, H. Van Wessel, V.J.H.M. Van Driel, A.H. Westra, P.A.F. Doevendans, F.H.M. Wittkampf, High-frequency irreversible electroporation for cardiac ablation using an asymmetrical waveform, Biomed. Eng. Online 18 (2019), https://doi.org/10.1186/s12938-019-0693-7.

[70] V.Y. Reddy, P. Neuzil, J.S. Koruth, J. Petru, M. Funosako, H. Cochet, L. Sediva, M. Chovanec, S.R. Dukkipati, P. Jais, Pulsed Field Ablation for Pulmonary Vein Isolation in Atrial Fibrillation, J. Am. Coll. Cardiol. 74 (2019) 315–326, https://doi.org/10.1016/j.jacc.2019.04.021.

[71] B. Howard, D.E. Haines, A. Verma, D. Packer, N. Kirchhof, N. Barka, B. Onal, S. Fraasch, D. Miklavčič, M.T. Stewart, Reduction in Pulmonary Vein Stenosis and Collateral Damage with Pulsed Field Ablation Compared with Radiofrequency Ablation in a Canine Model, Circ. Arrhythmia Electrophysiol. 13 (2020), https://doi.org/10.1161/CIRCEP.120.008337.

[72] W.G. Marshall, B.A. Boone, J.D. Burgos, S.I. Gografe, M.K. Baldwin, M.L. Danielson, M.J. Larson, D.R. Caretto, Y. Cruz, B. Ferraro, L.C. Heller, K.E. Ugen, M.J. Jaroszeski, R. Heller, Electroporation-mediated delivery of a naked DNA plasmid expressing VEGF to the porcine heart enhances protein expression, Gene Ther. 17 (2010) 419–423, https://doi.org/10.1038/gt.2009.153.

[73] A.A. Bulysheva, B. Hargrave, N. Burcus, C.G. Lundberg, L. Murray, R. Heller, Vascular endothelial growth factor-A gene electrotransfer promotes angiogenesis in a porcine model of cardiac ischemia, Gene Ther. 23 (2016) 649–656, https://doi.org/10.1038/gt.2016.35.

[74] S. Dong, C. Yao, Y. Zhao, Y. Lv, H. Liu, Parameters optimization of bipolar high frequency pulses on tissue ablation and inhibiting muscle contraction, IEEE Trans. Dielectr. Electr. Insul. 25 (2018) 207–216, https://doi.org/10.1109/TDEI.2018.006303.

[75] K.N. Aycock, Y. Zhao, M.F. Lorenzo, R.V. Davalos, A theoretical argument for extended interpulse delays in therapeutic high-frequency irreversible electroporation treatments, IEEE Trans. Biomed. Eng. (2021), https://doi.org/10.1109/TBME.2021.3049221.

[76] C. Günter, J. Delbeke, M. Ortiz-Catalan, Safety of long-term electrical peripheral nerve stimulation: Review of the state of the art, J. NeuroEng. Rehabil. 16 (2019), https://doi.org/10.1186/s12984-018-0474-8.

[77] M.B. Sano, C.B. Arena, K.R. Bittleman, M.R. Dewitt, H.J. Cho, C.S. Szot, D. Saur, J. M. Cissell, J. Robertson, Y.W. Lee, R.V. Davalos, Bursts of Bipolar Microsecond Pulses Inhibit Tumor Growth, Sci. Rep. 5 (2015), https://doi.org/10.1038/srep14999.

[78] C. Delteil, J. Teissié, M.P. Rols, Effect of serum on in vitro electrically mediated gene delivery and expression in mammalian cells, Biochim. Biophys. Acta - Biomembr. 1467 (2000) 362–368, https://doi.org/10.1016/S0005-2736(00)00235-2.

[79] M. Bosnjak, B.C. Lorente, Z. Pogacar, V. Makovsek, M. Cemazar, Different incubation times of cells after gene Electrotransfer in fetal bovine serum affect

cell viability, but not Transfection efficiency, J. Membr. Biol. 247 (2014) 421–428, https://doi.org/10.1007/s00232-014-9649-9.

[80] M. Golzio, J. Teissié, M.P. Rols, Direct visualization at the single-cell level of electrically mediated gene delivery, Proc. Natl. Acad. Sci. U. S. A. 99 (2002) 1292–1297, https://doi.org/10.1073/pnas.022646499.

[81] S. Haberl, D. Miklavčič, M. Pavlin, Effect of Mg ions on efficiency of gene electrotransfer and on cell electropermeabilization, Bioelectrochemistry 79 (2010) 265–271, https://doi.org/10.1016/j.bioelechem.2010.04.001.

[82] G. Pucihar, J. Krmelj, M. Reberšek, T.B. Napotnik, D. Miklavčič, Equivalent pulse parameters for electroporation, IEEE Trans. Biomed. Eng. 58 (2011) 3279–3288, https://doi.org/10.1109/TBME.2011.2167232.

[83] A. Liew, F.M. André, L.L. Lesueur, M.A. De Ménorval, T. O'Brien, L.M. Mir, Robust, efficient, and practical electrogene transfer method for human mesenchymal stem cells using square electric pulses, Hum. Gene Ther. Methods 24 (2013) 289–297, https://doi.org/10.1089/hgtb.2012.159.

[84] M.-P. Rols, D. Coulet, J. Teissie, Highly efficient transfection of mammalian cells by electric field pulses: Application to large volumes of cell culture by using a flow system, Eur. J. Biochem. 206 (1992) 115–121, https://doi.org/10.1111/j.1432-1033.1992.tb16908.x.

[85] S. Yao, S. Rana, D. Liu, G.E. Wise, Electroporation optimization to deliver plasmid DNA into dental follicle cells, Biotechnol. J. 4 (2009) 1488–1496, https://doi.org/10.1002/biot.200900039.

[86] G. Cheng, J. Zhong, J. Chung, F.V. Chisari, Double-stranded DNA and double-stranded RNA induce a common antiviral signaling pathway in human cells, Proc. Natl. Acad. Sci. U. S. A. 104 (2007) 9035–9040, https://doi.org/10.1073/pnas.0703285104.

[87] K.J. Ishii, T. Kawagoe, S. Koyama, K. Matsui, H. Kumar, T. Kawai, S. Uematsu, O. Takeuchi, F. Takeshita, C. Coban, S. Akira, TANK-binding kinase-1 delineates innate and adaptive immune responses to DNA vaccines, Nature 451 (2008) 725–729, https://doi.org/10.1038/nature06537.

[88] S. Chopra, P. Ruzgys, M. Maciulevičius, M. Jakutavičiute, S. Šatka, Investigation of plasmid DNA delivery and cell viability dynamics for optimal cell electrotransfection in vitro, Appl. Sci. 10 (2020), https://doi.org/10.3390/app10176070.

[89] R.N. Cohen, M.A.E.M. van der Aa, N. Macaraeg, A.P. Lee, F.C. Szoka, Quantification of plasmid DNA copies in the nucleus after lipoplex and polyplex transfection, J. Control. Release 135 (2009) 166–174, https://doi.org/10.1016/j.jconrel.2008.12.016.

[90] Y.C. Tsai, T.H. Tsai, C.P. Chang, S.F. Chen, Y.M. Lee, S.K. Shyue, Linear correlation between average fluorescence intensity of green fluorescent protein and the multiplicity of infection of recombinant adenovirus, J. Biomed. Sci. 22 (2015), https://doi.org/10.1186/s12929-015-0137-z.

[91] S. Haberl, M. Kandušer, K. Flisar, D. Hodžić, V.B. Bregar, D. Miklavčič, J.M. Escoffre, M.P. Rols, M. Pavlin, Effect of different parameters used for in vitro gene electrotransfer on gene expression efficiency, cell viability and visualization of plasmid DNA at the membrane level, J. Gene Med. 15 (2013) 169–181, https://doi.org/10.1002/jgm.2706.

[92] D.E. Chafai, A. Mehle, A. Tilmatine, B. Maouche, D. Miklavčič, Assessment of the electrochemical effects of pulsed electric fields in a biological cell suspension, Bioelectrochemistry 106 (2015) 249–257, https://doi.org/10.1016/j.bioelechem.2015.08.002.

[93] T. Kotnik, D. Miklavčič, L.M. Mir, Cell membrane electropermeabilization by symmetrical bipolar rectangular pulses: Part II. Reduced electrolytic contamination, Bioelectrochemistry (2001) 91–95, https://doi.org/10.1016/S1567-5394(01)00115-3.

[94] T. Potočnik, D. Miklavčič, A. Maček Lebar, Effect of electroporation and recovery medium pH on cell membrane permeabilization, cell survival and gene transfer efficiency in vitro, Bioelectrochemistry 130 (2019), https://doi.org/10.1016/j.bioelechem.2019.107342.

[95] M. Corrotte, T. Castro-Gomes, Lysosomes and plasma membrane repair, Curr. Top. Membr. (2019) 1–16, https://doi.org/10.1016/bs.ctm.2019.08.001.

[96] J.R. Casey, S. Grinstein, J. Orlowski, Sensors and regulators of intracellular pH, Nat. Rev. Mol. Cell Biol. 11 (2010) 50–61, https://doi.org/10.1038/nrm2820.

[97] M. Kandušer, M. Šentjurc, D. Miklavčič, The temperature effect during pulse application on cell membrane fluidity and permeabilization, Bioelectrochemistry 74 (2008) 52–57, https://doi.org/10.1016/j.bioelechem.2008.04.012.

[98] A. Donate, A. Bulysheva, C. Edelblute, D. Jung, M.A. Malik, S. Guo, N. Burcus, K. Schoenbach, R. Heller, Thermal Assisted In Vivo Gene Electrotransfer, Curr. Gene Ther. 16 (2016) 83–89, https://doi.org/10.2174/1566523216666160331125810.

[99] A. Bulysheva, J. Hornef, C. Edelblute, C. Jiang, K. Schoenbach, C. Lundberg, M.A. Malik, R. Heller, Coalesced thermal and electrotransfer mediated delivery of plasmid DNA to the skin, Bioelectrochemistry 125 (2019) 127–133, https://doi.org/10.1016/j.bioelechem.2018.10.004.

13

2.3. EFFICIENT GENE TRANSFECTION BY ELECTROPORATION - *IN VITRO* AND *IN SILICO* STUDY OF PULSE PARAMETERS

Gene electrotransfer (GET) is a widely used method for nucleic acids' delivery into cells. We explored, evaluated, and demonstrated the potential use of different pulses for introducing plasmid DNA (pDNA) into cells *in vitro* and compared the efficiency and dynamics of transgene expression after GET. We performed experiments on cell suspensions of 1306 fibroblasts and C2C12 myoblasts across the range of pulse durations (nanosecond to millisecond) including high-frequency bipolar (HF-BP) pulses. Six different concentrations of pDNA encoding green fluorescent protein were used. We show that GET can be achieved with nanosecond pulses even at low pulse repetition rate (10 Hz). GET efficiency depends on the pDNA concentration and cell line. Time dynamics of transgene expression are comparable between nanosecond, HF-BP, microsecond, and millisecond, pulses but vary between cell lines. Lastly, based on the data obtained in the experiments of pDNA concentration effect on GET the model of the probability of pDNA and cell membrane contact during GET was developed. The model shows that pDNA migration is dominated by diffusion for nanosecond and HF-BP pulses and by electrophoresis for micro- and millisecond pulses. Modeling results can provide valuable guidance for further experiments and interpretations of the results obtained by various pulse protocols.

*applied
sciences*

MDPI

Article

Efficient Gene Transfection by Electroporation—In Vitro and In Silico Study of Pulse Parameters

Tjaša Potočnik [ID], Shaurya Sachdev [ID], Tamara Polajžer, Alenka Maček Lebar [ID] and Damijan Miklavčič *[ID]

Faculty of Electrical Engineering, University of Ljubljana, Tržaška 25, 1000 Ljubljana, Slovenia
* Correspondence: damijan.miklavcic@fe.uni-lj.si

Abstract: Gene electrotransfer (GET) is a widely used method for nucleic acids' delivery into cells. We explored, evaluated, and demonstrated the potential use of different pulse durations for introducing plasmid DNA (pDNA) into cells in vitro and compared the efficiency and dynamics of transgene expression after GET. We performed experiments on cell suspensions of 1306 fibroblasts and C2C12 myoblasts with four ranges of pulse durations (nanosecond, high frequency bipolar (HF-BP), and micro- and millisecond). Six different concentrations of pDNA encoding green fluorescent protein were used. We show that GET can be achieved with nanosecond pulses with a low pulse repetition rate (10 Hz). The GET's efficiency depends on the pDNA concentration and cell line. Time dynamics of transgene expression are comparable between millisecond, microsecond, HF-BP, and nanosecond pulses but depend greatly on cell line. Lastly, based on the data obtained in the experiments of pDNA concentration effect on GET the model of the probability of pDNA and cell membrane contact during GET was developed. The model shows that pDNA migration is dominated by diffusion for nanosecond and HF-BP pulses and by electrophoresis for micro- and millisecond pulses. Modeling results can provide valuable guidance for further experiments and interpretations of the results obtained by various pulse protocols.

Keywords: gene electrotransfer; nanosecond pulses; high frequency bipolar pulses; electroporation; plasmid DNA

1. Introduction

Gene electrotransfer (GET), or gene transfection by electroporation, is a widely used method for nucleic acids' delivery into cells based on the phenomenon of electroporation where electric pulses cause temporarily increased cell membrane permeability [1]. GET has been shown to markedly enhance the efficiency of naked plasmid DNA (pDNA) transfer, and has been widely used to introduce nucleic acids into various types of cells in vitro, ex vivo, and in vivo [1,2].

In clinical settings, GET is also considered as a promising method for the delivery of CRISPR/Cas9 gene editing complexes [3]. GET can also be used for vaccination against infectious diseases, with a DNA vaccine currently being developed for vaccination against COVID-19 [4–6]. In oncology, GET is used for the treatment of and vaccination against various cancers [7–10]. GET can also be used for ex vivo genetic engineering. More and more treatments against cancers are based on the ex vivo genetic engineering of T cells to express chimeric antigen receptors (CARs), which bind tumor antigens or tumor-associated antigens in a human leukocyte antigen (HLA)-independent manner [11]. Viral vectors are effective for the genetic engineering of human primary cells but have serious limitations such as high manufacturing cost, long production timelines, and genotoxic risks derived from their semi-random chromosomal integration profiles [12]. In contrast to viral vectors, GET has become the simplest and most appealing nonviral deliver technology with its ability to introduce diverse biomolecules to millions of cells per treatment. The limitation

of most electroporation protocols used for cell therapy is, however, the low transfection efficiency and cell death [13].

The efficiency of GET can be measured in different ways and may depend on the GET application, most often as percentage of transfected cells (referred as GET in our paper), which gives information about the percentage of cells that were successfully transfected among the cells that survived the treatment [14]. This could be useful in applications where cells which can rapidly multiply are used, such as bacteria. For applications of GET in gene therapy, it may be crucial that the majority of cells survive the treatment. In this case, it is important that the results of GET efficiency also include cell survival. GET efficiency representing the percentage of transfected cells based on the number of cells that were exposed to electric pulses is referred to as the overall GET in the paper [15]. Furthermore, GET efficiency, if cells are transfected with fluorescent proteins, can be measured with median fluorescence intensity (MFI), representing the quantity of produced transfected protein [16]. This is important in applications where the goal is the production of high levels of therapeutic proteins such as in DNA vaccination. In this paper, we present results of GET in vitro using all three types of GET efficiency determination, namely, GET, MFI, and overall GET.

In GET applications, pulse parameters (amplitude, duration, repetition frequency, and number) are usually varied to achieve cell membrane permeabilization and at the same time prevent excessive cell damage [17]. The choice of appropriate parameters of electric pulses is one of the most relevant steps of GET. GET can be applied equally to all cell types and at all stages of the cell cycle, but GET efficiency depends on and varies greatly between different cell types. The origins of these differences are not yet well understood. Generally smaller cells require a higher electric field to permeabilize their cell membrane. This is an important consideration for ex vivo gene delivery, especially to hematopoietic cells. Electroporation thresholds for different cells in a heterogeneous tissue thus vary [18,19].

Currently, gene transfer by electroporation is believed to rely on cell membrane permeabilization and electrophoresis of pDNA during pulse delivery. Electrophoresis, which is present during electric field delivery, acts on negatively charged pDNA molecules and enables a higher number of pDNA molecules to come in contact with the cell membrane than would do so solely by diffusion [20]. Small molecules (equal to or smaller than 15 bp [21]) can enter the cell with electrophoresis; however, large pDNA molecules form aggregates on cell membrane during electric field delivery, which later enter the cell with endocytosis [1,22–24]. Because of its role in the formation of pDNA aggregates during electric field delivery, the lack of electrophoresis could represent an important weakness for the use of short pulses in GET [25,26]. The presence of electrophoretic migration of pDNA is the reason why, usually, long millisecond pulses are used for GET. Although leading to efficient GET, these pulses are associated with triggering muscle contractions, pH changes, and electrolysis at the electrode electrolyte interface causing electrochemical reactions [27–33].

Recently suggested high-frequency bipolar pulses (HF-BP), first predominantly used for irreversible electroporation applications–HFIRE [34]—were demonstrated to also enable GET in vitro [15]. One of the characteristics of HF-BP pulses are reduced electrochemical reactions and less metal ions released from the electrodes compared to longer pulses [29,35]. Furthermore, HF-BP pulses induce less muscle contractions and pain during pulse delivery [36–39].

In addition, nanosecond pulses have already been used for GET. When applying 200 ns pulses (10–18 kV/cm) in bursts of ten with a varied pulse repetition rate (up to 1 MHz), it was shown that with the increase in the pulse repetition rate from 100 kHz to 1 MHz, GET increased, resulting in up to 17% GET with a minimal decrease in cell survival [40]. Furthermore, it was shown that with 100×300 ns pulses delivered at 1 MHz and at 5 kV/cm, up to 40% GET can be achieved, which is comparable to an efficiency of 4×100 μs, 1 Hz, 1.5 kV/cm pulse protocol [41].

Interestingly, nanosecond pulses have been suggested to disrupt nuclear envelope which could facilitate delivery of pDNA to the nucleus and thus increase GET [42–44]. Several papers have described using different combinations of nanosecond and milli- or microsecond pulses with the attempt to improve GET. Firstly, it was shown that GET could be increased about four times when cells were exposed to 3.5 ms pulse with 0.3 kV/cm followed by 60 ns pulse at 60 kV/cm after 30 min [45]. However, these results were not reproduced successfully. Later, no effects of nanosecond pulses on GET were observed by applying 8×5 ms or 4×200 µs pulses delivered at 1 Hz followed by 10, 12, or 15 ns pulses delivered at 10 Hz [46]. However, when the order of pulse delivery was reversed, a more pronounced effect of nanosecond pulses on GET was observed. Using the electroporation approach with a combination of nanosecond (600 ns, 100 kHz, 50 kV/cm) followed immediately by millisecond pulses (1×10 ms, 500 V/cm) more than doubled transgene expression; at the same time, cell survival levels were similar as in standard millisecond electroporation [42]. The combination of nanosecond pulses (23×60 ns, 1 Hz, 24 kV/cm) and millisecond electric pulses (1×5 ms, 50 V) led to a 40-fold increase in GET if nanosecond pulses were applied first followed by millisecond pulse, but not in the reverse order. This effect of nanosecond pulses was time restricted, with the highest efficiency occurring when nanosecond pulses were delivered 5 min before millisecond pulses [47].

Nanosecond pulses can potentially offer a solution to limitations that are present in GET with longer milli- and microsecond pulses. Namely, some cells exposed to GET may lose viability due to excessive heat, pH changes, and ionic imbalance [3]. Nanosecond pulses decrease electrochemical reactions during pulse delivery and in vivo settings offer more patient-friendly treatment, with reduced muscle contractions [40,48]. Heating is also decreased during nanosecond pulses application, which lowers the thermal effects of treatment [48,49]. Nanosecond pulses widen the use of electroporation while also having an effect on intracellular structures. It has been shown that nanosecond pulses can penetrate the cell interior and permeabilize membranes of internal organelles, such as endosomal vesicles, endoplasmic reticulum, nuclear envelope, and cytoskeleton, leading to the disruption of intracellular vesicles, release of calcium from endoplasmic reticulum, and immediate and prolonged loss of mitochondrial membrane potential [44,50–54]. Successful GET with shorter (i.e., less than 10 µs) pulses in vitro is, however, mostly achieved with high pDNA concentrations, which might be challenging to reach in in vivo settings, at least over a larger volume [2].

Conventional GET, using micro- to millisecond-long pulses, generally relies on electrophoresis to bring the pDNA molecules to the cell membrane for successful transfection [55]. However, for nanosecond duration pulses, electric field/electrophoresis might not be present for sufficient time to ensure a pDNA cell membrane contact. Even with HF-BP pulses, net electrophoretic movement is balanced out due to the bipolar nature of pulses. For these pulses (nanosecond and HF-BP), pDNA molecules then have to rely on diffusion to reach the cell membrane. Moreover, there is only a limited window of time during which the cell membrane is permeable and competent enough to absorb pDNA molecules for successful GET [1,56]. Therefore, depending on how far the pDNA molecule is from the cell membrane, or how concentrated the pDNA solution is, the efficiency of GET for the wide variety of pulse durations (nanosecond to millisecond) can be analyzed using the framework of how electrophoresis and diffusion influence the probability of pDNA molecule reaching the permeabilized cell membrane. A theoretical framework based on the drift-diffusion equation of probability density and the one-dimensional Fokker–Planck equation was used in this work to determine such probabilities [57]. A similar probabilistic framework has also been used earlier to evaluate probabilities of successful pDNA translocation through an electropore in the cell membrane, along with its qualitative comparison to experimental GET efficiencies [58], and has also been compared to experimental pDNA translocation efficiencies in model systems [59].

The purpose of this paper is to explore, evaluate, and demonstrate the potential use of different pulses for introducing pDNA into cells in vitro and to compare GET efficiency and dynamics of gene expression after GET. We performed experiments in vitro, on cell suspensions of immortalized human skin fibroblasts 1306 cell line and on C2C12 myoblasts, covering a range of pulse durations from 200 ns to 5 ms, monopolar and the recently used microsecond bipolar, so-called HFIRE pulses. To clarify the role of electrophoresis in the transport of pDNA in the electroporation medium during GET with different durations of electric pulses, we also developed a simple mathematical model that gives the probability of pDNA contact with the cell membrane during GET and compared experimental results with those calculated by the model.

2. Materials and Methods

2.1. Cells

Immortalized human skin fibroblasts 1306 cell line and C2C12 murine skeletal myoblasts cell line, both from European Collection of Authenticated Cell Cultures (cat no. #90011887 and #91031101, respectively) were used. Cells were grown in 25–150 mm^2 culture flasks (TPP, Trasadingen, Switzerland) for 2–4 days in an incubator (Kambič, Semič, Slovenia) at 37 °C, in a humidified atmosphere of 5% CO_2 in air for 1306 cell line and 10% CO_2 in air for C2C12 cell line. 1306 cells were cultured in Eagle's Minimum Essential Medium (EMEM) growth medium (Sigma Aldrich, Darmstadt, Germany) supplemented with 15% fetal bovine serum (Sigma Aldrich, Darmstadt, Germany), L-glutamine (StemCell, Vancouver, BC, Canada), and antibiotics penicillin/streptomycin (PAA, Vienna, Austria) and gentamycin (Sigma Aldrich, Darmstadt, Germany). C2C12 cells were cultured in Dulbecco's Modified Eagle's Medium (DMEM) growth medium (Sigma Aldrich, Darmstadt, Germany) supplemented with 10% fetal bovine serum (Sigma Aldrich, Darmstadt, Germany), L-glutamine (StemCell, Vancouver, BC, Canada), and antibiotics penicillin/streptomycin (PAA, Vienna, Austria) and gentamycin (Sigma Aldrich, Darmstadt, Germany).

For experiments cells in exponential growth phase were trypsinized using trypsin–EDTA; 5 g trypsin/2 g EDTA in 0.9% NaCl (Sigma Aldrich, Darmstadt, Germany) 10 × diluted in Hanks' Balanced Salt solution (Sigma Aldrich, Darmstadt, Germany). From the obtained cell suspension, trypsin and growth medium were removed by centrifugation at 180× *g* for 5 min at room temperature (Sigma 3–15 K, Welwyn Garden City, UK). The cell pellet was then resuspendend in EMEM growth medium for 1306 cell line or DMEM growth medium for the C2C12 cell line to obtain a final cell density of 2 × 10^6 cells/mL.

2.2. Cell Size Measurement

Cells in suspension were transferred to Lab-Tek chamber and imaged with inverted Thunder Imager Live Cell system. Moreover, 16-bit images were acquired with a deep-cooled 4.2 MP sCMOS Leica DFC9000 Gt fast camera in the Leica Application Suite X (LAS X) software. Cell diameter was measured using the ImageJ software (accessed on 10 May 2022, http://imagej.nih.gov/ij/). For each cell line 20 cells were measured. Results are presented as mean ± standard deviation. Measured diameters were used in calculating the pDNA to membrane distance.

2.3. Nanosecond Pulses

Pulses of 200 ns or 500 ns duration were delivered by CellFX System electroporator (Pulse Biosciences, Hayward, CA, USA). The electric field strength (E) was calculated from the voltage measured by 1 kΩ resistor and Pearson current monitor model 2877 (1 V/1 A, 200 MHz) (Pearson Electronics, Palo Alto, CA, USA) during the experiment divided by the distance between the electrodes. We also measured the current during each pulse by Pearson current monitor model 2878 (1 V/10 A, 70 MHz) (Pearson Electronics, Palo Alto, CA, USA). Voltage and current measurements were monitored by the oscilloscope WaveSurfer 3024Z, 200 MHz (Teledyne LeCroy, Chestnut Ridge, NY, USA). 25, 100, or

300 pulses were delivered with 5 or 10 Hz pulse repetition frequency at electric field range of 0–19 kV/cm.

2.4. High Frequency Bipolar Pulses

For the delivery of 2 µs high-frequency bipolar pulses, a prototype high-frequency pulse generator L-POR was used (mPOR, Ljubljana, Slovenia). The L-POR electroporator is intended for laboratory use. It enables the generation of high-frequency symmetric and asymmetric bipolar electroporation pulses up to 1400 V and duration of pulses from 500 ns with a pulse repetition rate of up to 1 MHz. It also enables the generation of pulses in bursts. The pulses delivered were monitored by a high-voltage differential probe HVD3605A (Teledyne LeCroy, Chestnut Ridge, NY, USA), current probe CP031 (Teledyne LeCroy, Chestnut Ridge, NY, USA) and HDO6000 High-Definition oscilloscope (Teledyne LeCroy, Chestnut Ridge, NY, USA). In HF-BP pulse protocol, bipolar pulses of 2 µs duration of positive and negative phase were applied. The pause between positive and negative pulse phase and pause between bipolar pulses were 2 µs. 100 bursts were applied, and in each burst, 32 pulses were delivered. Burst repetition rate was 1 Hz [15]. We tested electric field range 0–2.5 kV/cm.

2.5. Micro and Millisecond Pulses

Monopolar rectangular pulses of 100 µs or 5 ms duration were delivered with a laboratory prototype pulse generator (University of Ljubljana), based on H-bridge digital amplifier with 1 kV MOSFETs (DE275-102N06A, IXYS, Milpitas, CA, USA) [60]. Pulse delivery was monitored by the oscilloscope WaveSurfer 422, 200 MHz with high-voltage differential voltage probe ADP305 and current probe CP030 (Teledyne LeCroy, Chestnut Ridge, NY, USA). For microsecond pulses, eight 100 µs pulses with electric fields 0–2 kV/cm and for millisecond pulses eight 5 ms pulses with electric fields 0–1.25 kV/cm were tested.

2.6. Permeabilization

Cell membrane permeabilization of 1306 and C2C12 cells in suspension was expressed as percentage of propidium iodide (PI) fluorescent cells. First, 5 µL of 1.5 mM PI was added to 200 µL of cells in growth medium at concentration 2×10^6 cells/mL in electroporation cuvette with 2 mm gap (VWR International, Radnor, PA, USA). Emission of PI fluorescence was detected by flow cytometry (Attune NxT, Carlsbad, CA, USA) using a blue laser excitation at 488 nm and detecting the emitted fluorescence through a 574/26 nm band-pass filter, 3 min after exposure of cells to electric pulses. Data for percentage of permeabilized cells and their median fluorescence intensity were collected. At every measurement 10,000 events were recorded. Data obtained were analyzed with the Attune NxT software (version 3.1.2).

2.7. Temperature Measurement during Pulse Delivery

The temperature of the cell sample was monitored during pulse delivery for all five pulse protocols and for both cell lines. The fiber optic sensor system (opSens, Québec, QC, Canada), which consisted of ProSens signal conditioner and a fiber optic temperature sensor OTG-M170, was used. The fiber optic sensor was carefully placed in the cell suspension in the middle of the gap between the electrodes in the cuvette. Sampling frequency was 1000 Hz. Two measurements were taken for each of the five pulse protocols and for both cell lines.

2.8. Cell Survival after Permeabilization

For cell survival experiments, 200 µL of cells in suspension in growth medium at concentration 2×10^6 cells/mL was pipetted in a 2 mm gap electroporation cuvette (VWR International, Radnor, PA, USA) and exposed to electric pulses. After pulse application, 50 µL of fetal bovine serum (Sigma Aldrich, Darmstadt, Germany) was added to cell suspension. Cells were incubated for 5 min at 37 °C [61]; afterwards, 1×10^4 C2C12

myoblasts or 2×10^4 1306 fibroblasts from cuvette were seeded in 100 µL of growth medium in a 96-well plate (TPP, Trasadingen, Switzerland). Cells were seeded in triplicates. The plate was then incubated for 24 h (37 °C, 10% CO_2 for C2C12 and 37 °C, 5% CO_2 for 1306). Cell survival was determined with the MTS-based Cell Titer 96 AQueous One Solution Cell Proliferation Assay (Promega, Madison, WI, USA). After incubation, 20 µL of MTS reagent were added to each well and cells were incubated for additional 2 h in the incubator (37 °C, 10% CO_2 for C2C12 and 37 °C, 5% CO_2 for 1306). Absorption at 490 nm wavelength was measured with a Tecan Infinite M200 spectrophotometer (Tecan, Männedorf, Switzerland). An average absorption obtained in the samples containing only growth medium was subtracted from the absorption measured in cell samples. To calculate the percentage of viable cells the absorption of each cell sample was divided by an average absorption of the control cell samples, where cells were treated as described but not exposed to electric pulses.

2.9. Plasmids

A 4.7 kb plasmid pEGFP-N1 (Clontech Laboratories Inc., Mountain View, CA, USA) and a 3.5 kb plasmid pmaxGFP (Lonza, Basel, Switzerland) both encoding green fluorescent protein (GFP) under the control of CMV promotor were used. pDNA was amplified using Escherichia coli and isolated with HiSpeed Plasmid Maxi Kit (Qiagen, Hilden, Germany). pDNA concentration was spectrophotometrically determined at 260 nm. We tested six different pDNA concentrations, namely, 40, 60, 80, 100, 250, and 500 µg/mL.

2.10. Gene Electrotransfer and Cell Survival after Gene Electrotransfer

A volume of 200 µL of cell suspension with different concentrations of pDNA was exposed to electric pulses in electroporation cuvettes with a 2 mm gap (VWR International, Radnor, PA, USA). After pulse delivery, 50 µL of fetal bovine serum (Sigma Aldrich, Darmstadt, Germany) was added to each cuvette, and cells were incubated 5 min at 37 °C [61,62]. After incubation, 1×10^5 1306 cells and 5×10^4 C2C12 cells from cuvette were transferred to a 24-well plate (TPP, Trasadingen, Switzerland) and seeded in growth medium for gene electrotransfer determination. From the rest of the cell sample in cuvette, 1×10^4 C2C12 myoblasts or 2×10^4 1306 fibroblasts were seeded in triplicates in 100 µL of growth medium in a 96-well plate (TPP, Trasadingen, Switzerland) to determine cell survival. Both plates were incubated for 24 h (37 °C, 10% CO_2 for C2C12 and 37 °C, 5% CO_2 for 1306).

After incubation, cells in 24-well plates were trypsinized and resuspended in 200 µL of PBS. Percentage of GFP-positive cells and median fluorescence intensity (MFI) of GFP-positive cells were detected using flow cytometer (Attune NxT, Carlsbad, CA, USA) with a blue laser at 488 nm and a 530/30 nm bandpass filter. At every measurement, 10,000 events were recorded. Data obtained were analyzed with the Attune NxT software (version 3.1.2).

Cell survival was determined with the MTS-based Cell Titer 96 AQueous One Solution Cell Proliferation Assay (Promega, Madison, WI, USA). After incubation, 20 µL of MTS reagent was added to each well, and cells were incubated for an additional 2 h in the incubator (37 °C, 10% CO_2 for C2C12 and 37 °C, 5% CO_2 for 1306). Absorption at 490 nm wavelength was measured with a Tecan Infinite M200 spectrophotometer (Tecan, Switzerland). An average absorption obtained in the samples containing only growth medium was subtracted from the absorption measured in cell samples. To calculate the percentage of viable cells the absorption of each sample was divided by an average absorption of the control samples.

2.11. Overall Gene Electrotransfer

When reporting GET efficiency, we distinguish between percentage of transfected cells among cells that survived the treatment and overall gene electrotransfer (overall GET), which represents the percentage of transfected cells relative to the initial population, which

considers both the efficiency of transfection and cell survival. Overall, GET was calculated as: overall GET (%) = GET (%) × cell survival (%)/100.

2.12. The Time Dynamics of Transgene Expression

Cells were electrotransfected with 500 μg/mL of pEGFP-N1 plasmid as described in point gene electrotransfer and cell survival after gene electrotransfer. After incubation, sample was divided into 14 parts, and cells were seeded in different numbers (1×10^5–5×10^3) to a 24-well plate (TPP, Trasadingen, Switzerland) and placed in the incubator (37 °C, 5% CO_2). For the next 5 days, every 8 h, cells from one well of the 24-well plate (TPP, Trasadingen, Switzerland) were trypsinized and resuspended in 200 μL of PBS and percentage of GFP-positive cells and median fluorescence intensity of GFP-positive cells were detected using flow cytometer (Attune NxT, Carlsbad, CA, USA) with a blue laser at 488 nm and a 530/30 nm bandpass filter. At every measurement 10,000 events were recorded. Data obtained were analyzed with the Attune NxT software (version 3.1.2).

2.13. Statistical Analysis

All results are reported as a mean value of 3 or 4 experiments. The spread of the data is given by standard deviation. The significance between the experimental groups was analyzed in SigmaPlot 11.0 (Systat Software Inc., Chicago, IL, USA) and determined using One-way ANOVA test followed by Tukey's multiple comparison test. Statistically significant difference was assumed at $p < 0.05$.

2.14. Modeling the Probability of pDNA and Cell Membrane Contact during GET

To determine the probability of pDNA and cell membrane contact, the distance of a pDNA molecule from the cell membrane needs to be determined. This pDNA–cell membrane distance depends on the concentration of pDNA. To determine the pDNA–cell membrane distance, we followed [16,55].

The radius of the cell is R_{cell}, and there is a total of N_{cells} in the suspension. The total volume occupied by the cells in suspension is thus $V_{cells} = N_{cells} \cdot \left(\frac{4}{3} \pi R_{cell}^3 \right)$. For a solution volume (V_{sol}), the volume space left to be occupied by pDNA molecules is:

$$V_{DNA} = V_{sol} - N_{cells} \cdot \left(\frac{4}{3} \pi R_{cell}^3 \right) \tag{1}$$

For pDNA molecules at a concentration (c_{DNA}) and with molecular weight (M_w), the total number of pDNA molecules in the solution is $N_{DNA} = \frac{c_{DNA} \cdot V_{sol} \cdot N_A}{M_w}$, where N_A is the Avogadro's number. Assuming the space available to a single pDNA molecule is defined by a sphere of radius of R_{DNA} (Figure 1), the volume occupied by pDNA molecules in the solution is $V_{DNA} = N_{DNA} \cdot \frac{4}{3} \pi R_{DNA}^3$ or:

$$V_{DNA} = \left(\frac{c_{DNA} \cdot V_{sol} \cdot N_A}{M_w} \right) \cdot \frac{4}{3} \pi R_{DNA}^3 \tag{2}$$

Thus, equating (1) and (2), we obtain $\left(\frac{c_{DNA} \cdot V_{sol} \cdot N_A}{M_w} \right) \cdot \frac{4}{3} \pi R_{DNA}^3 = V_{sol} - N_{cells} \cdot \left(\frac{4}{3} \pi R_{cell}^3 \right)$, or the space available to a single pDNA molecule in a sphere, is defined by radius R_{DNA} as follows:

$$R_{DNA} = \left(\frac{1 - \rho_{cell} \cdot \left(\frac{4}{3} \pi R_{cell}^3 \right)}{\frac{4}{3} \pi \cdot \left(\frac{c_{DNA} \cdot N_A}{M_w} \right)} \right)^{1/3} \tag{3}$$

where $\rho_{cell} = \frac{N_{cells}}{V_{sol}}$. R_{DNA} was then calculated using Equation (3) for different values of c_{DNA} and is shown in Supplementary Table S1. The following set of parameters were used— cell density (ρ_{cell}) = 2×10^6 cells/mL, molecular weight of pDNA (M_w) = 660 g/mol/bp ×

4700 bp = 3,102,000 g/mol for pEGFP-N1 pDNA, Avogadro's constant (N_A) = 6.023 × 10^{23}, R_{cell}(C2C12) = 8.4 μm, and R_{cell}(1306) = 7.15 μm.
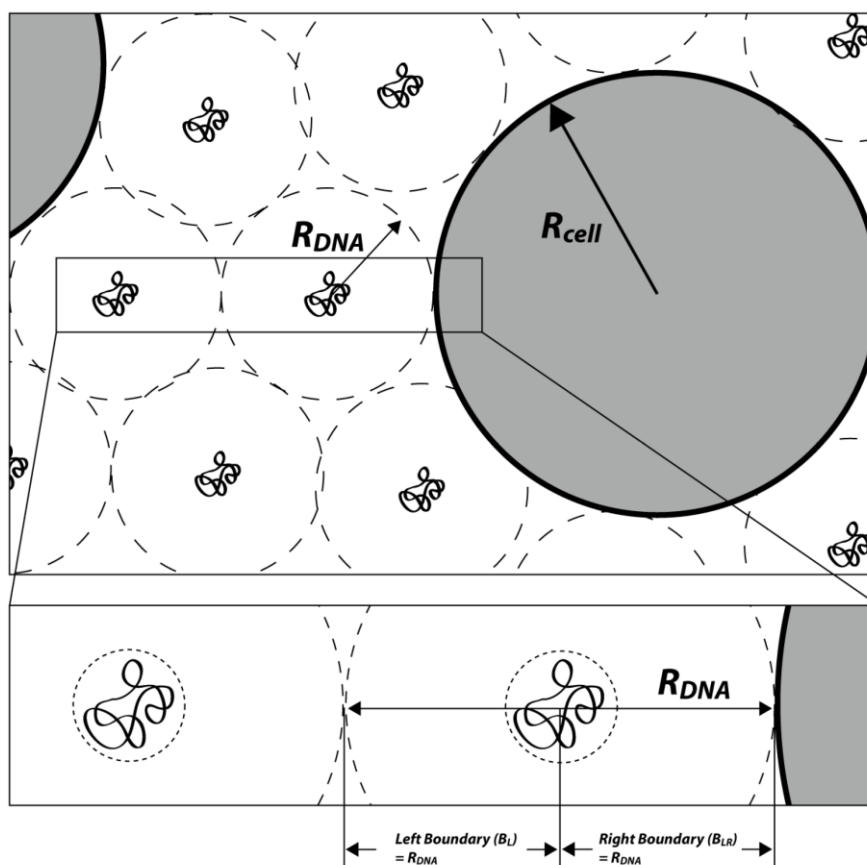
Figure 1. Schematic of distribution of pDNA molecules and cells in suspension. R_{cell} represents the radius of the cell, R_{DNA} represents the radius of the (nominal/free) spherical space available to the pDNA molecule. Subset in figure shows the boundaries within which a pDNA molecule close the cell membrane is allowed to move.

R_{DNA} can be considered as an estimate for the distance between a pDNA molecule and the nearest cell membrane. Furthermore, the boundaries within which a pDNA molecule can move needs to be defined for the model which determines the probability of pDNA molecule coming in contact with the cell membrane. Based on Figure 1, a natural choice for the right boundary (B_R), which constitutes the cell membrane, is R_{DNA}. Since R_{DNA} is the radius of spherical space available to the pDNA in the solution, the left boundary (B_L) is also considered as R_{DNA}. Other estimates of B_L and B_R can be considered, such as R_{DNA}, $R_{DNA} - R_g$ and $2R_{DNA} - 2R_g$, where R_g is the radius of gyration of the pDNA molecule. These are explained in the Supplementary Figure S1.

To determine the probability that a pDNA molecule reaches the permeabilized cell membrane, we assume a 1D case where a pDNA molecule can only move along the one axis (direction of applied electric field) bounded by the left and the right boundaries (Figure 2). The fundamental contribution of electrophoresis and diffusion to the probability of a pDNA molecule reaching the permeabilized cell membrane can be captured in 1D (in the direction of the electric field). We expect that the addition of extra dimensions will not contribute significantly to a more detailed picture of the process with the probabilistic framework described below.
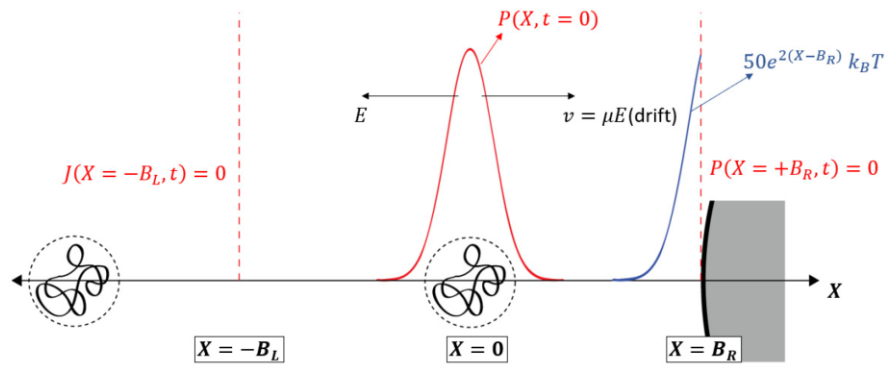
Figure 2. Schematic of the biased random walk of pDNA molecule along the *X*-axis due to drift (electrophoresis), diffusion, and a free energy barrier. Electric field acts along the negative *X*-axis, which creates a drift in the pDNA molecule along the positive *X*-axis. The pDNA molecule is initially centered at $X = 0$ with the initial condition defined by a narrow-band Gaussian distribution. The boundary conditions at the right ($X = +B_R$) and left ($X = -B_L$) of the domain are the absorbing and reflecting boundary conditions, respectively. A free energy barrier between the pDNA molecule and the cell membrane is present at the right boundary ($X = +B_R$).

The simplicity of such a 1D assumption enhances the pedagogical aspect of inferring the role of diffusion and electrophoresis in bringing the pDNA molecule to the permeabilized membrane (a prerequisite for GET) for a wide variety of experimental conditions used (e.g., pulse durations ranging from nanosecond to millisecond and concentrations ranging from 40 µg/mL to 500 µg/mL). The purpose of the model is not an estimation and/or prediction of experimental outcomes such as GET efficiency or MFI.

The probability density ($P(X, t)$) of finding the pDNA molecule at particular location along the *X*-axis at time *t* can be described using the following drift–diffusion equation of probability density [57]:

$$\frac{\partial P(X,t)}{\partial t} = -v\frac{\partial P(X,t)}{\partial X} + D\frac{\partial^2 P(X,t)}{\partial X^2} \qquad (4)$$

Equation (4) does not assume any interaction between the pDNA molecule and the cell membrane. However, a pDNA and cell membrane interaction free energy $F(X)$ can be assumed between the pDNA molecule and the cell membrane. In this case, the probability density of finding a particle at a particular location along the *X*-axis at time *t* can be described using the one-dimensional Fokker–Planck equation [57]:

$$\frac{\partial P(X,t)}{\partial t} = \frac{D}{k_B T}\frac{\partial}{\partial X}\left[\frac{\partial F(X)}{\partial X}P(X,t)\right] - v\frac{\partial P(X,t)}{\partial X} + D\frac{\partial^2 P(X,t)}{\partial X^2} \qquad (5)$$

51

The free energy barrier $F(X)$ is assumed to be $F(X) = 50e^{2(X-B_R)} k_B T$, i.e., a barrier with a height of 50 $k_B T$ that steeply decays exponentially away from the cell membrane at $X = +B_R$ (Figure 2). Such a barrier is inspired from [63]. The drift term in Equations (4) and (5) is due to the electrophoresis of the pDNA molecule and is given by $v = \mu E$, where μ is the electrophoretic mobility of the pDNA molecule ($\mu = -3.75 \times 10^{-8}$ m^{2}V^{-1}s^{-1}) [59,64,65] and E is the electric field intensity. The diffusion coefficient of pDNA is taken as $D = 10^{-12}$ m^{2}s^{-1} [65]. Equation (4) describes the process of finding pDNA at a particular location along the X-axis as a biased random walk, where the bias is due to electrophoresis of pDNA molecule. Equation (5) describes the same process of finding pDNA at a particular location along the X-axis based on a bias (electrophoresis), diffusion, and free energy interaction (barrier) with the cell membrane. The drift term in Equations (4) and (5) is non-zero only when the electric field pulse is present and is zero otherwise.

Equations (4) and (5) are solved for the probability density function $P(X, t)$ in the domain $X \in [B_L, B_R]$ with appropriate boundary and initial conditions using the pdepe() function in MATLAB® (R2021b). The initial condition for the pDNA molecule is considered as a narrow-band Gaussian/normal distribution with zero mean (centered at $X = 0$, Figure 2) and a standard deviation of 10 nm. The boundary at the right (positive end of the domain), i.e., the cell membrane, is considered an absorbing boundary condition, implying that once pDNA reaches the cell membrane, it is absorbed into the cell membrane, i.e., it is internalized and expressed by the cell. The resulting boundary condition at $X = +B_R$ is thus $P(X = +B_R, t) = 0$. The left boundary is considered to be a reflective barrier, implying that once the pDNA molecule reaches the left boundary, it is reflected back into the domain, i.e., the flux in the probability density function is zero. Flux for Equation (4) is given by $J(X, t) = vP(X, t) - D\frac{\partial P}{\partial X}(X, t)$ and for Equation (5) by $J(X, t) = \frac{D}{k_B T}\left[-\frac{\partial F(X)}{\partial X}\right]P(X, t) + vP(X, t) - D\frac{\partial P}{\partial X}(X, t)$. Thus, the resulting left boundary condition for Equation (4) is $vP(X = -B_L, t) - D\frac{\partial P}{\partial X}(X = -B_L, t) = 0$ and for Equation (5) is $\frac{D}{k_B T}\left[-\frac{\partial F(X = -B_L)}{\partial X}\right]P(X = -B_L, t) + vP(X = -B_L, t) - D\frac{\partial P}{\partial X}(X = -B_L, t) = 0$.

The concentration dependance of the experimental results is modeled by varying the location of the right (B_R) and the left (B_L) boundaries. These boundaries are defined by the free sphereical space (R_{DNA} in Figure 1) available to the pDNA molecule which shrinks or expands depending upon high or low concentration, respectively. Various estimates of R_{DNA} are given in Supplementary Table S1 for different concentrations. Since concentrations in the experiments in the current work vary from 40 μg/mL to 500 μg/mL, $B_L, B_R = R_{DNA}$ is varied from 312 nm to 134 nm, respectively. However, values of R_{DNA} as small as 77 nm (corresponding to 2500 μg/mL) and as high as 433 nm (corresponding to 15 μg/mL) are also considered to analyse a larger spectrum of concentrations that could be commonly found in GET experiments. It should be noted that boundaries of the domain $X \in [B_L, B_R]$ are defined using $B_L, B_R = R_{DNA}$ (Figure 1), the values for which are given in Supplementary Table S1 for different concentrations. However, other definitions of B_L, B_R can be used (see Figure S1), the values for which are given in Supplementary Table S2. Finally, Equations (4) and (5) are solved for the probability density function $P(X, t)$ in the domain $X \in [B_L, B_R]$.

3. Results

In this paper, different electric pulses were used to introduce pDNA into cells in vitro. We compared GET efficiency and the time dynamics of transgene expression after GET performed by using different pulses. The experiments were performed on cell suspensions of 1306 fibroblasts and on C2C12 myoblasts with a range of pulse durations from 200 ns to 5 ms, monopolar and bipolar pulses. The results are presented as the percentage of transfected cells (GET), quantity of produced transgene measured as median fluorescence intensity (MFI) and as the percentage of transfected cells considering cell survival (overall GET).

We first determined the optimal electric field amplitudes used in GET for each pulse protocol based on permeabilization and survival curves. After determining optimal electric field amplitude, the effect of pDNA concentration on GET, MFI, cell survival, and overall GET was determined. We compared the overall GET and MFI of all pulse durations at the highest pDNA concentration. Furthermore, with a subset of pulses, we explored the effect of different pDNA sizes on GET, MFI, cell survival, and overall GET. We also monitored the time dynamics of pDNA expression after GET with different pulse durations. Lastly, based on the data obtained in the experiments of the pDNA concentration effect on GET, the model of the probability of pDNA and cell membrane contact during GET was developed. The model was compared to GET efficiency using different pulse durations, with the aim to determine the importance of diffusive and electrophoretic movement of pDNA.

3.1. Determining Optimal Electric Field Amplitude for GET

In order to determine the optimal parameters for GET (intersections of permeabilization and survival curves) for C2C12 myoblast and 1306 fibroblast cell lines, we varied the nanosecond pulse parameters—pulse duration: 200 or 500 ns; pulse number: 25, 100, or 300 pulses; pulse repetition frequency: 5 or 10 Hz, and delivered electric field: 0–19 kV/cm.

In both cell lines, C2C12 myoblasts and 1306 fibroblasts, we achieved >90% cell membrane permeabilization, with different pulse durations of 200 ns and 500 ns and different tested pulse numbers, 25, 100, and 300 pulses (Supplementary Figures S2 and S3). No significant difference in permeabilization, survival, and PI MFI curves was observed when changing pulse repetition frequency (5 or 10 Hz) for 200 ns and 500 ns pulses for all three pulse numbers tested in C2C12 myoblasts (data not shown). Based on this, we decided to use only a 10 Hz pulse repetition frequency for experiments with 1306 fibroblasts.

Intersections of permeabilization and survival curves were observed at similar electric fields for C2C12 myoblasts and 1306 fibroblasts, except for 25 × 200 ns pulses, where the intersection of permeabilization and survival curves was observed at a lower electric field in 1306 cells—12–14 kV/cm compared to 15–18 kV/cm for C2C12 myoblasts (Supplementary Figure S2). Since cell size can influence the permeabilization threshold, we measured the diameters of cells in suspension, which were 16.8 ± 1.8 μm for C2C12 myoblasts and 14.3 ± 1.4 μm for 1306 fibroblasts.

A higher MFI of PI-positive cells was observed with 500 ns pulses compared to 200 ns duration pulses; additionally, the MFI increased with the increasing number of pulses from 25 to 300 in both pulse durations tested. Comparing MFI between C2C12 myoblasts and 1306 fibroblasts, lower MFI was observed in 1306 fibroblasts with both 200 ns and 500 ns pulses but only at high electric field amplitudes (Supplementary Figure S4).

The HF-BP pulse protocol consisted of bipolar pulses of 2 μs duration of positive and negative phase, 2 μs pause between positive and negative pulse phase, and pause between bipolar pulses. We applied 100 bursts, each containing 32 pulses. The burst repetition rate was 1 Hz, and the applied electric field was 0–2.5 kV/cm. For microsecond pulses we delivered: 8 × 100 μs, 1 Hz pulse repetition frequency, with the applied electric filed, 0–2 kV/cm and for millisecond pulses; 8 × 5 ms, 1 Hz pulse repetition frequency and applied electric filed, 0–1.25 kV/cm.

Permeabilization and survival curves for HF-BP pulse protocol behave similarly as permeabilization and survival curves of 8 × 100 μs pulse protocol for both cell lines. Permeabilization was achieved at lower values of electric field for 8 × 5 ms compared to 8 × 100 μs pulse protocol and survival deceased at lower values of electric field for 8 × 5 ms compared to 8 × 100 μs pulse protocol in both cell lines. MFI of permeabilized cells was higher at lower values of electric field when longer millisecond pulses were applied. Similarly, as for nanosecond pulses permeabilization, the MFI of permeabilized cells with a high electric field with HF-BP, micro-, and millisecond pulses was lower in 1306 cells compared to C2C12 myoblasts (Supplementary Figures S5 and S6).

After the initial parameters were determined, based on the permeabilization and survival curve, further optimization for every pulse protocol was performed. Performing

GET, we tested three different electric field amplitudes in the range of slightly below to slightly above the intersection of permeabilization and survival curve to determine the electric field at which the overall GET was the best (data not shown). Pulse protocols with chosen electric fields used to determine the effect of pDNA concentration and the time dynamics of transgene expression are given Table 1.

Table 1. Pulse protocols used to determine the effect of pDNA concentration.

C2C12 (16.8 ± 1.8 μm)	1306 (14.3 ± 1.4 μm)
25 × 200 ns, 10 Hz, 15.8 kV/cm	25 × 200 ns, 10 Hz, 12.8 kV/cm
100 × 500 ns, 10 Hz, 4.1 kV/cm	25 × 500 ns, 10 Hz, 6.5 kV/cm
2-2-2-2, 32 p, 100 b, 1 Hz, 1.25 kV/cm	2-2-2-2, 32 p, 100 b, 1 Hz, 1 kV/cm
8 × 100 μs, 1 Hz, 1.25 kV/cm	8 × 100 μs, 1 Hz, 1.25 kV/cm
8 × 5 ms, 1 Hz, 0.4 kV/cm	8 × 5 ms, 1 Hz, 0.6 kV/cm

For each cell line, only one 200 ns and one 500 ns pulse protocol were used to determine the effect of the pDNA concentration on GET. We chose pulse protocols with which the best overall GET of 500 μg/mL of pEGFP-N1 was obtained (Table 1).

3.2. Effect of pDNA Concentration on GET, MFI, Cell Survival, and Overall GET

In determining the effect of pDNA concentration on GET, MFI, cell survival, and overall GET, six different concentrations of pEGFP-N1 were tested, namely, 0, 40, 80, 100, 250, and 500 μg/mL..

The GET in C2C12 myotubes was significantly higher with HF-BP, 8 × 100 μs, and 8 × 5 ms pulses compared to nanosecond pulses for all pDNA concentrations tested (Figure 3A). Interestingly, in 1306 fibroblasts, the GET was higher with HF-BP, 8 × 100 μs, and 8 × 5 ms pulses compared to nanosecond pulses up to 250 μg/mL of pDNA. However, at the highest pDNA concentration in 1306 fibroblast, there were no significant differences in the GET between all pulse protocols (Figure 3C).

The effect of the pDNA concentration on GET depends on the cell line. However, the efficiency of nanosecond pulses depends more on the pDNA concentration compared to HF-BP, 8 × 100 μs, and 8 × 5 ms pulses in both cell lines.

The MFI of cells is indicative of how many pDNA copies were successfully transcribed and translated into fluorescent protein. The MFI of GFP-positive cells was higher in 1306 fibroblasts at all pDNA concentrations when compared to C2C12 myoblasts for all pulse protocols. The MFI of C2C12 myoblast was the highest with 8 × 5 ms pulse protocol followed by 8 × 100 μs, HF-BP, and the lowest with nanosecond pulse protocols. Interestingly, the MFI of C2C12 myoblasts slowly increased up to 250 μg/mL of pDNA and then reached a plateau. For pulse protocols 8 × 5 ms and 8 × 100 μs, there was a small increase in MFI from 250 μg/mL to 500 μg/mL pDNA concentration, but not statistically significant (Figure 3B).

Similarly, MFI of 1306 fibroblasts was also different compared to C2C12 myoblasts. At the highest pDNA concentration, the MFI of 1306 fibroblasts was the highest with the 8 × 100 μs pulse protocol followed by the nanosecond, HF-BP, and 8 × 5 ms pulse protocols. The MFI after the HF-BP and 8 × 5 ms pulse protocols increased gradually with increasing pDNA concentration. With the 8 × 100 μs pulse protocol, a significant increase was observed between 100 μg/mL and 250 μg/mL pDNA concentration. Interestingly, the MFI of 1306 fibroblasts increased significantly from 250 μg/mL to of 500 μg/mL pDNA concentration with both 200 ns and 500 ns pulse protocols (Figure 3D). The MFI of GFP-positive cells is cell-line-dependent and increases with increasing pDNA concentration.
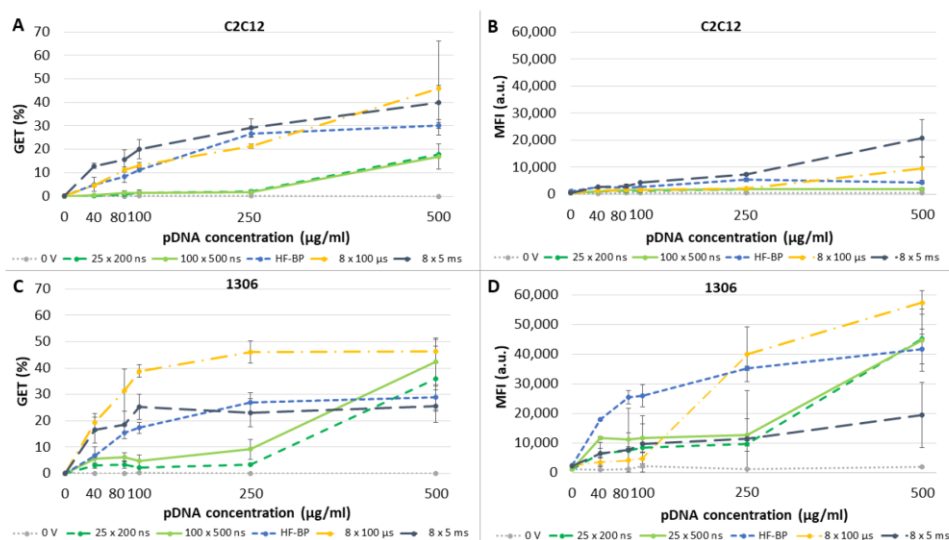
Figure 3. GET and median fluorescence intensity (MFI) of GFP-positive cells with different concentrations of pEGFP-N1 pDNA. (**A**) GET of C2C12 myoblasts, pulses: 25×200 ns: 25×200 ns, 10 Hz, 15.8 kV/cm; 100×500 ns: 100×500 ns, 10 Hz, 4.1 kV/cm; HF-BP: 2-2-2-2, 32p, 100b, 1 Hz, 1.25 kV/cm; 8×100 µs: 8×100 µs, 1 Hz, 1.25 kV/cm; and 8×5 ms: 8×5 ms, 1 Hz, 0.4 kV/cm. (**B**) MFI of C2C12 myoblasts, pulses: 25×200 ns: 25×200 ns, 10 Hz, 15.8 kV/cm; 100×500 ns: 100×500 ns, 10 Hz, 4.1 kV/cm; HF-BP: 2-2-2-2, 32p, 100b, 1 Hz, 1.25 kV/cm; 8×100 µs: 8×100 µs, 1 Hz, 1.25 kV/cm; and 8×5 ms: 8×5 ms, 1 Hz, 0.4 kV/cm. (**C**) GET of 1306 fibroblasts, pulses: 25×200 ns: 25×200 ns, 10 Hz, 12.8 kV/cm; 25×500 ns: 25×500 ns, 10 Hz, 6.5 kV/cm; HF-BP: 2-2-2-2, 32p, 100b, 1 Hz, 1 kV/cm; 8×100 µs: 8×100 µs, 1 Hz, 1.25 kV/cm; and 8×5 ms: 8×5 ms, 1 Hz, 0.6 kV/cm. (**D**) MFI of 1306 fibroblasts, pulses: 25×200 ns: 25×200 ns, 10 Hz, 12.8 kV/cm; 25×500 ns: 25×500 ns, 10 Hz, 6.5 kV/cm; HF-BP: 2-2-2-2, 32p, 100b, 1 Hz, 1 kV/cm; 8×100 µs: 8×100 µs, 1 Hz, 1.25 kV/cm; and 8×5 ms: 8×5 ms, 1 Hz, 0.6 kV/cm. 0 V represents control where cells were not exposed to electric pulses. Results are represented as an average of 3 repetitions. Statistical differences are given in the text. Bars represent standard deviation.

High concentration of pDNA used for GET was reported to affect cell survival [16]. In our study, however, with 8×5 ms pulses, we did not observe any decrease in cell survival with increasing pDNA concentrations compared to cells that were exposed just to electric pulses in both cell lines. In addition, in C2C12 myoblasts, pDNA concentration did not have any effect on cell survival after GET with 500 ns and 200 ns pulse protocols. With the 8×100 µs pulse protocol in C2C12, survival was significantly lower, with 500 µg/mL of pDNA. Interestingly, with HF-BP pulses in C2C12 myoblasts, a significant decrease in cell survival was observed already with the lowest pDNA concentration (40 µg/mL). In 1306 fibroblasts with the 500 ns and 200 ns pulse protocols, survival was significantly lower, with 500 µg/mL of pDNA. With HF-BP pulses with concentrations higher than 100 µg/mL and with the 8×100 µs pulse protocol, survival was significantly lower with 250 µg/mL and 500 µg/mL of pDNA (Figure 4). Our results suggest that the decrease in survival after GET with high pDNA concentrations is cell-line-dependent.

Figure 4. Cell survival with different concentrations of pEGFP-N1 pDNA. (**A**) C2C12 myoblasts, pulses: 25×200 ns: 25×200 ns, 10 Hz, 15.8 kV/cm; 100×500 ns: 100×500 ns, 10 Hz, 4.1 kV/cm; HF-BP: 2-2-2-2, 32p, 100b, 1 Hz, 1.25 kV/cm; 8×100 µs: 8×100 µs, 1 Hz, 1.25 kV/cm; and 8×5 ms: 8×5 ms, 1 Hz, 0.4 kV/cm; and (**B**) 1306 fibroblasts, pulses: 25×200 ns: 25×200 ns, 10 Hz, 12.8 kV/cm; 25×500 ns: 25×500 ns, 10 Hz, 6.5 kV/cm; HF-BP: 2-2-2-2, 32p, 100b, 1 Hz, 1 kV/cm; 8×100 µs: 8×100 µs, 1 Hz, 1.25 kV/cm; and 8×5 ms: 8×5 ms, 1 Hz, 0.6 kV/cm. 0 V represents control where cells were not exposed to electric pulses. Results are represented as an average of 3 repetitions. Statistical differences are given in the text. Bars represent standard deviation.

When also considering cell survival, i.e., calculating overall GET, we obtained the results presented in Figure 5. The overall GET increased with the increasing pDNA concentration for all pulse protocols and both cell lines. In C2C12 myoblasts, the highest overall GET was reached with 8×5 ms and 8×100 µs pulse protocols, followed by HF-BP, 500 ns, and 200 ns protocols. With all five pulse protocols, the overall GET increased up to the highest pDNA concentration used, i.e., 500 µg/mL. In C2C12 myoblasts, the overall GET with 40, 80, and 100 µg/mL pDNA concentrations was, however, below 1% with both 200 ns and 500 ns pulses (Figure 5A).

In 1306 fibroblasts, the highest overall GET was observed with 8×100 µs pulse protocol regardless of pDNA concentration used. Interestingly, with the highest pDNA concentration, i.e., 500 µg/mL, using the 8×5 ms pulse protocol, we achieved the lowest overall GET, even lower than the nanosecond and HF-BP pulse protocols. In addition, the overall GET increase with the increasing pDNA concentration was different compared to C2C12 myoblasts. In 1306 fibroblasts with the 8×100 µs, 8×5 ms, and HF-BP

pulse protocols, a plateau in the overall GET was observed between 100 μg/mL and 500 μg/mL pDNA concentrations, where the overall GET did not increase significantly with the increasing pDNA concentration. In contrast, with nanosecond pulse protocols, a significant increase in overall GET was observed between 250 μg/mL and 500 μg/mL pDNA concentration (Figure 5B).
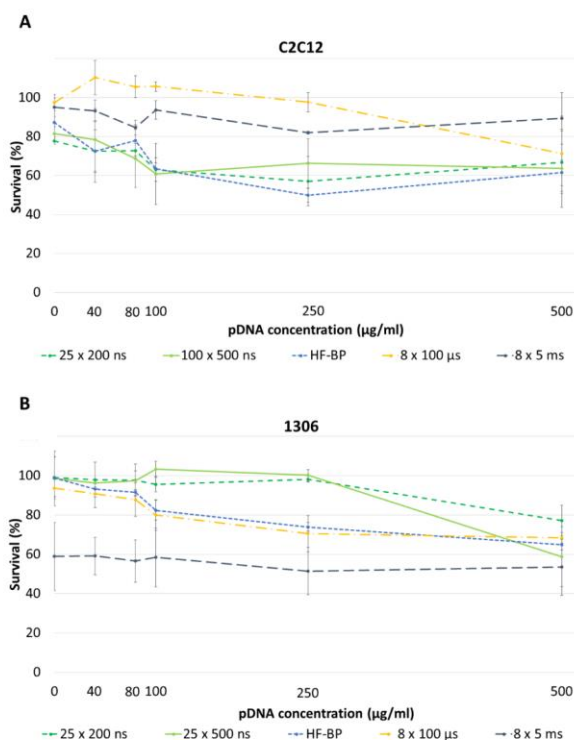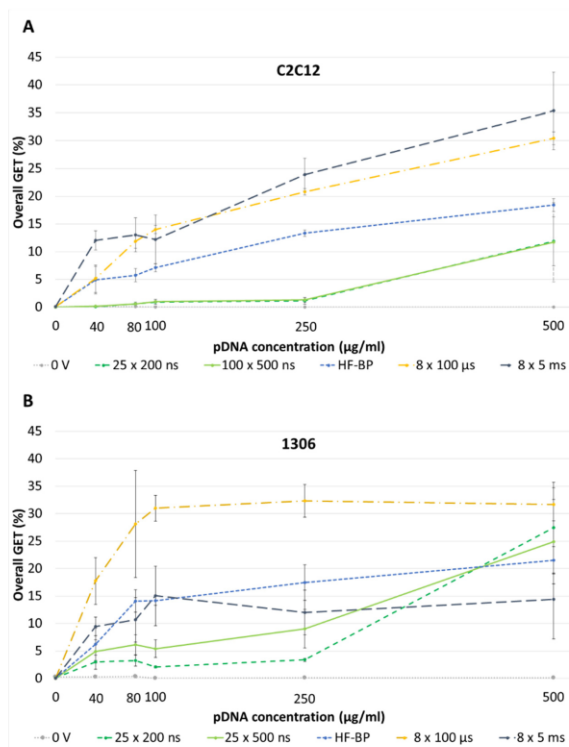

Figure 5. Overall GET with different concentrations of pEGFP-N1 pDNA. (**A**) C2C12 myoblasts, pulses: 25 × 200 ns: 25 × 200 ns, 10 Hz, 15.8 kV/cm; 100 × 500 ns: 100 × 500 ns, 10 Hz, 4.1 kV/cm; HF-BP: 2-2-2-2, 32p, 100b, 1 Hz, 1.25 kV/cm; 8 × 100 μs: 8 × 100 μs, 1 Hz, 1.25 kV/cm; and 8 × 5 ms: 8 × 5 ms, 1 Hz, 0.4 kV/cm; and (**B**) 1306 fibroblasts, pulses: 25 × 200 ns: 25 × 200 ns, 10 Hz, 12.8 kV/cm; 25 × 500 ns: 25 × 500 ns, 10 Hz, 6.5 kV/cm; HF-BP: 2-2-2-2, 32p, 100b, 1 Hz, 1 kV/cm; 8 × 100 μs: 8 × 100 μs, 1 Hz, 1.25 kV/cm; and 8 × 5 ms: 8 × 5 ms, 1 Hz, 0.6 kV/cm. 0 V represents control where cells were not exposed to electric pulses. Results are represented as an average of 3 repetitions. Statistical differences are given in the text. Bars represent standard deviation.

The importance of pDNA concentration is most noticeable with nanosecond pulses, where overall GET is less than a half in both cell lines already at pDNA concentration 250 μg/mL. With the lowest pDNA concentration, 40 μg/mL, overall GET in 1306 fibroblast was 3% and 5% for 200 and 500 ns pulses, respectively. In C2C12 myoblasts, the overall GET with 40, 80, and 100 μg/mL pDNA concentrations was below 1% with both 200 ns and 500 ns pulses (Figure 5). Based on these results, a pDNA concentration of 500 μg/mL was chosen to achieve robust overall GET.

3.3. Effect of Different pDNA Size on GET

Since pDNA size is reported to have an effect on GET efficiency, we performed experiments using two different size pDNA, comparing a 3.5 kb plasmid pmaxGFP and a 4.7 kb plasmid pEGFP-N1, both encoding GFP under the control of a CMV promotor. The concentrations of both plasmids in all experiments were 500 μg/mL, meaning that the number of pDNA copies added was $1.34 \times$ higher for the smaller pDNA. We performed experiments with pmaxGFP for both cell lines for pulse protocols which gave the highest GET with pEGFP-N1 plasmid (Table 1).

As we can observe in Figure 6A, in C2C12 myoblasts with smaller pDNA, significantly higher overall GET was observed only for 8×100 μs pulse protocol. Overall GET with 200 ns, 500 ns and HF-BP protocol was comparable. Interestingly, overall GET with 8×5 ms was lower with smaller pDNA compared to larger pDNA.
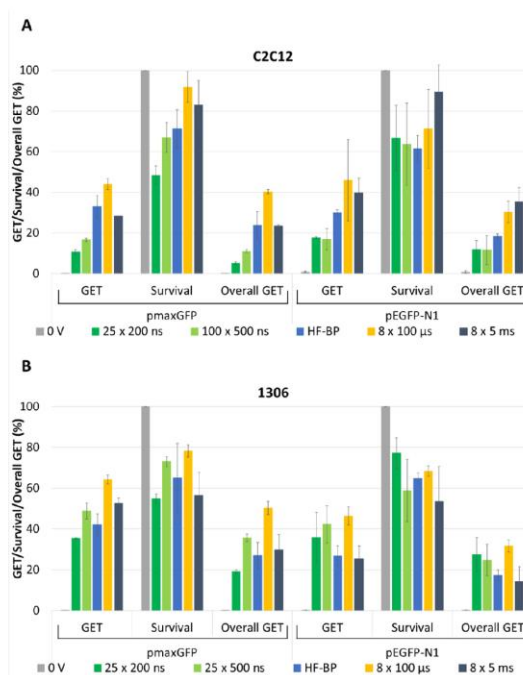
Figure 6. GET, cell survival, and overall GET with 500 μg/mL of pmaxGFP and pEGFP-N1 pDNA with different pulse protocols for (**A**) C2C12 myoblasts, 25×200 ns: 25×200 ns, 10 Hz, 15.8 kV/cm; 100×500 ns: 100×500 ns, 10 Hz, 4.1 kV/cm; HF-BP: 2-2-2-2, 32 pulses, 100 bursts, 1 Hz, 1.25 kV/cm; 8×100 μs: 8×100 μs, 1 Hz, 1.25 kV/cm; 8×5 ms: 8×5 ms, 1 Hz, 0.4 kV/cm; and (**B**) 1306 fibroblasts, 25×200 ns: 25×200 ns 10 Hz, 12.8 kV/cm;, 25×500 ns: 25×500 ns, 10 Hz, 6.5 kV/cm; HF-BP: 2-2-2-2, 32 pulses, 100 bursts, 1 Hz, 1. kV/cm; 8×100 μs: 8×100 μs, 1 Hz, 1.25 kV/cm; 8×5 ms: 8×5 ms, 1 Hz, 0.6 kV/cm. 0 V represents cells not exposed to electric pulses. Results are represented as an average of 3 repetitions. Bars represent standard deviation.

Similar results were obtained for 1306 fibroblasts (Figure 6B). Overall GET was significantly higher with smaller pDNA only for 8×100 μs protocol when compared to larger pDNA. With the 200 ns, 500 ns, HF-BP, and 8×5 ms protocols, comparable overall GET was observed with both pDNA sizes.

When comparing MFI of all pulse protocols between different pDNA sizes a marked difference was observed between the two cell lines. In C2C12 myoblasts, the MFI of the GFP-positive cells was significantly higher with smaller pDNA (pmaxGFP) after GET with the 200 ns, 500 ns, and HF-BP protocols (Figure 7A), while 1306 fibroblasts exhibited significantly higher MFI with smaller pDNA after 8×100 μs and 8×5 ms protocols (Figure 7B).
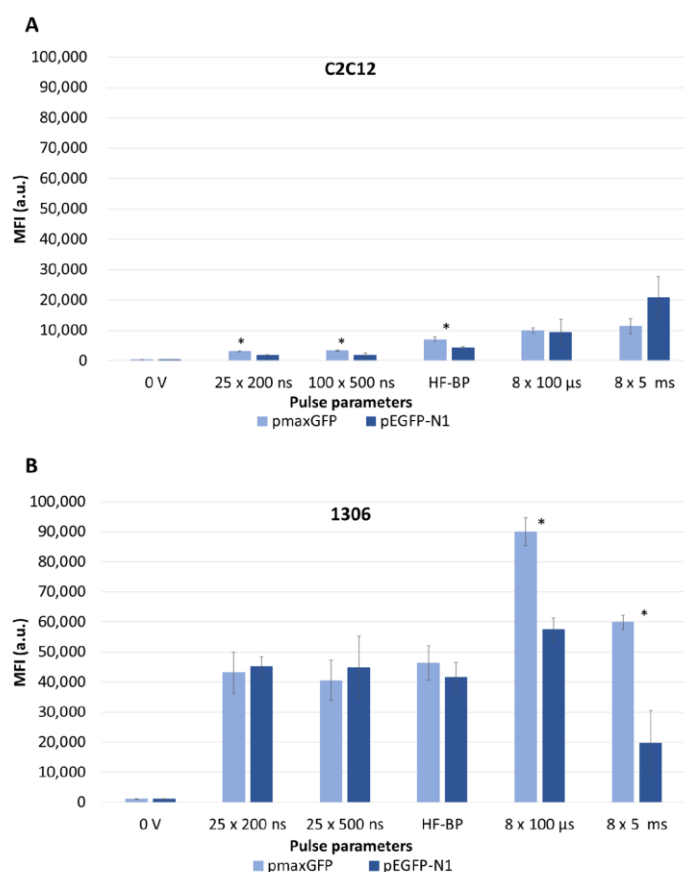
Figure 7. Median fluorescence (MFI) of GFP-positive cells with 500 μg/mL of pmaxGFP and pEGFP-N1 pDNA with different pulse protocols for (**A**) C2C12 myoblasts, 25×200 ns: 25×200 ns, 10 Hz, 15.8 kV/cm; 100×500 ns: 100×500 ns, 10 Hz, 4.1 kV/cm; HF-BP: 2-2-2-2, 32 pulses, 100 bursts, 1 Hz, 1.25 kV/cm; 8×100 μs: 8×100 μs, 1 Hz, 1.25 kV/cm; 8×5 ms: 8×5 ms, 1 Hz, 0.4 kV/cm; and (**B**) 1306 fibroblasts, 25×200 ns: 25×200 ns, 10 Hz, 12.8 kV/cm; 25×500 ns: 25×500 ns, 10 Hz, 6.5 kV/cm; HF-BP: 2-2-2-2, 32 pulses, 100 bursts, 1 Hz, 1. kV/cm; 8×100 μs: 8×100 μs, 1 Hz, 1.25 kV/cm; 8×5 ms: 8×5 ms, 1 Hz, 0.6 kV/cm. 0 V represents cells not exposed to electric pulses. Results are represented as an average of 3 repetitions. Bars represent standard deviation. Asterisk * represents statistically significant ($p < 0.05$) difference between pmaxGFP and pEGFP-N1 for the same pulse protocol.

59

3.4. Effect of Pulse Parameters on Overall GET and MFI

We compared overall GET of different pulse protocols after GET with 500 µg/mL of pEGFP-N1 since this were the conditions which led to the highest overall GET.

As we can observe in Figure 8, we achieved around a 35% overall GET with the 8×5 ms pulse protocol in C2C12 myoblast. The overall GET with the 8×5 ms pulse protocol was, however, significantly lower in 1306 fibroblast, 15%. The overall GET with the 8×100 µs pulses was comparable in both cell lines, at approximately 30%, as well as for the HF-BP pulse protocol, at 20%. On the contrary, the overall GET with nanosecond pulses was interestingly higher in 1306 fibroblasts compared to C2C12 myoblasts, with the overall GET using the 25×500 ns and 300×200 ns pulse protocols being significantly higher.

Figure 8. Overall GET with different pulse protocols for C2C12 myoblasts and 1306 fibroblasts with 500 µg/mL of pEGFP-N1. **C2C12:** 25×200 ns: 25×200 ns, 10 Hz, 15.8 kV/cm; 100×200 ns: 100×200 ns, 10 Hz, 6.9 kV/cm; 300×200 ns: 300×200 ns, 10 Hz, 6.3 kV/cm; 25×500 ns: 25×500 ns, 10 Hz, 6.9 kV/cm; 100×500 ns: 100×500 ns, 10 Hz, 4.1 kV/cm; 300×500 ns: 300×500 ns, 10 Hz, 2.4 kV/cm; HF-BP: 2-2-2-2, 32 pulses, 100 bursts, 1 Hz, 1.25 kV/cm; 8×100 µs: 8×100 µs, 1 Hz, 1.25 kV/cm; 8×5 ms; 8×5 ms, 1 Hz, 0.4 kV/cm. **1306:** 25×200 ns: 25×200 ns, 10 Hz, 12.8 kV/cm; 100×200 ns: 100×200 ns, 10 Hz, 6.9 kV/cm; 300×200 ns: 300×200 ns, 10 Hz, 4.2 kV/cm; 25×500 ns: 25×500 ns, 10 Hz, 6.5 kV/cm; 100×500 ns: 100×500 ns, 10 Hz, 3.5 kV/cm; 300×500 ns: 300×500 ns, 10 Hz, 2.7 kV/cm; HF-BP: 2-2-2-2, 32 pulses, 100 bursts, 1 Hz, 1 kV/cm; 8×100 µs: 8×100 µs, 1 Hz, 1.25 kV/cm; 8×5 ms; 8×5 ms, 1 Hz, 0.6 kV/cm. 0 V represents cells not exposed to electric pulses. Results are represented as an average of 3 repetitions. Bars represent standard deviation. Asterisk * represents statistically significant ($p < 0.05$) difference between cell lines for the same pulse protocol.

With respect to pulse parameters, overall GET with the highest pDNA concentration tested in C2C12 myoblasts was significantly higher with 8×5 ms compared to HF-BP and nanosecond pulse protocols. In addition, overall GET with 8×100 µs protocol was significantly higher compared to nanosecond pulse protocols. The overall GET in C2C12 myoblasts was significantly higher with HF-BP pulses compared to the 300×500 ns and 300×200 ns pulse protocols. However, due to the high variability, in 1306 fibroblasts, there was no significant difference in the overall GET when comparing 8×5 ms, 8×100 µs, HF-BP, and nanosecond pulse protocols.

With 8×100 µs pulses, the overall GET was comparable between both cell lines. The overall GET was significantly lower in 1306 fibroblasts for the 8×5 ms protocol and significantly higher for the 300×200 ns and 25×500 ns pulse protocols compared to the overall GET in C2C12 myoblasts. In addition, overall GET with 8×100 µs and

nanosecond pulses in 1306 fibroblasts, although not significantly, was higher as overall GET with 8×5 ms pulses (Supplementary Tables S3 and S4).

The MFI of GFP-positive cells was significantly higher in 1306 fibroblast with all pulse protocols, except for the 8×5 ms pulse protocol. The MFI of C2C12 myoblasts was up to 20,000 a.u. and was significantly different only between 8×5 ms and 300×500 ns pulse protocols. MFI of 1306 fibroblast was up to 60,000 a.u. There was no significant difference in MFI between different pulse protocols in 1306 fibroblasts (Figure 9).

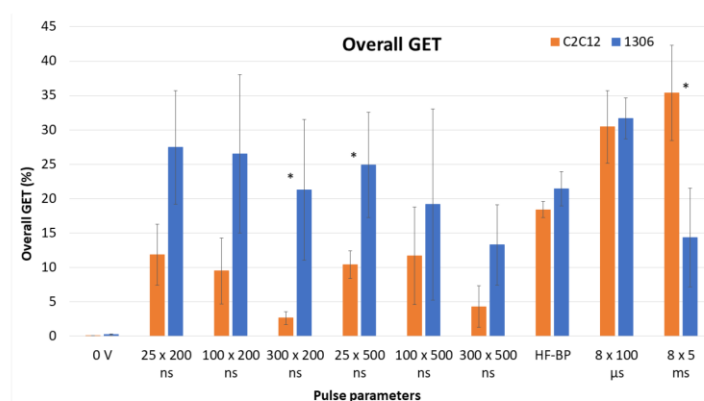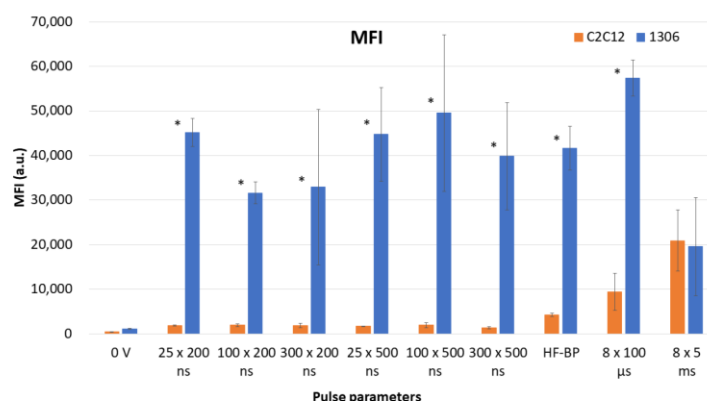**Figure 9.** Median fluorescence intensity (MFI) of GFP-positive cells with different pulse protocols for C2C12 myoblasts and 1306 fibroblasts with 500 μg/mL of pEGFP-N1. **C2C12:** 25×200 ns: 25×200 ns, 10 Hz, 15.8 kV/cm; 100×200 ns: 100×200 ns, 10 Hz, 6.9 kV/cm; 300×200 ns: 300×200 ns, 10 Hz, 6.3 kV/cm; 25×500 ns: 25×500 ns, 10 Hz, 6.9 kV/cm; 100×500 ns: 100×500 ns, 10 Hz, 4.1 kV/cm; 300×500 ns: 300×500 ns, 10 Hz, 2.4 kV/cm; HF-BP: 2-2-2-2, 32 pulses, 100 bursts, 1 Hz, 1.25 kV/cm; 8×100 μs: 8×100 μs, 1 Hz, 1.25 kV/cm; 8×5 ms; 8×5 ms, 1 Hz, 0.4 kV/cm. **1306:** 25×200 ns: 25×200 ns, 10 Hz, 12.8 kV/cm; 100×200 ns: 100×200 ns, 10 Hz, 6.9 kV/cm; 300×200 ns: 300×200 ns, 10 Hz, 4.2 kV/cm; 25×500 ns: 25×500 ns, 10 Hz, 6.5 kV/cm; 100×500 ns: 100×500 ns, 10 Hz, 3.5 kV/cm; 300×500 ns: 300×500 ns, 10 Hz, 2.7 kV/cm; HF-BP: 2-2-2-2, 32 pulses, 100 bursts, 1 Hz, 1 kV/cm; 8×100 μs: 8×100 μs, 1 Hz, 1.25 kV/cm; 8×5 ms; 8×5 ms, 1 Hz, 0.6 kV/cm. 0 V represents cells not exposed to electric pulses. Results are represented as an average of 3 repetitions. Bars represent standard deviation. Asterisk * represents statistically significant ($p < 0.05$) difference between cell lines for the same pulse protocol.

3.5. Time Dynamics of pDNA Expression

The time dynamics of pDNA expression was also monitored for both cell lines for those pulse protocols with which we obtained the best overall GET with 500 μg/mL of pEGFP-N1 plasmid (Table 1). The percentage of GFP-positive cells and their MFI were measured every 8 h for 6 days. Since we did not measure cell survival at each time point, the results for time dynamics of pDNA expression are presented as GET (not overall GET).

Our results show that the dynamics of the onset of GFP expression (both percentage of GFP-positive cells and their MFI) are comparable for all pulse protocols tested (i.e., from 200 ns up to 5 ms pulse durations) but varied greatly between the two cell lines (Figures 10 and 11).
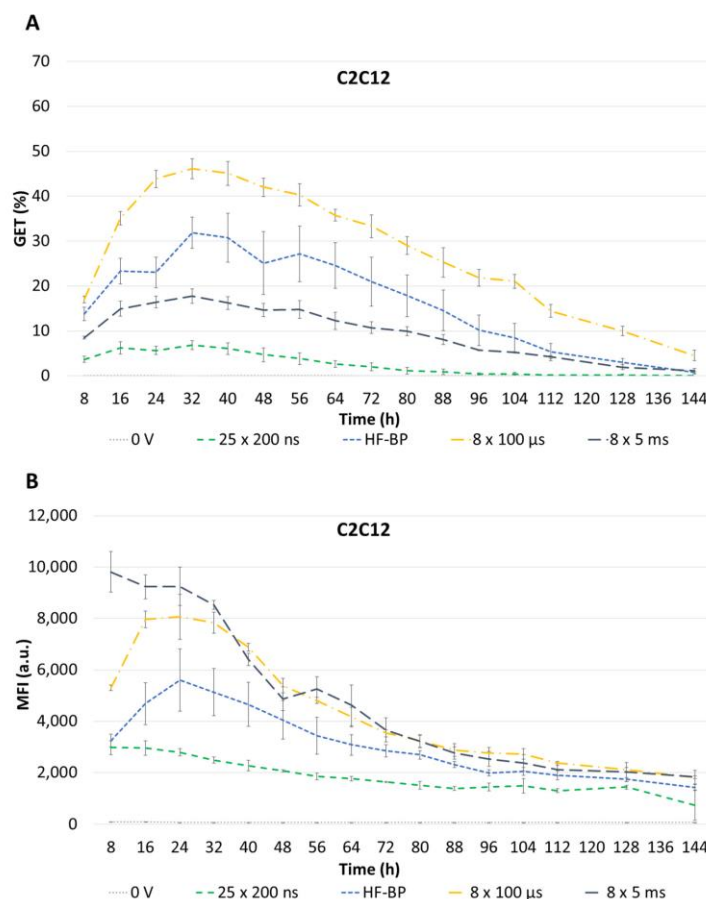
Figure 10. (**A**) GET and (**B**) median fluorescence intensity (MFI) of GFP-positive C2C12 myoblasts with 500 µg/mL pEGFP-N1 pDNA with different pulse protocols on 1306 fibroblasts, 25×200 ns: 25×200 ns, 10 Hz, 12.8 kV/cm; HF-BP: 2-2-2-2, 32 pulses, 100 bursts, 1 Hz, 1.25 kV/cm; 8×100 µs: 8×100 µs, 1 Hz, 1.25 kV/cm; 8×5 ms: 8×5 ms, 1 Hz, 0.6 kV/cm, 0 V represents control where cells were not exposed to electric pulses. Results are represented as an average of 3 repetitions. Bars represent standard deviation.

In C2C12 myoblasts, the GET increased with all pulse protocols reaching a maximum at 32 h after GET. The best GET was achieved with the 8×100 µs pulse protocol (46.2%), followed by HF-BP (31.9%), 8×5 ms (17.8%) and 25×200 ns (6.9%). Afterwards the GET started to decline and after 144 h (i.e., 6 days) decreased below 10% for all pulse protocols reaching 4.5%, 0.7%, 1.1%, and 0.02% for the 8×100 µs, HF-BP, 8×5 ms, and 25×200 ns pulse protocols, respectively (Figure 10A).
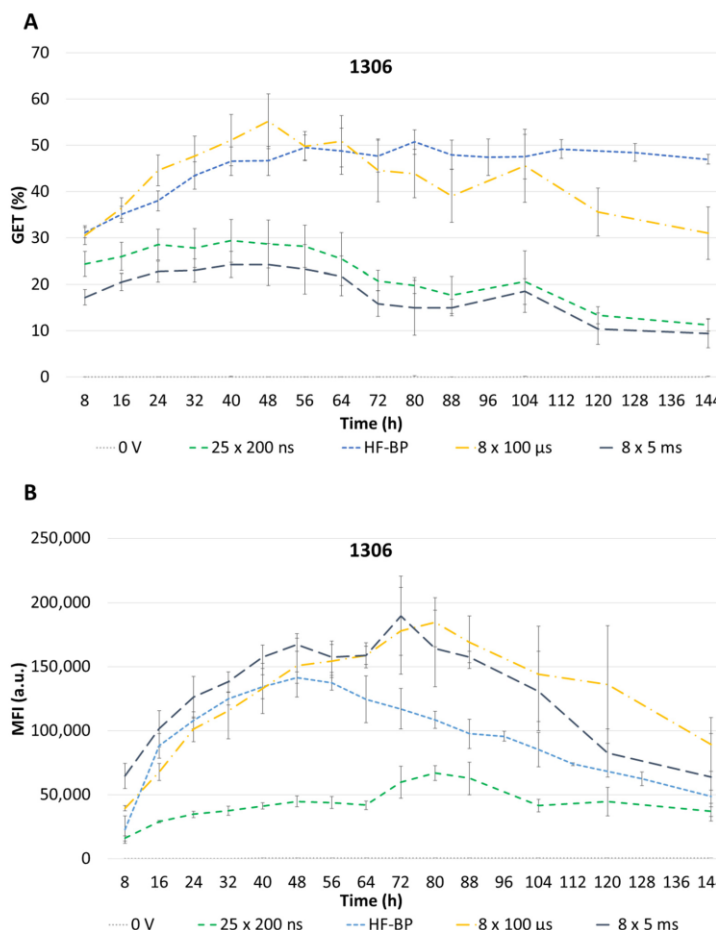
Figure 11. (**A**) GET and (**B**) median fluorescence intensity (MFI) of GFP-positive 1306 fibroblasts with 500 μg/mL pEGFP-N1 pDNA with different pulse protocols on 1306 fibroblasts, 25 × 200 ns: 25 × 200 ns, 10 Hz, 12.8 kV/cm; HF-BP: 2-2-2-2, 32 pulses, 100 bursts, 1 Hz, 1 kV/cm; 8 × 100 μs: 8 × 100 μs, 1 Hz, 1.25 kV/cm; 8 × 5 ms: 8 × 5 ms, 1 Hz, 0.6 kV/cm. 0 V represents control where cells were not exposed to electric pulses. Results are represented as an average of 3 repetitions. Bars represent standard deviation.

A similar dynamic was observed for MFI of GFP positive in C2C12 myoblasts. MFI reached the peak at 24 h after GET with 8 × 100 μs and HF-BP protocols and then stated to decline. Interestingly, MFI after the 8 × 5 ms and 25 × 200 ns protocols peaked already at 8 h after GET, after which it declined steadily (Figure 10B).

Contrary to C2C12 myoblasts, broad peaks in GET were observed in 1306 fibroblasts for all pulse protocols tested. The maximum percentage of GFP-positive cells was reached between 8 and 64 h for the 8 × 5 ms and 25 × 200 ns pulse protocols, between 24 and 104 h after GET with the 8 × 100 μs pulse protocol, and between 40 and 112 h after GET with

the HF-BP pulse protocol. The best GET was achieved with the 8 × 100 μs pulse protocol (max at 48 h, 55.2%), followed by the HF-BP (max at 80 h, 50.8%), 25 × 200 ns (max at 40 h, 29.2%) and 8 × 5 ms protocols (max at 40 h, 24.3%). Interestingly, higher GET was achieved with 25 × 200 ns compared to 8 × 5 ms protocol. After reaching a peak, the percentage of GFP-positive cells started to decrease slowly, except for the HF-BP protocol, where it remained at the same level for the entire time of observation. On day 6 (i.e., 144 h) after GET, 31.1%, 47.0%, 11.3%, and 9.5% of cells were still GFP-positive for the 8 × 100 μs, HF-BP, 25 × 200 ns, and 8 × 5 ms pulse protocols, respectively (Figure 11A).

In addition, in MFI, broad peaks were observed for all pulse protocols in 1306 fibroblasts. The MFI reached a peak later than the maximum percentage of GFP-positive cells between 24 and 104 h after GET with the 25 × 200 ns pulse protocol, between 40 and 104 h after GET with the 8 × 100 μs and 8 × 5 ms pulse protocols, and between 32 and 72 h after GET with the HF-BP pulse protocol. Comparable MFIs were observed between the 8 × 5 ms, 8 × 100 μs, and HF-BP protocols, which were higher compared to the 25 × 200 ns protocol (Figure 11B).

3.6. Modeling the Probability of pDNA and Cell Membrane Contact during GET

3.6.1. 200 ns and 500 ns Pulses

Equation (4) is first solved for a single pulse of 200 ns at an electric field intensity of 15.8 kV/cm. These were the conditions used in the experiments for C2C12 cells (Table 1). The results of the solution of Equation (4) are shown in Figure 12A below for B_L, B_R = 134 nm, representing 500 μg/mL pDNA solution concentration. The solid lines represent the evolution of $P(X, t)$ during the pulse, and the dashed lines represent the evolution of $P(X, t)$ after the pulse. Equation (4) is solved for t = 100 ms since the ns pulses are applied at a frequency of 10 Hz (implying 100 ms between pulses). During the pulse (t = 0 ns to t = 200 ns), the initial narrow band normal/Gaussian distribution drifts towards the right by electrophoresis and spreads only a little by diffusion. After the pulse, there is no drift, and the distribution spreads purely by diffusion. The time between two successive pulses is long enough for $P(X, t)$ to become almost flat before the onset of the second pulse (t = 100 ms).

To calculate the Probability of Successful Contact $PSC(t)$, the flux $P(X, t)$ is collected at the cell membrane, i.e., at $X = B_R$. $PSC(t)$ is calculated as $PSC(t) = 1 - \int_{-B_L}^{+B_R} P(X, t) dX$. This represents the probability that a pDNA molecule will successfully establish contact with, and be absorbed by, the cell membrane, which is pre-requisite for a successful GET. As observed from Figure 12B, $PSC(t)$ remains negligibly small during and after the 200 ns pulse, implying a negligible probability of pDNA establishing contact with the cell membrane. Only from around $t \sim 1$ ms does $PSC(t)$ start to rise (due to diffusion), attaining a non-negligible probability.

To determine the influence of concentration (i.e., of the distance between the pDNA and the cell membrane (in Figure 1)), another simulation using B_L, B_R = 433 nm, representing 15 μg/mL pDNA solution concentration, is shown in Figure 12C,D. Due to the lower concentration (or a larger distance between the pDNA and the cell membrane), the domain has expanded (Figure 12C), and the pDNA molecule has to travel a larger distance before it can reach the cell membrane. Due to insufficient electrophoresis, the pDNA molecule relies on diffusion after the cessation of pulse to cover this large distance and reach the cell membrane. For B_L, B_R = 433 nm, $PSC(t)$ starts to rise at a much later time and attains a lower $PSC(t)$ at t = 100 ms (Figure 12D), compared to B_L, B_R = 134 nm (Figure 12B).
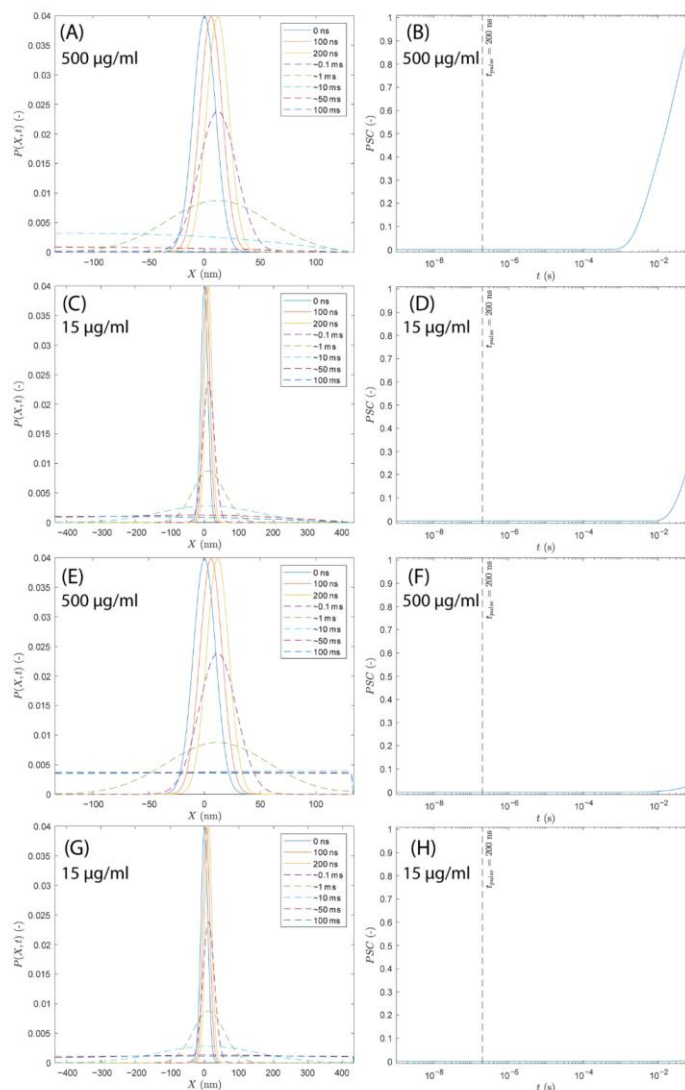
Figure 12. The 200 ns pulse: Evolution of $P(X,t)$ and the corresponding Probability of Successful Contact $PSC(t) = 1 - \int_{-B_L}^{+B_R} P(X,t)dX$ for $B_L, B_R = 134$ nm in (**A,B,E,F**) and for $B_L, B_R = 433$ nm in (**C,D,G,H**); (**A–D**) represent cases without free energy barrier and (**E–H**) represent cases with free energy barrier. Solid lines in (**A,C,E,G**) correspond to times during the pulse, and dashed lines in (**A,C,E,G**) correspond to times after the pulse. The dashed lines in (**B,D,F,H**) represent the time at which the 200 ns pulse ends.

Evolution of $P(X,t)$, as calculated using Equation (5), i.e., in the presence of a free energy barrier between the pDNA and the cell membrane, is shown in Figure 12E for

65

$B_L, B_R = 134$ nm (500 μg/mL) and in Figure 12G for $B_L, B_R = 433$ nm (15 μg/mL); the corresponding $PSC(t)$ values are shown in Figure 12F,H, respectively. The presence of a high free energy barrier (barrier height of 50 $k_B T$) signficantly reduces the probability of pDNA reaching the cell membrane. For a 200 ns pulse, electrophoresis acts for an insufficient amount of time to bring the pDNA molecule close to the cell membrane and for it to influence the pDNA molecule in overcoming the free energy barrier. Due to the nature of the free energy barrier considered in this study ($50 e^{2(X-B_R)} k_B T$), the free energy is negligibly small at distance greater than ∼2 nm away from the cell membrane, and it rises sharply as we approach the cell membrane. Therefore, for the electric field (and electrophoresis) to overcome this barrier, the pDNA molecule must already be present very close to the cell membrane, or the electric field should be applied for a longer duration such that electrophoresis first drags the pDNA molecule close to the cell membrane and then subsequently helps the pDNA molecule in overcoming this barrier. Thus, the pDNA molecule which relies on diffusion to reach the cell membrane is also repulsed by the free energy barrier, resulting in lower $PSC(t)$ compared to the case when no free energy barrier was present (comparing Figure 12B,D vs. Figure 12F,H). Since the probability of pDNA being absorbed by the cell membrane is low in the presence of a free energy barrier, the probability of finding the pDNA molecule in the domain $X \in [-B_L, B_R]$ at $t=100$ ms is higher (comparing Figure 12A,C vs. Figure 12E,G at $t=100$ ms). For 200 ns pulses, the time between pulses ($t = 100$ ms) is large enough for $P(X, t)$ to become almost flat (by diffusion) before the onset of the second pulse. This is the case for both – without the free energy barrier (Figure 12A,C) and the with free energy barrier (Figure 12E,G). This implies that it is almost equally probable to find the pDNA molecule at any X for $X \in [-B_L, B_R]$. Thus, for both cases, a uniform distribution of $P(X, t)$ in $X \in [-B_L, B_R]$ can be considered as an initial condition for the second pulse. For a uniform distribution, there is a higher probabilty of pDNA being close to the cell membrane compared to the narrow-band Gaussian distribution with a standard deviation of 10 nm centered around $X = 0$, the tail of which is neglibly small at $X = -B_L, +B_R$. Therefore, we expect that electrophoresis provided by the second pulse would contribute more to the rise in $PSC(t)$ during the second pulse compared to the first pulse for which the rise in $PSC(t)$ was negligible during the pulse (Figure 12B,D,F,H). However, since the pulse duration is small, we further expect that the rise in $PSC(t)$ will still not be significant to completely ensure the absorption of pDNA at the cell membrane. $PSC(t)$ will still have to rely on the diffusion post-second pulse. We expect this process to continue in the subsequent pulses until diffusion increases $PSC(t)$ to a value of 1. The role of any additional pulses after $PSC(t)$ reaches 1 is not accounted for by the model since the pDNA is absorbed by the cell membrane and $P(X, t) = 0$ in $X \in [-B_L, B_R]$. In such cases, additional pulses can be thought to add more pDNA molecules to the cell membrane.

To illustrate the point that ns pulses can be analysed in isolation, we can look at the Peclet number defined as the ratio of distance covered during electrophoresis to the distance covered during diffusion post pulse ($Pe = \frac{\mu E t_p}{\sqrt{2D t_{bp}}}$, where t_p is the pulse duration and t_{bp} is the duration between pulses). For the 200 ns pulse, $E = 15.8$ kV/cm, $t_p = 200$ ns, and $t_{bp} = 100$ ms, which gives a $Pe = 0.03$ (< 1), indicating that $P(X, t)$ would spread more by diffusion and reach the cell membrane while becoming flat than it would be drifted towards the cell membrane by electrophoresis over a single phase (during pulse and post-pulse). As a result, the role of electric field pulses can be studied in isolation without the confounding/compounding effects of multiple pulses.

Furthermore, for pedagogical purposes, and to study the effect of concentration on pDNA being absorbed by the cell membrane (a pre-requisite for GET) in isolation as a function different pulse durations and electric field intensities, we have decided to simulate only one pulse. Such an analysis effectivly allows us to infer and isolate the roles of electropohoresis and diffusion for different kinds of pulses/pulse durations used for GET as a function of concentration and will allow us to draw more general conclusions.

66

$PSC(t)$ is evaluated for the 200 ns pulse and 500 ns pulse at the corresponding electric field intensities (Table 1 for C2C12 cells) using (B_L, B_R) ranging from 77 nm to 433 nm (corresponding to concentrations ranging from 2500 μg/mL to 15 μg/mL, respectively) and is shown in Figure 13A–D. For all ranges of (B_L, B_R) tested, $PSC(t)$ rises post pulse termination (for both 200 ns and 500 ns pulses) through the diffusive process. As seen from Figure 13A,C (without the free energy barrier), $PSC(t)$ starts to rise from $t \sim 0.2$ ms for the lowest $(B_L, B_R) = 77$ nm. The time at which $PSC(t)$ begins to rise depends on (B_L, B_R), and $PSC(t)$ starts to rise earlier for lower (B_L, B_R), since the pDNA molecule is initially located close to the cell membrane and thus has a higher probability of reaching the cell membrane (through diffusion) first. Similar profiles (rise times) of $PSC(t)$ can be seen for 200 ns and 500 ns pulses as $PSC(t)$ rises predominantly by diffusion with little contribution from electrophoresis. For the case with free energy barrier (Figure 13B,D), the rise in $PSC(t)$ is delayed. $PSC(t)$ starts to rise from $t \sim 10$ ms for the lowest $((B_L, B_R) = 77$ nm) and attains a lower final $PSC(t)$ at $t = 100$ ms compared to the case without a free energy barrier. Similar profiles of $PSC(t)$ were obtained for both the 200 ns and 500 ns pulse in the presence of the free energy barrier as well, further indicating the dominating effect of the diffusive process with little contribution from electrophoresis.
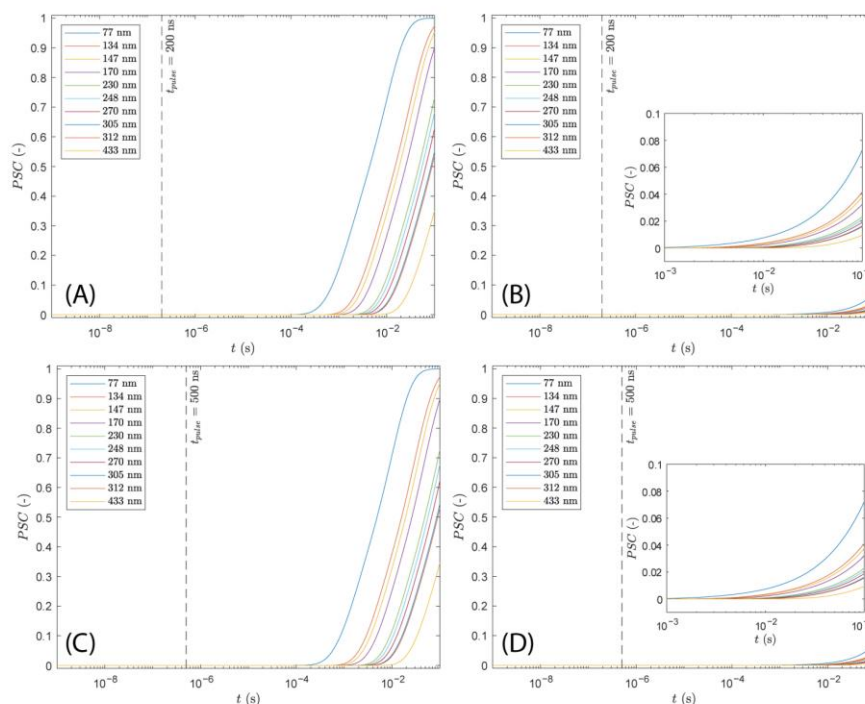
Figure 13. Evolution of $PSC(t)$ for different (B_L, B_R) ranging from 77 nm to 433 nm, corresponding to concentrations ranging from 2500 μg/mL to 15 μg/mL, respectively. (**A,B**) The 200 ns pulse at 15.8 kV/cm: (**A**) without free energy barrier, (**B**) with free energy barrier. (**C,D**) The 500 ns pulse at 4.1 kV/cm: (**C**) without free energy barrier, (**D**) with free energy barrier. Dashed lines represent the time at which nanosecond pulse ends. Insets in (**B,D**) show zoomed-in plots for rise in $PSC(t)$ from 1 ms.

For the 200 ns and 500 ns pulses, and for both – without and with free energy barrier, the final $PSC(t)$, i.e., $PSC(t = 100 \text{ ms})$ depends upon (B_L, B_R); thus, we can expect GET to depend on concentrations ranging from 2500 µg/mL to 15 µg/mL.

3.6.2. HF-BP Pulses

Equation (4) is solved using $B_L, B_R = 134$ nm (representing 500 µg/mL pDNA solution concentration) for 32 bipolar pulses (constituting 1 burst out of a 100 bursts) as described by the protocol given in Table 1 for C2C12 cells. Figure 14A–C show the evolution of $P(X,t)$ during the 32 pulses, whereas Figure 14D shows shows the evolution of $P(X,t)$ after termination of 32 pulses, i.e., 1 burst. The domain length considered was $B_L, B_R = 134$ nm, corresponding to 500 µg/mL.

Figure 14A shows the evolution of $P(X,t)$ during the first bipolar pulse. During the first 2 µs of the pulse, when the electric field is applied in the negative X direction, $P(X,t)$ moves to the right due to electrophoresis and only spreads slightly due to diffusion. During the next 2 µs, when the electric field is absent, the peak of $P(X,t)$ remains at the same X location, and $P(X,t)$ spreads slightly by diffusion. During the next 2 µs, the electric field is applied in the positive X direction and the peak of $P(X,t)$ moves to the left due to electrophoresis and spreads slightly by diffusion. During the last 2 µs of the pulse, the electric field is absent again, and the peak of $P(X,t)$ remains at the same location, spreading slightly by diffusion. The same pattern is repeated for 32 such bipolar pulses. Figure 14B shows the evolution of $P(X,t)$ during pulse number 15 and Figure 14C shows the evolution of $P(X,t)$ during pulse number 32. It can be seen from Figure 14B,C that the peak $P(X,t)$ remains close to $X = 0$ nm during the 32 pulses, as there is a net zero drift in $P(X,t)$ due to the bipolar nature of the pulses. $P(X,t)$, however, spreads by diffusion during the 32 pulses. Finally, after the cessation of 32 bipolar pulses (i.e., after 1 burst), or after $t = 256$ µs, $P(X,t)$ only spreads by diffusion and becomes almost flat until the onset of the next burst (at $t = 1$ s).

The Probability of Successful Contact, $PSC(t)$, is calculated as $PSC(t) = 1 - \int_{-B_L}^{+B_R} P(X,t)dX$ and is shown in Figure 14E. $PSC(t)$ remains negligibly small during the burst of 32 bipolar pulses, i.e., until $t = 256$ µs, as indicated by the dotted vertical line. Only from around $t \sim 1$ ms does $PSC(t)$ start to rise (due to diffusion), attaining a non-negligible probability. $PSC(t)$ reaches a final probability of 1 before the onset of the next burst of bipolar pulses (at $t = 1$ s).

To see the influence of the free energy barrier, Equation (5) is solved using $B_L, B_R = 134$ nm (representing 500 µg/mL pDNA solution concentration) for 32 bipolar pulses, and the the evolution of $P(X,t)$ is shown in Figure 14F–H during the 32 pulses and in Figure 14I after the termination of the 32 pulses. Similar to the case with no free energy barrier, the domain length considered was $B_L, B_R = 134$ nm, corresponding to 500 µg/mL. The evolution of $P(X,t)$ during 32 pulses for the case with the free energy barrier (Figure 14F–H) was similar to the the evolution of $P(X,t)$ during the 32 pulses without the free energy barrier (Figure 14A–C). This could be due to the fact that $P(X,t)$ is not able to spread enough by diffusion during the burst (and net electrophoresis is also negligible due to the bipolar nature of the pulses) to have a signficant portion other than the thin tail of $P(X,t)$ close to the cell membrane where the free energy barrier is present. Therefore, the evolution of $P(X,t)$ with the free energy barrier would be similar to the case without the free energy barrier for the large enough domain considered here ($B_L, B_R = 134$ nm, corresponding to 500 µg/mL). For smaller domain lengths (or concentrations > 500 µg/mL), this might not be the case.

68
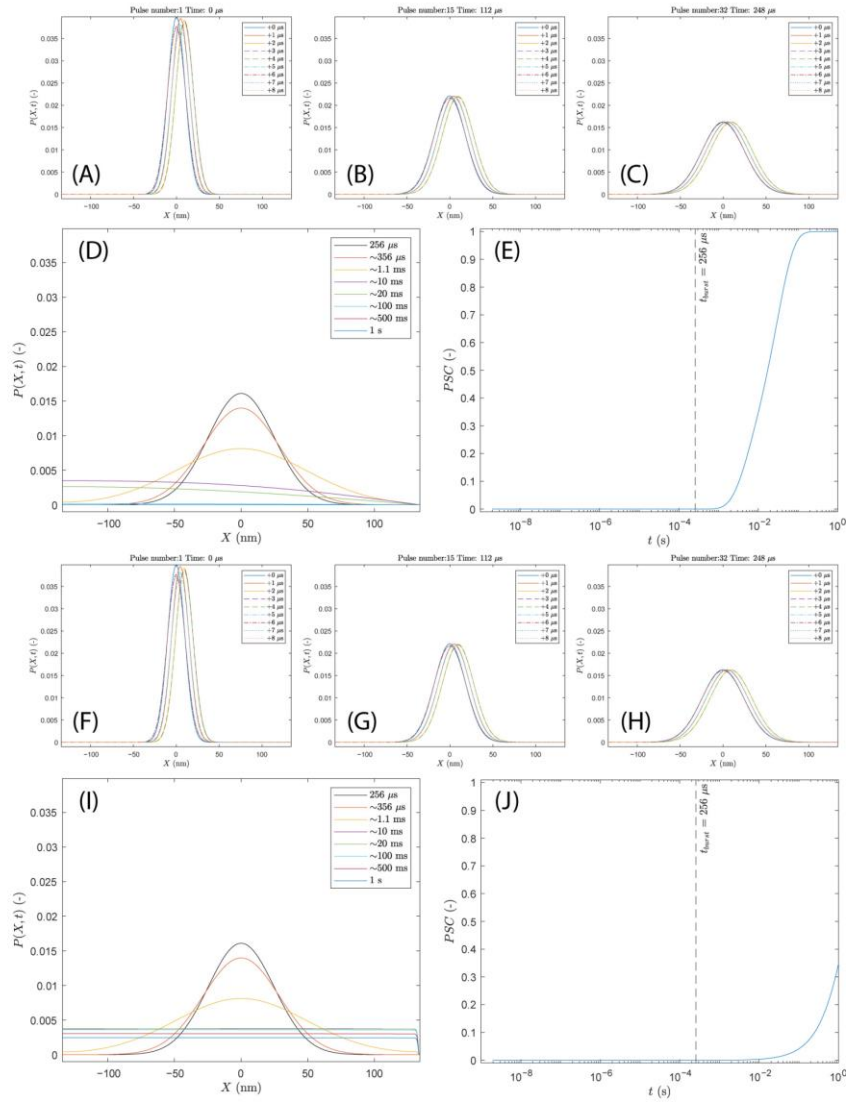
Figure 14. HF-BP pulses: Evolution of $P(X,t)$ and the corresponding Probability of Successful Contact $PSC(t) = 1 - \int_{-B_L}^{+B_R} P(X,t)dX$ for $B_L, B_R = 134$ nm (corresponding to 500 µg/mL) during a sequence of 32 bipolar pulses (1 burst) at an electric field intensity of 1.25 kV/cm (Table 1 for C2C12 cells). (**A–E**) represent cases without free energy barrier and (**F–J**) represent cases with free energy barrier. The dashed lines in (**E,J**) represent the time at which the sequence of 32 pulses (i.e., 1 burst) ends.

The difference between the cases without and with the free energy barrier can be seen in the evolution of $P(X, t)$ after the burst (comparing Figure 14D with Figure 14I). Similar to ns pulses, it is less probable for the pDNA molecule to come in contact with the cell membrane by diffusion only in the presence of the free energy barrier. As a result, there is higher probability for the pDNA molecule to stay within the domain $X \in [-B_L, B_R]$. Correspondingly, $PSC(t)$ begins to rise at a much later time in the presence of the free energy barrier (Figure 14J) compared to the case without the free energy barrier (Figure 14E). $PSC(t)$ also reaches a lower final value of only silightly greater than 0.3 at the end of the burst.

$PSC(t)$ is evaluated using (B_L, B_R) ranging from 77 nm to 433 nm, corresponding to concentrations ranging from 2500 µg/mL to 15 µg/mL, respectively, and is shown in Figure 15A for the case without the free energy barrier and in Figure 15B for the case with the free energy barrier. For all ranges of (B_L, B_R) tested, $PSC(t)$ rises post-burst termination (32 bipolar pulses) through the diffusive process. As seen from Figure 15A, and similar to nanosecond pulses, $PSC(t)$ starts to rise from $t \sim 0.2$ ms for the lowest $(B_L, B_R) = 77$ nm. Furthermore, the time at which $PSC(t)$ begins to rise depends on (B_L, B_R), and $PSC(t)$ starts to rise earlier for lower (B_L, B_R). A similar trend was observed for the case with the free energy barrier; however, the rise in $PSC(t)$ was delayed (to $t \sim 10$ ms for the lowest $(B_L, B_R) = 77$ nm) and $PSC(t)$ attains a lower final value (at = 1 s) compared to the case without the free energy barrier.
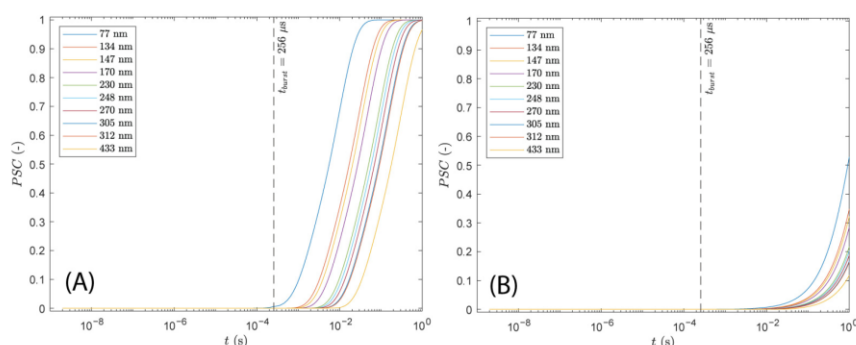
Figure 15. Evolution of $PSC(t)$ for different (B_L, B_R) ranging from 77 nm to 433 nm, corresponding to concentrations ranging from 2500 µg/mL to 15 µg/mL, respectively, for a sequence of 32 bipolar pulses (1 burst) at an electric field intensity of 1.25 kV/cm (Table 1 for C2C12 cells): (**A**) without free energy barrier and (**B**) with free energy barrier. Dashed lines represent the time at which the sequence of 32 pulses (i.e., 1 burst) ends.

The evolution of $PSC(t)$ is similar for nanosecond and HF-BP pulses. Figure 16 shows $PSC(t)$ using $B_L, B_R = 134$ nm (500 µg/mL) for a 200 ns pulse, a 500 ns pulse, and a bipolar burst. Irrespective of the pulse duration (200 ns, 500 ns, or a burst of 2 µs bipolar pulses), $PSC(t)$ starts to rise post-pulse/burst termination from around $t \sim 1$ ms (for the case without the free energy barrier Figure 16A) and $t \sim 20$ ms (for the case with the free energy barrier Figure 16B) and rises at the same rate. This indicates that the electrophoresis provided by these nanosecond and HF-BP pulses is insufficient to establish a pDNA contact with the cell membrane, and $PSC(t)$ rises due to diffusion. The solid vertical line in Figure 16A,B represents the onset of the next 200 ns or 500 ns pulse (pulse repition rate for ns pulses is 10 Hz).

Figure 16. Evolution of $PSC(t)$ for a single 200 ns pulse, a single 500 ns pulse and a single burst (32 bipolar pulses) for (B_L, B_R) = 134 nm, corresponding to 500 µg/mL: (**A**) without free energy barrier and (**B**) with free energy barrier. Dashed lines represent the time at which the ns pulses end or the sequence of 32 pulses (i.e., 1 burst) ends. The solid vertical line represents the onset of the next 200 ns or 500 ns pulse (pulse repetition rate for ns pulses is 10 Hz). The next burst of HF-BP pulses starts at 1 s (burst repetition frequency is 1 Hz).

It is worthwhile to note that for ns pulses, a single pulse was considered, whereas for HF-BP pulses, 32 bipolar pulses (or 1 burst) were considered. As mentioned previously, the Peclet number ($Pe = \frac{\mu E t_p}{\sqrt{2D t_{bp}}}$) during a single phase (pulse + post pulse) of the 200 ns pulse was $Pe = 0.03$ (< 1), indicating that diffusion dominated the process during the phase and that the initial narrow-band Gaussian distribution drifts very little due to electrophoresis and becomes nearly flat by spreading due to diffusion by the end of the phase. As a result, ns pulses can be studied in isolation. However, for a sequence of 32 bipolar pulses, pulse duration $t_p = 2$ µs and time between pulses $t_{bp} = 2$ µs is not large. For an electric field intensity of 1.25 kV/cm, the Peclet number for HF-BP pulses is $Pe = 4.69$ (> 1), indicating the electrophoresis during the pulse dominates the diffusion in between pulses, and there is very little time for diffusion to spread the distribution. As a result, there could be a compounding effect of subsequent pulses due to which the entire sequence of 32 pulses was considered. However, if we consider pulse duration $t_p = 2$ µs and the time between bursts $t_{bp} = 1$ s, the Peclet number for a single burst is $Pe = 0.01$ (< 1), indicating that diffusion dominates over electrophoresis and spreads the distribution, making it almost flat by the end of the burst. As a result, the individual bursts can be studied in isolation. The assumption of $t_p = 2$ µs as opposed to $t_p = 32 \times 2$ µs is valid, as there is net zero electrophoresis/drift during the 32 pulses.

For HF-BP pulses, the time between bursts ($t = 1$ s) is large enough for $P(X, t)$ to become almost flat (by diffusion) before the onset of the second burst. For the case without the free energy barrier, $PSC(t)$ for (B_L, B_R) ranging from 77 nm to 433 nm reaches 1 before the onset of the second burst (Figure 15A). This should imply that without the free energy barrier, GET should be independent of concentration. This is unlike the 200 ns pulse and 500 ns pulse protocols, where, although the time between pulses was large ($t = 100$ ms), it was not large enough to esnure $PSC(t)$ reaches 1 for (B_L, B_R) ranging from 77 nm to 433 nm (Figure 13A,C), thus implying GET dependance on concentration even without the free energy barrier for 200 and 500 ns pulses. Furthermore, since $PSC(t)$ reaches 1 before the onset of the second burst, the model does not account for the second burst since $P(X, t) \sim 0$ in $X \in [-B_L, B_R]$. In this case, additional bursts can be thought to add more pDNA molecules to the cell membrane.

For the case with free energy barrier, $PSC(t)$ does not reach a value of 1, and the final value depends on (B_L, B_R) ranging from 77 nm to 433 nm (Figure 15B). This implies that

71

GET should depend on concentration when the free energy barrier is present. However, since the time between bursts is large ($t = 1$ s), $P(X, t)$ becomes almost flat (but non-zero) before the onset of the second burst (Figure 14I at $t = 1$ s). Therefore, as with 200 ns pulses, a uniform distribution of $P(X, t)$ in $X \in [-B_L, B_R]$ can be considered as an initial condition for the second burst. For a uniform distribution, there is a higher probabilty of pDNA being close to the cell membrane compared to the narrow-band Gaussian distribution with a standard deviation of 10 nm centered around $X = 0$, the tail of which is neglibly small at $X = -B_L, +B_R$. Therefore, we expect that electrophoresis provided by the second burst pulses would contribute more to the rise of $PSC(t)$ during burst compared to the first burst for which the rise in $PSC(t)$ was negligible during burst. However, due to the bipolar nature of the pulses and due to the free energy barrier, we further expect that the rise in $PSC(t)$ will not be significant during the sequence of 32 bipolar pulses of the second burst. $PSC(t)$ will still have to rely on diffusion post-second pulse. We expect this process to continue in the subsequent bursts till diffusion rises $PSC(t)$ to a value of 1. The role of any additional bursts after $PSC(t)$ reaches 1 is not accounted for by the model since the pDNA is absorbed by the cell membrane and $P(X, t) = 0$ in $X \in [-B_L, B_R]$. In such cases, additional pulses can be thought to add more pDNA molecules to the cell membrane.

3.6.3. 100 μs Pulses

Equations (4) and (5) were solved using B_L, $B_R = 134$ nm (representing 500 μg/mL pDNA solution concentration) for a 100 μs (monopolar) pulse at an electric field intensity of 1.25 kV/cm, corresponding to experimental conditions for C2C12 cells (Table 1). The evolution of $P(X, t)$ is shown in Figure 17A for the case without the free energy barrier and in Figure 17C for the case with free energy barrier. For the case without the free energy barrier, electophoresis shifts the peak of $P(X, t)$ towards the cell membrane and acts for a sufficient amount of time to ensure that the pDNA molecule reaches the cell membrane during the pulse. This is further evident from the evolution of $PSC(t)$ in Figure 17B, where $PSC(t)$ remains negligibly small until around $t \sim 20$ μs and then suddenly increases to a final value of 1 well before the pulse terminates at $t = 100$ μs. This is further evident from $P(X, t) = 0$ in $X \in [B_L, B_R]$ for times $t > 20$ μs in Figure 17A, indicating that the pDNA has been absorbed by the cell membrane by this time.

For the case with the free energy barrier, similar to the case without the free energy barrier, electrophoresis drives the peak of $P(X, t)$ towards the cell membrane during the pulse (Figure 17C). When nearing the cell membrane, and while electrophoresis is still present, electrophoresis is driving the pDNA molecule to establish a contact with the cell membrane, and at the same time, it is facing the free energy barrier preventing the pDNA molecule from being absorbed at the cell membrane. As a result of this, there is a high probability of finding the pDNA molecule close to the cell membrane (see the peak at $t \sim$ 50 μs in Figure 17C, also notice the change in scale of the Y-axis between Figure 17A,C) Eventually, with electophoresis acting on the pDNA molecule, the probability of pDNA overcoming the free energy barrier and establishing a contact with the cell membrane increases. Simultaneously, the probability of the pDNA molecule being located close to the cell membrane decreases, as is evident in the decrease in the peak of $P(X, t)$ from $t \sim 50$ μs to $t \sim 100$ μs (Figure 17C).

Similar inferences can be made from the evolution of $PSC(t)$ in Figure 17D. Similar to the case without the free energy barrier (Figure 17B), $PSC(t)$ begins to rise at $t \sim 20$ μs in Figure 17D; however, the rise is not as steep as was with the case without the free energy barrier. The free energy barrier slows down the rise in $PSC(t)$. Furthermore, it also prevents $PSC(t)$ from attaining a vlaue of 1 during the pulse. Once the pulse is terminated, $PSC(t)$ begins to rise by diffusion. However, the rise is negligibly small since the free energy barrier is too strong/high to be overcome by diffusion.

Figure 17. The 100 μs pulses: Evolution of $P(X,t)$ and the corresponding Probability of Successful Contact $PSC(t) = 1 - \int_{-B_L}^{+B_R} P(X,t)dX$ for B_L, B_R = 134 nm (500 μg/mL) for a 100 μs pulse at an electric field intensity of 1.25 kV/cm (Table 1 for C2C12 cells). (**A,B**) represent cases without free energy barrier and (**C,D**) represent cases with free energy barrier. The dashed lines in (**B,D**) represent the time at which the 100 μs pulse ends. For (A), $P(X,t) = 0$ in $X \in [B_L, B_R]$ for legends in $t \geq 50$ μs, as a result of which $P(X,t)$ is not visible in (A) for these values of t. For (C), $P(X,t) \sim 0$ in $X \in [B_L, B_R]$ for legends in $t \geq 1$ ms, as a result of which $P(X,t)$ is not visible in (C) for these values of t.

$PSC(t)$ is evaluated for (B_L, B_R) ranging from 77 nm to 433 nm, corresponding to concentrations ranging from 2500 μg/mL to 15 μg/mL, respectively, and is shown in Figure 18A for the case without the free energy barrier. For most ranges of (B_L, B_R) tested, $PSC(t)$ rises steeply through electrophoresis and attains a final value of 1 before the 100 μs pulse. For (B_L, B_R) = 433 nm (corresponding to the lowest concentration of 15 μg/mL), $PSC(t)$ just falls short of reaching a value of 1 before the 100 μs pulse's termination; however, $PSC(t)$ reaches a value of 1 post-pulse termination. The time at which $PSC(t)$ begins to rise depends on (B_L, B_R), and $PSC(t)$ starts to rise earlier for lower (B_L, B_R), i.e., for higher concentrations. For the 100 μs pulse, the rise in $PSC(t)$ happens before the termination of the pulse, unlike nanosecond and HF-BP pulses, where $PSC(t)$ rises post-pulse/burst termination through the diffusive process.
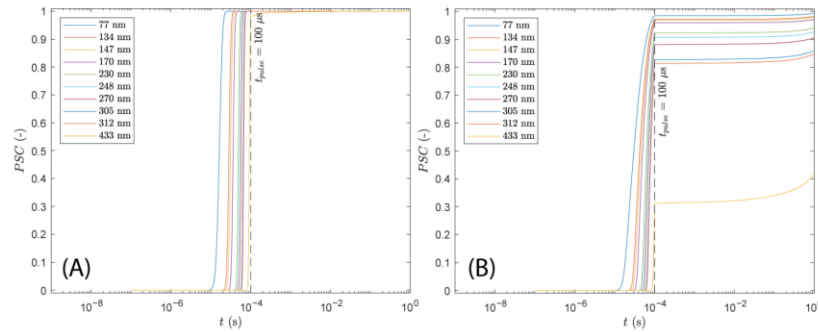
Figure 18. Evolution of $PSC(t)$ for different (B_L, B_R) ranging from 77 nm to 433 nm, corresponding to concentrations ranging from 2500 μg/mL to 15 μg/mL, for a 100 μs pulse at an electric field intensity of 1.25 kV/cm (Table 1 for C2C12 cells): (**A**) without free energy barrier and (**B**) with free energy barrier. Dashed lines represent the time at which the 100 μs pulse ends.

For the case with the free energy barrier (Figure 18B), $PSC(t)$ begins to rise before $t = 100$ μs and continues to rise until $t = 100$ μs (due to electrophoresis) for all (B_L, B_R) ranging from 77 nm to 433 nm, corresponding to concentrations ranging from 2500 μg/mL to 15 μg/mL, respectively. The rise is not as steep as it is for the case without the free energy barrier. Moreover, $PSC(t)$ does not attain a value of 1 at $t = 100$ μs, and the value of $PSC(t)$ at $t = 100$ μs depends on (B_L, B_R). After $t = 100$ μs (pulse termination), $PSC(t)$ increases slowly through the diffusive process. However, the post-pulse diffusive rise is small since diffusion is not strong enough to efficiently overcome the high free energy barrier.

These results indicate that even though the electrophoresis provided by the 100 μs pulse aids in overcoming the free energy barrier (as indicated by the higher $PSC(t)$ observed compared to the nanosecond and HF-BP pulses), they are not entirely sufficient to completely ensure that the pDNA molecule comes in contact with the cell membrane during pulse.

It is interesting to note that the final $PSC(t)$ before the onset of the second pulse, i.e., $PSC(t = 1$ s$)$ does not depend upon (B_L, B_R)/concentration for no free energy barrier (Figure 18A), whereas it depends on the (B_L, B_R)/concentration with the free energy barrier (Figure 18B). Therefore, similar to HF-BP pulses, depending on the presence of a free energy barrier and its strength/height, the results for the 100 μs pulse at an electric field strength of 1.25 kV/cm may depend on the concentration.

Furthermore, the Peclet number during a single phase (pulse + post-pulse) is $Pe = \frac{\mu E t_p}{\sqrt{2D t_{bp}}} = 0.33$, considering $t_p = 100$ μs, time between pulses $t_{bp} = 1$ s, and $E = 1.25$ kV/cm. Such a value of Peclet number, although < 1, does not convince us entirely of either electrophoresis or of diffusion dominating the process during the single phase (pulse + postpulse). Therefore, there could be a confounding role of subsequent pulses, and individual pulses cannot be inferred in isolation. For the case with the free energy barrier, we expect the additional pulses to increase the probability of pDNA reaching the cell membrane and contribute to the further rise in $PSC(t)$. For the case without the free energy barrier, $PSC(t)$ already reaches 1 before 100 μs pulse termination, and $P(X, t) = 0$ in $X \in [-B_L, B_R]$ before the onset of the second pulse. As mentioned previously, the model does not account for the second (or additional) pulse. Therefore, additional pulses can be thought to add additional pDNA molecules to the cell membrane.

3.6.4. 5 ms Pulses

Equations (4) and (5) were solved using B_L, $B_R = 134$ nm (representing 500 μg/mL pDNA solution concentration) for a 5 ms pulse at an electric field intensity of 0.6 KV/cm

corresponding to experimental conditions for C2C12 cells (Table 1), and the results are shown in Figure 19A,B for the case without the free energy barrier and in Figure 19C,D for the case with the free energy barrier. For the case in which no free energy barrier is present, the evolution of $P(X, t)$ is shown in Figure 19A. Similar to a 100 μs pulse without a free energy barrier, electrophoresis with a 5 ms pulse drives the peak of $P(X, t)$ towards the cell membrane. The 5 ms pulse is long enough to ensure that the pDNA molecule is able to reach the cell membrane. This is also evident from the evolution of $PSC(t)$ in Figure 19B. $PSC(t)$ remains negligibly small until $t \sim 40$ μs and then suddenly rises to attain a final value of 1 well before the 5 ms pulse ends. For a 100 μs pulse without free energy barrier Figure 17B, $PSC(t)$ remains negligibly small until $t \sim 20$ μs, then rising suddenly to reach a final of 1. The difference in the time when $PSC(t)$ begins to rise can be explained by the difference in the electric field intensities used. For the 100 μs pulse, the electric field was 1.25 kV/cm, whereas for the 5 ms pulse, the electric field was 0.6 kV/cm. As a result, it takes approximately twice the amount of time for $PSC(t)$ to become non-negligible and then rise suddenly (steeply) for the 5 ms pulse conditions. $P(X, t) = 0$ in $X \in [B_L, B_R]$ for times $t > 50$ μs in Figure 19A, indicating that the pDNA has been absorbed by the cell membrane by this time.
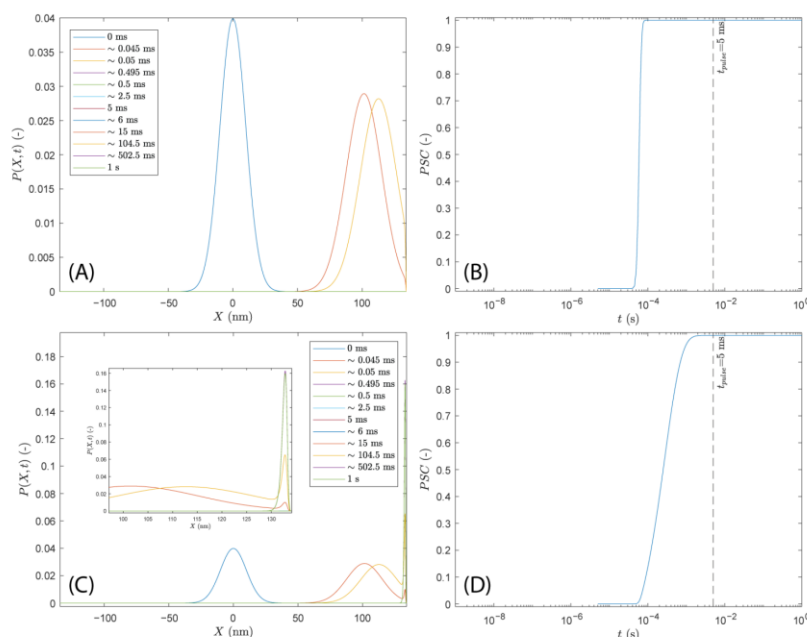
Figure 19. The 5 ms pulses: Evolution of $P(X, t)$ and the corresponding Probability of Successful Contact $PSC(t) = 1 - \int_{-B_L}^{+B_R} P(X, t)dX$ for $B_L, B_R = 134$ nm (500 μg/mL) for a 5 ms pulse at an electric field intensity of 0.6 kV/cm (Table 1 for C2C12 cells). (**A,B**) represent cases without free energy barrier and (**C,D**) represent cases with free energy barrier. The dashed lines in (**B,D**) represent the time at which the 5 ms pulse ends. For (**A**), $P(X, t) = 0$ in $X \in [B_L, B_R]$ for legends in $t \geq 0.495$ ms, as a result of which $P(X, t)$ is not visible in (**A**) for these values of t. For (**C**), $P(X, t) = 0$ in $X \in [B_L, B_R]$ for legends in $t \geq 2.5$ ms, as a result of which $P(X, t)$ is not visible in (**C**) for these values of t.

When a free energy barrier is present between the pDNA molecule and the cell membrane, similar to the 100 μs pulse, electrophoresis from the 5 ms pulses drives the

peak towards the cell membrane (Figure 19C). However, in the presence of the free energy barrier, when the $P(X, t)$ distribution reaches the cell membrane, electrophoresis is driving the probability for the pDNA to be absorbed at the cell membrane and, at the same time, the free energy barrier is preventing pDNA from being absorbed. This competition between electrophoresis and the free energy barrier leads to another peak of $P(X, t)$ being formed close to the cell membrane, which rises with time (Figure 19C at $t \sim 0.045$ ms and $t \sim 0.05$ ms, also note the difference in the scale of the Y-axis between Figure 19A,C). Eventually, the distribution of $P(X, t)$ becomes concentrated to a single peak with a narrow distribution (Figure 19C at $t \sim 0.495$ ms and inset). As electrophoresis continues to act, the probability of pDNA overcoming the free energy barrier and of pDNA being absorbed by the cell membrane increases, reducing the peak of narrow band $P(X, t)$ (Figure 19C at $t \sim 0.495$ ms and $t \sim 0.5$ ms and inset). Eventually, electrophoresis acts long enough to ensure that the pDNA molecule is absorbed by the cell membrane.

Similar inferences can be made from the evolution of $PSC(t)$ for the case with the free energy barrier (Figure 19D). $PSC(t)$ remains negligibly small until $t \sim 40$ μs and then begins to rise. Compared to the case without the free energy barrier (Figure 19B), the rise in $PSC(t)$ is slower, owing to the competing effect of electrophoresis and free energy barrier. Eventually, electrophoresis is able to overcome the free energy barrier, and $PSC(t)$ reaches a final value of 1 before the end of the pulse.

$PSC(t)$ is also evaluated for (B_L, B_R) ranging from 77 nm to 433 nm (representing 2500 μg/mL to 15 μg/mL pDNA solution concentration, respectively) and is shown in Figure 20A for the case without the free energy barrier. For all ranges of (B_L, B_R) tested, $PSC(t)$ rises steeply and attains a final value of 1 before pulse termination through electrophoresis. The time at which $PSC(t)$ begins to rise depends on (B_L, B_R), and $PSC(t)$ starts to rise earlier for lower (B_L, B_R) (i.e., higher concentrations). These observations are similar to the case without the free energy barrier for a 100 μs pulse (Figure 18A) and unlike for nanosecond pulses and HF-BP pulses, where $PSC(t)$ rises post-pulse/burst termination through the diffusive process (Figure 13A,C, Figures 15A and 16A).
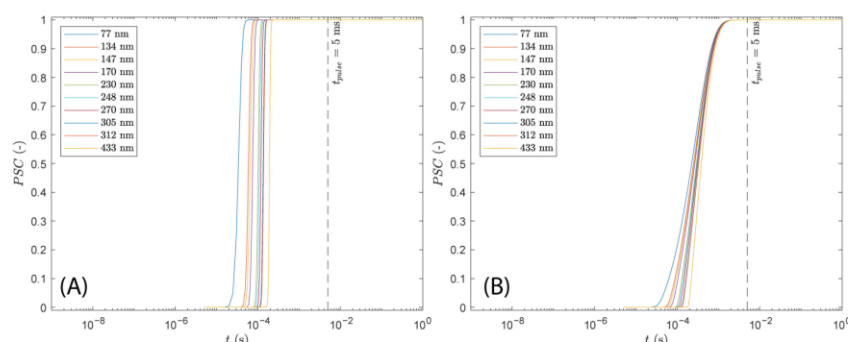
Figure 20. Evolution of $PSC(t)$ for different (B_L, B_R) ranging from 77 nm to 433 nm (corresponding to concentrations ranging from 2500 μg/mL to 15 μg/mL) for a 5 ms pulse at an electric field intensity of 0.6 kV/cm (Table 1 for C2C12 cells): (**A**) without free energy barrier and (**B**) with free energy barrier. Dashed lines represent the time at which the 5 ms pulse ends.

For the case with the free energy barrier, $PSC(t)$ begins to rise before pulse termination at $t = 5$ ms for (B_L, B_R) raning from 77 nm to 433 nm (representing 2500 μg/mL to 15 μg/mL pDNA solution concentration, respectively) (Figure 20B). The time at which $PSC(t)$ begins to rise depends on (B_L, B_R), and the rate of the rise in $PSC(t)$ is slower compared the case without the free energy barrier. For a 5 ms pulse at an electric field intensity of 0.6 kV/cm, the electrophoresis acts for a sufficient amount of time to ensure that $PSC(t)$ reaches a final

value of 1 before pulse termination for all (B_L, B_R) tested. This is unlike the case for a 100 μs pulse with the free energy barrier, where $PSC(t)$ could not attain a final value of 1 for the range of (B_L, B_R) tested, even though twice as strong of an electric field, with an intensity of 1.25 kV/cm, was applied.

The results in Figure 20 indicate that irrespective of the presence of free energy barrier, $PSC(t)$ reaches a final value of 1 before the 5 ms pulse termination for all (B_L, B_R) tested, indicating that GET should not depend on the concentration for these pulse parameters.

We can further calculate the Peclet number as $Pe = \frac{\mu E t_p}{\sqrt{2D t_{bp}}} = 7.95$; considering $t_p = 5$ ms, time between pulses $t_{bp} = 1$ s, and $E = 0.6$ kV/cm. $Pe = 7.95$ indicates that electrophoresis dominates diffusion during the phase (pulse + post pulse), and individual pulses cannot be inferred in isolation. However, the pulse duration is long enough to ensure that $PSC(t)$ reaches a final value of 1 before pulse termination for both – with and without the free energy barrier. So, even though the model does not account for multiple pulses since $P(X, t) = 0$ in $X \in [B_L, B_R]$ before the onset of the next pulse, subsequent pulses can be thought to add more pDNA molecules to the cell membrane.

4. Discussion

Electroporation with long pulses in vitro and in vivo is a well-established and efficient method for GET [55,66]. Most often, a train of pulses in the range of few to several tens of millisecond is used, although even shorter, i.e., 100–500 μs, pulses are used. With expanding the use of GET from in vitro to in vivo, the need to avoid pain and undesirable muscle contractions emerged. It was also suggested that electrochemical reactions could negatively affect GET efficiency [27–33]. The approval of cell therapies, where cells are transfected ex vivo, further strengthen the need to reduce electrochemical reactions during treatment because, usually, the number of available cells is low; consequently, it is important that most of the cells survive the treatment. Currently, when GET is performed ex vivo, the high voltage required for electroporation poses risks of cytotoxicity and loss of cytoplasmic content, which can adversely affect GET efficiency [67].

The use of shorter pulses in GET provides a potential mitigation of the above-mentioned drawbacks of long pulses, but the HF-BP and nanosecond pulse range remains poorly explored. Currently, there are only a few studies reporting the use of HF-BP and nanosecond pulses for GET [15,40,41]. Therefore, the aim of this study was to further explore the nanosecond range of pulse durations and HF-BP pulses. We aimed to find optimal parameters for GET with 200 ns and 500 ns pulses in two different cell lines and compare efficiency and expression dynamics of different pulse durations, up to 5 ms, including HF-BP. Since the electrophoretic effect of electric pulses on pDNA in GET is considered important, we also developed a theoretical framework of the diffusive and electrophoretic movement of pDNA during different pulse protocols and compared the results to those obtained experimentally.

4.1. Cell Membrane Permeabilization and Cell Survival

For GET, it is critical to use pulse parameters which achieve cell membrane permeabilization and at the same time maintain high cell survival. It was postulated that membrane permeabilization is prerequisite for successful GET. GET, however, is a complex process comprised of several consecutive steps, with cell membrane permeabilization alone not being a guarantee for successful GET [1,55]. Nevertheless, cell membrane permeabilization was first determined by using PI. Because the electric field at the intersection of the permeabilization and survival curves is not necessarily optimal also for GET, we also determined GET efficiency at slightly larger and slightly lower electric fields. With all tested pulse protocols, we were able to determine the optimal electric field for GET, which usually resulted in around 80% cell membrane permeabilization and higher than 60% cell survival. As expected, using longer pulses and/or higher numbers of applied pulses, cell membrane permeabilization was reached at lower electric fields [48,68]. The optimal electric field for GET was similar for both cell lines (Supplementary Tables S3 and S4). We electroporated

cells in suspension, which means they are of similar round shape, their size does not differ significantly (Table 1), and they are evenly distributed between electrodes, which all leads to a similar electric field needed for having the majority of cells permeabilized [69].

4.2. Effect of pDNA Concentration on Overall Gene Electrotransfer

The high concentration of pDNA can have a negative effect on cell survival [16] and consequently on GET efficiency, but it is also needed to obtain GET with nanosecond and HF-BP pulses [15,49]. Pathogen-associated molecular patterns that are associated with pDNA, for example, unmethylated CpG motifs in pDNA, can be recognized by TLR9 and can induce an innate immune response in tissue, which can lead to apoptosis activation [70,71]. pDNA concentrations used in our experiments were higher than concentrations usually used in in vitro experiments, which are most often between 10 and 100 μg/mL [14,72–75]. On the other hand, it has been shown that pDNA concentration affects GET efficiency and that, with higher pDNA concentration, efficient GET can also be achieved with shorter pulses [15,16,25,76]. The effect of the pDNA concentration was observed in our experiments, where a decreasing pDNA concentration led to a significant decrease in the overall GET. This was especially observed in 1306 fibroblasts, where, at pDNA concentrations up to 100 μg/mL, the overall GET was higher with 8×100 μs, HF-BP, and 8×5 ms pulses compared to 500 ns and 200 ns pulses, whereas, at 500 μg/mL of pDNA, there was no significant difference in the overall GET between different pulse protocols. Interestingly, this was not observed in C2C12 myoblasts where the overall GET rose with increasing pDNA concentration for all pulse protocols. At the highest pDNA concentration (500 μg/mL), the overall GET was, however, still significantly higher with longer pulse protocols (8×100 μs and 8×5 ms), where electrophoresis acts for a longer period of time compared to shorter pulse protocols (HF-BP, 500 ns, and 200 ns) (Figure 5). Difference in overall GET between two cell lines confirms that the efficiency of GET does not depend solely on parameters of applied pulses. GET is a multistep process including various intracellular mechanisms (cell membrane repair mechanism, DNA sensors activation, endocytic pathways, cytoskeleton reorganization) which can differ between cell lines [77,78].

Contrary to our previous results on a CHO cell line [15], in C2C12 myoblasts and 1306 fibroblasts, we observed some decrease in cell survival with increasing pDNA concentration, however, not for all pulse protocols. With 8×5 ms pulses, we did not observe a decrease in cell survival with increasing pDNA concentrations (in both cell lines). In addition, in C2C12 myoblasts, pDNA concentration did not have an effect on cell survival after GET with the HF-BP, 100×500 ns, and 25×200 ns pulse protocols. A decrease in cell survival with 250 μg/mL of pDNA was only observed in 1306 fibroblasts after the 8×100 μs pulse protocol; with other pulse protocols, decreased survival was observed only with the highest pDNA concentration, 500 μg/mL (Figure 4). Our results are similar to [79], where the authors observed decreased cell survival with pDNA concentrations higher than 400 μg/mL. However, the decrease in cell survival in our experiments was not high enough to cause a drop in the overall GET at 500 μg/mL of pDNA. These and our previous results [15] show that decreases in cell survival following GET with high pDNA concentration seem to be cell-line-dependent. pDNA by itself was not toxic to cells, as observed before [15,80]. High pDNA concentration could trigger a decrease in cell survival in different steps of GET. We have shown previously that higher pDNA concentration leads to larger pDNA aggregates formed on cell membrane [15] during pulse delivery, which could slow down or obstruct cell membrane repair. Furthermore, high pDNA concentration in endosomes or cytoplasm could activate endosomal and/or cytoplasmic DNA sensors which can induce programmed cell death [81]. Finally, cell death could be triggered by high number of pDNA copies in nucleus or by the high number of transgenes being produced [82].

78

4.3. Gene Electrotransfer Using Different Plasmid Sizes

Since pDNA size is reported to have an influence on GET efficiency, we compared GET, cell survival, and overall GET with a 4.7 kb and a 3.5 kb pDNA having the same CMV promoter and both encoding GFP. We did not observe any difference in GET and cell survival between different pDNA sizes. Interestingly, smaller pDNA led to higher overall GET only when using the 8×100 μs pulse protocol in both cell lines. For other pulse protocols, we did not observe a significant increase in the overall GET with smaller pDNA, although the copy number of smaller pDNA was 1.34 times higher compared to the larger pDNA, as we used the same concentration of pDNA (500 μg/mL) (Figure 6). Similarly, it was previously shown that GFP knockdown with pDNA sizes from 1.9 to 4.3 kb was equally efficient when the same moles of pDNA were used applying 2×30 ms pulses [83]. Our results show that smaller pDNA did not have a strong effect on overall GET, which is contrary to observations by [41], where they report higher sub-microsecond high-frequency GET with smaller pDNA. Reducing pDNA size also improved GET efficiency in other studies [84,85]. The difference in the size of the pDNA used in our study was only 25%, which might be the reason why we did not observe a significant increase in overall GET efficiency with smaller pDNA.

Interestingly, when comparing MFI of GFP-positive cells transfected with pDNA of different sizes in C2C12 myoblasts, a significantly higher MFI with smaller pDNA was observed after GET with the 200 ns, 500 ns, and HF-BP pulses. On the contrary, in 1306 fibroblasts, a higher MFI with smaller pDNA was observed after GET with 8×100 μs and 8×5 ms (Figure 7) pulses. This means that in C2C12 myoblasts, shorter pulses enabled more copies of smaller pDNA to reach the nucleus. With longer pulses, the MFIs after GET with both pDNA sizes were comparable. The situation seems to be reversed in 1306 fibroblasts, where longer pulses enabled more copies of smaller pDNA to reach the nucleus. This suggests that not only cell line and pDNA size but also pulse parameters influence the degree of transgene expression.

4.4. Effect of Pulse Parameters on Overall Gene Electrotransfer

We achieved GET in both cell lines with all pulse protocols, but with variable efficiency (Figure 8). Differences in GET efficiency between different cell lines have been reported before [86–88] and are still not well understood. It has been suggested that differences in GET efficiency can be the consequence of various biophysical factors such as the fluidity of the cell membrane or biological parameters such as different mechanisms that are present or activated in cells and the ability of cells to recover after the delivery of electric pulses [89,90]. If the difference would be the consequence of different cell membrane composition or fluidity or induced transmembrane voltage, then we would expect to also observe the difference in cell membrane permeabilization. Since permeabilization and survival curves were similar for both cell lines, the difference in GET efficiency is more likely the consequence of the difference in the presence and degree of activity of intrinsic cellular mechanisms and pathways. Furthermore, in in vitro experiments, the composition of the electroporation medium can also influence GET efficiency [91–93]. The GET of each cell line in our experiments was performed in their recommended growth medium. For C2C12 myoblasts, this was DMEM, and for 1306 fibroblasts, this was EMEM. They are both variations of basic medium used for primary and diploid cultures, but DMEM has a higher concentration of amino acids and vitamins compared to EMEM. DMEM also contains iron in the form of ferric sulfate, which is absent in EMEM [94].

We performed GET in growth medium, which is more like in vivo extracellular fluid compared to other buffers used for GET. Growth medium is highly conductive, which results in high currents and increased electrochemical reactions such as electrolysis, the generation of radicals, and the release of metal ions from the electrodes during pulse delivery [28,95]. It was shown previously that short, i.e., nanosecond, pulses and bipolar pulses decrease metal release from electrodes compared to longer pulses [29,35,48,96]. Furthermore, high medium conductivity also results in high currents, leading to heating

and temperature increases in the sample during pulse delivery. The temperature increase is more pronounced when longer or more pulses are applied [35]. In our experiments, the temperature of the sample never exceeded 32 °C, meaning that thermal effects were negligible (Supplementary Table S5).

In addition to achieving a higher percentage of transfected cells in 1306 fibroblasts, the MFI of the GFP-positive cells was higher (Figure 9). Fluorescence intensity is reported to be dependent on the number of pDNA copies inside the cell that have reached the cell nucleus and have been successfully transcribed and translated into fluorescent proteins [97,98]. In this respect, this could mean that the higher number of pDNA copies was transferred to 1306 fibroblasts during pulse delivery compared to C2C12 myoblasts. Other factors, such as the availability and degree of activity of the cellular machinery for transcription and translation, also affect production of proteins from transfected pDNA [97,98]. Based on this, higher GET efficiency in 1306 fibroblasts could also mean that the rate of pDNA transcription and translation into fluorescent protein is higher in 1306 fibroblasts compared to C2C12 myoblasts.

4.5. Time Dynamics of pDNA Expression

Measurements of pDNA expression every 8 h over a six-day period (Figures 10 and 11) show that the onsets of GFP expression (both percentage of GFP-positive cells and their MFI) are comparable for the 200 ns, HF-BP, 8×100 µs, and 8×5 ms pulse protocols but depend greatly on the cell line. Similar time dynamics of the GET and MFI for all pulse durations in one cell line suggest that all pulse protocols triggered the same mechanisms responsible for pDNA translocation through the cytoplasm to the cell nucleus.

In C2C12 myoblasts, the GFP-positive cells and their MFI reached a peak soon after GET and then declined steadily, falling below 10% for all four pulse durations at day 6. Similar time dynamics were observed for human mesenchymal stem cells [86]. On the contrary, in 1306 fibroblasts, peaks of the maximum GFP-positive cells and their MFI were broad and not very pronounced. After reaching a peak, the percentage of GFP-positive cells started to decrease slowly. On day 6 after GET with all pulse durations, around half of the cells were still GFP-positive (Figures 10 and 11). Differences in time dynamics and duration of transgene expression after GET between cell lines have been reported previously [99]. Differences in curves for the GET and MFI for all pulse protocols between cell lines suggest that mechanisms of pDNA translocation through the cytoplasm to the cell nucleus and the duration of the transcription of pDNA are most probably different in different cell lines.

The lower percentage of GFP-positive cells and their lower MFIs in C2C12 myoblasts could be a consequence of the higher number or degree of activation of DNA sensors in this cell line, which could trigger pDNA degradation to a larger extent compared to 1306 fibroblasts. During GET, pDNA could activate endosomal DNA sensors during translocation to the nucleus with endocytosis mediated pathways or cytoplasmic DNA sensors by entering the cell through cell membrane defects caused during pulse delivery. Additionally, cytosolic DNA sensors might be triggered by pDNA released to cytosol after endosomal escape. It was already shown that GET with pDNA led to the upregulation of several proposed cytosolic DNA sensors in different tumor cell types [78,100] and also in C2C12 myoblasts [82]. Other reasons for the observed decrease in transgene expression over time in C2C12 myoblasts could be the loss of the pDNA through the nuclear pores, loss of the pDNA at each mitosis, de novo pDNA methylation preventing pDNA transcription, or pDNA degradation by endonucleases [80].

We continuously observed differences in the overall GET and MFI between the two cell lines studied. These differences might be the consequence of variations in cell membrane composition [101], endocytic pathways specific to certain cell lines, or the degree of activation of endocytic pathways [102,103], as well as the presence of cytosolic nucleases [104].

Our results show that MFI of GFP-positive cells is more unpredictable and unrepeatable than the percentage of GFP-positive cells. The MFI of 1306 fibroblasts in our experiments with increasing pDNA concentration (Figure 3D) was much lower than the

MFI of 1306 fibroblasts transfected with the same concentration (500 μg/mL) of pDNA and with the same pulse protocols in the experiments of time dynamics of pDNA expression (Figure 11B). At the same time, the GET efficiency in both experiments was comparable with the same pulse protocols. Contrarily, in C2C12 myoblasts, the MFI was comparable in both experiments, but GET after 8×5 ms was much lower in the experiments of the time dynamics of the pDNA expression (Figure 10A) compared to the experiments with increasing pDNA concentration (Figure 3A). It was shown previously that the time after cell passage at which cells are exposed to electric pulses affects GET efficiency. The GET and MFI of all plasmid concentrations differed significantly when comparing cells transfected 24 h and 48 h after passage. The GET and MFI were higher in cells which were transfected 24 h after passage compared to cells transfected 48 h after passage. Observed differences in the transfection efficiency of the cells passaged at different times before the experiment could be the consequence of the differences in cell cycle phases at which GET was performed [79]. Biological factors, such as cell growth phase, which determine cell shape, size, and, probably most important, composition, and the integrity of the nuclear envelope play an important role in cell response to electric pulse delivery and the ability to repair damage after pulse delivery. During cell ageing, the cell membrane composition changes due to the increase in the total amount of proteins and cholesterol, potentially affecting cell membrane permeabilization [18,105]. In our experiments, we used cells 2–4 days after cell passage for GET, so this could be the reason for differences observed in GET and MFI of GFP-positive cells [79].

4.6. Modeling the Probability of pDNA Cell Membrane Contact during GET

From results of modeling the probability of pDNA cell membrane contact during GET, it can be inferred that the process of a pDNA molecule reaching the cell membrane and being absorbed by it is mediated by diffusion for 200 ns, 500 ns pulse and HF-BP pulses, whereas for the 100 μs and 5 ms pulse, the process is mediated by electrophoresis. As done in the results section, one can define a Peclet number as: $Pe = \frac{\mu E t_p}{\sqrt{2D t_{bp}}}$, where t_p is the pulse duration, t_{bp} is the duration between pulses, E is the electric field intensity, μ is the electrophoretic mobility and D is the diffusion coefficient. Alternatively, the time between pulses can be inferred as the frequency (f, Hz), in which case $Pe = \frac{\mu E t_p}{\sqrt{2D/f}}$. The values of Pe used in experiments, and mentioned in the results, are given below again in Table 2. Such a Pe gives the relative contributions of electrophoresis and diffusion during the single phase of pulse/burst. Inferring the role of electrophoresis for different types of pulses used (ns, HF-BP, μs, and ms) using this parameter helps to correctly identify the role electrophoresis and diffusion as inferred from the model results.

Table 2. Values of Pe for various experimental conditions for C2C12 cells.

	200 ns	500 ns	HF-BP	100 μs	5 ms
Frequency, f (Hz)	10.00	10.00	1.00	1.00	1.00
t_{bp} (s)	0.10	0.10	1.00	1.00	1.00
t_p (s)	2×10^{-7}	5×10^{-7}	2×10^{-6}	1×10^{-4}	5×10^{-3}
E (kV/cm)	15.80	4.10	1.25	1.25	0.60
Pe	0.03	0.02	0.01	0.33	7.95

$Pe \ll 1$ for the 200 ns, 500 ns, and HF-BP pulses indicates the dominant role of diffusion in bringing the pDNA molecule to the cell membrane. For the 100 μs pulse, $Pe = 0.33$ or $Pe \sim 1$, indicating that neither diffusion nor electrophoresis dominates the process of pDNA coming in contact with the cell membrane. From the model results of the 100 μs pulse, we saw that $PSC(t)$ begins to rise sharply before $t = 100$ μs, for both–with and without the free energy barrier. It could be possible that for the range of (B_L, B_R) tested from 77 nm to 433 nm corresponding to concentrations from 2500 μg/mL

to 15 µg/mL, the pDNA molecule was close to the cell membrane, and electrophoresis played the dominant role in bringing the pDNA molecules to the cell membrane On further reducing the concentration to <15 µg/mL, one might find that electrophoresis is insufficient to bring the pDNA molecule close to the cell membrane. As already seen for $(B_L, B_R) = 433$ nm, corresponding to 15 µg/mL (Figure 18A,B), $PSC(t)$ begins to rise very close to pulse termination (dotted line in Figure 18A,B). Therefore, one can argue that for $(B_L, B_R) > 433$ nm (or concentrations < 15 µg/mL), electrophoresis will be insufficient to bring the pDNA molecule to the cell membrane, and the process will have to partly rely on diffusion, indicating the dominance of neither. For the 5 ms pulse, $Pe = 7.95$ indicates the dominant role of electrophoresis in bringing the pDNA molecule close to the cell membrane. This is also seen from Figure 20A,B, where $PSC(t)$ begins to rise and attains a value of 1 much before pulse termination for both—with and without the free energy barrier, indicating electrophoresis as the dominant mechanism.

For 200 ns, 500 ns, and HF-BP, the electric field acts for a short duration, which is not sufficient to drive the pDNA molecule to the cell membrane through electrophoresis. The pDNA molecule thus diffuses to the cell membrane, and the distance (l) that the pDNA molecule travels by diffusion variers with time as $l^2 \sim Dt$. Therefore, normalizing the time in Figure 13A,C for nanosecond pulses and in Figure 15A for HF-BP pulses with l^2 should collapse the curves for different domain lengths $l = (B_L, B_R)$ ranging from 77 nm to 433 nm (corresponding concentration ranging from 2500 µg/mL to 15 µg/mL). The normalization (and the corresponding collapse) is shown in Figure 21A for the 200 ns pulse, in Figure 21C for the 500 ns pulse, and in Figure 21E for the HF-BP pulses for the case without the free energy barrier. This collapse further indicates that the process for pDNA reaching the cell membrane in the absence of a free energy barrier is purely diffusive for 200 ns, 500 ns, and HF-BP pulses.

For the case with the free energy barrier for 200 ns, 500 ns, and HF-BP pulses (Figures 13B,D and 15B), normalizing the time with l^2 does not produce a good collapse. Rather, normalizing with l collapses all the curves onto a single master curve (Figure 21B,D,F). Such a collapse with l indicates that the process for 200 ns, 500 ns, and HF-BP pulses with the free energy barrier is not entirely diffusive.

For 100 µs and 5 ms pulses without the free energy barrier, the process of pDNA reaching the cell membrane is electrophoretic for (B_L, B_R) ranging from 77 nm to 433 nm (corresponding concentration ranging from 2500 µg/mL to 15 µg/mL). The electrophoretic distance traveled by the pDNA molecule in the presence of an electric field is given by $l = \mu Et$; therefore, normalizing the curves with l in Figures 18A and 20A should collapse them into a single master curve. The collapse is shown as $PSC(t)$ vs. t/l in Figure 21G for the 100 µs pulse and in Figure 21I for the 5 ms pulse. This indicates that the process by which the pDNA molecule establishes contact with the cell membrane in the absence of the free energy barrier is driven by electrophoresis for 100 µs and 5 ms pulses.

For 100 µs and 5 ms pulses, in the case when the free energy barrier is present, we can follow the same process of normalizing the curves in Figures 18B and 20B by l and check the collapse. This is shown in Figure 21H,J for the 100 µs and 5 ms pulse, respectively. As can be seen from these figures, the collapse for times t when $PSC(t)$ begins to rise is good; however, for later times or far larger $PSC(t)$, the collapse is not satisfactory. This indicates that in the presence of free energy barrier, the process by which the pDNA molecule moves close to the cell membrane (since that is when $PSC(t)$ begins to rise) is driven by electrophoresis. However, the process of a pDNA molecule coming into contact with the cell membrane by overcoming the free energy barrier is not entirely electrophoretic. It is observed from Figure 20B that $PSC(t)$ is already collapsed for late times (i.e., for $PSC(t)$ close to 1) without normalizing, implying that $PSC(t)$ is independent of $l = (B_L, B_R)$ for the range of l tested between 77 nm and 433 nm.

Figure 21. (**A**) Results for 200 ns pulse in Figure 13A plotted as $PSC(t)$ vs. t/l^2; (**B**) Results for 200 ns pulse in Figure 13B plotted as $PSC(t)$ vs. t/l; (**C**) Results for 500 ns pulse in Figure 13C plotted as $PSC(t)$ vs. t/l^2; (**D**) Results for 500 ns pulse in Figure 13D plotted as $PSC(t)$ vs. t/l; (**E**) Results for HF-BP pulses in Figure 15A plotted as $PSC(t)$ vs. t/l^2; (**F**) Results for HF-BP pulses in Figure 15B
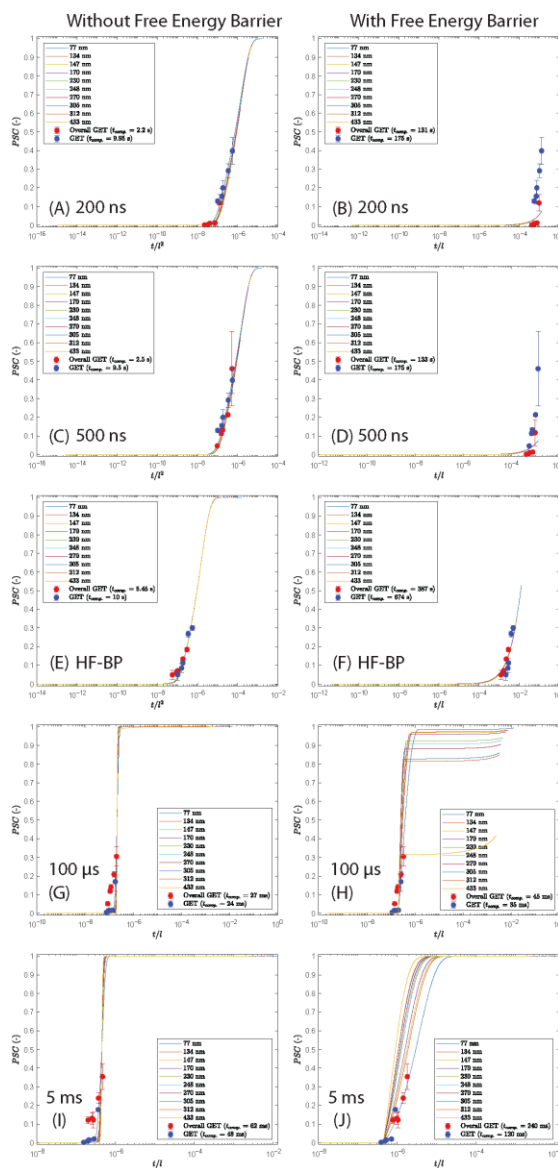
plotted as $PSC(t)$ vs. t/l; (**G**) Results for 100 μs pulse in Figure 18A plotted as $PSC(t)$ vs. t/l; (**H**) Results for 100 μs pulse in Figure 18B plotted as $PSC(t)$ vs. t/l; (**I**) Results for 5 ms pulse in Figure 20A plotted as $PSC(t)$ vs. t/l; (**J**) Results for 5 ms pulse in Figure 20B plotted as $PSC(t)$ vs. t/l. Also shown as dots are Overall GET (Figure 5) and GET (Figure 3) for C2C12 cells plotted against $t_{competent}/l^2$ or against $t_{competent}/l$, where l for the corresponding concentration was taken as R_{DNA} from Supplementary Table S1 and $t_{competent}$ was determined by fitting Overall GET/GET to $PSC(t)$ for $l = 77$ nm.

Also shown in Figure 21A–J are the results for overall GET and GET for the respective pulse parameters. Overall GET (Figure 5) and GET (Figure 3) for C2C12 myoblasts are plotted against $t_{competent}/l$ or against $t_{competent}/l^2$. Values of l for the respective concentrations are taken from R_{DNA} from Supplementary Table S1. $t_{competent}$ is taken to be the time for which the cell membrane remains competent to accept/absorb the incoming pDNA molecule. $t_{competent}$ was determined by varying $t_{competent}$ and minimizing the root mean squared error (RMSE) between Overall GET/GET vs. $t_{competent}/l^2$ and $PSC(t)$ vs. t/l^2 (at $l = 77$ nm) in Figure 21A,C,E. For Figure 21B,D,F,G–J, $t_{competent}$ was determined by varying $t_{competent}$ and minimizing the root mean squared error (RMSE) between Overall GET/GET vs. $t_{competent}/l$ and $PSC(t)$ vs. t/l (at $l = 77$ nm). $l = 77$ nm was chosen since the curves are collapsed for various values of l, and fitting to $l = 77$ nm would imply fitting to all the collapsed curves. The best fit values are given in the legends in Figure 21A–J against their respective Overall GET and GET.

It should be noted that this exercise of plotting Overall GET/GET vs. $t_{competent}/l^2$ or $t_{competent}/l$ along with $PSC(t)$ vs. t/l^2 or t/l should not be considered as a direct one-to-one comparison between the model and the experiment. Such an exercise is only performed to place the experiments within the context of the model. Overall GET and GET cannot be directly compared to $PSC(t)$, as overall GET and GET represent efficiencies which also include downstream processes of pDNA translocation across the cell membrane, migration through the cytoplasm, entering the nucleus, transcription, translation, and protein expression. $PSC(t)$, on the other hand, only represents the probability of pDNA establishing contact with the cell membrane. However, in a first approximation, only those cells on which pDNA molecules have established contact with the cell membrane can be expected to be transfected. Therefore, $PSC(t)$ can be considered as an upper limit of transfection efficiency. Moreover, different durations of pulses (short nanosecond pulses, HF-BP, or long micro- and millisecond pulses) can permeabilize the cell membrane in different ways. This can in turn result in the cell membrane being competent in different ways to absorb the pDNA molecule for different durations of pulses. Different durations of pulses can also alter the free energy barrier between the pDNA and the cell membrane, further influencing the results. Different types of cells themselves can be sensitive in different ways to permeabilization by the pulses, yielding different transfection efficiencies, as seen in Figure 3 for C2C12 myoblasts and 1306 fibroblasts. The models based on $PSC(t)$ do not account for such parameters and differences. An experimental observable that can perhaps be better compared to the $PSC(t)$ could therefore be the fraction of cells forming pDNA aggregates on the cell membrane [21,56].

From the fitting parameters of $t_{competent}$ in Figure 21A–J, it can be observed that $t_{competent}$ for 200 ns, 500 ns, and HF-BP, where the process is diffusive, is much larger than $t_{competent}$ for 100 μs and 5 ms pulses, where the process is mainly electrophoretic. Absolute values $t_{competent}$ cannot be considered, as $t_{competent}/l$ or $t_{competent}/l^2$ are not non-dimensional; however, from fitting, $t_{competent}$ for 200 ns, 500 ns, and HF-BP is around two orders of magnitude larger than $t_{competent}$ for 100 μs and 5 ms pulses. Furthermore, adding a free energy barrier between the pDNA and the cell membrane shifts the rise in $PSC(t)$ vs. t/l^2 or t/l to the right, indicating that it is harder for the pDNA molecule to be absorbed by the cell membrane in the presence of free energy. One can then argue that the cell membrane needs to be competent for a longer amount of time in the presence of a free energy barrier to absorb the incoming pDNA molecule. As a result, larger $t_{competent}$ was

observed for the cases with free energy barrier (Figure 21B,D,F,H,J) compared to the cases without free energy barrier (Figure 21A,C,E,G,I).

To determine the time it takes for the pDNA molecule to reach the cell membrane by diffusion or by electrophoresis, some estimates can be considered. The time it takes for the pDNA molecule to reach the cell membrane at a distance l by diffusion is given by $t = l^2/2D$ (for 200 ns, 500 ns, and HF-BP pulses), whereas time it takes for the pDNA molecule to reach the cell membrane at distance l by electrophoresis is given by $t = l/\mu E$ (for 100 µs and 5 ms pulse). These estimates are given in Figure 22 for l ranging from 77 nm to 433 nm, corresponding to concentrations ranging from 2500 µg/mL to 15 µg/mL. E is taken as 0.6 kV/cm for the 5 ms pulse and 1.25 kV/cm for the 100 µs pulse. One can observe that the time it takes for pDNA to reach the cell membrane by diffusion varies from around $O(1)$ ms (for $l = 77$ nm, 2500 µg/mL) to around $O(100)$ ms (for $l = 433$ nm, 15 µg/mL). For electrophoresis, the time it takes to reach the cell membrane varies from around $O(0.01)$ ms (for $l = 77$ nm, 2500 µg/mL) to $O(0.1)$ ms (for $l = 433$ nm, 15 µg/mL). It can be inferred that the cell membrane should be competent for at least $O(100)$ ms, i.e., $t_{competent} \sim 100$ ms, for transfection by 200 ns, 500 ns, and HF-BP pulses, whereas the cell membrane should be competent for at least $O(0.1)$ ms, i.e., $t_{competent} \sim 100$ µs, for transfection by 100 µs and 5 ms pulses. There is a 2–3 orders of magnitude difference in $t_{competent}$ for 200 ns, 500 ns, and HF-BP and $t_{competent}$ for 100 µs and 5 ms pulses, as also inferred from the fitting parameters in Figure 21.
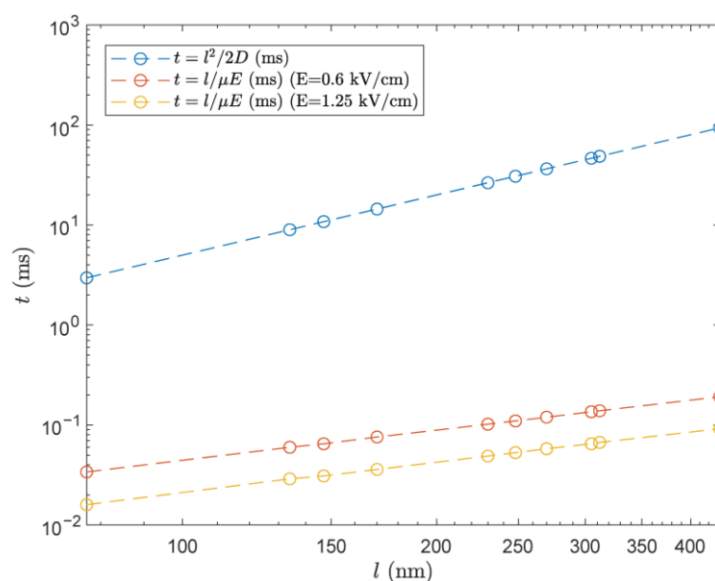
Figure 22. Time it takes for a pDNA molecule to cover a distance by diffusion and by electrophoresis. l ranges from 77 nm too 433 nm, corresponding to concentrations ranging from 2500 µg/mL to 15 µg/mL.

One can also observe from Figure 21 that for very large values of t/l or t/l^2, $PSC(t)$ reaches a final value of 1, and the results should not depend on l (or concentration). That is, if the cell membrane is able to absorb the pDNA molecule for a very large amount of time, then irrespective of l (or concentration), the pDNA molecule will have an equally high probability of reaching the cell membrane. Since we see a concentration dependence

for 200 ns, 500 ns, and HF-BP pulses, one can argue that $t_{competent}$ is around $O(1–100)$ ms, since this the amount of time it takes for the pDNA to reach the cell membrane by diffusion (Figure 22). The time it takes for the pDNA to reach the cell membrane by electrophoresis is $O(0.01–0.1)$ ms (Figure 22). For a large $t_{competent}$ of around $O(1–100)$ ms, we should not observe a concentration dependence for 100 μs and 5 ms pulses. However, since we do observe a concentration dependence for Overall GET and GET for 100 μs and 5 ms pulses, it could be that the $t_{competent}$ is different—and shorter (around $O(0.01–0.1)$ ms)—for these pulses. It has been observed experimentally that the cell membrane remains permeable for a longer amount of time with ns pulses compared to μs and ms pulses [48].

Recently, 300 ns pulses have been successfully used for GET [106]. However, 100 pulses were used at a pulse repetition frequency of 1 MHz. This high frequency of pulse repetition, or the corresponding short duration between successive pulses, could imply that the cumulative effect of 100 pulses at 1 MHz pulse repetition frequency is equivalent to a single pulse of duration 100 μs. To test this, Equation (4) was solved for 100 pulses of duration 300 ns and an electric field intensity of 7 kV/cm at a pulse repetition frequency of 1 MHz and a pDNA cell membrane distance of 170 nm (corresponding to 250 μg/mL, Supplementary Table S1), similar to the conditions used in [106]. The evolution of $P(X, t)$ is shown in Figure 23 for pulse numbers 1, 5, 10, 20, and 30. From Figure 23A, it can be seen that during the first pulse, the peak shifts towards the right due to electrophoresis (until 300 ns) and also spreads only slightly due to diffusion. After the cessation of first pulse, the peak stays at the same place, and the distribution spreads only slightly due to diffusion from 300 ns to 1 μs. During the second pulse, this peak is then further driven to the right by electrophoresis, spreading only slightly by diffusion. After the end of the second pulse, the distribution spreads only slightly by diffusion, until the time the third pulse acts and the process repeats (see Figure 23B for pulse number 5). By the 10th pulse, the peak of the distribution has already migrated a distance greater than 50 nm towards the right, spreading only slightly by diffusion (as seen by a broadening of $P(X, t)$ and a decrease in the maximum value of $P(X, t)$) (Figure 23C). By pulse number 20 (starting at $t = 19$ μs), the peak of the distribution has already drifted to the right by $\sim$150 nm by electrophoresis indicating a non negligible $PSC(t)$ by $t \sim$19 μs (Figure 23D,F). Figure 23E, corresponding to the 30th pulse (or $t = 29$ μs), indicates that the pDNA molecule has already been absorbed at the cell membrane as $P(X, t) = 0$ in $X \in [B_L, B_R]$ by $t = 29$ μs. This is further evident from Figure 23F, which shows that $PSC(t)$ has risen sharply and reached a final value of 1 before $t \sim 30$ μs.

The results in Figure 23 corresponding to the high frequency of 1 MHz differ from the results of Figure 12 corresponding to the low frequency of 10 Hz. In both cases, electrophoresis drives the peak of $P(X, t)$ towards the right (cell membrane) during the pulse while spreading it only slightly by diffusion. Once the pulse ends, the distribution of $P(X, t)$ is allowed to spread by diffusion. For the low frequency of 10 Hz case, the time between the subsequent pulses or the time allowed for the distribution to relax by diffusion is significantly higher ($t \sim 100$ ms). This large time allows the spread of $P(X, t)$ by diffusion and flattens it out in a way that enough flux of $P(X, t)$ can be collected at the cell membrane and $PSC(t)$ starts to rise by diffusion. However, for the high frequency of 1 MHz, the time between subsequent pulses or the time allowed for the distribution to relax by diffusion is small, corresponding to $t < 1$ μs. This time is too small for the distribution of $P(X, t)$ to spread by diffusion and reach the cell membrane. Soon after, the next pulse acts on the pDNA molecule driving the still narrow $P(X, t)$ distribution to the right. Cumulatively, this is how $P(X, t)$ is driven to the right by electrophoresis; if enough pulses are delivered (in this case $\sim$20), the pDNA molecule reaches the cell membrane by electrophoresis, as seen by the early and sharp rise in $PSC(t)$.
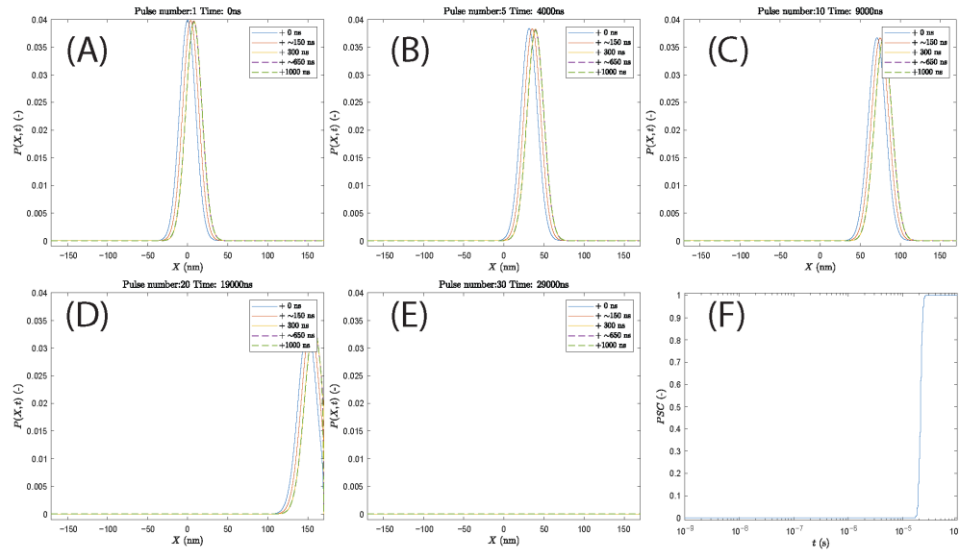
Figure 23. (**A–E**) Evolution of $P(X, t)$ without free energy barrier (Equation (4)) for 100 pulses of 300 ns and 7 kV/cm applied at a high frequency of 1 MHz and for a pDNA and cell membrane distance of 170 nm (corresponding to 250 µg/mL). The pulse numbers for each pulse and corresponding time are shown on top of (**A–E**). Solid lines indicate the during pulse $P(X, t)$ and dotted lines represent after pulse $P(X, t)$. (**F**) Evolution of $PSC(t)$ without free energy barrier.

The process of high-frequency ns pulses can also be analyzed from the point of view of Peclet number defined as $Pe = \frac{\mu E t_p}{\sqrt{2D/f}}$. For experimental conditions in [106], $t_p = 300$ ns, $E = 7$ kV/cm, and $f = 1$ MHz, which gives $Pe = 5.57$, indicating that electrophoresis is dominating the transport of pDNA to the cell membrane, and multiple pulses at such a high pulse repetition frequency can be thought of as a single long pulse providing the electrophoresis. For the experimental conditions in this work, $t_p = 200$ ns, $E = 15.8$ kV/cm, $f = 10$ Hz, and $Pe = 0.03$ (see Table 2), indicating that the pDNA molecule reaches the cell membrane predominantly by diffusion. Thus, the Peclet number defined as $Pe = \frac{\mu E t_p}{\sqrt{2D/f}}$ can be used as useful parameter to infer the role of electrophoresis and diffusion for a variety of pulses used in this work and in [106].

5. Conclusions

In summary, we showed that GET can also be achieved with nanosecond pulses (with low pulse repetition rate, i.e., 10 Hz) in addition to widely used millisecond and microsecond pulses and previously shown HF-BP pulses. GET efficiency depends on pDNA concentration, cell line, and pulse parameters. In our experiments, smaller pDNA did not significantly improve GET efficiency, but it had an effect on the degree of transgene expression. We showed that the time dynamics of transgene expression are comparable between millisecond, microsecond, HF-BP, and nanosecond pulses but differ greatly between the two cell lines. A simple mathematical model of the probability of pDNA and cell membrane contact during GET shows that pDNA migration for nanosecond (at low repetition frequency) and HF-BP pulses is dominated by diffusion, and for micro- and millisecond pulses, the process is dominated by electrophoresis. A Peclet (Pe) number has been defined that can be used to infer the role of diffusion and electrophoresis in a wide

variety of pulsing conditions. However, for the process of pDNA molecules coming into contact with the cell membrane in the presence of a strong free energy barrier close to the cell membrane, the role of diffusion and electrophoresis cannot be isolated as effectively. Nevertheless, the migration of pDNA close to the cell membrane can still be inferred based on electrophoresis and diffusion. The developed model and modeling results can provide valuable guidance for further experiments and interpretations of results obtained by various pulse protocols.

Supplementary Materials: The following supporting information can be downloaded at: https://www.mdpi.com/article/10.3390/app12168237/s1, Figure S1: Schematic of distribution of pDNA molecules and cells in suspension; Figure S2: Comparison of permeabilization and survival curves of C2C12 myoblast and 1306 fibroblasts with 200 ns pulses and 10 Hz pulse repetition rate; Figure S3: Comparison of permeabilization and survival curves of C2C12 myoblast and 1306 fibroblasts with 500 ns pulses and 10 Hz pulse repetition rate; Figure S4: Comparison of MFI of permeabilized C2C12 myoblast and 1306 fibroblasts; Figure S5: Comparison of permeabilization, survival curves, and MFI of C2C12 myoblast and 1306 fibroblasts with 8×100 μs and 8×5 ms pulses; Figure S6: Comparison of permeabilization, survival curves, and MFI of C2C12 myoblast and 1306 fibroblasts with HF-BP pulses; Table S1: Various estimates of the distance between a pDNA molecule and the nearest cell membrane (R_{DNA}); Table S2: Various estimates of the distance between a DNA molecule and the nearest cell membrane and between two pDNA molecules; Table S3: Nanosecond, HF-BP, micro and millisecond pulse protocols with which the best overall GET with 500 μg/mL of pEGFP-N1 was achieved in C2C12 myoblasts; Table S4: Nanosecond, HF-BP, micro and millisecond pulse protocols with which the best overall GET with 500 μg/mL of pEGFP-N1 was achieved in 1306 fibroblasts; Table S5: Maximum temperature increases of the cell sample during pulse delivery. References [107,108] are cited in the supplementary materials.

Author Contributions: Conceptualization: T.P. (Tjaša Potočnik), S.S., A.M.L. and D.M.; experiments: T.P. (Tjaša Potočnik) and T.P. (Tamara Polajžer); model, S.S. and A.M.L.; investigation: T.P. (Tjaša Potočnik), S.S. and A.M.L.; data curation: T.P. (Tjaša Potočnik) and S.S.; writing—original draft preparation: T.P. (Tjaša Potočnik) and S.S.; writing—review and editing: T.P. (Tjaša Potočnik), S.S., A.M.L. and D.M.; visualization: T.P. (Tjaša Potočnik) and S.S.; supervision: A.M.L. and D.M.; funding acquisition: D.M. All authors have read and agreed to the published version of the manuscript.

Institutional Review Board Statement: Not applicable.

Informed Consent Statement: Not applicable.

Data Availability Statement: Data are available from the corresponding author on request.

Conflicts of Interest: The authors declare no conflict of interest. The funders had no role in the design of the study, in the collection, analyses or interpretation of data; in the writing of the manuscript, or in the decision to publish the results.

References

1. Rosazza, C.; Haberl Meglic, S.; Zumbusch, A.; Rols, M.-P.; Miklavcic, D. Gene Electrotransfer: A Mechanistic Perspective. *Curr. Gene Ther.* **2016**, *16*, 98–129. [CrossRef] [PubMed]
2. Sokołowska, E.; Błachnio-Zabielska, A.U. A Critical Review of Electroporation as a Plasmid Delivery System in Mouse Skeletal Muscle. *Int. J. Mol. Sci.* **2019**, *20*, 2776. [CrossRef] [PubMed]

3. Fajrial, A.K.; He, Q.Q.; Wirusanti, N.I.; Slansky, J.E.; Ding, X. A Review of Emerging Physical Transfection Methods for CRISPR/Cas9-Mediated Gene Editing. *Theranostics* **2020**, *10*, 5532–5549. [CrossRef] [PubMed]

4. Folegatti, P.M.; Bittaye, M.; Flaxman, A.; Lopez, F.R.; Bellamy, D.; Kupke, A.; Mair, C.; Makinson, R.; Sheridan, J.; Rohde, C.; et al. Safety and Immunogenicity of a Candidate Middle East Respiratory Syndrome Coronavirus Viral-Vectored Vaccine: A Dose-Escalation, Open-Label, Non-Randomised, Uncontrolled, Phase 1 Trial. *Lancet Infect. Dis.* **2020**, *20*, 816–826. [CrossRef]

5. Morrow, M.P.; Kraynyak, K.A.; Sylvester, A.J.; Shen, X.; Amante, D.; Sakata, L.; Parker, L.; Yan, J.; Boyer, J.; Roh, C.; et al. Augmentation of Cellular and Humoral Immune Responses to HPV16 and HPV18 E6 and E7 Antigens by VGX-3100. *Mol. Ther. Oncolytics* **2016**, *3*, 16025. [CrossRef] [PubMed]

6. Topol, E.J. Messenger RNA Vaccines against SARS-CoV-2. *Cell* **2021**, *184*, 1401. [CrossRef] [PubMed]

7. Algazi, A.P.; Twitty, C.G.; Tsai, K.K.; Le, M.; Pierce, R.; Browning, E.; Hermiz, R.; Canton, D.A.; Bannavong, D.; Oglesby, A.; et al. Phase II Trial of IL-12 Plasmid Transfection and PD-1 Blockade in Immunologically Quiescent Melanoma. *Clin. Cancer Res.* **2020**, *26*, 2827–2837. [CrossRef] [PubMed]

8. Bhatia, S.; Longino, N.V.; Miller, N.J.; Kulikauskas, R.; Iyer, J.G.; Ibrani, D.; Blom, A.; Byrd, D.R.; Parvathaneni, U.; Twitty, C.G.; et al. Intratumoral Delivery of Plasmid IL12 via Electroporation Leads to Regression of Injected and Noninjected Tumors in Merkel Cell Carcinoma. *Clin. Cancer Res.* **2020**, *26*, 598–607. [CrossRef] [PubMed]

9. Heller, R.; Heller, L.C. Gene Electrotransfer Clinical Trials. *Adv. Genet.* **2015**, *89*, 235–262. [CrossRef]

10. Geboers, B.; Scheffer, H.J.; Graybill, P.M.; Ruarus, A.H.; Nieuwenhuizen, S.; Puijk, R.S.; Van Den Tol, P.M.; Davalos, R.V.; Rubinsky, B.; De Gruijl, T.D.; et al. *High-Voltage Electrical Pulses in Oncology: Irreversible Electroporation, Electrochemotherapy, Gene Electrotransfer, Electrofusion, and Electroimmunotherapy*; Radiological Society of North America (RSNA): Oak Brook, IL, USA, 2020; Volume 295, pp. 254–272.

11. Alzubi, J.; Lock, D.; Rhiel, M.; Schmitz, S.; Wild, S.; Mussolino, C.; Hildenbeutel, M.; Brandes, C.; Rositzka, J.; Lennartz, S.; et al. Automated Generation of Gene-Edited CAR T Cells at Clinical Scale. *Mol. Ther. Methods Clin. Dev.* **2021**, *20*, 379–388. [CrossRef]

12. Mingozzi, F.; High, K.A. Immune Responses to AAV in Clinical Trials. *Curr. Gene Ther.* **2011**, *11*, 321–330. [CrossRef] [PubMed]

13. Stewart, M.P.; Sharei, A.; Ding, X.; Sahay, G.; Langer, R.; Jensen, K.F. In Vitro and Ex Vivo Strategies for Intracellular Delivery. *Nature* **2016**, *538*, 183–192. [CrossRef] [PubMed]

14. Haberl, S.; Kanduser, M.; Flisar, K.; Hodžić, D.; Bregar, V.B.; Miklavčič, D.; Escoffre, J.M.; Rols, M.P.; Pavlin, M. Effect of Different Parameters Used for in Vitro Gene Electrotransfer on Gene Expression Efficiency, Cell Viability and Visualization of Plasmid DNA at the Membrane Level. *J. Gene Med.* **2013**, *15*, 169–181. [CrossRef]

15. Potočnik, T.; Miklavčič, D.; Maček Lebar, A. Gene Transfer by Electroporation with High Frequency Bipolar Pulses in Vitro. *Bioelectrochemistry* **2021**, *140*, 107803. [CrossRef] [PubMed]

16. Chopra, S.; Ruzgys, P.; Maciulevičius, M.; Jakutavičiute, M.; Šatka, S. Investigation of Plasmid DNA Delivery and Cell Viability Dynamics for Optimal Cell Electrotransfection in Vitro. *Appl. Sci.* **2020**, *10*, 6070. [CrossRef]

17. Gehl, J.; Mir, L.M. Determination of Optimal Parameters for in Vivo Gene Transfer by Electroporation, Using a Rapid in Vivo Test for Cell Permeabilization. *Biochem. Biophys. Res. Commun.* **1999**, *261*, 377–380. [CrossRef]

18. Young, J.L.; Dean, D.A. Electroporation-Mediated Gene Delivery. *Adv. Genet.* **2015**, *89*, 49–88. [CrossRef]

19. Čemažar, M.; Jarm, T.; Miklavčič, D.; Lebar, A.M.; Ihan, A.; Kopitar, N.A.; Serša, G. Effect of Electric-Field Intensity on Electropermeabilization and Electrosensitivity of Various Tumor-Cell Lines in vitro. *Electro Magn.* **1998**, *17*, 263–272. [CrossRef]

20. Faurie, C.; Rebersek, M.; Golzio, M.; Kanduser, M.; Escoffre, J.M.; Pavlin, M.; Teissie, J.; Miklavcic, D.; Rols, M.P. Electro-Mediated Gene Transfer and Expression Are Controlled by the Life-Time of DNA/Membrane Complex Formation. *J. Gene Med.* **2010**, *12*, 117–125. [CrossRef]

21. Sachdev, S.; Feijoo Moreira, S.; Keehnen, Y.; Rems, L.; Kreutzer, M.T.; Boukany, P.E. DNA-Membrane Complex Formation during Electroporation Is DNA Size-Dependent. *Biochim. Biophys. Acta Biomembr.* **2020**, *1862*, 183089. [CrossRef]

22. Wu, M.; Yuan, F. Membrane Binding of Plasmid DNA and Endocytic Pathways Are Involved in Electrotransfection of Mammalian Cells. *PLoS ONE* **2011**, *6*, e20923. [CrossRef] [PubMed]

23. Wang, L.; Miller, S.E.; Yuan, F. Ultrastructural Analysis of Vesicular Transport in Electrotransfection. *Microsc. Microanal.* **2018**, *24*, 553–563. [CrossRef] [PubMed]

24. Rosazza, C.; Deschout, H.; Buntz, A.; Braeckmans, K.; Rols, M.P.; Zumbusch, A. Endocytosis and Endosomal Trafficking of DNA After Gene Electrotransfer In Vitro. *Mol. Ther. Nucleic Acids* **2016**, *5*, e286. [CrossRef] [PubMed]

25. Pavlin, M.; Flisar, K.; Kandušer, M. The Role of Electrophoresis in Gene Electrotransfer. *J. Membr. Biol.* **2010**, *236*, 75–79. [CrossRef] [PubMed]

26. André, F.M.; Gehl, J.; Sersa, G.; Préat, V.; Hojman, P.; Eriksen, J.; Golzio, M.; Cemazar, M.; Pavselj, N.; Rols, M.P.; et al. Efficiency of High- and Low-Voltage Pulse Combinations for Gene Electrotransfer in Muscle, Liver, Tumor, and Skin. *Hum. Gene Ther.* **2008**, *19*, 1261–1271. [CrossRef]

27. Sano, M.B.; Fan, R.E.; Cheng, K.; Saenz, Y.; Sonn, G.A.; Hwang, G.L.; Xing, L. Reduction of Muscle Contractions during Irreversible Electroporation Therapy Using High-Frequency Bursts of Alternating Polarity Pulses: A Laboratory Investigation in an Ex Vivo Swine Model. *J. Vasc. Interv. Radiol.* **2018**, *29*, 893–898.e4. [CrossRef]

28. Chafai, D.E.; Mehle, A.; Tilmatine, A.; Maouche, B.; Miklavčič, D. Assessment of the Electrochemical Effects of Pulsed Electric Fields in a Biological Cell Suspension. *Bioelectrochemistry* **2015**, *106*, 249–257. [CrossRef]

29. Vižintin, A.; Vidmar, J.; Ščančar, J.; Miklavčič, D. Effect of Interphase and Interpulse Delay in High-Frequency Irreversible Electroporation Pulses on Cell Survival, Membrane Permeabilization and Electrode Material Release. *Bioelectrochemistry* **2020**, *134*, 107523. [CrossRef]

30. Klein, N.; Guenther, E.; Botea, F.; Pautov, M.; Dima, S.; Tomescu, D.; Popescu, M.; Ivorra, A.; Stehling, M.; Popescu, I. The Combination of Electroporation and Electrolysis (E2) Employing Different Electrode Arrays for Ablation of Large Tissue Volumes. *PLoS ONE* **2019**, *14*, e0221393. [CrossRef]

31. Maglietti, F.; Michinski, S.; Olaiz, N.; Castro, M.; Suárez, C.; Marshall, G. The Role of Ph Fronts in Tissue Electroporation Based Treatments. *PLoS ONE* **2013**, *8*, e80167. [CrossRef]

32. Olaiz, N.; Signori, E.; Maglietti, F.; Soba, A.; Suárez, C.; Turjanski, P.; Michinski, S.; Marshall, G. Tissue Damage Modeling in Gene Electrotransfer: The Role of PH. *Bioelectrochemistry* **2014**, *100*, 105–111. [CrossRef] [PubMed]

33. Turjanski, P.; Olaiz, N.; Maglietti, F.; Michinski, S.; Suárez, C.; Molina, F.V.; Marshall, G. The Role of PH Fronts in Reversible Electroporation. *PLoS ONE* **2011**, *6*, e17303. [CrossRef] [PubMed]

34. Sano, M.B.; Arena, C.B.; Bittleman, K.R.; Dewitt, M.R.; Cho, H.J.; Szot, C.S.; Saur, D.; Cissell, J.M.; Robertson, J.; Lee, Y.W.; et al. Bursts of Bipolar Microsecond Pulses Inhibit Tumor Growth. *Sci. Rep.* **2015**, *5*, 14999. [CrossRef]

35. Mahnič-Kalamiza, S.; Miklavčič, D. Scratching the Electrode Surface: Insights into a High-Voltage Pulsed-Field Application from in Vitro & in Silico Studies in Indifferent Fluid. *Electrochim. Acta* **2020**, *363*, 137187. [CrossRef]

36. Yao, C.; Dong, S.; Zhao, Y.; Lv, Y.; Liu, H.; Gong, L.; Ma, J.; Wang, H.; Sun, Y. Bipolar Microsecond Pulses and Insulated Needle Electrodes for Reducing Muscle Contractions during Irreversible Electroporation. *IEEE Trans. Biomed. Eng.* **2017**, *64*, 2924–2937. [CrossRef]

37. Mercadal, B.; Arena, C.B.; Davalos, R.V.; Ivorra, A. Avoiding Nerve Stimulation in Irreversible Electroporation: A Numerical Modeling Study. *Phys. Med. Biol.* **2017**, *62*, 8060–8079. [CrossRef]

38. Aycock, K.N.; Zhao, Y.; Lorenzo, M.F.; Davalos, R.V. A Theoretical Argument for Extended Interpulse Delays in Therapeutic High-Frequency Irreversible Electroporation Treatments. *IEEE Trans. Biomed. Eng.* **2021**, *68*, 1999–2010. [CrossRef]

39. Cvetkoska, A.; Maček-Lebar, A.; Trdina, P.; Miklavčič, D.; Reberšek, M. Muscle Contractions and Pain Sensation Accompanying High-Frequency Electroporation Pulses. *Sci. Rep.* **2022**, *12*, 8019. [CrossRef] [PubMed]

40. Ruzgys, P.; Novickij, V.; Novickij, J.; Šatkauskas, S. Nanosecond Range Electric Pulse Application as a Non-Viral Gene Delivery Method: Proof of Concept. *Sci. Rep.* **2018**, *8*, 15502. [CrossRef]

41. Novickij, V.; Balevičiūtė, A.; Ruzgys, P.; Šatkauskas, S.; Novickij, J.; Zinkevičienė, A.; Girkontaitė, I. Sub-Microsecond Electrotransfection Using New Modality of High Frequency Electroporation. *Bioelectrochemistry* **2020**, *136*, 107594. [CrossRef]

42. Chang, A.Y.; Liu, X.; Tian, H.; Hua, L.; Yang, Z.; Wang, S. Microfluidic Electroporation Coupling Pulses of Nanoseconds and Milliseconds to Facilitate Rapid Uptake and Enhanced Expression of DNA in Cell Therapy. *Sci. Rep.* **2020**, *10*, 6061. [CrossRef]

43. Thompson, G.L.; Roth, C.C.; Kuipers, M.A.; Tolstykh, G.P.; Beier, H.T.; Ibey, B.L. Permeabilization of the Nuclear Envelope Following Nanosecond Pulsed Electric Field Exposure. *Biochem. Biophys. Res. Commun.* **2016**, *470*, 35–40. [CrossRef]

44. Batista Napotnik, T.; Reberšek, M.; Vernier, P.T.; Mali, B.; Miklavčič, D. Effects of High Voltage Nanosecond Electric Pulses on Eucaryotic Cells (in Vitro): A Systematic Review. *Bioelectrochemistry* **2016**, *110*, 1–12. [CrossRef]

45. Beebe, S.J.; Blackmore, P.F.; White, J.; Joshi, R.P.; Schoenbach, K.H. Nanosecond Pulsed Electric Fields Modulate Cell Function through Intracellular Signal Transduction Mechanisms. *Physiol. Meas.* **2004**, *25*, 1077–1093. [CrossRef]

46. Chopinet, L.; Batista-Napotnik, T.; Montigny, A.; Rebersek, M.; Teissié, J.; Rols, M.P.; Miklavčič, D. Nanosecond Electric Pulse Effects on Gene Expression. *J. Membr. Biol.* **2013**, *246*, 851–859. [CrossRef] [PubMed]

47. Guo, S.; Jackson, D.L.; Burcus, N.I.; Chen, Y.J.; Xiao, S.; Heller, R. Gene Electrotransfer Enhanced by Nanosecond Pulsed Electric Fields. *Mol. Ther. Methods Clin. Dev.* **2014**, *1*, 14043. [CrossRef] [PubMed]

48. Vižintin, A.; Marković, S.; Ščančar, J.; Miklavčič, D. Electroporation with Nanosecond Pulses and Bleomycin or Cisplatin Results in Efficient Cell Kill and Low Metal Release from Electrodes. *Bioelectrochemistry* **2021**, *140*, 107798. [CrossRef]

49. Novickij, V.; Balevičiute, A.; Malysko, V.; Želvys, A.; Radzevičiute, E.; Kos, B.; Zinkeviciene, A.; Miklavčič, D.; Novickij, J.; Girkontaite, I. Effects of Time Delay between Unipolar Pulses in High Frequency Nano-Electrochemotherapy. *IEEE Trans. Biomed. Eng.* **2022**, *69*, 1726–1732. [CrossRef]

50. Schoenbach, K.H.; Beebe, S.J.; Buescher, E.S. Intracellular Effect of Ultrashort Electrical Pulses. *Bioelectromagnetics* **2001**, *22*, 440–448. [CrossRef] [PubMed]

51. Tekle, E.; Oubrahim, H.; Dzekunov, S.M.; Kolb, J.F.; Schoenbach, K.H.; Chock, P.B. Selective Field Effects on Intracellular Vacuoles and Vesicle Membranes with Nanosecond Electric Pulses. *Biophys. J.* **2005**, *89*, 274–284. [CrossRef] [PubMed]

52. Napotnik, T.B.; Wu, Y.H.; Gundersen, M.A.; Miklavčič, D.; Vernier, P.T. Nanosecond Electric Pulses Cause Mitochondrial Membrane Permeabilization in Jurkat Cells. *Bioelectromagnetics* **2012**, *33*, 257–264. [CrossRef] [PubMed]

53. Vernier, P.T.; Sun, Y.; Marcu, L.; Salemi, S.; Craft, C.M.; Gundersen, M.A. Calcium Bursts Induced by Nanosecond Electric Pulses. *Biochem. Biophys. Res. Commun.* **2003**, *310*, 286–295. [CrossRef] [PubMed]

54. Ford, W.E.; Ren, W.; Blackmore, P.F.; Schoenbach, K.H.; Beebe, S.J. Nanosecond Pulsed Electric Fields Stimulate Apoptosis without Release of Pro-Apoptotic Factors from Mitochondria in B16f10 Melanoma. *Arch. Biochem. Biophys.* **2010**, *497*, 82–89. [CrossRef] [PubMed]

55. Sachdev, S.; Potočnik, T.; Rems, L.; Miklavčič, D. Revisiting the Role of Pulsed Electric Fields in Overcoming the Barriers to in Vivo Gene Electrotransfer. *Bioelectrochemistry* **2022**, *144*, 107994. [CrossRef] [PubMed]

56. Golzio, M.; Teissié, J.; Rols, M.P. Direct Visualization at the Single-Cell Level of Electrically Mediated Gene Delivery. *Proc. Natl. Acad. Sci. USA* **2002**, *99*, 1292–1297. [CrossRef] [PubMed]
57. Muthukumar, M. Polymer Translocation. Murugappan. Available online: https://books.google.si/books?hl=sl&lr=&id=PcuT-ibRtRIC&oi=fnd&pg=PP1&dq=Muthukumar,+Murugappan.+Polymer+translocation.+CRC+press,+2016.&ots=K0bz9eAsWT&sig=LYEClwUyYngqBXZ5CsyHdcy3Wjc&redir_esc=y#v=onepage&q=Muthukumar%2C (accessed on 9 June 2022).
58. Yu, M.; Tan, W.; Lin, H. A Stochastic Model for DNA Translocation through an Electropore. *Biochim. Biophys. Acta Biomembr.* **2012**, *1818*, 2494–2501. [CrossRef] [PubMed]
59. Sachdev, S.; Muralidharan, A.; Choudhary, D.K.; Perrier, D.L.; Rems, L.; Kreutzer, M.T.; Boukany, P.E. DNA Translocation to Giant Unilamellar Vesicles during Electroporation Is Independent of DNA Size. *Soft Matter* **2019**, *15*, 9187–9194. [CrossRef] [PubMed]
60. Sweeney, D.C.; Reberšek, M.; Dermol, J.; Rems, L.; Miklavčič, D.; Davalos, R.V. Quantification of Cell Membrane Permeability Induced by Monopolar and High-Frequency Bipolar Bursts of Electrical Pulses. *Biochim. Biophys. Acta Biomembr.* **2016**, *1858*, 2689–2698. [CrossRef]
61. Bosnjak, M.; Lorente, B.C.; Pogacar, Z.; Makovsek, V.; Cemazar, M. Different Incubation Times of Cells after Gene Electrotransfer in Fetal Bovine Serum Affect Cell Viability, but Not Transfection Efficiency. *J. Membr. Biol.* **2014**, *247*, 421–428. [CrossRef] [PubMed]
62. Delteil, C.; Teissié, J.; Rols, M.P. Effect of Serum on in Vitro Electrically Mediated Gene Delivery and Expression in Mammalian Cells. *Biochim. Biophys. Acta Biomembr.* **2000**, *1467*, 362–368. [CrossRef]
63. Antipina, A.Y.; Gurtovenko, A.A. Molecular-Level Insight into the Interactions of DNA with Phospholipid Bilayers: Barriers and Triggers. *RSC Adv.* **2016**, *6*, 36425–36432. [CrossRef]
64. Stellwagen, N.C.; Gelfi, C.; Righetti, P.G. The Free Solution Mobility of DMA. Available online: https://onlinelibrary.wiley.com/doi/epdf/10.1002/%28SICI%291097-0282%28199711%2942%3A6%3C687%3A%3AAID-BIP7%3E3.0.CO%3B2-Q (accessed on 9 June 2022).
65. Portet, T.; Favard, C.; Teissié, J.; Dean, D.S.; Rols, M.P. Insights into the Mechanisms of Electromediated Gene Delivery and Application to the Loading of Giant Vesicles with Negatively Charged Macromolecules. *Soft Matter* **2011**, *7*, 3872–3881. [CrossRef]
66. Potter, H.; Heller, R. Transfection by Electroporation. *Curr. Protoc. Mol. Biol.* **2018**, *2018*, 9.3.1–9.3.13. [CrossRef] [PubMed]
67. Atsavapranee, E.S.; Billingsley, M.M.; Mitchell, M.J. Delivery Technologies for T Cell Gene Editing: Applications in Cancer Immunotherapy. *EBioMedicine* **2021**, *67*, 103354. [CrossRef] [PubMed]
68. Pucihar, G.; Krmelj, J.; Reberšek, M.; Napotnik, T.B.; Miklavčič, D. Equivalent Pulse Parameters for Electroporation. *IEEE Trans. Biomed. Eng.* **2011**, *58*, 3279–3288. [CrossRef] [PubMed]
69. Vera-Tizatl, C.E.; Talamás-Rohana, P.; Vera-Hernández, A.; Leija-Salas, L.; Rodríguez-Cuevas, S.A.; Chávez-Munguía, B.; Vera-Tizatl, A.L. Cell Morphology Impact on the Set-up of Electroporation Protocols for in-Suspension and Adhered Breast Cancer Cells. *Electromagn. Biol. Med.* **2020**, *39*, 323–339. [CrossRef] [PubMed]
70. Harris, E.; Elmer, J.J. Optimization of Electroporation and Other Non-Viral Gene Delivery Strategies for T Cells. *Biotechnol. Prog.* **2021**, *37*, e3066. [CrossRef] [PubMed]
71. Michieletto, D.; Lusic, M.; Marenduzzo, D.; Orlandini, E. Physical Principles of Retroviral Integration in the Human Genome. *Nat. Commun.* **2019**, *10*, 575. [CrossRef] [PubMed]
72. Pavlin, M.; Kandušer, M. New Insights into the Mechanisms of Gene Electrotransfer—Experimental and Theoretical Analysis. *Sci. Rep.* **2015**, *5*, 9132. [CrossRef] [PubMed]
73. Zhang, Z.; Qiu, S.; Zhang, X.; Chen, W. Optimized DNA Electroporation for Primary Human T Cell Engineering. *BMC Biotechnol.* **2018**, *18*, 4. [CrossRef]
74. Yu, L.; Reynaud, F.; Falk, J.; Spencer, A.; Di Ding, Y.; Baumlé, V.; Lu, R.; Castellani, V.; Yuan, C.; Rudkin, B.B. Highly Efficient Method for Gene Delivery into Mouse Dorsal Root Ganglia Neurons. *Front. Mol. Neurosci.* **2015**, *8*, 2. [CrossRef] [PubMed]
75. Markowicz, S.; Niedzielska, J.; Kruszewski, M.; Ołdak, T.; Gajkowska, A.; Machaj, E.K.; Kurzak, H.; Pojda, Z. Nonviral Transfection of Human Umbilical Cord Blood Dendritic Cells Is Feasible, but the Yield of Dendritic Cells with Transgene Expression Limits the Application of This Method in Cancer Immunotherapy. *Acta Biochim. Pol.* **2006**, *53*, 203–211. [CrossRef] [PubMed]
76. Kandušer, M.; Miklavčič, D.; Pavlin, M. Mechanisms Involved in Gene Electrotransfer Using High- and Low-Voltage Pulses—An in Vitro Study. *Bioelectrochemistry* **2009**, *74*, 265–271. [CrossRef] [PubMed]
77. Frandsen, S.K.; McNeil, A.K.; Novak, I.; McNeil, P.L.; Gehl, J. Difference in Membrane Repair Capacity Between Cancer Cell Lines and a Normal Cell Line. *J. Membr. Biol.* **2016**, *249*, 569–576. [CrossRef] [PubMed]
78. Znidar, K.; Bosnjak, M.; Cemazar, M.; Heller, L.C. Cytosolic DNA Sensor Upregulation Accompanies DNA Electrotransfer in B16.F10 Melanoma Cells. *Mol. Ther. Nucleic Acids* **2016**, *5*, e322. [CrossRef] [PubMed]
79. Chopra, S.; Ruzgys, P.; Maciulevičius, M.; Šatkauskas, S. Effect of Cell Passage Time on the Electrotransfection Efficiency. *Biol. Bull.* **2020**, *47*, 441–447. [CrossRef]
80. Lesueur, L.L.; Mir, L.M.; André, F.M. Overcoming the Specific Toxicity of Large Plasmids Electrotransfer in Primary Cells In Vitro. *Mol. Ther. Nucleic Acids* **2016**, *5*, e291. [CrossRef] [PubMed]
81. Zahid, A.; Ismail, H.; Li, B.; Jin, T. Molecular and Structural Basis of DNA Sensors in Antiviral Innate Immunity. *Front. Immunol.* **2020**, *11*, 3094. [CrossRef] [PubMed]
82. Semenova, N.; Bosnjak, M.; Markelc, B.; Znidar, K.; Cemazar, M.; Heller, L. Multiple Cytosolic DNA Sensors Bind Plasmid DNA after Transfection. *Nucleic Acids Res.* **2019**, *47*, 10235–10246. [CrossRef] [PubMed]

83. Hornstein, B.D.; Roman, D.; Arévalo-Soliz, L.M.; Engevik, M.A.; Zechiedrich, L. Effects of Circular DNA Length on Transfection Efficiency by Electroporation into HeLa Cells. *PLoS ONE* **2016**, *11*, e0167537. [CrossRef] [PubMed]
84. Molnar, M.J.; Gilbert, R.; Lu, Y.; Liu, A.B.; Guo, A.; Larochelle, N.; Lochmuller, H.; Petrof, B.J.; Nalbantoglu, J.; Karpati, G. Factors Influencing the Efficacy, Longevity, and Safety of Electroporation-Assisted Plasmid-Based Gene Transfer into Mouse Muscles. *Mol. Ther.* **2004**, *10*, 447–455. [CrossRef] [PubMed]
85. Ribeiro, S.; Mairhofer, J.; Madeira, C.; Diogo, M.M.; Lobato Da Silva, C.; Monteiro, G.; Grabherr, R.; Cabral, J.M. Plasmid DNA Size Does Affect Nonviral Gene Delivery Efficiency in Stem Cells. *Cell. Reprogram.* **2012**, *14*, 130–137. [CrossRef]
86. Smirnikhina, S.A.; Lavrov, A.V.; Bochkov, N.P. Dynamics of Elimination of Plasmids and Expression of VEGF121 Gene Transfected into Human Mesenchymal Stem Cells by Different Methods. *Bull. Exp. Biol. Med.* **2011**, *151*, 121–125. [CrossRef] [PubMed]
87. Čegovnik, U.; Novaković, S. Setting Optimal Parameters for in Vitro Electrotransfection of B16F1, SA1, LPB, SCK, L929 and CHO Cells Using Predefined Exponentially Decaying Electric Pulses. *Bioelectrochemistry* **2004**, *62*, 73–82. [CrossRef]
88. Bodwell, J.; Swift, F.; Richardson, J. Long Duration Electroporation for Achieving High Level Expression of Glucocorticoid Receptors in Mammalian Cell Lines. *J. Steroid Biochem. Mol. Biol.* **1999**, *68*, 77–82. [CrossRef]
89. Tsong, T.Y. Electroporation of Cell Membranes. *Biophys. J.* **1991**, *60*, 297–306. [CrossRef]
90. Kotnik, T.; Rems, L.; Tarek, M.; Miklavcic, D. Membrane Electroporation and Electropermeabilization: Mechanisms and Models. *Annu. Rev. Biophys.* **2019**, *48*, 63–91. [CrossRef] [PubMed]
91. Sherba, J.J.; Hogquist, S.; Lin, H.; Shan, J.W.; Shreiber, D.I.; Zahn, J.D. The Effects of Electroporation Buffer Composition on Cell Viability and Electro-Transfection Efficiency. *Sci. Rep.* **2020**, *10*, 3053. [CrossRef]
92. Haberl, S.; Miklavčič, D.; Pavlin, M. Effect of Mg Ions on Efficiency of Gene Electrotransfer and on Cell Electropermeabilization. *Bioelectrochemistry* **2010**, *79*, 265–271. [CrossRef]
93. Potočnik, T.; Miklavčič, D.; Maček Lebar, A. Effect of Electroporation and Recovery Medium PH on Cell Membrane Permeabilization, Cell Survival and Gene Transfer Efficiency in Vitro. *Bioelectrochemistry* **2019**, *130*, 107342. [CrossRef]
94. Arora, M. Cell Culture Media: A Review. *Mater. Methods* **2013**, *3*, 24. [CrossRef]
95. Saulis, G.; Rodaitė-Riševičienė, R.; Dainauskaitė, V.S.; Saulė, R. Electrochemical Processes during High-Voltage Electric Pulses and Their Importance in Food Processing Technology. *Adv. Food Biotechnol.* **2015**, *35*, 575–591. [CrossRef]
96. Kotnik, T.; Miklavčič, D.; Mir, L.M. Cell Membrane Electropermeabilization by Symmetrical Bipolar Rectangular Pulses: Part II. Reduced Electrolytic Contamination. *Bioelectrochemistry* **2001**, *54*, 91–95. [CrossRef]
97. Cohen, R.N.; van der Aa, M.A.E.M.; Macaraeg, N.; Lee, A.P.; Szoka, F.C. Quantification of Plasmid DNA Copies in the Nucleus after Lipoplex and Polyplex Transfection. *J. Control. Release* **2009**, *135*, 166–174. [CrossRef]
98. Tsai, Y.C.; Tsai, T.H.; Chang, C.P.; Chen, S.F.; Lee, Y.M.; Shyue, S.K. Linear Correlation between Average Fluorescence Intensity of Green Fluorescent Protein and the Multiplicity of Infection of Recombinant Adenovirus. *J. Biomed. Sci.* **2015**, *22*, 31. [CrossRef]
99. Chicaybam, L.; Barcelos, C.; Peixoto, B.; Carneiro, M.; Limia, C.G.; Redondo, P.; Lira, C.; Paraguassú-Braga, F.; De Vasconcelos, Z.F.M.; Barros, L.; et al. An Efficient Electroporation Protocol for the Genetic Modification of Mammalian Cells. *Front. Bioeng. Biotechnol.* **2017**, *4*, 99. [CrossRef]
100. Znidar, K.; Bosnjak, M.; Semenova, N.; Pakhomova, O.; Heller, L.; Cemazar, M. Tumor Cell Death after Electrotransfer of Plasmid DNA Is Associated with Cytosolic DNA Sensor Upregulation. *Oncotarget* **2018**, *9*, 18665–18681. [CrossRef]
101. Rosazza, C.; Phez, E.; Escoffre, J.M.; Cézanne, L.; Zumbusch, A.; Rols, M.P. Cholesterol Implications in Plasmid DNA Electrotransfer: Evidence for the Involvement of Endocytotic Pathways. *Int. J. Pharm.* **2012**, *423*, 134–143. [CrossRef]
102. Mao, M.; Wang, L.; Chang, C.C.; Rothenberg, K.E.; Huang, J.; Wang, Y.; Hoffman, B.D.; Liton, P.B.; Yuan, F. Involvement of a Rac1-Dependent Macropinocytosis Pathway in Plasmid DNA Delivery by Electrotransfection. *Mol. Ther.* **2017**, *25*, 803–815. [CrossRef]
103. Chang, C.C.; Wu, M.; Yuan, F. Role of Specific Endocytic Pathways in Electrotransfection of Cells. *Mol. Ther. Methods Clin. Dev.* **2014**, *1*, 14058. [CrossRef]
104. Cervia, L.D.; Chang, C.C.; Wang, L.; Yuan, F. Distinct Effects of Endosomal Escape and Inhibition of Endosomal Trafficking on Gene Delivery via Electrotransfection. *PLoS ONE* **2017**, *12*, e0171699. [CrossRef] [PubMed]
105. Cervia, L.D.; Chang, C.C.; Wang, L.; Mao, M.; Yuan, F. Enhancing Electrotransfection Efficiency through Improvement in Nuclear Entry of Plasmid DNA. *Mol. Ther. Nucleic Acids* **2018**, *11*, 263–271. [CrossRef] [PubMed]
106. Radzevičiūtė, E.; Malyško-Ptašinskė, V.; Novickij, J.; Novickij, V.; Girkontaitė, I. Transfection by Electroporation of Cancer and Primary Cells Using Nanosecond and Microsecond Electric Fields. *Pharmaceutics* **2022**, *14*, 1239. [CrossRef] [PubMed]
107. Robertson, R.M.; Smith, D.E. Self-Diffusion of Entangled Linear and Circular DNA Molecules: Dependence on Length and Concentration. *Macromolecules* **2007**, *40*, 3373–3377. [CrossRef]
108. Robertson, R.M.; Laib, S.; Smith, D.E. Diffusion of Isolated DNA Molecules: Dependence on Length and Topology. *Proc. Natl. Acad. Sci. USA* **2006**, *103*, 7310–7314. [CrossRef] [PubMed]

2.4 REVISITING THE ROLE OF PULSED ELECTRIC FIELDS IN OVERCOMING THE BARRIERS TO *IN VIVO* GENE ELECTROTRANSFER

Gene therapies are revolutionizing medicine by providing a way to cure hitherto incurable diseases. Scientific and technological advances have enabled the first gene therapies to become clinically approved. In addition, with the ongoing COVID-19 pandemic, we are witnessing record speeds in the development and distribution of gene-based vaccines. For gene therapy to take effect, the therapeutic nucleic acids (RNA or DNA) need to overcome several barriers before they can execute their function of producing a protein or silencing a defective or overexpressing gene. This includes the barriers of the interstitium, the cell membrane, the cytoplasmic barriers and (in case of DNA) the nuclear envelope. Gene electrotransfer (GET), i.e., transfection by means of pulsed electric fields, is a non-viral technique that can overcome (some of) these barriers enabling a safe and effective GET. GET has reached the clinical stage of investigations where it is currently being evaluated for its therapeutic benefits across a wide variety of indications. In this review, we formalize our current understanding of GET from a biophysical perspective and critically discuss the mechanisms by which electric field can aid in overcoming identified barriers. We also identify and highlight the gaps in current knowledge that hinder optimization of GET *in vivo*.

Revisiting the role of pulsed electric fields in overcoming the barriers to *in vivo* gene electrotransfer

Shaurya Sachdev, Tjaša Potočnik, Lea Rems, Damijan Miklavčič *

University of Ljubljana, Faculty of Electrical Engineering, Tržaška cesta 25, 1000 Ljubljana, Slovenia

ARTICLE INFO

ABSTRACT

Gene therapies are revolutionizing medicine by providing a way to cure hitherto incurable diseases. The scientific and technological advances have enabled the first gene therapies to become clinically approved. In addition, with the ongoing COVID-19 pandemic, we are witnessing record speeds in the development and distribution of gene-based vaccines. For gene therapy to take effect, the therapeutic nucleic acids (RNA or DNA) need to overcome several barriers before they can execute their function of producing a protein or silencing a defective or overexpressing gene. This includes the barriers of the interstitium, the cell membrane, the cytoplasmic barriers and (in case of DNA) the nuclear envelope. Gene electrotransfer (GET), i.e., transfection by means of pulsed electric fields, is a non-viral technique that can overcome these barriers in a safe and effective manner. GET has reached the clinical stage of investigations where it is currently being evaluated for its therapeutic benefits across a wide variety of indications. In this review, we formalize our current understanding of GET from a biophysical perspective and critically discuss the mechanisms by which electric field can aid in overcoming the barriers. We also identify the gaps in knowledge that are hindering optimization of GET *in vivo*.

Contents

1. Introduction

Gene therapy is revolutionising the field of medicine by offering potential unprecedented treatments to devastating diseases of various origins, with cancer, inheritable diseases, infectious diseases and cardio-vascular diseases currently holding the major share of indications [1,2]. Treatments based on (cell and) gene therapy have been approved for cancers such as head and neck squamous cell carcinoma, Acute Lymphoblastic Leukaemia, B-cell Lymphoma and unresectable Metastatic Melanoma, and for inheritable diseases such as Lipoprotein Lipase Deficiency, Adenosine Deaminase Deficiency - Severe Combined Immunodeficiency or ADA-SCID and Retinal Dystrophy [1,3]. Approval of these therapies, especially

* Corresponding author.
   E-mail address: damijan.miklavcic@fe.uni-lj.si (D. Miklavčič).

with the advent of Chimeric Antigen Receptor T-Cell (CAR-T cell) therapy which is contingent upon genetic engineering of T-cells, represents a hallmark in the field of medicine since they provide supreme remission rates to untenable cancers [4]. Additionally, gene-based vaccines made of ribonucleic acid (RNA) (BNT1262b2 and mRNA-1273) were the first to receive approval for vaccination against the infectious Corona Virus Disease − 2019 (COVID-19) pandemic at a record breaking speed of less than 12 months [5]. Their safety, potency, low cost, rapid production and scalability following identification of the virion make them superior to previous generation vaccines [6-8]. With gene editing technologies, especially CRISPR/Cas9, gene therapies are no longer limited to adding a specific gene to the target cells but are now also capable of editing entire defective genetic sequences [9]. Although still in the nascent stage, such gene editing technologies have not only expanded the indications falling under the gambit of gene therapies but have also elevated the potential impact of gene therapies in the field of medicine.

For gene therapies to take effect, DNA or RNA (deoxyribonucleic acid or ribonucleic acid) must enter the cell to produce a protein or to silence a defective or overexpressing gene. This entails the nucleic acid to overcome several barriers before it can reach the cytoplasm of the cell (for RNA) or the nucleus of the cell (for DNA) to enable its therapeutic action. These barriers are: the interstitial barriers, the cell membrane barrier, the cytoplasmic barriers and the nuclear envelope. After the pioneering work of Wolff *et al.* [10], who injected naked DNA and RNA into mouse skeletal muscle *in vivo* and observed *trans*-gene (protein) expression, it soon became clear that these barriers severely limit the efficiency of gene therapies mediated by naked DNA and RNA injection. Following DNA or RNA injection into the muscle, only minute amounts can enter the cell. For instance, DNA starts to degrade as soon as 5 min after injection into mouse muscles [11]. Thus, researchers are actively investigating possibilities to devise strategies that can overcome these barriers.

So far, viral and non-viral vectors have been researched for DNA and RNA delivery. Viral vectors possess excellent capability to overcome the barriers and are now being approved for treating diseases. Till date, 13 gene therapies have been approved *in vivo* based on using viral vectors to overcome the barriers [12]. However, viral vectors have some alarming drawbacks: pre-existing immunity and immune reactions following injection of viral vectors can reduce the effectiveness of the therapy and cause immunotoxicity - precluding the use of particular viruses in certain geographic locations and certain patients [13]. While most of these concerns related to viral vectors are being addressed by modifying and engineering the viral vectors, non-viral vectors are gaining traction as feasible and, in some cases, even superior (at least in terms of safety) alternatives to viral gene delivery [14]. Non-viral vectors that are being developed fall broadly into the categories of chemical vectors (e.g., polymer, lipid-based and various inorganic nano-carriers *etc.*) and physical vectors (e.g., ballistic, laser, ultrasound, electroporation *etc.*). Non-viral vectors are in principle devoid of an immune response per se but they lack the high efficiency of viral vectors *in vivo* [1,3,14,15].

A non-viral method which shows great promise is naked DNA injection followed by the application of pulsed electric field (PEF). DNA transfection, referred to as cellular uptake of DNA and subsequent gene expression, mediated by PEF is known as Gene Electrotransfer (GET). DNA transfection, GET and a few other terms that will be used throughout the review are formally defined in Section 2. Although GET is applicable to both DNA and RNA, we will be restricting the purview of this review, and of GET, to only DNA as it has been the prevalent molecule under investigation in GET literature. GET increases transfection rates of DNA by 100–2000 times and improves reproducibility of transfection compared

to naked DNA injection without the application of PEF [16-20]. Several clinical trials are underway evaluating the efficacy of GET in oncology for treatment of, and vaccination against, cancer, and for vaccination against infectious diseases [21-33]. A GET based DNA vaccine [34,35] is currently under Phase (2/3) investigation for COVID-19 pandemic (NCT04336410 and the INNOVATE trial - NCT04642638). Further, since GET is capable of delivering large genetic payloads, it is considered as a promising technique for CRISPR/Cas9 gene editing applications [36,37]. CRISPR/Cas9 applications mediated by GET greatly amplify the prospect of GET in the field of medicine and therapeutics.

Although, several clinical investigations indicate that GET is a safe and an effective clinical technique providing therapeutic benefits, it has taken around 40 years to reach this stage. Over the years, efforts have been made to improve GET. GET of DNA encoding for monoclonal antibodies in large animals such as non-human primates provides a quantitative example to illustrate how optimizations have led to an improvement in the efficiency: dose finding studies in combination with optimizing devices and delivery protocols have led to an increase in the serum antibody levels from a few ng/ml to greater than 30 µg/ml [38]. Some of these optimizations were based on targeting the interstitial barrier using extracellular matrix digesting enzymes and aiding in better distribution of DNA in the interstitium. While GET has taken several strides to reach the clinic, much of the success can be attributed to our increased understanding of how DNA molecules, due to PEF, overcame the barriers they encountered on their way and reached the nucleus. The knowledge of how DNA molecules interact and overcome the barriers during GET is scattered over the literature, which dates as far back as 1982 with the first report of *in vitro* GET [39]. The purpose of this review is to revisit the role of PEF in overcoming the barriers to GET *in vivo*. Since the cell membrane and intracellular barriers are discussed in detail along with the interstitial barrier, the review is also relevant for understanding GET *in vitro*. We, thus, critically review existing literature that helps formalize the current understanding of GET and barriers limiting its efficiency. We also identify gaps in current understanding and suggest directions of future research to further enable an enhanced understanding of DNA delivery to cells using GET.

2. Brief overview and current understanding of mechanisms involved in gene electrotransfer

GET is a complex process and to get a good grip on the current understanding of GET it is prudent to explain the process based on *in vitro* systems which are more amenable to investigative rigour even though they are oversimplified compared to processes *in vivo*. According to *in vitro* experiments, GET is a multi-step process which involves (i) interaction of DNA with the cell membrane (Fig. 1 B.1) (ii) translocation through the cell membrane (Fig. 1 B.2) (iii) migration across the cytoplasm (Fig. 1 C.1) (iv) translocation through the nuclear envelope (Fig. 1 D) and (v) gene expression. *In vivo*, an additional step involving the distribution of DNA from the site of injection to enough number of cells in the target tissue needs to be considered. This step entails overcoming the interstitial barriers (Fig. 1 A). The subsequent steps (i-v) are the same both *in vivo* and *in vitro*.

In vitro, the DNA molecules suspended in the solution uniformly surround the cells shortly after addition. Once PEF is applied, DNA molecules (being negatively charged) are electrophoretically pushed from the cathode towards the anode (Fig. 1 A). In the process, they encounter the cells, specifically, the cell membrane on the cathode facing side of the cell. PEF, in addition to electrophoretically pushing the DNA molecules towards the cell membrane, also increases the permeability of the cell membrane via a
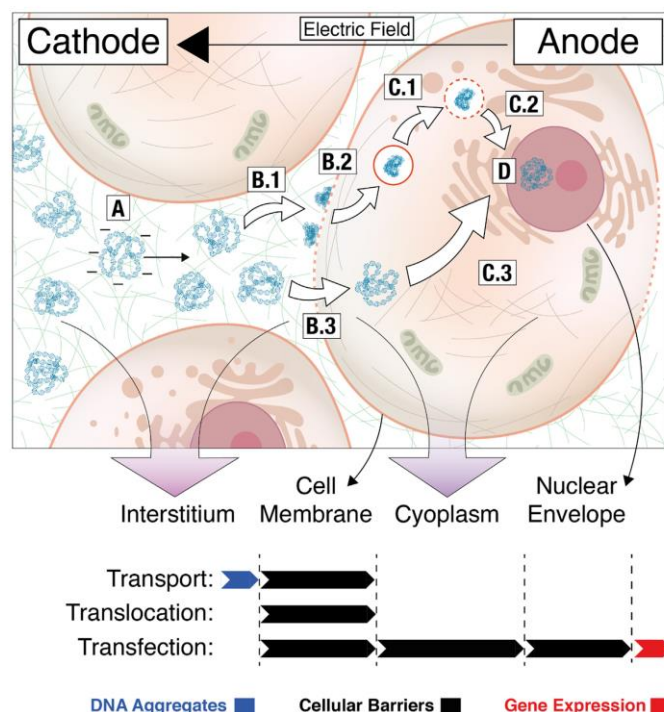
Fig. 1. Overview of the gene electrotransfer (GET) process and definitions of the terminologies used. (A) Negatively charged DNA molecules are electrophoretically pushed towards the cell membrane. (B.1–3) Events taking place at the membrane level during GET. (B.1) Formation of DNA-membrane complexes or DNA aggregates at the cell membrane. (B.2) Endocytic translocation of DNA aggregates. (B.3) Direct DNA translocation into the cell without the formation of DNA aggregates. (C.1–3) Events taking place inside the cytoplasm during GET. (C.1) Intra-cellular trafficking of endocytic vesicles (endosomes) containing DNA aggregates. (C.2) Escape of DNA molecules from endocytic vesicles. (C.3) Intracellular trafficking of naked DNA molecules which have gained direct access to the cytoplasm by translocating through the membrane without forming DNA aggregates. (D) DNA transport across the nuclear envelope.

phenomenon termed electropermeabilization (also referred to as electroporation). Experiments have suggested that DNA enters the cells only if the PEF intensity is similar to, or higher than, that required for electropermeabilization [40,41].

Electropermeabilization, or the transient increase of membrane permeability due to PEF, is attributed to formation of hydrophilic pores in the lipid domains of the cell membrane (Fig. 2 A), oxidation of membrane lipids (Fig. 2 B), denaturation of membrane proteins (Fig. 2 C) and/or a combination of these [42]. These mechanisms of electropermeabilization, depicted in Fig. 2, explain a large number of observations related to *trans*-membrane transport of ions and small molecules which is primarily governed by electrophoresis and diffusion [43-49]. The *"threshold"* PEF intensity leading to electropermeabilization, known as the electropermeabilization threshold, is usually determined as the minimum PEF intensity required for detecting such ions or small molecules (e.g., propidium iodide dye) inside the cells [50].

Only if the PEF intensity is above the electropermeabilization threshold, the entry of DNA molecules into cells can be detected. There are two possible pathways of DNA entry. In the first, and the most widely accepted, pathway the DNA molecules, which are electrophoretically pushed towards the cells, interact with the permeabilized membrane on the cathode facing side of the cell

(Fig. 1 B.1-B.2). The DNA interaction with the permeabilized membrane can be visualized in terms of DNA aggregates or DNA-membrane complexes (Fig. 1 B.1). Such trapped (or immobilized) DNA molecules, henceforth referred to as DNA aggregates, are internalized *via* endocytosis and appear inside the cell in the minutes following PEF application [40,51,52].

In the second pathway, which is less accepted, the electrophoretically pushed DNA enters the cell directly by translocating through the permeabilized membrane on the cathode facing side of the cell (Fig. 1 B.3). In this pathway, the DNA molecules, prior to and/or during translocation, might interact with the cell membrane in the form of DNA adsorption on the cell membrane. Using molecular dynamics (MD) simulations, siRNA molecules have shown to translocate through hydrophilic pores by being adsorbed to the lipid bi-layer [53]. DNA interaction with the cell membrane in the form of DNA adsorption is different from DNA aggregation at the permeabilized membrane.

Before proceeding, we would like to define a few terms that will be used repeatedly through the text and could potentially lead to a confusion if they are not explicitly defined. The event of DNA crossing the cell membrane is a multi-step process which involves interaction of DNA with the permeabilized membrane in the form of DNA aggregates and subsequent internalization of the DNA aggre-

3
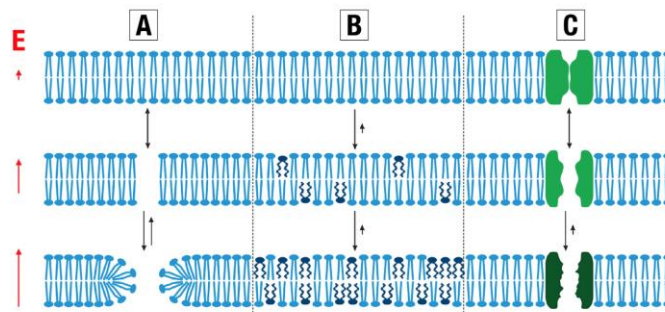
Fig. 2. (A-C) Mechanisms of cell membrane permeabilization due to its exposure to pulsed electric fields (PEF). Image reproduced from [42] with permission. Lipid molecules are depicted in blue and membrane protein is depicted in green. The electric field is represented by a red arrow on the left. The length of the arrow depicts the strength of the electric field and the arrow points in the direction of the electric field. The black arrows in between membrane states depict the transition between the states and the length of the arrow depicts the transition rates. Longer arrows depict faster transition rates and shorter arrows depict slower transition rates. All arrows are not drawn to scale. (A) Formation of hydrophilic pores in lipid bilayers from its pre-cursor hydrophobic pores in the presence of an electric field. (B) Chemical modification (e.g. lipid peroxidation) of lipids, specifically their tails, leading to their deformation resulting in increased permeability. (C) Denaturation of membrane proteins (e.g., voltage gated ion-channels) in the presence of an electric field, making them non-selectively permeable. Both (B) and (C), and/or their combination, can be responsible for prolonged permeability observed in cells which is of $O(10-15)$ mins. (For interpretation of the references to color in this figure legend, the reader is referred to the web version of this article.)

gates into the cell *via* endocytosis. We will refer to the combination of these steps i.e. DNA aggregate formation and subsequent internalization *via* endocytosis, including any intermediate steps, as DNA transport across the cell membrane. For instance, processes B.1 and B.2 in Fig. 1 represent a DNA transport event. We will exclusively refer to DNA translocation as an event in which DNA only crosses the permeabilized cell membrane and reaches the cytoplasm. For instance, endocytosis of aggregated DNA, i.e. Fig. 1 B.2, is a translocation event. In addition, DNA translocating through the permeabilized membrane without the formation of DNA aggregates and directly reaching the cytoplasm, i.e. Fig. 1 B.3, is also a translocation event. Further, we consider DNA transfection (or transfection) to imply (and be inclusive of) the complete sequence of events - DNA translocation across the cell membrane, DNA transport through the cytoplasm, DNA transport across the nuclear envelope and gene expression. GET is referred to as DNA transfection mediated by PEF. See bottom half of Fig. 1 for elucidation. Thus, GET efficiency implies DNA transfection efficiency in which DNA transfection is mediated by PEF. Lastly, throughout the text, we have used the notation of '$O(n)$ [units]' to quantify various parameters in appropriate units. The '$O(n)$ [units]' simply implies that the value of the parameter is *approximately* n in the given [units]. E.g., "...*electrophoretic migration of O(1) μm..*" implies that the electrophoretic migrations is *approximately* 1 μm. Rather than concerning with precise values, we have used this notation to provide approximate values or order of magnitude estimates, which are often sufficient to illustrate our point.

Along with electropermeabilization, electrophoresis is also believed to be necessary for GET. So much so that these two processes need to take place simultaneously. If DNA molecules are added after the application of PEF, DNA transfection is not observed even though the membrane is permeable to small molecules [41,54]. Role of electrophoresis is further evident from the fact that DNA aggregates are formed only on the cathode facing side of the cells [40]. Moreover, DNA molecules are electrophoretically added to the existing DNA aggregates in subsequent pulses [51], and DNA transfection is a vectorial process that depends on the direction of PEF [54]. Recent experiments have suggested that small DNA molecules of size 15–25 base pairs (bp) and siRNA molecules have direct access to the cytoplasm (without forming DNA or RNA aggregates) and they enter the cell from the permeabi-

lized membrane on the cathode facing side of cell, indicating an electrophoretic DNA and RNA translocation across permeabilized membrane [55,56].

Overall, PEF is thought to play a dual role in GET. One role is to permeabilise the cell membrane. The other role is to electrophoretically push the DNA molecules and bring them close to the permeabilized membrane, allowing DNA molecules to either form DNA aggregates at the permeabilized membrane (Fig. 1 B.1) which later appear inside the cytoplasm *via* endocytosis (Fig. 1 B.2) or translocate through the permeabilized membrane directly into the cytoplasm (Fig. 1 B.3). While both, membrane permeabilization and electrophoresis, appear to be necessary for GET, the reason for this necessity as well as their precise role in GET still remains elusive.

The cell membrane has a residual negative charge on the outer surface [57]. For negatively charged DNA to interact with the permeabilized membrane and form DNA aggregates, DNA must overcome an electrostatic barrier. The role of electrophoresis could thus be to, directly or indirectly, overcome the electrostatic barrier, enabling the interaction of DNA with the permeabilized membrane and enabling the formation of DNA aggregates (Fig. 1 B.1). In case of DNA molecules that have direct access to the cytoplasm, electrophoresis could help drive the translocation of DNA molecule through the permeabilized membrane during PEF (Fig. 1 B.3) [58]. Another possible role of electrophoresis (specific to *in vivo*) could be to transport DNA in the interstitial space through the dense network of the Extra-Cellular Matrix (ECM) fibres. For instance, diffusion is negligible compared to electrophoresis in the ECM, and the DNA molecules primarily rely on electrophoresis as the dominant mode of transport [59-61]. Thus, another role of electrophoresis could be to overcome the interstitial barriers by transporting DNA in the tissue and improving the interstitial distribution of DNA molecules.

The pathways by which the DNA is translocated across the cell membrane are understood only to a limited extent. Direct translocation of DNA in its native configuration through hydrophilic pores formed in the permeabilized membrane (Fig. 2 A) could explain the internalization of DNA molecules that have direct access to the cytoplasm (Fig. 1 B.3) [55,62]. However, research has mainly focussed on investigating DNA aggregate formation. As a result, there is now increasing evidence that DNA aggregates are translocated *via* endocytic pathways [63-65]. Understanding the mecha-

4

nism(s) of DNA translocation are crucial for successful GET since the intra-cellular fate of the DNA molecules depends on whether they have direct access to the cytoplasm or they are endocytosed inside vesicles.

Once internalized, irrespective of the translocation pathway, the DNA molecules are presented with yet another barrier - the cytoplasm, which primarily comprises of the dense cytoskeleton network. DNA aggregates that have been endocytosed are encapsulated in endocytic vesicles (endosomes - Fig. 1 B.2) and are protected against degradation by intra-cellular nuclease(s). DNA molecules inside endosomes rely on endosomal trafficking mediated by the actin and the microtubule network and their associated molecular motors (myosin and dynein) to reach the nucleus (or its vicinity) (Fig. 1 C.1) [65,66]. However, the endosomal membrane presents an extra barrier since the DNA molecules must escape from the endosome (Fig. 1 C.2) in order to cross the nuclear envelope and get expressed.

DNA molecules that gain direct access to the cytoplasm (Fig. 1 B.3), however, have to rely on hindered diffusion to reach the nucleus (Fig. 1 C.3). The diffusion of molecules inside the cytoplasm is size dependent and is hindered by the actin network [67,68]. Large DNA molecules, such as the plasmid DNA (pDNA) of around 5 kbp, have extremely low diffusion coefficients and are practically immobile [68]. They are, thus, highly susceptible to degradation by the intracellular nuclease(s) [69,70]. However, experiments have shown that naked DNA molecules are able to complex with intra-cellular proteins that may aid in their trafficking inside the cytoplasm [71].

The final (physical) barrier to GET is the nuclear envelope. DNA molecules in the *peri*-nuclear space that are not trapped in endosomes (endocytic vesicles), need to cross the nuclear envelope to reach the nucleus for transcription. The nuclear envelope is temporarily disrupted during cell division and synchronising GET (or gene transfer in general) with the mitotic phase of cells has shown to increase DNA transfection efficiency [72,73]. DNA molecules can also enter the nucleus of non-dividing, slow-dividing and terminally-differentiated cells using specific gene sequences in the DNA molecule that are able to bind to proteins in the cytoplasm that facilitate the entry of DNA molecules into the nucleus [71]. However, transfection has also been obtained with DNA molecules lacking these specific gene sequences [74].

Nanosecond PEF have shown to permeabilize membranes of intra-cellular organelles, vesicles and vacuoles [75-77]. However, results on applying nanosecond PEF after conventional PEF to improve GET efficiency by disrupting or permeabilizing the nuclear membrane have been inconclusive [78-81].

Various mechanisms of nuclear import have also been proposed for DNA molecules trapped within endosomes. For instance, endosomes containing DNA aggregates could fuse with the endoplasmic reticulum, transferring their (DNA) load to the endoplasmic reticulum. DNA molecules could then utilize the network between reticulum and nuclear membrane to enter into the nucleus [82]. Alternatively, or additionally, nuclear envelope associated endosomes could transfer DNA to the nucleus by fusing with the nuclear envelope [83].

3. Interstitial barriers

The interstitial space, or the interstitium, constitutes the environment surrounding the cells. Apart from cell-cell junctions, the interstitial space comprises of a network of macromolecules known as the Extra-Cellular Matrix (ECM). The major components of the ECM are polysaccharides - glycosaminoglycans (such as hyaluronan, chondroitin sulphate, dermatan sulphate, heparan sulphate) and fibrous proteins (such as collagen, elastin, fibronectin,

laminin) [84]. Physical impediments of cell–cell junctions, ECM and cell-ECM junctions, along with specific interaction of DNA with these components (e.g., electrostatic interactions), significantly limit mobility and distribution of DNA in target tissues and prevent DNA molecules to come in contact with large number of cells. In addition, DNA is highly susceptible to degradation by extracellular nuclease(s). Nucleases are present in the intra-cellular as well as in the extra-cellular (i.e. the interstitial) space [85]. While the precise function of nucleases is still debated, they are expected to regulate the extra-cellular concentration of DNA through the action of DNA cleavage [86]. Nevertheless, they pose a great threat to the functionality of DNA introduced into tissues for therapeutic purposes. Some studies have reported that DNA starts to degrade as soon as 5 mins after injection into mouse muscles [11], whereas others have reported half-life of 120 mins in the tumour interstitium [87]. Hindered distribution of DNA due to structural components of the interstitium and degradation of DNA by the nucleases present in the interstitium make it a potentially limiting barrier to GET *in vivo*.

Scale-up studies have shown that higher levels of connective tissue/ECM in muscles of larger/older animals correspond to lower levels of DNA transfection compared to smaller/younger animals [88-91]. This suggests that ECM is a limiting barrier to GET. Enzymes that can digest certain components of the ECM have, thus, been used to increase the efficiency of GET. For instance, hyaluronidase, an enzyme digesting hyaluronan, has been used to increase GET efficiency [92]. In another study, tumours with different levels of ECM were treated with ECM digesting enzymes - hyaluronidase and collagenase, and the transfection efficiency was compared for each type of tumour. Tumours with different levels of ECM responded differently to GET post the enzymatic treatment. It was observed that tumours with high levels of ECM responded better to GET post enzymatic treatment compared to tumours with low levels of ECM [93].

Several studies mimicking an *in vivo* environment have also demonstrated that cell–cell junctions and components of the ECM indeed limit the distribution of DNA, contributing to diminished GET efficiency. For instance, experiments on 3D spheroid models mimicking an *in vivo* environment revealed that cells only on the outer layer of the spheroid interacted with the DNA molecules even though the cells deep inside the spheroid were permeabilized as was evident by the uptake of small propidium iodide dye [94]. In another study, less than 1% of the cells in the spheroid could be transfected even though a transfection efficiency greater than 20% was achieved for cells in suspension under similar electroporation (PEF) conditions [95]. The low efficiency of GET can predominantly be attributed to the lack of DNA distribution inside the spheroid due to a dense cell arrangement with corresponding cell–cell junctions and possibly some ECM that can be deposited from cells within the spheroid [94]. In addition, non-uniform distribution of electric field and a reduced induced transmembrane voltage due to dense packing of cells inside a spheroid could also be a reason for limited electropermeabilization and concomitant reduced DNA transfection [95-97]. Reduced uptake of another molecule (Calcein) *via* PEF by cells in a spheroid was attributed to diminished distribution of Calcein due to dense packing of cells, reduced electric field inside the spheroid and lower induced transmembrane voltage for cells inside the spheroid [98]. Other components of the ECM such as collagen fibres also hinder diffusion and electrophoresis of DNA in the interstitium as determined by experiments in reconstructed tissues *in vitro* [99] and in *ex-vivo* models [60].

The ECM, thus, severely limits the distribution of molecules including DNA in the tissues. While PEF overcomes the cell membrane barrier by permeabilizing the cell membrane and allowing the entry of DNA into cells, PEF also provides the necessary push
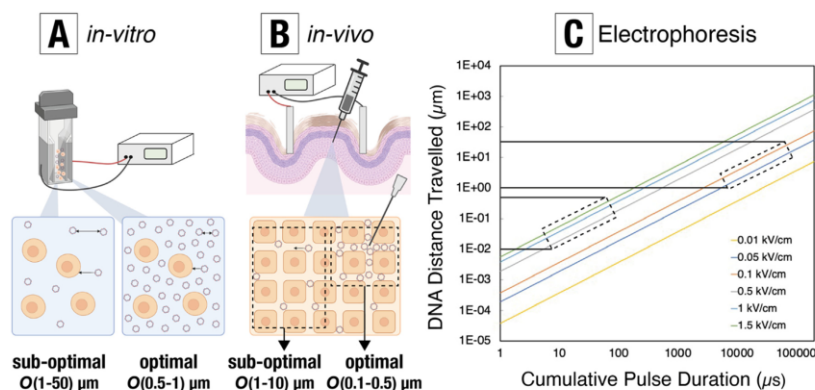
5

Fig. 3. Distribution of DNA *in vitro* and *in vivo*. (A) Distribution of DNA molecules *in vitro* under sub-optimal/low and optimal/high DNA concentrations. The DNA molecules are in the suspension and homogenously distribute throughout the suspension. (B) Distribution of DNA molecules *in vivo*. Due to interstitial barriers, the injected DNA molecules are heterogeneously distributed such that regions of sub-optimal/low and optimal/high DNA concentrations exist in the target tissue. The average cell-DNA/DNA-DNA distance is given in (A) and (B) for high/optimal and low/sub-optimal DNA concentrations. The distances have been calculated according to calculations in Appendix A. (C) Electrophoretic migration of DNA molecules (5900 bp) as a function of accumulated time for different electric field intensities. The calculations of electrophoretic migration by the DNA molecule are presented in Appendix B.

to DNA *via* electrophoresis and possibly overcomes, at least partially, the interstitial barrier as well.

To further investigate the role of electrophoresis, a strategy consisting of high voltage (HV) "short" pulses along with low voltage (LV) "long" pulses were employed *in vivo* [100,101]. This strategy was first proposed for *in vitro* experiments [62,102], and the purpose was two-fold - (i) to decouple the process of electropermeabilization from electrophoresis and (ii) to enhance the electrophoresis. The HV pulses were above the electropermeabilization threshold with an electric field amplitude of $O(100)$ V/cm and with a pulse duration of $O(100)$ μs. Since these pulses were of shorter duration, the HV pulses did not provide enough electrophoresis compared to LV pulses. The LV pulses were below the electropermeabilization threshold with an electric field amplitude of $O(10)$ V/cm, but with a longer duration of $O(100)$ ms to enhance the electrophoresis of DNA.

Increase in GET efficiency was observed for the combination of HV + LV pulses compared to using HV or LV pulses alone [100,101]. Since the LV pulse alone did not result in significant electropermeabilization [100,101], even though some transfection was observed for the LV pulse alone [100], the increase in GET efficiency was attributed to direct effect of LV pulses on DNA assuming that LV pulses are contributing to electrophoresis. Enhanced GET efficiency was obtained if DNA was added either before the HV pulse or in between the HV and the LV pulses of the HV + LV protocol, indicating the crucial role of electrophoresis in enhancing the efficiency of GET [101].

The strategy consisting of HV pulses for permeabilization and LV pulses for electrophoresis was employed leading to a higher efficiency of GET *in vivo* in further studies [103-105]. Long duration pulses are currently being employed in clinical settings. For instance, CELLECTRA® devices by Inovio Pharmaceuticals employ electric current-controlled (0.2 A for intra-dermal and 0.5 A for intra-muscular) long-duration pulses of 52 ms for its GET based DNA vaccination programs [29,32,34,35,106]. Interestingly, exponentially decaying pulses that have been successfully used in early studies of GET have a leading high peak, corresponding to HV component, and a long tail, corresponding to the LV component [102]. In light of these observations regarding long duration pules of

52 ms, it is also important to note that short duration pulses of 100 μs (at 1.3–1.5 kV/cm) are also being successfully used for GET in clinical settings [24-27,33].

The results on improved GET efficiency *in vivo* as a result of employing HV + LV pulses (or enhancing electrophoresis with separate LV pulses for electrophoresis) were, however, not observed in subsequent *in vitro* studies. At optimal DNA concentrations for *in vitro*, HV + LV pulses did not lead to higher transfection efficiency compared to HV pulses alone; however, for sub-optimal DNA concentrations, HV + LV resulted in an increased transfection efficiency compared to HV alone [107,108]. In this case, optimal concentration was defined as concentration beyond which transfection efficiency did not increase with an increase in DNA concentration, and transfection efficiency was defined as the percentage of transfected cells. Experiments at these sub-optimal and optimal DNA concentrations *in vitro* revealed the role of HV + LV pulses and of electrophoresis (Fig. 3 A). Due to hindered distribution of DNA in target tissues, regions of suboptimal DNA concentrations are expected to always exist *in vivo* (Fig. 3 B). Employing HV + LV pulses *in vivo* is thus expected to enhance GET efficiency due to the presence of these regions of sub-optimal DNA concentrations.

Although HV + LV pulse experiments *in vitro* and *in vivo* provide a possible mechanism of how LV pulses, through electrophoresis, enhance GET efficiency *in vivo*, it is worthwhile to look deeper into the role of electrophoresis in this enhancement. As argued by Bureau *et al.* [100], electrophoresis could enhance efficiency of GET by (i) improving DNA diffusion (distribution) in tissues (ii) by improving the contact between DNA molecules and the cell membrane (iii) by allowing DNA molecules to interact with and/or "insert" into the permeabilized cell membrane, i.e., DNA aggregation (Fig. 1 B.1) and (iv) aiding direct DNA translocation through the permeabilized membrane (Fig. 1 B.3). Possibilities (iii) and (iv) require the membrane to be permeabilized, whereas this is not necessary for (i) and (ii).

Bureau et al. further ruled out the possibilities (i) and (ii) by arguing that the application of LV pulses before HV pulses or LV pulses alone did not lead to an enhancement in GET efficiency, implying that a permeabilized state of the membrane is necessary to observe the effect of LV electrophoresis [100]. Usually, LV pulses
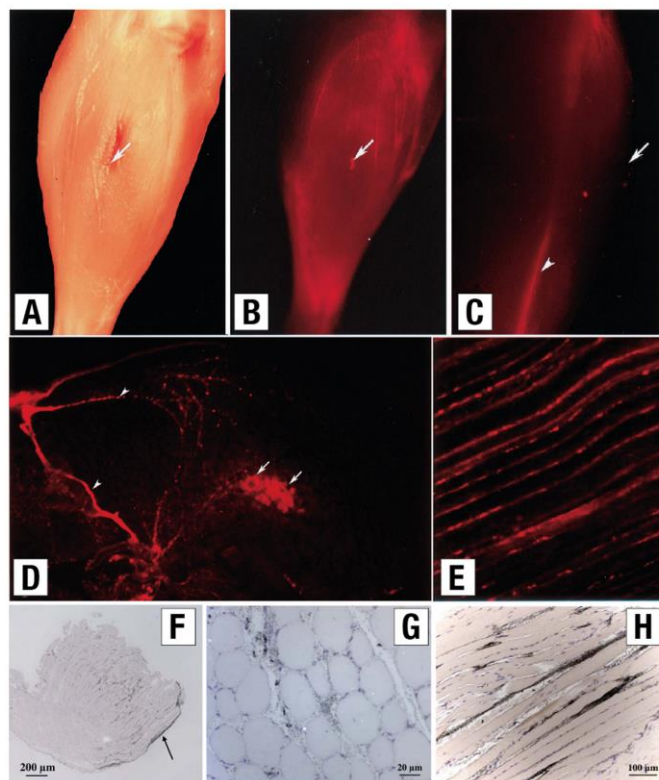
6

Fig. 4. Distribution of intramuscularly injected DNA. (A-E) Tibialis anterior muscle of mice; images from [113] Copyright 2000. The American Association of Immunologists, Inc. (A) Brightfield image of tibialis anterior muscle. White arrow marks the site injection. (B) Fluorescent image of the whole tibialis anterior muscle with DNA (labelled) in red, 5 mins after injection. White arrow marks the site of injection. (C) Fluorescent image of the lateral view of tibialis anterior muscle with DNA (labelled) in red, 5 mins after injection. White arrow marks the point of injection and white arrowhead points to accumulated DNA along the myotendinous junction. (D) Fluorescent image of vibratome transverse section (150 μm) of the tibialis anterior muscle with DNA (labelled) in red, 5 mins after injection. White arrowheads mark DNA in between muscle fibres/cells and white arrows mark DNA inside muscle fibres/cells. (E) Vibratome longitudinal section of the tibialis anterior muscle with DNA (labelled) in red, 5 mins after injection. DNA is located between muscle fibres/cells. (F-H) Tibial cranial muscle of mice with DNA (radioactively labelled) in black; images from [11]. (F) Transverse section of the tibial cranial muscle, 5 mins after injection. Black arrow shows accumulation of DNA between the muscle fibres and the overlaying fascia. (G) Higher magnification of a transverse section of the tibial cranial muscle, 3 h after injection. (H) Longitudinal section of the tibial cranial muscle, 5 after injection. (For interpretation of the references to color in this figure legend, the reader is referred to the web version of this article.)

are applied after HV pulses to increase the efficiency of GET. However, applying LV pulse before the HV pulse has been shown to marginally (although not statistically significantly) enhance DNA transfection compared to HV pulses alone in certain *in vitro* experiments [108,109]. Lack of significant enhancement in GET efficiency when LV pulses are applied before HV pulses does provide some evidence against possibility (ii), further studies might, however, be required to completely rule out this possibility.

Maximum DNA migration observed in tumour interstitium *ex vivo* [60] and *in vivo* [61] was around 0.37 μm and 0.23 μm, respectively, for a 50 ms pulse duration. It should be noted that a pulse duration of 50 ms is representative of pulse durations used in LV GET protocols. Even with the application of 10 such pulses, only a microscopic distribution of $O(1)$ μm is achieved. Thus, electrophoresis (by LV pulses) is not sufficient to improve DNA distribution in target tissues, effectively ruling out possibility (i). It is

likely that the distribution of DNA observed over macroscopic distances is due to the convection forces through injection [110-112].

It then appears that a permeabilized membrane is indeed necessary to observe the effect of electrophoresis provided by the LV pulses, and role of electrophoresis is to enhance the local concentration around the permeabilized membrane so that more DNA molecules can interact with the permeabilized membrane forming DNA aggregates, i.e., possibility (iii) (Fig. 1 B.1) or DNA molecules can directly translocate through the permeabilized membrane, i.e., possibility (iv) (Fig. 1 B.3).

According to our estimates, the DNA-cell distance is $O(0.5-1)$ μm *in vitro* and $O(0.1-0.5)$ μm *in vivo*, in regions with high/optimal DNA concentration (see Fig. 3 A and B, and refer to Appendix A for calculations). Thus, for high/optimal DNA concentrations which can be easily achieved *in vitro* and almost impossible to achieve *in vivo*, there already are DNA molecules in close proximity to

7

101

the cell. In this case, HV pulses alone are sufficient in bringing enough DNA molecules close to the permeabilized membrane for the purpose of DNA aggregation and/or direct DNA translocation. The DNA electrophoretic migration (electrophoresis) provided by HV pulses is $O(0.1–1)$ μm (Fig. 3 C, Appendix B for calculations) which is similar to the cell-DNA distance in regions with high/optimal DNA concentrations. Therefore, LV pulses add little to nothing in their contribution to bring enough DNA molecules close to the cell *via* electrophoretic migration (electrophoresis).

On the contrary, we estimate the DNA-cell distance to be $O(1–50)$ μm *in vitro* and $O(1–10)$ μm *in vivo* at low/sub-optimal DNA concentrations (Fig. 3 A and B, Appendix A for calculations). As a result, the number of DNA molecules close enough to make contact

Table 1
Values of hydraulic conductivities for different types of tissues and tumors. From [114].

	Tissue Type	Hydraulic Conductivity (K') [cm^3/mm Hg s $\times 10^{-8}$]
Normal Tissue	Rat abdominal muscle	15–78
	Rat dermis	5.33
	Mouse tail skin	70–150
	Subcutaneous plane	0.6–0.85
	Subcutaneous slice	6
	Aortic media and intima	0.4–2.0
Tumors	MCaIV tumor	248
	LS174T tumor	45
	U87 tumor	65, 7000
	HSTS26T tumor	9.2
	Rat fibrosarcoma	1.36–1360
	B16.F10 murine tumor	4100–11000
	4T1 murine tumor	950–2300
	Hepatoma	0.8–4.1, 28

with the cell membrane is low. Electrophoretic migration (electrophoresis) provided by the LV pulse is $O(1–100)$ μm (Fig. 3 C, Appendix B for calculations). In this case, LV pulse aids in electrophoretically migrating DNA molecules from far away to the cells, bringing enough DNA molecules close to the permeabilized membrane for the purpose of DNA aggregation and/or direct DNA translocation.

As mentioned above, the experimental electrophoretic migration observed for 50 ms long pulses (i.e., in the LV pulse regime) in tumour interstitium *ex vivo* was $O(0.1–1)$ μm [60,61]. Therefore, electrophoretic migration of $O(1–100)$ μm by LV pulses based on Fig. 3 C and calculations presented in Appendix B should be taken as an upper limit to the electrophoretic migration.

Overall, both HV and LV pulses are crucial for GET *in vivo*, whereby LV pulses, and the associated electrophoresis, appear to be especially critical for enhancing the efficiency of GET *in vivo*. *In vivo*, the interstitium limits the distribution of DNA molecules, providing a heterogenous distribution of DNA in the target tissue (Fig. 3 B). As a result, regions of low/sub-optimal DNA concentrations exist in the target tissue. LV pulses are able to offset the low efficiency of GET which results from the existence of these regions of low/sub-optimal DNA concentrations [107,108]. LV pulses accomplish this by electrophoretically bringing more DNA molecules close to the permeabilized membrane for DNA-aggregation and/or direct DNA translocation.

The question that then arises is - *how are DNA molecules distributed over macroscopic distances in the target tissue? Further, is the distribution inhomogeneous leading to zones of sub-optimal DNA concentrations?*

For intra-muscular injections in the tibialis anterior muscles of mice, DNA was distributed in the entire muscle 5 min after injection as shown in Fig. 4 A-C [113]. The white arrows mark the point of injection whereas the white arrowhead indicate the accumula-

Fig. 5. Influence of convective forces from injection of fluids on their macroscopic distribution in target tissues. (A-B) Injection of insulin in (pig) adipose tissue; images from [110]. (A) Histologically stained cross section of the sub-cutaneous tissue (pig adipose) with injected insulin shown in red. Injection fluid volume was 100μl and the scale bar corresponds to 1mm implying distribution over macroscopic distances. (B) X-ray computed tomographic scan of a similar sub-cutaneous injection process. The injection channel is visible along with the back-flow of the fluid to the skin surface. (C-D) Injection of Urografin fluid into adipose tissue; images first published in Journal of Mechanics and Material Structures in Vol. 6 (2011), No 1, published by Mathematical Sciences Publishers [111]. (C) A composite of X-ray image of 500μl of 150 Urografin fluid (opaque dye) injected into porcine adipose tissue. (D) Cross-section from a 3D reconstruction of 720 X-ray images of the dye-injection in (C). (E-G) Injection of dye (blue) into pig adipose tissue; images from [112]. (E) Images after single 100μl dye injection into adipose tissue and squeezing the site in-between electrodes. (F) Sagittal plane of the dye injection site after dissection to show the distribution of dye within the tissue. The dye is primarily found between the collagenous septa diving adipose lobes. (G) Distribution of dye in adipose tissue after 5 injections of 50μl each. (For interpretation of the references to color in this figure legend, the reader is referred to the web version of this article.)

Table 2
Interstitial fluid volume and ECM composition for different types of tissues and tumors. From [117].

	Tissue Type	Interstitial Fluid Volume (ml/g wet weight)	Collagen (mg/g wet weight)	Glycosaminoglycans (mg/g wet weight)	Hyaluron (mg/g wet weight)
Normal Tissue	Skin	0.40–0.45	170–190	3.7–4.2	0.5–1.6
	Muscle	0.07–0.12	10–13	2.2	0.09–0.13
	Lung	0.24	5–35	6.1	0.07–0.13
Tumors	Mammary carcinoma (murine) MCa1V Host: Mouse		1.7 ± 0.4		0.22 ± 0.02
	Colon adenocarcinoma (human) (LS174T) Host: Mouse		1.8 ± 0.7		0.10 ± 0.04
	Glioblastoma (human) (U87) Host: Mouse		9 ± 4		0.10 ± 0.04
	Soft tissue sarcoma (human) (HSTS) Host: Mouse		6 ± 1		0.22 ± 0.03
	Mammary carcinoma (DMBA induced) Host: Rat	0.39 ± 0.02	4.6 ± 0.7		1.9 ± 0.3
	Ovarian carcinoma (OVCAR-3) Host: Mouse	0.60 ± 0.03	7.7 ± 0.5		0.08 ± 0.04
	Ovarian carcinoma (SKOV-3) Host: Mouse	0.53 ± 0.11	9 ± 3		0.20 ± 0.02

tion of DNA (labelled in red) along the myotendinous junction of the tibialis anterior muscle. Closer inspection of the transverse and longitudinal sections of the muscles revealed local distribution of DNA (labelled in red) within the tissue, 5 mins after injection. DNA was distributed in between the muscle cells as observed in transverse (Fig. 4 D) and longitudinal (Fig. 4 E) sections. For the transverse section, the white arrowheads mark the accumulation of DNA in the space between the cells, whereas the white arrows mark the DNA inside cells at the point of injection. Observations on a whole transverse sections of tibial cranial muscles of mice also showed a macroscopic distribution of radio-labelled DNA 5 mins after injection (Fig. 4 F) [11]. Higher magnifications of the transverse (Fig. 4 G) and longitudinal (Fig. 4 H) sections, 3 h and 5 mins after injection, respectively, reveal that the DNA is located in the inter-fibrillar space (i.e., space in between the muscle cells). One can infer similar patterns of DNA distribution in the inter-fibrillar space or the interstitium, after injection, from transverse sections shown in (Fig. 4 D and G) and longitudinal sections shown in (Fig. 4 E and H).

As mentioned earlier, the distribution over macroscopic distances *in vivo* is likely due to the convection forces while injecting the bolus of DNA solution into the tissue. Injection studies have shown that sub-ml (100 µl) bolus injections into the subcutaneous region led to a "depot" which spans approx. 1 cm in length (Fig. 5 A and B) [110]. The "depot" can be described as a region (or a volume space) within which the injected bolus/dye can be found. In another study, 0.5 ml (500 mm³) bolus occupied a volume of 2300 mm³ once injected into the adipose tissue, implying a macroscopic distribution (Fig. 5 C and D) [111]. Similar observations were made in dye injection studies in which adipose tissue was considered as a target for DNA vaccination using GET (Fig. 5 E-G) [112]. Distribution of fluid in target tissues also depends on the type of tissue (muscle, fat/adipose and skin/dermis) as each of these have different resistances and permeabilities to the injected fluid.

To obtain information of how the tissue type influences the distribution of injected fluid, one can consider the Darcy's equation which describes the flow through porous media (tissue/tumors) as: $\bar{v} = -(K/\mu)\nabla p = -K'\nabla p$, where $\bar{v}$ is bulk-averaged velocity, p is pressure, μ is viscosity, K is specific permeability and K' is hydraulic conductivity [114]. Different types of tissues have different hydraulic conductivities and will influence the convection-based distribution of injected (DNA) solution. Hydraulic conductivities of common types of tissues used as a target during GET is given in Table 1 [114].

There are, however, a few points to be kept in mind while using hydraulic conductivities to interpret convection-based flow. Firstly, hydraulic conductivity of soft porous media such as biological tissues and tumors was found to vary with infusion pressure; with the variations being attributed to pressure-induced deformation of tissues [115,116]. Secondly, hydraulic conductivity of tissues is largely dependent on fractional void volume of the interstitium, the composition of ECM components and the geometry of the ECM [114,117]. For instance, hydraulic conductivity and mechanical (deformative) properties of various tumors were found to be correlated to the constituents of the ECM, specifically the collagen [118]. Various tissues, which are targets for GET, can have widely varying compositions of the ECM constituents and, thus, very different hydraulic conductivities, as evident from Table 1. Composition of commonly used target tissues during GET and a few tumors is shown in Table 2 [117]. Note that one must be careful in correlating the hydraulic conductivity to the composition of the ECM as this approach might be oversimplistic [114]. Interestingly, the increase in GET efficiency correlated with the amount of ECM in tumors when ECM digesting enzymes – collagenase and hyaluronidase – were used [93].

Structural anisotropy in the target tissue can also influence DNA distribution in the interstitium. It was shown that the structural anisotropy in cerebellum, collagen gels and tumor models can lead to anisotropy in diffusion of small and large molecules in the interstitium [119,120]. In addition, drug solution was shown to preferentially permeate along the direction of alignment (i.e. longitudinal) of the muscle tissue and have a higher hydraulic conductivity along that direction compared to the transverse direction [121].

It should be noted that injected volume often exceeds the fluid (holding) capacity of the target tissue leading to swelling or post-injection re-adjustments. For instance, intra-dermal injections lead to the formation of blebs under the skin [122-126].

In case of intra-muscular injections, 50 µl of DNA injection (exceeding muscle capacity) caused swelling of the anterior epimysial sheath of tibialis anterior muscle of mice [113]. Soon after, the swelling subsided and redistributed the fluid throughout the muscle. Reducing the volume of the fluid during injection to 5 µl did not lead to swelling of epimysial sheath while still dispersing the DNA throughout the muscle, although to a lesser extent. Interestingly, in the absence of PEF, less DNA uptake (at the site of injection) and less overall transgene expression was observed for the 5 µl injection compared to 50 µl injection. The higher transgene expression for the 50 µl injection was attributed, although specula-

9

tively, to the swelling of the muscle and the hydrostatic pressure resulting from the excessive fluid volume compared to the fluid (holding) capacity of the muscle, which in turn induced the uptake of DNA by muscle cells.

According to the authors [113], this could potentially explain why naked DNA transfection efficiency is higher for smaller animals compared to larger animals. Dupuis *et al.* [113] argued, based on their experimental observations, that the ratio of the injected fluid volume to the fluid (holding) capacity of the muscle/tissue is higher for smaller animals, owing to the small size of the muscle/tissue. This leads to muscle/tissue swelling and additional (hydrostatic) pressure or mechanical forces being generated that can induce DNA uptake. Mechanically squeezing the cells in a microfluidic environment has led to an enhanced DNA transfection efficiency using GET [127]. On the contrary, muscles/tissues of larger animals have enough capacity to accommodate the incoming injected fluid. This generates less pressure and low (or not enough) mechanical forces in the environment which possibly results in reduced uptake of DNA by muscle cells.

Therefore, while convection forces due to fluid injection help/aid in macroscopic distribution of DNA in target tissues, other factors associated with injection procedure should be considered while evaluating and investigating GET. One such factor is tissue swelling as a result of injection volume exceeding the fluid holding capacity of the tissues and its associated impact/hydrostatic pressure on cells within the tissues and near the site of injection, leading to DNA uptake or DNA transfection.

Another method to improve macroscopic distribution of DNA is to use injections at multiple sites, as has been observed for GET in rat skeletal muscle [128]. However, the improvement in transfection efficiency due to multiple injections is not always consistent between animals. No variation in DNA transfection efficiency was observed for mice when multiple injections were used compared to a single injection, keeping the total DNA dose constant [129].

While it appears that DNA is distributed over macroscopic distances through convection by injection, studies have also revealed that distribution of DNA is inhomogeneous in the interstitium [130]. From Fig. 4 D and E, it can be observed that the intensity of fluorescently labelled DNA (in red) is unevenly distributed, implying inhomogeneous concentration of DNA in the target tissue/muscle. This is further evident from Fig. 4 G and H where distribution of radioactively labelled DNA (in black) is inhomogeneous in the interstitial space between muscle fibres.

The reason for this inhomogeneity is perhaps the dense environment of the interstitium. The interstitium prevents DNA concentration to be homogenous in the target tissue and allows for zones of low/sub-optimal DNA concentration to exist *in vivo*. As discussed previously, existence of these zones then allows LV electrophoresis, in the HV + LV protocol, to enhance the GET efficiency by pushing DNA molecules over microscopic distances and accumulating enough DNA molecules close to the permeabilized membrane of cells in the low concentration zones, thereby locally increasing the concentration near the permeabilized membrane. In zones where DNA is present at high/optimal concentrations, HV pulses alone are sufficient since enough DNA molecules are already present near the permeabilized membrane of cells.

Eventually, DNA being distributed (or present) over macroscopic distances in the tissue, due to convection by injection, enables DNA transfection into cells at locations where, in addition to DNA, sufficient electric field is present to allow membrane permeabilization.

As mentioned, membrane permeabilization is necessary for DNA transfection, which implies that sufficient electric field intensity which permeabilizes the cell membrane must be present at locations where DNA molecules are present (whether at optimal or sub-optimal concentrations).

A broader implication of this (necessity) is that only those cells which are within the electric field distribution emanating from the electrodes are possible targets for GET. This defines a limited geometric area (or volume) constrained by electrode configurations (and distances) within which cells can be transfected through GET [125]. Increasing the target area (or volume) by increasing the distance between electrodes along with sustaining a sufficient electric field for permeabilization is a severe limitation as this requires increasing the voltages to levels that are clinically not viable or are unsafe [131]. In case of viral vector mediated delivery, a wider area can be target based on injection alone as long as appropriate membrane receptors are present on the cells which can accept the viral/chemical vectors [132-135].

Another implication of the requirement of sufficient electric field for permeabilization is that all cells that fall within target area (or within the electrodes) might not get transfected. Electric field suffers the same fate of spatial inhomogeneity within the target area, as does DNA distribution, while going from *in vitro* to *in vivo*. Due to inhomogeneous distribution, there might be pockets well within the target area where electric field is not sufficient. The inhomogeneity arises due to multiple reasons which are discussed below.

Firstly, different tissues have vastly different electrical conductivities [91,136]. Electrical conductivities of different types of tissues are shown in Table 3. If the electric field is applied *trans*cutaneously i.e. the electrodes are in contact with the skin, electric field distribution emanating from the electrodes would be highly heterogenous due to different electrical conductivities of the underlying tissues – skin, adipose, muscle and/or tumor [137,138]. As a result, the electric field in underlying muscle or tumor is less compared to the overlaying skin due to the low electrical conductivity of skin (when an averaged value of all skin layers was considered) [137,139] or of *stratum corneum* [138]. This might result in insufficient electric field within the muscle or tumor for permeabilization and, as a result, for GET.

Secondly, within the same type of tissue, the electric field can be highly heterogenous, as shown numerically for muscles [137], skin [140-142] and tumors [138], and experimentally for tumors [143]. Skin itself is a heterogenous tissue with different layers (*stratum corneum* and the lower skin layers – epidermis and dermis) having different conductivities (Table 3). The inhomogeneity in electric field distribution within the same type of tissue, and even within the same layer of the tissue, arises due to conductivity changes resulting from permeabilization of cells within the tissue/layer. These effects have been modelled numerically [137,141,142,144]. Local conductivity changes and the resulting spatial heterogeneity in electrical conductivity arising due electroporation have also been observed experimentally in liver tissue [145]. Tumors can intrinsically have spatial variations in electrical conductivity [146,147]. Variations in electrical conductivity, whether naturally occurring in tissues or induced due permeabi-

Table 3
Electrical conductivities of different tissues. From [91,136].

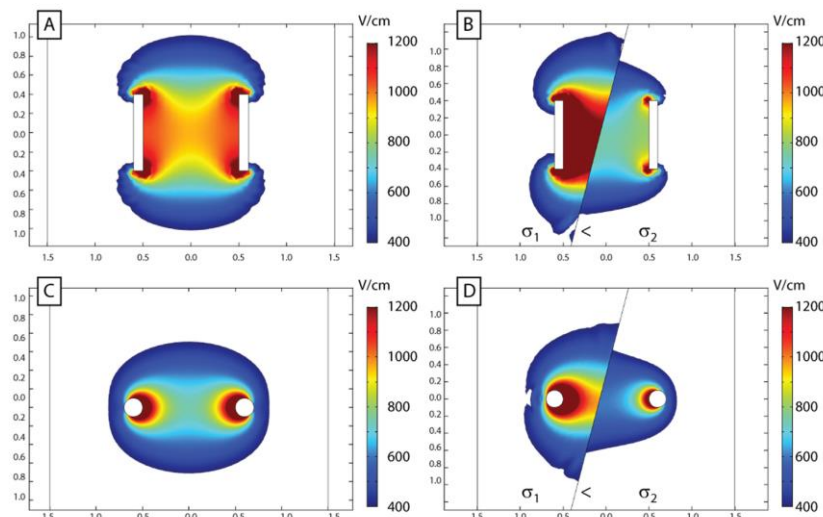| Tissue Type		Conductivity (S/m)
Tumor		0.22–0.4
Fat (Adipose)		0.02–0.04
Muscle	Transversal	0.04–0.14
	Longitudinal	0.3–0.8
Skin	*stratum corneum*	0.0000125
	Lower skin layers	0.227
Heart		0.06–0.4
Bone		0.01–0.06
Kidney		0.6
Liver		0.023–0.2
Lung (Inflated)		0.024–0.09

10

Fig. 6. Distribution of electric field in tissues for needle and plate electrodes. A voltage difference of 1000 V is applied between the electrodes which are 1 cm apart. The axis represents distances in (cm), and the color bar represents the electric field intensity in (V/cm). Distribution of electric field in a homogeneous tissue for plate (A) and needle (C) electrodes. Distribution of electric field in an inhomogeneous tissue for plate (B) and needle (D) electrodes. The inhomogeneous tissue is composed of tissues with conductivities σ_1 and σ_2, with $\sigma_2 = 3.\sigma_1$. From [148].

lization, lead to inhomogeneous distribution of electric field in the tissue.

Finally, the geometry of the electrodes can also influence the distribution of electric field *in vivo*. Electric field distribution for a homogenous tissue is shown for plate electrodes in Fig. 6 (A) and for needle electrodes in Fig. 6 (C) [148]. The tissue conductivity is same for both the cases and a voltage difference of 1000 V is applied between the electrodes which are 1 cm apart however, one can generally observe that the electric field distribution is more inhomogeneous for needle electrodes than for plate electrodes [130,148,149]. The electric field distribution is further influenced by the diameter of the needle electrodes [150,151]. The influence of tissue electrical conductivity on electric field distribution in an inhomogeneous tissue is shown in Fig. 6 (B) and (D) for plate and needle electrodes, respectively [148].

Orientation of cells with respect to electric field also have an influence on the efficiency of GET. For short $O(1)$ µs pulses, orientation of cells with respect to the electric field had a negligible effect on electroporation [152]. However, for longer $O(1-10)$ ms pulses, cells oriented parallel to the electric field were electroporated more than cells oriented perpendicular to the electric field [152]. For muscle fibers *in vivo*, a higher electroporation threshold of 200 V/cm was observed for perpendicular orientations of electric field compared to an electroporation threshold of only 80 V/cm for parallel orientations of electric field [153]. The orientations were defined with respect to the long axis of muscle fibers. Anisotropy in the muscle tissue is further evident from different electrical conductivities along longitudinal (parallel) and transversal (perpendicular) directions with respect to the long axis of muscle fibers, as depicted in Table 3.

Therefore, means that can improve the distribution of DNA molecules and electric field in target tissues, making the concentration of DNA and electric field homogenous, have tremendous potential in improving the efficiency and increasing the clinical

adoption of GET. For instance, electrolytic damage and cell death due to pH changes [154-158] and muscle contractions and pain associated with GET [159-163] can be minimized by potentially eliminating long mono-polar pulses.

Other PEF-related changes that can influence the interstitial barriers should also be considered. For instance, PEF has shown to directly affect the Gap Junction (GJ) membrane proteins involved in intercellular communication. Application of nanosecond PEF impairs the Gap Junction Intercellular Communication (GJIC), attributed to the disassembly of the membrane proteins involved in the cell–cell communication [164]. However, the GJIC disruption is time and field dependent, with time scale in the O (10) mins [164], similar to the time scale of DNA degradation in the interstitium [11,87]. In another study, cell–cell junctions were altered by the application of PEF in endothelial cells of blood vessels leading to an enhanced permeability to dextrans (70 kDa) [165]. Such alterations of gap junctions and cell–cell junctions imply that PEF alone can modulate the permeability of the interstitium, enabling a more homogenous distribution of solutes in the tissue.

4. Cell membrane

Once the DNA molecules overcome the interstitial barriers, they encounter the next barrier - the cell membrane. It is widely accepted that DNA transport across the cell membrane *via* GET is a multi-step process. As mentioned previously in Section 2, DNA transport at the membrane level involves interaction of the DNA with the membrane in the form of DNA aggregates (Fig. 1 B.1) followed by translocation of the aggregates *via* endocytic pathways (Fig. 1 B.2) [63-65]. The understanding that endocytic pathways are involved in DNA translocation does seem to provide a certain degree of control, albeit low. Lack of knowledge on endocytic precursor [52,91] i.e. the DNA-membrane interaction in the form of
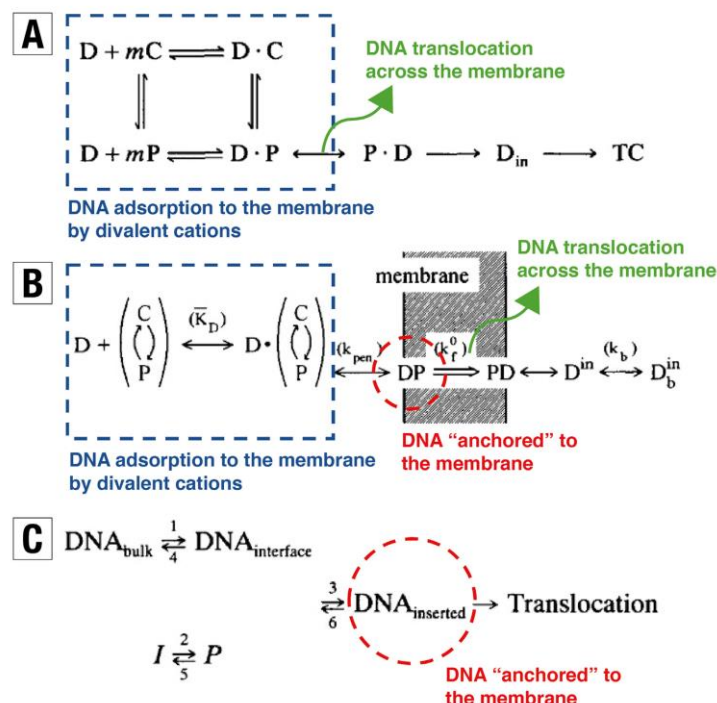
11

Fig. 7. Multi-step process of DNA and cell membrane interaction and internalization in the presence of an electric field. (a) Scheme from [172]; D – DNA, C - unpermeabilized membrane, P - permeabilized membrane, m – maximum number of binding sites, D.C - DNA associated with (or adsorbed to) the unpermeabilized membrane, D.P – DNA associated with (or adsorbed to) the permeabilized membrane, D.P ↔ P.D – DNA translocation across the membrane, D_{in} - internalised DNA and TC – final state of transfected cell. (b) Scheme from [174]; D - DNA, C - unpermeabilized membrane, P - permeabilized membrane, DP - DNA anchored to the membrane, DP ⇒ PD – DNA translocation across the membrane, D^{in} – internalised DNA and Db^{in} – internalised DNA bound to an internal cell structure to initiate genetic cell transformation. (c) Scheme from [41]; I - membrane in native state, P - permeabilized membrane.

DNA aggregation at the cell membrane (Fig. 1 B.1), still limits us to a trial-and-error based optimization using PEF parameters, yielding insufficient improvements.

Another possible way for DNA molecules to overcome the cell membrane barrier is by directly translocating across the permeabilized membrane without the formation of DNA aggregates (Fig. 1 B.3). However, a mechanism of direct DNA translocation through the permeabilized membrane is less widely accepted.

In order to evaluate the role of PEF in mediating DNA transport *via* DNA aggregate formation and subsequent endocytosis (Fig. 1 B.1-2) or in mediating a direct DNA translocation across the permeabilized membrane (Fig. 1 B.3), the existing body of evidence needs to be re-examined. Although such an exercise cannot provide an understanding of a definitive mechanism of DNA aggregate formation and/or DNA translocation, it can still point to the gaps, which when addressed, will lead to improved understanding of how DNA molecules overcome the cell membrane barrier during GET.

Since the initial reports of successful DNA transfection into mammalian cells [39], efforts were dedicated to understand the "motive" force or the mechanism of DNA translocation across the cell membrane [54,62]. Formation of hydrophilic pores (Fig. 2 A), initially described in [39,49,166,167], not only explained the transport of small molecules across the membrane during PEF but also

offered the possibility to explain DNA translocation through the permeabilized membrane.

Various modes of DNA translocation through the hydrophilic pores were considered: diffusion (or electro-diffusion as the authors termed it) through the hydrophilic pores [39], binding of the DNA to the membrane surface and lateral diffusion through the hydrophilic pores [168], translocation of DNA due to flow resulting from colloid-osmotic swelling [169] or from electro-osmotic flux [170] and electrophoretic translocation of DNA through the hydrophilic pores [54,62].

Diffusive translocation through hydrophilic pores was not consistent with the observation that transfection efficiency was drastically reduced when DNA was added only a few seconds after the application of PEF [54]. Further control experiments in the same study also did not support the hypothesis of DNA translocation through hydrophilic pores *via* flow resulting from colloid-osmotic swelling or electro-osmosis [54].

In the meantime, evidence was accumulated that DNA (pre-) adsorption on the cell membrane *via* divalent cations prior to PEF application enhanced DNA transfection [168,171]. In fact, DNA transfection was reduced by two orders of magnitude in the absence of divalent cations [168]. A scheme, shown in Fig. 7 A, was presented which conceptualised the role of divalent cations

in DNA transfection [172]. According to the scheme, DNA molecules (D), in the presence of (m) divalent cations, are adsorbed to the non-permeabilized membrane state (C) or to the permeabilized membrane state (P) as D.C and D.P, respectively. The translocation of DNA molecules across the permeabilized membrane is depicted as D.P ↔ P.D. Therefore, the scheme in Fig. 7 A assumed the adsorption of DNA on the cell membrane (permeabilized and/or non-permeabilized) as a precursor to DNA translocation. The scheme further assumed a membrane bound or membrane associated DNA translocation across the cell membrane. DNA inside the cytoplasm is depicted as D_{in} and the transfected state of the cell is depicted as TC.

DNA adsorption on the membrane mediated by the divalent cations can take place prior to, and without, the application of PEF in addition to taking place during the application of PEF. However, it was soon understood that there is another DNA membrane interaction that takes place due to, and in the presence of, PEF. This interaction represents the anchoring of the DNA molecule to the permeabilized membrane and is a strong(er) association than the interaction mediated by divalent cations [173].

A theoretical analysis of experimental results also predicted the existence of the step of DNA molecules being anchored to the permeabilized membrane [174]. According to the authors, the interaction is an "electro-diffusive" insertion of the DNA into the permeabilized membrane, and it represents a highly interactive step which takes place in the presence of PEF.

A refined scheme depicting the sequence of events at the membrane level, including the step of DNA anchoring to the membrane, was introduced and is shown in Fig. 7 B [174]. The scheme in Fig. 7 B is conceptually similar to the scheme in Fig. 7 A. However, an additional step of DNA being anchored to the membrane - depicted as DP and encircled in red is introduced in Fig. 7 B. This step of DNA anchoring or "inserting/penetrating" into the membrane is predicted to take place during, and in the presence of, PEF [174]. Whereas, the translocation of DNA across the membrane (DP => PD) is predicted to be a slow process that possibly takes place after the application of PEF and does not require the presence of PEF [40,91,173,174].

With a multi-step transport of DNA across the membrane (Fig. 7) it becomes imperative to understand the role of PEF in mediating this transport, in each of these steps. Meanwhile, other experiments at the time also predicted the DNA transport to be a multi-step process establishing a similar scheme as shown in Fig. 7 C [41]. Although the scheme in Fig. 7 C differs slightly from Fig. 7 A and B, it still acknowledges DNA anchoring or "inserting" into the membrane and DNA translocation across the membrane to be two separate steps. Of note is the fact that the scheme in Fig. 7 C does not assume any pre-adsorption of DNA on the membrane by divalent cations. Rather, it refers to accumulation of DNA at the membrane interface. Nevertheless, the authors were able to infer the role of PEF in this multi-step scheme of DNA transfection through their experiments.

Experiments revealed that the "threshold" electric field intensity required to transfect cells with DNA is the same as that required to permeabilize the cell membrane [41]. Further, DNA transport into the cells takes place only through those parts on the cell membrane that are made permeable [41,175]. However, permeabilization and DNA transport should be considered as two separate events (Fig. 7 C, processes 1,4 and 2,5). This is inferred from the observations that the conditions which optimize permeabilization are not the same as the ones that optimize DNA transfection [41]. In addition, the membrane permeabilization is long-lived ($O(1–10)$ minutes after PEF termination), whereas sites on the permeable membrane competent for DNA transport are short lived (within $O(1–2)$ s of PEF termination) [41,54]. Another role of PEF is to electrophoretically accumulate DNA at the membrane

(Fig. 7 C, Process 1). This is also discussed in Section 3 of this review.

The authors [41] further acknowledged the existence of the step in which DNA is inserted in (or anchored to) the cell membrane based on the observations that DNA translocation across the membrane is a slow process [173] and that the application of LV pulses after HV pulses improves DNA transfection [62]. The DNA insertion or anchoring step is depicted in Fig. 7 C as $DNA_{inserted}$. It should be carefully noted that the step of DNA anchoring or insertion to the cell membrane ($DNA_{inserted}$) is between interfacial accumulation ($DNA_{interface}$) and DNA 'Translocation' in Fig. 7 C, thus, also indicating a multi-step DNA transport across the cell membrane.

PEF, thus, influences GET at the membrane level in many ways [41]. First, PEF determines permeabilised area/cap where transmembrane potential exceeds a certain "threshold" value and permeabilization takes place; these areas become the competent sites for DNA transport (Fig. 7 C, Process 2). In addition, PEF accumulates DNA near the cell membrane (interfacial accumulation) through electrophoresis (Fig. 7 C, Process 1). Fig. 7 C can be reconciled with Fig. 7 A and B by assuming that the interfacial accumulation could lead to (an enhanced) adsorption of DNA molecules on the membrane *via* divalent cations.

There were no experimental evidences to infer the influence of PEF in anchoring or insertion of the DNA to the membrane (Fig. 7 C, Process 3) [41]. However, as mentioned previously, there were speculations from earlier studies that DNA anchoring or insertion to the membrane takes place in the presence of PEF. For instance, Neumann and co-workers termed this anchoring or insertion of DNA to the membrane as a "highly interactive" "electro-diffusive" process, suggesting that it is influenced by PEF [174].

Although the mechanism of DNA interaction and anchoring to the cell membrane and subsequent translocation were still unknown, such schemes, along with experimental and theoretical analysis [41,172,174], were instrumental in establishing the DNA transport through the permeabilized membrane as a multi-step process involving DNA anchoring to the cell membrane, DNA interaction (anchoring or "insertion") with the cell membrane and DNA translocation across the membrane, as opposed to a direct translocation through permeabilized membrane. While multiple steps involved in the process of GET convoluted the entire process, acknowledging the existence of the multi-step process was crucial in establishing a holistic view of GET and preventing its oversimplification.

It was not until 2002 that experiments confirmed the existence of PEF mediated DNA membrane interaction in the form DNA aggregates using fluorescently labelled DNA molecules and observations at the single-cell level [40]. The observation of DNA aggregates greatly influenced the understanding of DNA transport and DNA translocation across the membrane.

Efforts were then focused on characterizing these DNA aggregates and examining the role of PEF in the formation of these DNA aggregates. The first role of PEF in forming DNA aggregates at the cell membrane was already evident from the initial report [40]. Experiments revealed that only when the membrane was permeabilized (i.e. PEF was above the electropermeabilization threshold) that DNA aggregates were observed at the membrane [40]. This observation was consistent with previous reports of electropermeabilization threshold being same for DNA transfection and uptake of small molecules [41]. Moreover, a longer ms duration pulse was needed to observe DNA aggregate formation at the membrane, whereas the uptake of small propidium iodide was detected even with shorter µs pulses, indicating a role of electrophoresis [40]. However, a few studies have reported formation of DNA aggregates even with short µs pulses but with slightly higher electric field strengths [109]. Further evidence of the involvement of electrophoresis comes from the observations that

13

S. Sachdev, Tjaša Potočnik, L. Rems et al.

DNA aggregates are formed on the cathode facing side of the membrane [40,51,52,109].

In an attempt to characterize the kinetics of DNA aggregate formation, it was observed that DNA aggregates take around 1 s to form or become stabilized [52]. Under bi-polar conditions, reversing the polarity of PEF within 1 s does not lead to stable DNA aggregates, resulting in lowered gene expression [52]. Moreover, during the application of a train of pulses, the first pulse led to DNA aggregates on the membrane, whereas subsequent pulses did not lead to new aggregates being formed [51]. Rather, new DNA molecules were electrophoretically added to the existing aggregates [51].

Since DNA molecules interact with the membrane and form aggregates, there are two processes leading to DNA aggregation that need further attention - (i) DNA attaching to the cell membrane followed by (ii) DNA "condensing" on the cell membrane to form aggregates. Both these processes are peculiar since they (might) involve overcoming an electrostatic barrier. For DNA attaching to the cell membrane, the electrostatic barrier arises due to negatively charged DNA molecules attaching to a negatively charged cell membrane. For DNA "condensing" to form aggregates, the electrostatic barrier arises due to negatively charged DNA molecules condensing onto themselves. While a distinct condensed state of DNA molecules in the aggregates is still speculative and has not been explicitly proven, it can still be inferred that DNA molecules in the aggregates represent a state in which strands of DNA molecules are closer to each other than they are in their native "free" state.

We shall now look at the possible role of PEF in overcoming these electrostatic barriers arising due to DNA membrane interaction in the form of DNA aggregation at the cell membrane.

As discussed previously, the process of DNA adsorption to the membrane is mediated by divalent cations, and this process enhances DNA transfection [168,171,172,174]. It should be noted that DNA adsorption to the membrane *via* divalent cations is not equivalent to DNA aggregation at the cell membrane. DNA can adsorb on the membrane irrespective of PEF application whereas DNA will aggregate in the presence of, and possibly due to, PEF [63].

The questions arise – *How divalent cations help in overcoming the electrostatic barrier leading to DNA adsorption on the cell membrane?* and – *How, and if, PEF modulates the process of adsorption of DNA on the cell membrane by divalent cations?*

Divalent cations can facilitate adsorption of DNA on zwitterionic lipid membranes. This is based on the process of ion-exchange and is described in terms of an extended Poisson-Boltzmann framework [176]. Prior to adsorption, divalent cations are bound to the negatively charged phosphate moieties of the DNA molecule. When DNA molecules approach the membrane, the divalent cations that are bound to the DNA phosphate moieties, now bind to the phosphate moieties of the lipid head group. This causes a re-orientation of the lipid head group, exposing the positively charged moieties outward towards the approaching DNA molecule. These positively charged moieties of the lipid head-group now provide the counter-ion charge to stabilize the phosphate moieties of the DNA molecule. This is the ion exchange pro-
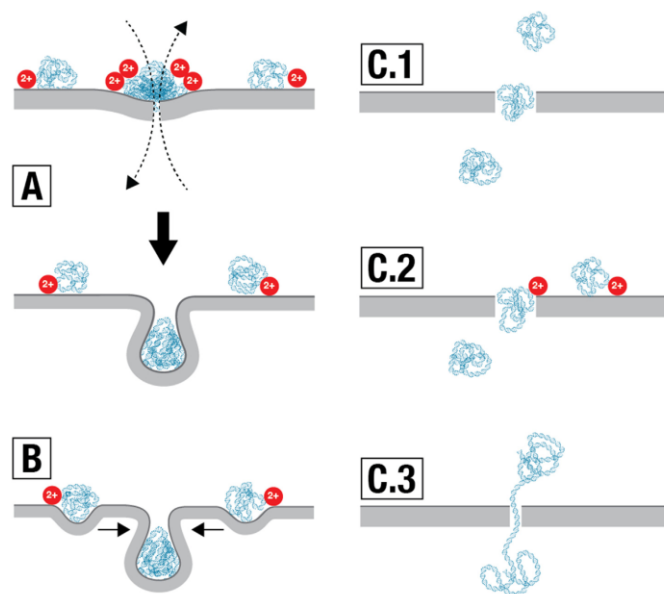
Fig. 8. Different modes of DNA translocation across the cell membrane. DNA is shown in blue, divalent cations are depicted as red circles and cell membrane is depicted in grey (A) DNA aggregation mediated by divalent cations and subsequent endocytosis. The dotted arrows represent ion influx/efflux through permeable sites on the membrane. (B) DNA aggregation mediated by curvature mediated interactions. (C.1–3) DNA translocation through hydrophilic pores without DNA aggregation. (C.1) DNA translocation through large hydrophilic pores without membrane adsorption. (C.2) DNA translocation through large hydrophilic pores with membrane adsorption. (C.3) Single file (i.e., single bp by bp) DNA translocation through a small hydrophilic pore. (For interpretation of the references to color in this figure legend, the reader is referred to the web version of this article.)

14

cess - where divalent cations first neutralizing the phosphate moieties of the DNA molecules, upon DNA adsorption, neutralize the phosphate moieties of the lipid head group. In return, the positively charged moieties of the lipid head group stabilize the phosphate moieties of the DNA molecule. This model was first proposed by McManus *et al.* who experimentally showed that divalent cations adsorbing to the zwitterionic membrane in the presence of DNA molecules effectively render the membrane positively charged [177].

Based on MD simulations it was shown that in the absence of divalent cations, there is a repulsive electrostatic barrier between a DNA molecule and a zwitterionic lipid membrane [178]. However, when enough divalent cations (Ca^{2+}) are adsorbed on the zwitterionic lipid membrane, they render the lipid membrane effectively positive. DNA molecules, on approaching the lipid membrane, now experience an attractive force indicating favourable adsorption to the membrane in the presence of divalent cations. According to the authors, the initial adsorption of DNA on the lipid membrane is driven by the net positive charge of the membrane induced by the divalent cations. Later, a stable adsorption is observed when the adsorbed divalent cations diffuse to the adsorbed DNA and form a tighter bond by bridging the phosphate moieties of the lipids to the phosphate moieties of the DNA [178].

Thus, based on extended Poisson-Boltzmann formalism of ion-exchange and/or MD formalism, divalent cations can help reduce the repulsive electrostatic free-energy barrier. At high enough concentrations, divalent cations can eventually overcome the barrier by inducing an attraction between zwitterionic lipid membranes and negatively charged DNA molecules [176-178].

Following plausible explanation of – *How divalent cations help in overcoming the electrostatic barrier leading to DNA adsorption on the cell membrane?* we shall now look at – *How, and if, PEF modulates the process of adsorption of DNA on the membrane by divalent cations?*

It appears that PEF could directly contribute to overcoming the electrostatic barrier between negatively charged DNA molecules and (predominantly negatively charged) cell membrane. According to MD simulations, PEF tends to align zwitterionic lipid dipoles along the outward membrane normal at the lipid mono-layer facing the cathode [179], thus creating favourable conditions for negatively charged DNA molecules to interact with the positive moieties of the zwitterionic lipid mono-layer. On the other hand, PEF tends to align zwitterionic lipid dipoles away from the outward membrane normal at the lipid monolayer facing the anode [179], indicating less favourable conditions for DNA molecules to interact with zwitterionic lipid mono-layer. Such orientations of zwitterionic lipid dipoles favour adsorption of DNA on the cathode facing side of the cell membrane based on the ion exchange process described above [176,177]. Moreover, PEF mediated alignment of dipoles at the lipid mono-layers facing the cathode and the anode is also consistent with DNA aggregates being observed at the cell membrane facing the cathode.

DNA can adsorb to the cell membrane even in the absence of PEF [63]. In this case, the role of PEF, at best, could be to accumulate enough DNA molecules near the cell membrane to facilitate their adsorption by divalent cations [41]. Since adsorption of DNA to the cell membrane enhances DNA transfection [168,171,172,174], PEF could indirectly contribute to this enhancement by facilitating DNA adsorption to the cell membrane.

However, it is still not clear how adsorption of DNA molecules to the cell membrane by divalent cations enhances DNA transfection. It is possible that adsorption of DNA to the membrane enhances DNA aggregate formation during PEF. It was shown that a high divalent cation (Mg^{2+}) concentration led to more DNA aggregates being formed [180]. However, the transfection efficiency also decreased with increasing divalent cation concentration (or

increasing DNA aggregate formation) [180], or showed bell-shaped curve with increasing divalent cation concentration [63]. This is inconsistent with the claim that adsorption of DNA molecules to the membrane enhances DNA transfection *via* DNA aggregate formation.

Further, with the knowledge of DNA aggregates formed at the membrane during PEF, the role and fate of these adsorbed DNA molecules (using divalent cations) is not explicit. A high divalent cation concentration leading to enhanced DNA aggregate formation implicitly implies that the adsorbed DNA molecules predominantly lead to formation of DNA aggregates. *Is there also some contribution of bulk, or non-adsorbed, DNA to the formation of DNA aggregates?* The source of DNA in the DNA aggregates formed on the membrane during the application of PEF has not been explicitly identified.

Divalent cations also offer some explanation to the observation/speculation that DNA molecules can overcome their own repulsive electrostatic barrier to aggregate at the cell membrane during PEF. Divalent cations have led to condensation of DNA molecules adsorbed on 2-dimensional (2-D) cationic lipid bi-layer [181]. Beyond a critical divalent cation concentration, there was an abrupt transition from a repulsive electrostatic state of adsorbed DNA molecules to an attractive state leading to DNA condensation [181]. The observations of DNA condensation using divalent cations on 2-D lipid surfaces are consistent with the GET experiments in which divalent cations lead to adsorption of DNA molecules at the membrane (2-D). Moreover, increasing the divalent cation (Mg^{2+}) concentration lead to an increase in DNA aggregates being formed [63,180], consistent with the possibility of divalent cations mediating DNA condensation on cationic lipid bi-layers [181].

Since the condensed state of DNA aggregates is observed only in the presence of PEF, the role of PEF could be to enhance divalent cation concentration which would trigger the transition of adsorbed DNA molecules to an aggregated and condensed state. For instance, PEF could lead to a locally enhanced divalent cation concentration at the permeable sites on the membrane due to divalent cation influx/efflux. This would lead to aggregation of DNA molecules at (or near) the permeable sites (Fig. 8 A). The aggregated DNA molecules could locally alter membrane properties that could then eventually lead to the translocation of DNA molecules by endocytic pathways (Fig. 8 A).

Other processes that can lead to DNA condensation and DNA aggregate formation are curvature-mediated interactions. It was observed that DNA molecules adsorbed on a cationic lipid bi-layer can condense onto themselves [182]. The fraction of condensed DNA molecules increases with increasing cationic lipid concentration. The condensation in this case is driven by curvature mediated interactions [183]. When DNA molecules are adsorbed on the lipid bi-layer membrane, the adsorption can lead to local changes in the membrane curvatures (Fig. 8 B). These local changes can in-turn drive curvature mediated collapse and condensation of DNA molecules at the membrane (Fig. 8 B). Once condensed and aggregated, the increasing membrane curvature at the site of aggregated DNA molecules can further attract incoming DNA molecules to the existing aggregate (Fig. 8 B) [184,185]. This can possibly explain why the number of DNA aggregates remained constant when a train of pulses was applied along with the author's explanation based on lowering of electric field elsewhere in the membrane upon the formation of conducting pores [51]. The high curvature induced by the DNA aggregates due to curvature mediated attraction can naturally lead to translocation of DNA aggregates by vesiculation or endocytic pathways [184].

DNA aggregation can thus be explained based on divalent cation (counter-ion) mediated attraction or curvature mediated interactions. However, it must be noted that these are only speculative

attempts to explain DNA aggregate formation. For instance, cationic lipids are not known to be naturally present in cell membranes, and extrapolation of possible mechanisms from the cationic bilayer system to cells undergoing GET should be done with caution. Thus, DNA aggregation mediated by divalent cations and/or curvature mediated interactions only offer a possibility of providing a basis towards a mechanistic understanding of DNA aggregate formation, or they offer possible starting points to investigate and further explore the underlying mechanism of DNA aggregate formation. Attempts to decipher the mechanisms of DNA aggregate formation during PEF/GET have been very scarce.

In view of DNA aggregate formation and the subsequent internalization *via* endocytic pathways (Fig. 1 B.1-2 and Fig. 8 A and B), a mechanism of direct DNA translocation across the permeabilized membrane has still not been completely abandoned (Fig. 1 B.3) [39,54,62,168]. Sukharev et al. showed that permeability of dye-molecules increased in the presence of DNA molecules, indicating that DNA interacts with hydrophilic pores in membrane during their passage across the membrane [62]. Although indirect, it still provided evidence that the interaction of DNA with the hydrophilic pores, which increases the permeability to dye molecules, is electrophoretic in nature and that DNA is directly translocating through the hydrophilic pores due to electrophoresis provided by PEF (Fig. 8 C.1-3).

Since then, various evidence have supported the mechanism of direct entry into the cell by DNA translocation through hydrophilic pores (without the formation of DNA aggregates) during PEF (Fig. 8 C.1-3), but only to minor extent. For instance, siRNA had direct access to the cytoplasm during the application of PEF, and entered the cells from the cell membrane on the cathode facing side of the cell [56]. However, siRNA molecules are small (~25 bp) compared to large pDNA molecules (~5000 bp), and a mechanism of direct translocation *via* hydrophilic pores for siRNA molecules cannot be trivially extrapolated to large DNA molecules. It was recently shown that irrespective of DNA size, two classes of DNA are observed: aggregated DNA at the membrane and DNA that has direct access to the cytoplasm [55]. Small DNA molecules (25–100 bp) had predominantly direct, and instant, access to the cytoplasm. However, increasing the DNA size shifted the tendency of DNA molecules to aggregate at the cell membrane. Most (but not all) of DNA of size 1000 bp became aggregated at the cell membrane. However, some large DNA still had direct access to the cytoplasm.

Theoretically speaking [186], hydrophilic pores could become large enough to accommodate DNA molecules (Fig. 8 C.1-2), provided that there are no constraints limiting the pore size. For example, in pure lipid systems like giant unilamellar vesicles, one can observe formation pores with diameters of $O(1)$ μm [187]. Other experiments with giant unilamellar vesicles and DNA have also indicated the existence of large enough hydrophilic pores allowing free passage to DNA translocation [58,188]. In planar lipid bilayers, pores can expand indefinitely until rupturing the membrane [167].

However, in a cell membrane the dense actin network that attaches to the membrane is thought to limit the pore size [47]. Indeed, formation of macropores was completely supressed in giant unilamellar vesicles encapsulated with actin networks [189]. Estimates of hydrophilic pore size in cells due to application of PEF are of $O(1)$ nm [190]. Some electroporation models in cells have even assumed a maximum hydrophilic pore size of 5–60 nm [186,191-193]. Radius of gyration for pDNA molecules (~5000 bp) is estimated to be ~ 100 nm [194]. Thus, hydrophilic pore sizes of size 10–60 nm can possibly accommodate pDNA molecules of size ~ 100 nm (~5000 bp) and enable a direct DNA translocation through hydrophilic pores. Even for small hydrophilic pores of $O(1)$ nm, a model has been developed in which DNA can

translocate through the hydrophilic pores in a single-file manner (base-pair by base-pair) similar to DNA translocation through O(1) nm solid-state nanopores [195] (Fig. 8 C.3). However, single-file DNA translocation models are applicable to linear DNA molecules rather than to circular DNA molecules such as plasmid DNA.

Altogether, these experiments and models do account for a mechanism in which DNA molecules translocate through the hydrophilic pores without the need for DNA aggregates being formed. However, it appears that a direct DNA translocation through hydrophilic pores in the membrane is not the dominant mode of DNA crossing the membrane during GET. A criticism to the mechanism of direct DNA translocation into cell has been the lack of naked DNA distribution inside the cell for large DNA molecules which makes them vulnerable to degradation by intracellular nucleases [68-70]. However, experiments have demonstrated that naked DNA molecules form complexes with intracellular proteins as early as 15 mins post their introduction into the cytoplasm [71]. The protein-DNA complexes can facilitate active trafficking inside the cytoplasm and nuclear import of DNA [71], thus providing a possible pathway for DNA molecules translocating through hydrophilic pores (and directly accessing the cytoplasm) to reach the nucleus.

4.1. Endocytosis

Observations that some of the DNA molecules form large aggregates on cell membrane, which are rapidly protected from degradation by cellular nucleases and appear on the intracellular side only several minutes after PEF treatment [40], pointed to endocytosis as possible mechanism for DNA translocation. DNA molecules in the aggregated form at the cell membrane could be recognized by the cell as cargo for endocytosis. Indeed, several studies have shown that the translocation of DNA molecules across cell membrane is mediated by endocytic-like processes during GET [63,196,197].

Endocytosis is a fundamental cellular process present in all cells. There are various endocytic trafficking pathways that coexist and are active concurrently in the same cell type [198]. However, endocytosis was initially not considered as a possible mechanism by which DNA could cross the cell membrane because of the absence of known cellular receptors for DNA. Nonetheless, it was shown that electrophoretically driven DNA can lead to membrane curvature large enough to initiate membrane invagination which can then activate endocytic vesicle formation where DNA is immobile and rapidly protected from extracellular nucleases degradation [54,62]. Overall, there are several possibilities how endocytosis could be involved in DNA uptake after PEF. For instance, DNA could be internalized by (intrinsic) endocytic pathways that are continuously present in cells. Alternatively, PEF could trigger "electroendocytosis" - an electric-field induced endocytic-like process that was first observed when DNA was internalised into large unilamellar vesicles *via* the formation of endosome-like vesicles when exposed to PEF [199]. "Electroendocytosis" was later reported in different cells *in vitro* as well [200-202]. However, it remains unclear whether "electroendocytosis" is specific to PEF or it is simply a native cellular response to membrane damage [203]. Namely, endocytosis is involved in cell membrane repair mechanisms which are activated in response to cell membrane damage. Within 30 s after wounding, the resulting cell membrane damage causes an influx of calcium ions from extracellular space into the cytoplasm triggering exocytosis of lysosomes followed by massive endocytosis. To be internalised into the cell, DNA molecules (aggregated) at the cell membrane could be piggybacked into cell during cell membrane repair after PEF treatment when damaged parts of cell membrane and proteins are being internalized into vesicles for recycling. As

16

another possibility - negatively charged DNA aggregates on cell membrane could trigger similar effects as do negatively charged PIP2 molecules. PIP2 is an important endocytosis and cytoskeleton regulator. Before endocytosis, PIP2 molecule is present in patches in the cell membrane where it is involved in regulation and recruitment of endocytic proteins to the cell membrane [204]. PIP2 molecules interact with many transmembrane proteins, for instance with Bin-Amphiphysin-Rvs (BAR) domain proteins, which are curvature sensing and are important in regulating membrane shape transitions during endocytosis [205].

In addition to cell membrane repair mechanisms, endocytosis could be linked to cytoskeleton disruption and remodelling following the application of PEF (more details on this are provided later). Cytoskeleton, particularly actin filaments and microtubules, are involved in all stages of endocytosis and post endocytic intracellular transport - from endocytic vesicle formation and early stages of endosomal transport, to transport of vesicles between different cell organelles, and transport to perinuclear space [206]. Shortly after the application of PEF, actin polymerization was observed at the side of the cell where DNA aggregates were formed, but only when DNA was present during PEF treatment [207]. High concentration of PIP2 molecule in cell membrane triggers actin polymerization by recruiting dynamin proteins which polymerize at areas of high membrane curvature [208,209]. Negatively charged DNA aggregates on cell membrane could trigger similar response leading to actin polymerization followed by endocytic vesicle formation [91].

Different endocytic pathways have been reported to participate in GET: caveolae- and clathrin-mediated endocytosis, macropinocytosis, and clathrin- independent carrier/GPI-enriched early endosomal compartment (CLIC/GEEC) pathway, both *in vitro* [63,64,197,207] and *in vivo* [210,211]. However, the contribution of each endocytic pathway, or a dominant endocytic pathway, during GET remains elusive. In order to determine which endocytic pathway is involved in DNA internalization during GET, majority of the studies have utilised endocytic inhibitors or have measured the co-localization of DNA and endocytic markers. Endocytic inhibitors are not entirely specific and can interrupt several endocytic mechanisms simultaneously. Even endocytic markers are not entirely specific and can therefore mark several different endocytic pathways. Further, endocytic pathways are complex and diverse. There are many fundamental questions that still remain unanswered including whether key components of specific endocytic pathway are conserved across cell lines and whether there is some overlap in functions of molecules known to participate in specific endocytic pathway [198]. In addition, various sizes of DNA aggregates (100–500 nm) formed on cell membrane during GET could simultaneously trigger multiple endocytic pathways [40,55,212].

4.2. Cytoskeleton disruption and its role in DNA translocation

PEF treatment leads to changes in conformation of all major cytoskeleton components - actin filaments, microtubules and intermediate filaments [213]. Cytoskeleton is highly dynamic and is capable of changing its constitution on a time-scale of $O(1–10)$ mins in response to an external stimulus, mechanical or biochemical in nature. Recovery of cytoskeleton components is reported to be achieved within hours following PEF treatment [214,215].

The cell membrane is connected to actin filaments *via* linker proteins. This provides stability and mechanical support to the lipid bilayer, which is otherwise very fluid. Therefore, disruption of cytoskeleton network due to (and following) PEF application can have a dual effect on GET efficiency. Firstly, it can alter the initiation and transport of endocytic pathways by affecting actin filaments and microtubules as described above. Secondly, it can contribute to mechanisms that participate in the increased mem-

brane permeability. Macropores are observed in the membrane of GUVs when they are treated with PEF [187]. However, macropores are not observed in membranes of cells or actin encapsulated GUVs suggesting that cytoskeletal, and/or associated proteins, can affect membrane permeability, particularly pore expansion and resealing [189,216]. The observation that permeabilized regions of the cell are not laterally mobile hints to the possibility of the cytoskeleton being linked to the permeabilized state and to the influence of cytoskeleton on permeabilization and GET [213,217].

To investigate how cytoskeleton structures impact membrane permeability post-PEF application, cytoskeleton disrupting agents were used. They, however, led to contradictory observations regarding the involvement of actin filaments in membrane permeabilization [213]. On one hand, studies showed that exposure to actin inhibiting or disrupting agents led to an increased membrane permeability after PEF application [218-221]. On the other hand, some studies reported significantly decreased PI uptake following PEF application in cells treated with actin inhibiting agents, suggesting a decreased membrane permeability [222,223]. Microtubule inhibition also led to a decreased PI uptake into cells indicative of a decreased membrane permeability. Additionally, shorter resealing time was observed following PEF application in cells treated with microtubule inhibiting agents [218,224]. Use of inhibiting agents thus requires careful attention to the concentration and the exposure of these agents because they can be toxic and can directly affect cell viability and permeability on their own. Additionally, different cell types and pulse parameters may result in different outcomes [213].

Pulses of different durations, from nanosecond to millisecond, can lead to cytoskeletal disruption [213]. However, the mechanism by which PEF leads to cytoskeletal disruption has not yet been elucidated. It was proposed that cytoskeletal disruption could be a consequence of interactions between PEF and cytoskeletal proteins (or associated proteins) in the form of conformation changes, electrophoresis and electromechanical effects. Experiments on actin-encapsulated GUVs compared mechanical and electrophoretic forces experienced by actin filaments. It was shown that 4 times higher electrophoretic forces are induced on actin filaments compared to mechanical forces [189]. In actin-encapsulated GUVs, where biological processes can be excluded and direct effects on actin can be investigated, breakdown of actin filaments was observed following PEF application. However, the force of mechanical disruption on the cell membrane was below the threshold that is required for actin filament rupture or depolymerization. This suggests that, upon membrane permeabilization, electrophoretic forces acting on the actin filaments play a major role in actin network disruption [225,226].

Microtubules are composed of α- and β-tubulin which are polar molecules with high negative charge at the c-terminus tail leading to a higher overall electrical charge and a higher dipole moment compared to other proteins. This makes microtubules a (highly susceptible) target for direct modulation by PEF. It has been shown that PEF can directly disrupt microtubules polymerization [227,228]. Further, electrophoretic forces are reported to decrease interactions between microtubules and motor proteins, thus affecting microtubules dynamics [227,228].

Apart from directly influencing cytoskeleton dynamics, PEF can also have secondary effects on cytoskeleton. One of the proposed secondary processes by which PEF application could lead to cytoskeletal disruption is through altering calcium dynamics. Calcium, as a signalling molecule, is involved in a large number of cellular processes and can consequently lead to diversity of cellular responses that can together disrupt the cytoskeleton. For instance, calcium modulates both major components of cytoskeleton - actin and microtubules, and its increased concentration in the cytoplasm can cause actin breakdown and microtubules depolymerization

17

[229,230]. Normally, calcium pumps maintain a 10,000 times lower calcium concentration inside the cells compared to the interstitium (or extracellular space). Following cell membrane permeabilization, extracellular calcium enters the cell by electrophoresis and diffusion through pores and/or through voltage-gated calcium channels. The resulting high concentration of calcium in the cytoplasm can lead to calcium induced calcium release from endoplasmic reticulum, leading to further amplification of calcium signals. In addition, cytoplasmic calcium levels can also increase due to permeabilization of various intracellular calcium stores, such as the endoplasmic reticulum and mitochondria after PEF application [231-233].

Other secondary processes triggered by PEF, such as ATP depletion, cell swelling, pH changes and reactive oxygen species generation may also lead to cytoskeletal disruption. However, respective contributions of each of these mechanisms to cytoskeletal disruption remain poorly characterized. When cell membrane becomes permeabilized, ATP can leak through pores in the cell membrane [234,235]. Additionally, during subsequent membrane resealing, ion concentrations in the cell have to be restored, which is an energy consuming process that requires ATP. Together, this can lead to severe ATP depletion after PEF application [236]. ATP depletion was also shown to inhibit linker proteins and lead to cell membrane separation from the underlying cytoskeleton [237]. Cell blebbing and rounding is often reported after PEF application [219,238,239]. Cell swelling can also lead to cytoskeletal disruption [238,239]. However, cytoskeletal disruption was observed also in the absence of cell swelling suggesting the involvement of alternate mechanisms [240]. In tissues, cell swelling after PEF application is limited compared to cells in suspension, but it could lead to narrowing of the interstitial (i.e., extracellular) space. Further, PEF application can also lead to pH changes in the vicinity of electrodes, with acidic pH at anode and alkaline pH at cathode [156]. Acidic pH was reported to promote actin rearrangement and cellular protrusion [241]. PEF also induce the generation of reactive oxygen species [242-244] which were reported to cause direct oxidation of actin and actin-regulatory proteins [245]. However, the precise role of oxidation of specific proteins in different cellular functions remains to be elucidated.

5. Cytoplasmic barriers

Majority of studies have focused on cell membrane as a barrier to GET. But for GET to be efficient, DNA must overcome additional cellular barriers of the cytoplasm and the nuclear envelope i.e., DNA must travel through cytoplasm to reach the perinuclear space and cross the nuclear envelope to enter the cell nucleus. It was observed that naked DNA diffusion is almost negligible within the dense cytoplasm which consists of cytoskeleton network, various cellular organelles and large amounts of proteins among other molecules. In addition, naked DNA is degraded within minutes by nucleases present in cell cytoplasm [70]. Cytoplasm, thus, presents itself as another significant barrier which cannot be ignored when considering GET optimization. Nevertheless, since GET leads to transgene expression, there must be mechanisms by which DNA circumvents cytoplasmic obstacles.

DNA molecules that have had direct access to the cytoplasm do not stay naked or un-complexed for very long in the cytoplasm. Negatively charged plasmid DNA is quickly coated with cytoplasmic proteins, some of them being sequence-specific DNA-binding proteins, and cations. This, in turn could help in their transport through the cytoplasm. For instance, it was proposed that DNA moves to perinuclear space by active transport, meaning that naked DNA in cell cytoplasm connects with adapter proteins, enabling their binding to the cytoskeleton motor proteins [246].

Proteins that bind to DNA could also act as adaptor proteins to motor proteins which enable transport along cytoskeletal network [70,247]. Results have indeed confirmed that naked DNA, either after endosomal escape or translocation through pores in the cell membrane, complexes with various proteins such as microtubule-directed motor proteins, heterogeneous nuclear ribonucleoproteins (hnRNP), mRNA binding proteins, proteins involved in nuclear import and as well as export and transcription factors. For instance, formation of plasmid DNA-protein complexes has been observed as early as 15 min post PEF application [71]. It should be noted that DNA-protein complex formation could also result in DNA charge neutralization leading to DNA condensation. DNA condensation in turn leads to reduction of its size which could increase diffusion and mobility of DNA. Also, DNA-protein complex formation could protect DNA from degradation.

When DNA is endocytosed, endocytic vesicles containing DNA already possess proteins that interact with motor proteins facilitating their (active) transport [206]. Results have indeed shown that DNA molecules in cell cytoplasm co-localize with early endosomes, recycling endosomes, late endosomes and lysosomes indicative of active transport [64,65]. Contradictory results were obtained regarding endosomal escape of DNA molecules. On one hand, inhibition of endosomal fusion or lysosomal translocation was reported to prevent gene expression [248]. On the other hand, studies reported that DNA molecules must escape endosomes prior to fusion with lysosomes, otherwise they are lost to degradation [249]. Nevertheless, DNA molecules are reported to accumulate in the perinuclear space within 1–2 h following PEF [64].

Importantly, we should note that care must be taken when interpreting results using labelled DNA molecules. DNA markers used for investigating intracellular trafficking of DNA molecules, such as TOTO-1 and BrdU, can change the properties of DNA molecules such as their size, configuration and net effective charge, and consequently DNA transport. For instance, BrdU labelled DNA molecules may become more resistant to lysosomal degradation and might also alter the kinetics of nuclear accumulation of DNA molecules [248]. Further, when DNA is labelled with a high fluorophore to DNA ratio, the ability of DNA to enter the nucleus and its transcriptional activity are reduced [250]. These observations demonstrate that labelling of DNA molecules alters, and possibly interferes with, the behaviour of DNA molecules.

There are only a handful of studies reporting on the role of cytoskeleton network on DNA transport following PEF application. It was observed that pre-treatment with latrunculin B, a molecule that disrupts actin cytoskeleton, decreased the number of cells transfected with DNA molecules as well as the fluorescence intensity (resulting from reporter gene expression) [207]. On the contrary, stabilization of the microtubule network resulted in enhancement of electro-transfected DNA expression. It was also demonstrated that DNA molecules can interact with motor proteins and be actively transported along the microtubule network [66,251]. Cytoskeleton network is a complex and a diverse mesh of various interacting proteins. Different types of cells have different cytoskeleton organization, leading to variations in the cellular responses to external stimuli [237,252]. Various studies have shown that cancerous cells, which have a cytoskeletal network adapted for proliferation and infiltration and consequently have reduced stiffness, have a different response to damage by PEF application compared to healthy cells [252-254]. For instance, following the same PEF treatment, cytoskeleton was conserved in fibroblasts whereas cancer cells showed a loss of cytoskeleton [255].

Transport of DNA thorough cytoplasm remains yet another GET barrier that is still not fully understood. Altogether, above mentioned findings point to different mechanisms which are involved in DNA transport through cytoplasm to perinuclear space. How-

18

ever, further studies are needed to elucidate which mechanisms, and to what extent, or possibly the dominant mechanism, that participate in DNA transport through cytoplasm, lead to successful GET.

6. Nuclear envelope

The nuclear envelope controls the traffic between the cytoplasm and the nucleus for all macromolecules - proteins, DNA, RNA and oligonucleotides. Even in the cells that expressed the transgene, 24 h after GET most of the DNA molecules were visible as aggregates located in the perinuclear space. Apparently, only some DNA molecules crossed the nuclear envelope, but even this small fraction was enough to lead to gene expression [40].

DNA molecules can reach cell nucleus during mitosis when the nuclear envelope is disassembled in a process referred to as nuclear envelope breakdown. DNA transfection efficiency can be increased by synchronization with the mitotic phase [72]. Alternatively, DNA must be transported through the nuclear pore complex to reach cell nucleus where they can be transcribed. In general, nondividing cells are known to be harder to transfect [256]. Majority of cells in tissues are either terminally differentiated or they divide with doubling times ranging from weeks to months. There must then be a way for DNA molecules to enter cell nucleus in the absence of cell division. Indeed, DNA has been delivered to quiescent cells. For instance, pDNA was directly microinjected into the cytoplasm of individual primary skeletal muscle cells, leading to gene expression [257]. In fact, among non-dividing cells, muscle cells seem to be the easiest to transfect with physical methods [258].

In the absence of cell division, the nuclear import of DNA molecules was shown to depend on specific DNA sequences, known as DNA nuclear targeting sequence (DTS), that drive nuclear import better compared to other sequences [259]. The first such sequence discovered was SV40 - a 72 bp long Simian virus 40 enhancer that binds to multiple ubiquitous general transcription factors and facilitates nuclear import of DNA, consequently increasing gene transfer efficiency [260,261]. DTS have binding sites for various transcription factors which are assembled in the cytoplasm and transported to the nucleus with importins - proteins involved in the nuclear import. After binding to DTS, transcription factors interact with importins and enable transport of DNA molecules to the nucleus [71,256,262]. In fact, 30 min after PEF application, over 300 unique proteins were bound to DNA molecules with DTS compared to only 60 proteins which were bound to DNA molecules without DTS [71]. This suggests that DNA molecules with DTS have a higher chance of translocation to the nucleus from the cytoplasm. However, gene transfer and expression have been obtained also with DNA molecules that lack DTS. It was shown that when cytoplasm of a mouse skeletal muscle cell *in vivo* was injected with DNA molecules, at least some of the DNA molecules were able to cross the nuclear envelope and be imported into the nucleus independent of any DTS [74].

While exposure of cells to micro- and millisecond PEF leads to cell membrane permeabilization, nanosecond PEF have shown to permeabilize cell organelles such as intracellular granules [75], endocytic vesicles [76] and large endocytosed vacuoles [77]. They can also release calcium from the endoplasmic reticulum [80]. Since nanosecond PEF permeabilize intra-cellular organelle membranes, they might also have an effect on the nuclear envelope. In this way GET efficiency could be enhanced by facilitating the access of DNA molecules to the nucleus. However, when cells were exposed to nanosecond PEF after the application of conventional PEF, improvement in GET efficiency in terms of transgene expression and percentage of transfected cells was observed only in some

Table AT.1
Parameters in equation (A.6) and their values.

Parameter	Value	Reference/Justification
R_{cell}	7.5 μm	[46,267]
M_w (5900 bp DNA molecule)	3894000 g/mol	5900 bp × 660 g/mol/bp
c (sub-optimal)	$\leq 1\ \mu g/ml$	[107,108]
c (optimal)	$\geq 10\ \mu g/ml$	[107,108]
ρ_{cell} (*in vitro*)	2×10^{12} cells/m³	[180,266]
ρ_{cell} (*in vivo*)	5.5×10^{14} cells/m³	*

* Considering a total number of N_{cells} in a space of volume V_{space}, the sphere of volume available to a single cell is V_{space}/N_{cells} or $1/\rho_{cell}$. For extremely dense suspensions or densely packed cells, as is the case for tissues or *in vivo*, the sphere of volume ($1/\rho_{cell}$) available to a single cell equals the volume of a single cell ($\frac{4}{3}\pi R_{cell}^3$) i.e., $1/\rho_{cell} = \frac{4}{3}\pi R_{cell}^3$. Using $R_{cell} = 7.5$ μm, we obtain $\rho_{cell} \sim 5.5 \times 10^{14}$ cells/m³.

cases [80,81]. In other cases, no improvement in GET efficiency was observed [78]. In contrast, applying nanosecond PEF before conventional PEF did show improved GET efficiency, which was attributed to calcium independent and dependent effects of nanosecond PEF on GET [263].

A hypothesis that endosomes with DNA molecules could interact and fuse with endoplasmic reticulum and thus release DNA molecules into the lumen of reticulum was also proposed. DNA molecules could then reach the nucleus through the continuous network between the nuclear and reticulum membranes, bypassing the steps of endosomal escape and of crossing the nuclear envelope [82].

Finally, DNA molecules could be translocated to the nucleus with nuclear envelope-associated endosomes. Nuclear envelope-associated endosomes are early endosomes that were observed to localize in the perinuclear space and fuse with the nuclear envelope, thus enabling cell surface proteins and extracellular molecules direct access to cell nucleus [83]. Further, it was shown that lipid vesicles can spontaneously fuse with permeabilized membrane [264,265], implying that permeabilization of intracellular organelle membranes could facilitate the fusion of pDNA-containing endosomes with the endoplasmic reticulum or the nuclear envelope. A theoretical study suggested that permeabilization of the endoplasmic reticulum can occur not only when exposing cells to nsPEF, but also when exposing them to longer and more conventional pulses [191]. However, additional studies are needed to clarify if the above-mentioned mechanisms are involved in the transfer of DNA molecules to the nucleus following PEF application.

7. Conclusion

In vivo barriers of the interstitium, cell-membrane, cytoplasm and nuclear envelope contribute in their own unique ways to prevent DNA molecules from reaching the nucleus of the cell. PEF helps to overcome (some of) these barriers and allow DNA molecules to reach the nucleus. We have revisited the existing literature and formalized the past and the current understanding of the GET process, explaining in detail how DNA molecules interact with each of the barriers and transport through them sequentially. In doing so, we have identified the factors limiting the transport of DNA through the barriers if the transport process is known, such as for the interstitium. We also identified gaps in the understanding of the transport process through the barriers if the transport process is still unknown, such as for the cell membrane, the cytoplasm and the nuclear envelope. Identifying the mechanisms of transport and addressing the transport limitations – each of which have been discussed – will enable further enhancement of GET efficiency *in vitro* as well as in *in vivo* across (length) scales, cell types,

19

Table AT.2
DNA – Cell distances for concentrations ranging from sub-optimal to optimal.

Regime	Concentration (µg/ml)	DNA - Cell Distance [D in eq. (A.6)] (µm)			
		in vitro		*in vivo*	
sub-optimal	0.01	10.72	$O(1-50)$	3.28	$O(1-10)$
	0.1	4.97		1.52	
	1	2.31		0.71	
	5	1.35		0.41	
optimal	10	1.07	$O(0.5-1)$	0.33	$O(0.1-0.5)$
	50	0.63		0.19	
	100	0.50		0.15	

tissue types and species; a privilege which is not afforded by the current trial-and-error based optimisations of GET.

Declaration of Competing Interest

The authors declare that they have no known competing financial interests or personal relationships that could have appeared to influence the work reported in this paper.

Acknowledgements

Appendix A. DNA – Cell distance

The approach used to calculate the DNA – cell distance is similar to the one in [266]. Considering a total number of N_{cells} in a space of volume V_{space}, the total volume occupied by cells is $N_{cells} \cdot \frac{4}{3}\pi R_{cell}^3$; where R_{cell} is the radius of the cell and $\frac{4}{3}\pi R_{cell}^3$ is the volume of a single cell. The volume left to be occupied by the DNA molecules is:

$$V_{DNA} = V_{space} - N_{cells} \cdot \frac{4}{3}\pi R_{cell}^3 \tag{A.1}$$

The volume space available to single a DNA molecule can be considered as $\frac{4}{3}\pi R_{DNA}^3$; where R_{DNA} is the radius of the sphere available to a DNA molecule. The volume occupied by a total of N_{DNA} molecules is then:

$$V_{DNA} = N_{DNA} \cdot \frac{4}{3}\pi R_{DNA}^3 \tag{A.2}$$

If the concentration of DNA molecules is c (g/ml), then the number of DNA molecules in the space (V_{space}) can be calculated as:

$$N_{DNA} = \frac{c \cdot V_{space} \cdot N_A}{M_w} \tag{A.3}$$

where M_w is the molecular weight (g/mol) of the DNA molecules and N_A is the Avogadro's number.

Combining equations (A.1), (A.2) and (A.3), we obtain the radius of the sphere available to single DNA molecules (R_{DNA}) as:

$$R_{DNA} = \left(\frac{V_{space} - N_{cells} \cdot \frac{4}{3}\pi R_{cell}^3}{\frac{4}{3}\pi \cdot \left(\frac{c \cdot V_{space} \cdot N_A}{M_w} \right)} \right)^{1/3} \tag{A.4}$$

Assuming the cells and DNA molecules are evenly distributed, the average distance between two DNA molecules or a DNA molecule and a cell can be considered as $D = 2.R_{DNA}$, or:

$$D = 2. \left(\frac{V_{space} - N_{cells} \cdot \frac{4}{3}\pi R_{cell}^3}{\frac{4}{3}\pi \cdot \left(\frac{c \cdot V_{space} \cdot N_A}{M_w} \right)} \right)^{1/3} \tag{A.5}$$

Considering, $\rho_{cell} = \frac{N_{cells}}{V_{space}}$ to be the cell density, equation (A.5) above can be rewritten as:

$$D = 2. \left(\frac{1 - \rho_{cell} \cdot \frac{4}{3}\pi R_{cell}^3}{\frac{4}{3}\pi \cdot \left(\frac{c N_A}{M_w} \right)} \right)^{1/3} \tag{A.6}$$

To get some estimates for DNA – DNA or DNA – cell distance, we consider the values in Table AT.1 for parameters in equation (A.6).

Values and approximate estimates for DNA – cell distances are given below in Table AT.2 below for different concentrations of DNA molecules ranging from sub-optimal to optimal. The calculations are based on Equation (A.6) and parameters in Table AT.1.

Appendix B. Electrophoretic migration

The electrophoretic migration (L) of a DNA molecule under an electric field (E) can be calculated according to:

$$L = \mu E T \tag{B.1}$$

Where μ is the electrophoretic mobility of the DNA molecule and T is the duration for which the electric field is applied. We have calculated electrophoretic migration for a DNA molecule with 5900 bp with $\mu = -3.75 \times 10^{-8}$ $m^2V^{-1}s^{-1}$ based on [268].

References

[1] S.L. Ginn, A.K. Amaya, I.E. Alexander, M. Edelstein, M.R. Abedi, Gene therapy clinical trials worldwide to 2017: An update, J. Gene Med. 20 (5) (2018) e3015, https://doi.org/10.1002/jgm.3015.

[2] X.M. Anguela, K.A. High, Entering the modern era of gene therapy, Annu. Rev. Med. 70 (1) (2019) 273–288, https://doi.org/10.1146/annurev-med-012017-043332.

[3] F. Capone, F. Nappi, M.C. Galli, Gene Therapy Clinical Trials: Past, Present and Future - ScienceDirect, in: Second Gener. Cell Gene-Based Ther., 2020: pp. 285–301. https://doi.org/10.1016/B978-0-12-812034-7.00011-X.

[4] A.K. Singh, J.P. McGuirk, CAR T cells: continuation in a revolution of immunotherapy, Lancet Oncol. 21 (3) (2020) e168–e178, https://doi.org/10.1016/S1470-2045(19)30823-X.

[5] E.J. Topol, Messenger RNA vaccines against SARS-CoV-2, Cell. 184 (6) (2021) 1401, https://doi.org/10.1016/j.cell.2020.12.039.

[6] N. Pardi, M.J. Hogan, F.W. Porter, D. Weissman, mRNA vaccines-a new era in vaccinology, Nat. Rev. Drug Discov. 17 (4) (2018) 261–279, https://doi.org/10.1038/nrd.2017.243.

[7] E.N. Gary, D.B. Weiner, DNA vaccines: prime time is now, Curr. Opin. Immunol. 65 (2020) 21–27, https://doi.org/10.1016/j.coi.2020.01.006.

[8] M.A. Kutzler, D.B. Weiner, DNA vaccines: Ready for prime time?, Nat Rev. Genet. 9 (10) (2008) 776–788, https://doi.org/10.1038/nrg2432.

[9] M.H. Porteus, A New Class of Medicines through DNA Editing, N. Engl. J. Med. 380 (10) (2019) 947–959, https://doi.org/10.1056/NEJMra1800729.

[10] J.A. Wolff, R.W. Malone, P. Williams, W. Chong, G. Acsadi, A. Jani, P.L. Felgner, Science 247 (80) (1990) 1465–1468, https://doi.org/10.1126/science.1690918.

[11] M.F. Bureau, S. Naimi, R. Torero Ibad, J. Seguin, C. Georger, E. Arnould, L. Maton, F. Blanche, P. Delaere, D. Scherman, Intramuscular plasmid DNA electrotransfer: Biodistribution and degradation, Biochim. Biophys. Acta -

Gene Struct. Expr. 1676 (2) (2004) 138–148, https://doi.org/10.1016/j.bbaexp.2003.11.005.

[12] Z. Zhao, A.C. Anselmo, S. Mitragotri, Viral Vector-Based Gene Therapies in the Clinic, Bioeng. Transl. Med. (2021), https://doi.org/10.1002/btm2.10258 e10258.

[13] J.M. Wilson, T.R. Flotte, Moving Forward After Two Deaths in a Gene Therapy Trial of Myotubular Myopathy, Hum. Gene Ther. 31 (13-14) (2020) 695–696, https://doi.org/10.1089/hum.2020.182.

[14] H. Yin, R.L. Kanasty, A.A. Eltoukhy, A.J. Vegas, J.R. Dorkin, D.G. Anderson, Non-viral vectors for gene-based therapy, Nat. Rev. Genet. 15 (8) (2014) 541–555, https://doi.org/10.1038/nrg3763.

[15] C.M. Wiethoff, C.R. Middaugh, Barriers to nonviral gene delivery, J. Pharm. Sci. 92 (2) (2003) 203–217, https://doi.org/10.1002/jps.10286.

[16] H. Aihara, J.-I. Miyazaki, Gene transfer into muscle by electroporation in vivo, Nat. Biotechnol. 16 (9) (1998) 867–870, https://doi.org/10.1038/nbt0998-867.

[17] L.M. Mir, M.F. Bureau, J. Gehl, R. Rangara, D. Rouy, J.-M. Caillaud, P. Delaere, D. Branellec, B. Schwartz, D. Scherman, High-efficiency gene transfer into skeletal muscle mediated by electric pulses, Proc. Natl. Acad. Sci. USA 96 (8) (1999) 4262–4267, https://doi.org/10.1073/pnas.96.8.4262.

[18] I. Mathiesen, Electropermeabilization of skeletal muscle enhances gene transfer in vivo, Gene Ther. 6 (4) (1999) 508–514, https://doi.org/10.1038/sj.gt.3300847.

[19] T. Nishi, K. Yoshizato, S. Yamashiro, H. Takeshima, K. Sato, K. Hamada, I. Kitamura, T. Yoshimura, H. Saya, J.I. Kuratsu, Y. Ushio, High-efficiency in vivo gene transfer using intraarterial plasmid DNA injection following in vivo electroporation, Cancer Res. 56 (1996) 1050–1055.

[20] R. Heller, M. Jaroszeski, A. Atkin, D. Moradpour, R. Gilbert, J. Wands, C. Nicolau, In vivo gene electroinjection and expression in rat liver, FEBS Lett. 389 (1996) 225–228, https://doi.org/10.1016/0014-5793(96)00590-X.

[21] R. Heller, L.C. Heller, Gene Electrotransfer Clinical Trials, Adv. Genet. 89 (2015) 235–262, https://doi.org/10.1016/bs.adgen.2014.10.006.

[22] L. Lambricht, A. Lopes, S. Kos, G. Sersa, V. Préat, G. Vandermeulen, Clinical potential of electroporation for gene therapy and DNA vaccine delivery, Expert Opin. Drug Deliv. 13 (2) (2016) 295–310, https://doi.org/10.1517/17425247.2016.1121990.

[23] B. Geboers, H.J. Scheffer, P.M. Graybill, A.H. Ruarus, S. Nieuwenhuizen, R.S. Puijk, P.M. van den Tol, R.V. Davalos, B. Rubinsky, T.D. de Gruijl, D. Miklavčič, M.R. Meijerink, High-Voltage Electrical Pulses in Oncology : Irreversible Electroporation, Electrochemotherapy, Gene Electrotransfer, Electrofusion, and Electroimmunotherapy, Radiology. 295 (2020) 254–272, https://doi.org/10.1148/radiol.2020192190.

[24] A.P. Algazi, C.G. Twitty, K.K. Tsai, M. Le, R. Pierce, E. Browning, R. Hermiz, D.A. Canton, D. Bannavong, A. Oglesby, M. Francisco, L. Fong, M.J. Pittet, S.P. Arlauckas, C. Garris, L.P. Levine, C. Bifulco, C. Ballesteros-Merino, S. Bhatia, S. Gargosky, R.H.I. Andtbacka, B.A. Fox, M.D. Rosenblum, A.I. Daud, Phase II Trial of IL-12 Plasmid Transfection and PD-1 Blockade in Immunologically Quiescent Melanoma, Clin. Cancer Res. 26 (12) (2020) 2827–2837, https://doi.org/10.1158/1078-0432.CCR-19-2217.

[25] A. Algazi, S. Bhatia, S. Agarwala, M. Molina, K. Lewis, M. Faries, L. Fong, L.P. Levine, M. Franco, A. Oglesby, C. Ballesteros-Merino, C.B. Bifulco, B.A. Fox, D. Bannavong, R. Talia, E. Browning, M.H. Le, R.H. Pierce, S. Gargosky, K.K. Tsai, C. Twitty, A.I. Daud, Intratumoral delivery of tavokinogene telseplasmid yields systemic immune responses in metastatic melanoma patients, Ann. Oncol. 31 (4) (2020) 532–540, https://doi.org/10.1016/j.annonc.2019.12.008.

[26] S. Bhatia, N.V. Longino, N.J. Miller, R. Kulikauskas, J.G. Iyer, D. Ibrani, A. Blom, D.R. Byrd, U. Parvathaneni, C.G. Twitty, J.S. Campbell, M.H. Le, S. Gargosky, R. H. Pierce, R. Heller, A.I. Daud, P. Nghiem, Intratumoral delivery of plasmid IL12 via electroporation leads to regression of injected and noninjected tumors in Merkel cell carcinoma, Clin. Cancer Res. 26 (3) (2020) 598–607, https://doi.org/10.1158/1078-0432.CCR-19-0972.

[27] S.K. Greaney, A.P. Algazi, K.K. Tsai, K.T. Takamura, L. Chen, C.G. Twitty, Li. Zhang, A. Paciorek, R.H. Pierce, M.H. Le, A.I. Daud, L. Fong, Intratumoral Plasmid IL12 Electroporation Therapy in Patients with Advanced Melanoma Induces Systemic and Intratumoral T-cell Responses, Cancer, Immunol. Res. 8 (2) (2020) 246–254, https://doi.org/10.1158/2326-6066.CIR-19-0359.

[28] C. Aggarwal, R. Cohen, M.P. Morrow, K.A. Kraynyak, A.J. Sylvester, D.M. Knoblock, J.M. Bauml, G.S. Weinstein, A. Lin, J. Boyer, L. Sakata, S. Tan, A. Anton, K. Dickerson, D. Mangrolia, R. Vang, M. Dallas, S. Oyola, S. Duff, M. Esser, R. Kumar, D. Weiner, I. Csiki, M.L. Bagarazzi, Immunotherapy targeting HPV16/18 generates potent immune responses in HPV-associated head and neck cancer, Clin. Cancer Res. 25 (1) (2019) 110–124, https://doi.org/10.1158/1078-0432.CCR-18-1763.

[29] K. Modjarrad, C.C. Roberts, K.T. Mills, A.R. Castellano, K. Paolino, K. Muthumani, E.L. Reuschel, M.L. Robb, T. Racine, M.-D. Oh, C. Lamarre, F.I. Zaidi, J. Boyer, S.B. Kudchodkar, M. Jeong, J.M. Darden, Y.K. Park, P.T. Scott, C. Remigio, A.P. Parikh, M.C. Wise, E.K. Duperret, K.Y. Kim, H. Choi, S. White, M. Bagarazzi, J.M. May, D. Kane, H. Lee, G. Kobinger, N.L. Michael, D.B. Weiner, S.J. Thomas, J.N. Maslow, Safety and immunogenicity of an anti-Middle East respiratory syndrome coronavirus DNA vaccine: a phase 1, open-label, single-arm, dose-escalation trial, Lancet Infect. Dis. 19 (9) (2019) 1013–1022, https://doi.org/10.1016/S1473-3099(19)30266-X.

[30] M.P. Morrow, K.A. Kraynyak, A.J. Sylvester, X. Shen, D. Amante, L. Sakata, L. Parker, J. Yan, J. Boyer, C. Roh, L. Humeau, A.S. Khan, K. Broderick, K. Marcozzi-Pierce, M. Giffear, J. Lee, C.L. Trimble, J.J. Kim, N.Y. Sardesai, D.B. Weiner, M.L. Bagarazzi, Augmentation of cellular and humoral immune responses to

HPV16 and HPV18 E6 and E7 antigens by VGX-3100, Mol. Ther. - Oncolytics. 3 (2016) 16025, https://doi.org/10.1038/mto.2016.25.

[31] M.P. Morrow, K.A. Kraynyak, A.J. Sylvester, M. Dallas, D. Knoblock, J.D. Boyer, J. Yan, R. Vang, A.S. Khan, L. Humeau, N.Y. Sardesai, J.J. Kim, S. Plotkin, D.B. Weiner, C.L. Trimble, M.L. Bagarazzi, Clinical and immunologic biomarkers for histologic regression of high-grade cervical dysplasia and clearance of HPV16 and HPV18 after immunotherapy, Clin. Cancer Res. 24 (2) (2018) 276–294, https://doi.org/10.1158/1078-0432.CCR-17-2335.

[32] C.L. Trimble, M.P. Morrow, K.A. Kraynyak, X. Shen, M. Dallas, J. Yan, L. Edwards, R.L. Parker, L. Denny, M. Giffear, A.S. Brown, K. Marcozzi-Pierce, D. Shah, A.M. Slager, A.J. Sylvester, A. Khan, K.E. Broderick, R.J. Juba, T.A. Herring, J. Boyer, J. Lee, N.Y. Sardesai, D.B. Weiner, M.L. Bagarazzi, Safety, efficacy, and immunogenicity of VGX-3100, a therapeutic synthetic DNA vaccine targeting human papillomavirus 16 and 18 E6 and E7 proteins for cervical intraepithelial neoplasia 2/3: A randomised, double-blind, placebo-controlled phase 2b trial, Lancet. 386 (10008) (2015) 2078–2088, https://doi.org/10.1016/S0140-6736(15)00239-1.

[33] A.I. Daud, R.C. DeConti, S. Andrews, P. Urbas, A.I. Riker, V.K. Sondak, P.N. Munster, D.M. Sullivan, K.E. Ugen, J.L. Messina, R. Heller, Phase I trial of interleukin-12 plasmid electroporation in patients with metastatic melanoma, J. Clin. Oncol. 26 (36) (2008) 5896–5903, https://doi.org/10.1200/JCO.2007.15.6794.

[34] T.R.F. Smith, A. Patel, S. Ramos, D. Elwood, X. Zhu, J. Yan, E.N. Gary, S.N. Walker, K. Schultheis, M. Purwar, Z. Xu, J. Walters, P. Bhojnagarwala, M. Yang, N. Chokkalingam, P. Pezzoli, E. Parzych, E.L. Reuschel, A. Doan, N. Tursi, M. Vasquez, J. Choi, E. Tello-Ruiz, I. Maricic, M.A. Bah, Y. Wu, D. Amante, D.H. Park, Y. Dia, A.R. Ali, F.I. Zaidi, A. Generotti, K.Y. Kim, T.A. Herring, S. Reeder, V. M. Andrade, K. Buttigieg, G. Zhao, J.M. Wu, D. Li, L. Bao, J. Liu, W. Deng, C. Qin, A.S. Brown, M. Khoshnejad, N. Wang, J. Chu, D. Wrapp, J.S. McLellan, K. Muthumani, B. Wang, M.W. Carroll, J.J. Kim, J. Boyer, D.W. Kulp, L.M.P.F. Humeau, D.B. Weiner, K.E. Broderick, Immunogenicity of a DNA vaccine candidate for COVID-19, Nat. Commun. 11 (2020) 1–13, https://doi.org/10.1038/s41467-020-16505-0.

[35] P. Tebas, ShuPing Yang, J.D. Boyer, E.L. Reuschel, A. Patel, A. Christensen-Quick, V.M. Andrade, M.P. Morrow, K. Kraynyak, J. Agnes, M. Purwar, A. Sylvester, J. Pawlicki, E. Gillespie, I. Maricic, F.I. Zaidi, K.Y. Kim, Y. Dia, D. Frase, P. Pezzoli, K. Schultheis, T.R.F. Smith, S.J. Ramos, T. McMullan, K. Buttigieg, M. W. Carroll, J. Ervin, M.C. Diehl, E. Blackwood, M.P. Mammen, J. Lee, M.J. Dallas, A.S. Brown, J.E. Shea, J.J. Kim, D.B. Weiner, K.E. Broderick, L.M. Humeau, Safety and immunogenicity of INO-4800 DNA vaccine against SARS-CoV-2: A preliminary report of an open-label, Phase 1 clinical trial, EClinicalMedicine. 31 (2021) 100689, https://doi.org/10.1016/j.eclinm.2020.100689.

[36] A.K. Fajrial, Q.Q. He, N.I. Wirusanti, J.E. Slansky, X. Ding, A review of emerging physical transfection methods for CRISPR/Cas9-mediated gene editing, Theranostics. 10 (12) (2020) 5532–5549, https://doi.org/10.7150/thno.43465.

[37] H.-X. Wang, M. Li, C.M. Lee, S. Chakraborty, H.-W. Kim, G. Bao, K.W. Leong, CRISPR/Cas9-Based Genome Editing for Disease Modeling and Therapy: Challenges and Opportunities for Nonviral Delivery, Chem. Rev. 117 (15) (2017) 9874–9906, https://doi.org/10.1021/acs.chemrev.6b00799.

[38] A. Patel, M.A. Bah, D.B. Weiner, In Vivo Delivery of Nucleic Acid-Encoded Monoclonal Antibodies, BioDrugs. 34 (3) (2020) 273–293, https://doi.org/10.1007/s40259-020-00412-3.

[39] E. Neumann, M. Schaefer-Ridder, Y. Wang, P.H. Hofschneider, Gene transfer into mouse lyoma cells by electroporation in high electric fields, EMBO J. 1 (7) (1982) 841–845, https://doi.org/10.1002/j.1460-2075.1982.tb01257.x.

[40] M. Golzio, J. Teissie, M.-P. Rols, Direct visualization at the single-cell level of electrically mediated gene delivery, Proc. Natl. Acad. Sci. U. S. A. 99 (3) (2002) 1292–1297, https://doi.org/10.1073/pnas.022646499.

[41] H. Wolf, M.P. Rols, E. Boldt, E. Neumann, J. Teissié, Control by pulse parameters of electric field-mediated gene transfer in mammalian cells, Biophys. J. 66 (2) (1994) 524–531, https://doi.org/10.1016/S0006-3495(94)80805-7.

[42] T. Kotnik, L. Rems, M. Tarek, D. Miklavčič, Membrane Electroporation and Electropermeabilization: Mechanisms and Models, Annu. Rev. Biophys. 48 (1) (2019) 63–91, https://doi.org/10.1146/annurev-biophys-052118-115451.

[43] K. Kinosita, T.Y. Tsong, Voltage-induced conductance in human erythrocyte membranes, Biochim. Biophys. Acta - Biomembr. 554 (2) (1979) 479–497, https://doi.org/10.1016/0005-2736(79)90386-9.

[44] J. Li, H. Lin, Numerical simulation of molecular uptake via electroporation, Bioelectrochemistry. 82 (1) (2011) 10–21, https://doi.org/10.1016/j.bioelechem.2011.04.006.

[45] K.A. DeBruin, W. Krassowska, Modeling electroporation in a single cell. I. Effects of field strength and rest potential, Biophys. J. 77 (3) (1999) 1213–1224, https://doi.org/10.1016/S0006-3495(99)76973-0.

[46] M. Schmeer, T. Seipp, U. Pliquett, S. Kakorin, E. Neumann, Mechanism for the conductivity changes caused by membrane electroporation of CHO cell-pellets, Phys. Chem. Chem. Phys., The Royal Soc. Chem. (2004) 5564–5574, https://doi.org/10.1039/b411037d.

[47] J.C. Weaver, Y.A. Chizmadzhev, Theory of electroporation: A review, Bioelectrochemistry Bioenerg. 41 (2) (1996) 135–160, https://doi.org/10.1016/S0302-4598(96)05062-3.

[48] L.V. Chernomordik, S.I. Sukharev, S.V. Popov, V.F. Pastushenko, A.V. Sokirko, I. G. Abidor, Y.A. Chizmadzhev, The electrical breakdown of cell and lipid membranes: the similarity of phenomenologies, BBA - Biomembr. 902 (3) (1987) 360–373, https://doi.org/10.1016/0005-2736(87)90204-5.

21

[49] K. Kinosita, T.Y. Tsong, Formation and resealing of pores of controlled sizes in human erythrocyte membrane, Nature 268 (5619) (1977) 438–441, https://doi.org/10.1038/268438a0.

[50] T. Batista Napotnik, D. Miklavčič, In vitro electroporation detection methods – An overview, Bioelectrochemistry. 120 (2018) 166–182, https://doi.org/10.1016/j.bioelechem.2017.12.005.

[51] J.-M. Escoffre, T. Portet, C. Favard, J. Teissié, D.S. Dean, M.-P. Rols, Electromediated formation of DNA complexes with cell membranes and its consequences for gene delivery, Biochim. Biophys. Acta - Biomembr. 1808 (6) (2011) 1538–1543, https://doi.org/10.1016/j.bbamem.2010.10.009.

[52] C. Faurie, M. Rebersek, M. Golzio, M. Kanduser, J.-M. Escoffre, M. Pavlin, J. Teissie, D. Miklavcic, M.-P. Rols, Electro-mediated gene transfer and expression are controlled by the life-time of DNA/membrane complex formation, J. Gene Med. 12 (1) (2010) 117–125, https://doi.org/10.1002/jgm.1414.

[53] M. Breton, L. Delemotte, A. Silve, L.M. Mir, M. Tarek, Transport of siRNA through lipid membranes driven by nanosecond electric pulses: An experimental and computational study, J. Am. Chem. Soc. 134 (34) (2012) 13938–13941, https://doi.org/10.1021/ja3052365.

[54] V.A. Klenchin, S.I. Sukharev, S.M. Serov, L.V. Chernomordik, Chizmadzhev YuA, Chizmadzhev YuA, Electrically induced DNA uptake by cells is a fast process involving DNA electrophoresis, Biophys. J. 60 (4) (1991) 804–811, https://doi.org/10.1016/S0006-3495(91)82115-4.

[55] S. Sachdev, S. Feijoo Moreira, Y. Keehnen, L. Rems, M.T. Kreutzer, P.E. Boukany, DNA-membrane complex formation during electroporation is DNA size-dependent, Biochim. Biophys. Acta - Biomembr. 1862 (2) (2020) 183089, https://doi.org/10.1016/j.bbamem.2019.183089.

[56] A. Paganin-Gioanni, E. Bellard, J.M. Escoffre, M.P. Rols, J. Teissie, M. Golzio, Direct visualization at the single-cell level of siRNA electrotransfer into cancer cells, Proc. Natl. Acad. Sci. USA 108 (26) (2011) 10443–10447, https://doi.org/10.1073/pnas.1103519108.

[57] O.V. Bondar, D.V. Saifullina, I.I. Shakhmaeva, I.I. Mavlyutova, T.I. Abdullin, Monitoring of the Zeta Potential of Human Cells upon Reduction in Their Viability and Interaction with Polymers, Acta Naturae. 4 (2012) 78–81, https://doi.org/10.32607/20758251-2012-4-1-78-81.

[58] S. Sachdev, A. Muralidharan, D.K. Choudhary, D.L. Perrier, L. Rems, M.T. Kreutzer, P.E. Boukany, DNA translocation to giant unilamellar vesicles during electroporation is independent of DNA size, Soft Matter. 15 (45) (2019) 9187–9194, https://doi.org/10.1039/C9SM01274E.

[59] D.A. Zaharoff, F. Yuan, Effects of pulse strength and pulse duration on in vitro DNA electromobility, Bioelectrochemistry. 62 (1) (2004) 37–45, https://doi.org/10.1016/j.bioelechem.2003.10.011.

[60] D.A. Zaharoff, R.C. Barr, C.-Y. Li, F. Yuan, Electromobility of plasmid DNA in tumor tissues during electric field-mediated gene delivery, Gene Ther. 9 (19) (2002) 1286–1290, https://doi.org/10.1038/sj.gt.3301799.

[61] J.W. Henshaw, D.A. Zaharoff, B.J. Mossop, F. Yuan, Electric field-mediated transport of plasmid DNA in tumor interstitium in vivo, Bioelectrochemistry. 71 (2) (2007) 233–242, https://doi.org/10.1016/j.bioelechem.2007.07.005.

[62] S.I. Sukharev, V.A. Klenchin, S.M. Serov, L.V. Chernomordik, Chizmadzhev YuA, Chizmadzhev YuA, Electroporation and electrophoretic DNA transfer into cells. The effect of DNA interaction with electropores, Biophys. J. 63 (5) (1992) 1320–1327, https://doi.org/10.1016/S0006-3495(92)81709-5.

[63] M. Wu, F. Yuan, J. Rao, Membrane binding of plasmid DNA and endocytic pathways are involved in electrotransfection of mammalian cells, PLoS One. 6 (6) (2011) e20923, https://doi.org/10.1371/journal.pone.0020923.

[64] C. Rosazza, H. Deschout, A. Buntz, K. Braeckmans, M.-P. Rols, A. Zumbusch, Endocytosis and Endosomal Trafficking of DNA After Gene Electrotransfer In Vitro, Mol. Ther. - Nucleic Acids. 5 (2016) e286, https://doi.org/10.1038/mtna.2015.59.

[65] C. Rosazza, A. Buntz, T. Rieß, D. Wöll, A. Zumbusch, M.-P. Rols, Intracellular tracking of single-plasmid DNA particles after delivery by electroporation, Mol. Ther. 21 (12) (2013) 2217–2226, https://doi.org/10.1038/mt.2013.182.

[66] E.E. Vaughan, D.A. Dean, Intracellular trafficking of plasmids during transfection is mediated by microtubules, Mol. Ther. 13 (2) (2006) 422–428, https://doi.org/10.1016/j.ymthe.2005.10.004.

[67] E. Dauty, A.S. Verkman, Actin cytoskeleton as the principal determinant of size-dependent DNA mobility in cytoplasm: A new barrier for non-viral gene delivery, J. Biol. Chem. 280 (9) (2005) 7823–7828, https://doi.org/10.1074/jbc.M412374200.

[68] G.L. Lukacs, P. Haggie, O. Seksek, D. Lechardeur, N. Freedman, A.S. Verkman, Size-dependent DNA mobility in cytoplasm and nucleus, J. Biol. Chem. 275 (3) (2000) 1625–1629, https://doi.org/10.1074/jbc.275.3.1625.

[69] L.D. Cervia, F. Yuan, Current Progress in Electrotransfection as a Nonviral Method for Gene Delivery, Mol. Pharm. 15 (9) (2018) 3617–3624, https://doi.org/10.1021/acs.molpharmaceut.8b00207.

[70] D. Lechardeur, K.-J. Sohn, M. Haardt, P.B. Joshi, M. Monck, R.W. Graham, B. Beatty, J. Squire, H. O'Brodovich, G.L. Lukacs, Metabolic instability of plasmid DNA in the cytosol: A potential barrier to gene transfer, Gene Ther. 6 (4) (1999) 482–497, https://doi.org/10.1038/sj.gt.3300867.

[71] M.A. Badding, J.D. Lapek, A.E. Friedman, D.A. Dean, Proteomic and functional analyses of protein-DNA complexes during gene transfer, Mol. Ther. 21 (4) (2013) 775–785, https://doi.org/10.1038/mt.2012.231.

[72] S. Brunner, E. Fürtbauer, T. Sauer, M. Kursa, E. Wagner, Overcoming the nuclear barrier: Cell cycle independent nonviral gene transfer with linear polyethylenimine or electroporation, Mol. Ther. 5 (1) (2002) 80–86, https://doi.org/10.1006/mthe.2001.0509.

[73] M. Golzio, J. Teissié, M.-P. Rols, Cell synchronization effect on mammalian cell permeabilization and gene delivery by electric field, Biochim. Biophys. Acta - Biomembr. 1563 (1-2) (2002) 23–28, https://doi.org/10.1016/S0005-2736(02)00369-3.

[74] J.K. Utvik, A. Nja, K. Gundersen, DNA injection into single cells of intact mice, Hum. Gene Ther. 10 (2) (1999) 291–300, https://doi.org/10.1089/10430349950019075.

[75] K.H. Schoenbach, S.J. Beebe, E.S. Buescher, Intracellular effect of ultrashort electrical pulses, Bioelectromagnetics. 22 (6) (2001) 440–448, https://doi.org/10.1002/bem.71.

[76] T.B. Napotnik, M. Reberšek, T. Kotnik, E. Lebrasseur, G. Cabodevila, D. Miklavčič, Electropermeabilization of endocytotic vesicles in B16 F1 mouse melanoma cells, Med. Biol. Eng. Comput. 48 (5) (2010) 407–413, https://doi.org/10.1007/s11517-010-0599-9.

[77] E. Tekle, H. Oubrahim, S.M. Dzekunov, J.F. Kolb, K.H. Schoenbach, P.B. Chock, Selective field effects on intracellular vacuoles and vesicle membranes with nanosecond electric pulses, Biophys. J. 89 (1) (2005) 274–284, https://doi.org/10.1529/biophysj.104.054494.

[78] L. Chopinet, T. Batista-Napotnik, A. Montigny, M. Rebersek, J. Teissié, M.-P. Rols, D. Miklavčič, Nanosecond electric pulse effects on gene expression, J. Membr. Biol. 246 (11) (2013) 851–859, https://doi.org/10.1007/s00232-013-9579-y.

[79] N. Chen, K.H. Schoenbach, J.F. Kolb, R. James Swanson, A.L. Garner, J. Yang, R.P. Joshi, S.J. Beebe, Leukemic cell intracellular responses to nanosecond electric fields, Biochem. Biophys. Res. Commun. 317 (2) (2004) 421–427, https://doi.org/10.1016/j.bbrc.2004.03.063.

[80] S.J. Beebe, J. White, P.F. Blackmore, Y. Deng, K. Somers, K.H. Schoenbach, Diverse Effects of Nanosecond Pulsed Electric Fields on Cells and Tissues, DNA Cell Biol. 22 (12) (2003) 785–796, https://doi.org/10.1089/104454903322624993.

[81] S.J. Beebe, P.F. Blackmore, J. White, R.P. Joshi, K.H. Schoenbach, Physiol. Meas., Physiol. Meas. 25 (4) (2004) 1077–1093, https://doi.org/10.1088/0967-3334/25/4/023.

[82] A. Elouahabi, J.-M. Ruysschaert, Formation and intracellular trafficking of lipoplexes and polyplexes, Mol. Ther. 11 (3) (2005) 336–347, https://doi.org/10.1016/j.ymthe.2004.12.006.

[83] A. Chaumet, G.D. Wright, S.H. Seet, K.M. Tham, N.V. Gounko, F. Bard, Nuclear envelope-associated endosomes deliver surface proteins to the nucleus, Nat. Commun. 6 (1) (2015), https://doi.org/10.1038/ncomms9218.

[84] B. Alberts, A. Johnson, J. Lewis, M. Raff, K. Roberts, P. Walter, Molecular Biology of the Cell, 4th Editio, Garland Science, New York, 2002.

[85] A.G. Baranovskii, V.N. Buneva, G.A. Nevinsky, Human deoxyribonucleases, Biochem. 69 (6) (2004) 587–601, https://doi.org/10.1023/B:BIRY.0000033731.50496.01.

[86] L. Lauková, B. Konečná, L. Janovičová, B. Vlková, P. Celec, Deoxyribonucleases and their applications in biomedicine, Biomolecules. 10 (2020) 1–20, https://doi.org/10.3390/biom10071036.

[87] T. Nomura, S. Nakajima, K. Kawabata, F. Yamashita, Y. Takakura, M. Hashida, Intratumoral Pharmacokinetics and in Vivo Gene Expression of Naked Plasmid DNA and Its Cationic Liposome Complexes after Direct Gene Transfer, Cancer Res. 57 (1997).

[88] I. Danko, P. Williams, H. Herweijer, G. Zhang, U.S. Latendresse, I. Bock, J.A. Wolff, High expression of naked plasmid DNA in muscles of young rodents, Hum. Mol. Genet. 6 (1997) 1435–1443, https://doi.org/10.1093/hmg/6.9.1435.

[89] D.J. Wells, G. Goldspink, Age and sex influence expression of plasmid DNA directly injected into mouse skeletal muscle, FEBS Lett. 306 (1992) 203–205, https://doi.org/10.1016/0014-5793(92)81000-C.

[90] S. Jiao, P. Williams, R.K. Berg, B.A. Hodgeman, L. Liu, G. Repetto, J.A. Wolff, Direct gene transfer into nonhuman primate myofibers in vivo, Hum. Gene Ther. 3 (1) (1992) 21–33, https://doi.org/10.1089/hum.1992.3.1-21.

[91] C. Rosazza, S. Haberl Meglic, A. Zumbusch, M.-P. Rols, D. Miklavcic, Gene Electrotransfer: A Mechanistic Perspective, Curr. Gene Ther. 16 (2) (2016) 98–129, https://doi.org/10.2174/1566523216666160331130040.

[92] J.M. McMahon, E. Signori, K.E. Wells, V.M. Fazio, D.J. Wells, Optimisation of electrotransfer of plasmid into skeletal muscle by pretreatment with hyaluronidase - Increased expression with reduced muscle damage, Gene Ther. 8 (16) (2001) 1264–1270, https://doi.org/10.1038/sj.gt.3301522.

[93] M. Cemazar, M. Golzio, G. Sersa, J.-M. Escoffre, A. Coer, S. Vidic, J. Teissie, Hyaluronidase and collagenase increase the transfection efficiency of gene electrotransfer in various murine tumors, Hum. Gene Ther. 23 (1) (2012) 128–137, https://doi.org/10.1089/hum.2011.073.

[94] L. Wasungu, J.-M. Escoffre, A. Valette, J. Teissie, M.-P. Rols, A 3D in vitro spheroid model as a way to study the mechanisms of electroporation, Int. J. Pharm. 379 (2) (2009) 278–284, https://doi.org/10.1016/j.ijpharm.2009.03.035.

[95] L. Chopinet, L. Wasungu, M.-P. Rols, First explanations for differences in electrotransfection efficiency in vitro and in vivo using spheroid model, Int. J. Pharm. 423 (1) (2012) 7–15, https://doi.org/10.1016/j.ijpharm.2011.04.054.

[96] M. Pavlin, N. Pavselj, D. Miklavcic, Dependence of induced transmembrane potential on cell density, arrangement, and cell position inside a cell system, IEEE Trans. Biomed. Eng. 49 (6) (2002) 605–612, https://doi.org/10.1109/TBME.2002.1001975.

[97] R. Susil, D. Šemrov, D. Miklavčič, Electric field-induced transmembrane potential depends on cell density and organization, Electro- and

Magnetobiology. 17 (3) (1998) 391–399, https://doi.org/10.3109/15368379809030739.

[98] P.J. Canatella, M.M. Black, D.M. Bonnichsen, C. McKenna, M.R. Prausnitz, Tissue Electroporation: Quantification and Analysis of Heterogeneous Transport in Multicellular Environments, Biophys. J. 86 (5) (2004) 3260–3268, https://doi.org/10.1016/S0006-3495(04)74374-X.

[99] M. Madi, M.-P. Rols, L. Gibot, Efficient In Vitro Electropermeabilization of Reconstructed Human Dermal Tissue, J. Membr. Biol. 248 (5) (2015) 903–908, https://doi.org/10.1007/s00232-015-9791-z.

[100] M.F. Bureau, J. Gehl, V. Deleuze, L.M. Mir, D. Scherman, Importance of association between permeabilization and electrophoretic forces for intramuscular DNA electrotransfer, Biochim. Biophys. Acta - Gen. Subj. 1474 (3) (2000) 353–359, https://doi.org/10.1016/S0304-4165(00)00028-3.

[101] S. Satkauskas, M.F. Bureau, M. Puc, A. Mahfoudi, D. Scherman, D. Miklavcic, L. M. Mir, Mechanisms of in vivo DNA electrotransfer: Respective contribution of cell electropermeabilization and DNA electrophoresis, Mol. Ther. 5 (2002) 133–140, https://doi.org/10.1006/mthe.2002.0526.

[102] G.L. Andreason, G.A. Evans, Optimization of electroporation for transfection of mammalian cell lines, Anal. Biochem. 180 (2) (1989) 269–275, https://doi.org/10.1016/0003-2697(89)90429-6.

[103] S. Šatkauskas, F. André, M.F. Bureau, D. Scherman, D. Miklavčič, L.M. Mir, Electrophoretic component of electric pulses determines the efficacy of in vivo DNA electrotransfer, Hum. Gene Ther. 16 (10) (2005) 1194–1201, https://doi.org/10.1089/hum.2005.16.1194.

[104] N. Pavšelj, V. Préat, DNA electrotransfer into the skin using a combination of one high- and one low-voltage pulse, J. Control. Release. 106 (3) (2005) 407–415, https://doi.org/10.1016/j.jconrel.2005.05.003.

[105] F. Andre, J. Gehl, G. Sersa, V. Preat, P. Hojman, J. Eriksen, M. Golzio, M. Cemazar, N. Pavselj, M.-P. Rols, D. Miklavcic, E. Neumann, J. Teissie, L.M. Mir, Efficiency of high and low voltage pulse combinations for gene electrotransfer in muscle, liver, tumor and skin, Hum. Gene Ther. 19 (2008) 1261–1271, https://doi.org/10.1089/hum.2008.060.

[106] M.C. Diehl, J.C. Lee, S.E. Daniels, P. Tebas, A.S. Khan, M. Giffear, N.Y. Sardesai, M.L. Bagarazzi, Tolerability of intramuscular and intradermal delivery by CELLECTRA® adaptive constant current electroporation device in healthy volunteers, Hum. Vaccines Immunother. 9 (10) (2013) 2246–2252, https://doi.org/10.4161/hv.24702.

[107] M. Kandušer, D. Miklavčič, M. Pavlin, Mechanisms involved in gene electrotransfer using high- and low-voltage pulses - An in vitro study, Bioelectrochemistry. 74 (2) (2009) 265–271, https://doi.org/10.1016/j.bioelechem.2008.09.002.

[108] M. Pavlin, K. Flisar, M. Kandušer, The role of electrophoresis in gene electrotransfer, J. Membr. Biol. 236 (1) (2010) 75–79, https://doi.org/10.1007/s00232-010-9276-z.

[109] M. Pavlin, M. Kandušer, New Insights into the Mechanisms of Gene Electrotransfer - Experimental and Theoretical Analysis, Sci. Rep. 5 (1) (2015), https://doi.org/10.1038/srep09132.

[110] M. Thomsen, A. Hernandez-Garcia, J. Mathiesen, M. Poulsen, D.N. Sørensen, L. Tarnow, R. Feidenhans'l, J.C.D. Alamo, Model study of the pressure build-up during subcutaneous injection, PLoS One. 9 (8) (2014) e104054, https://doi.org/10.1371/journal.pone.0104054.

[111] K. Comley, N. Fleck, Deep penetration and liquid injection into adipose tissue, J. Mech. Mater. Struct. 6 (1-4) (2011) 127–140, https://doi.org/10.2140/jomms.2011.6.127.

[112] P.D. Fisher, C.J. Brambila, J.R. McCoy, W.B. Kiosses, J.M. Mendoza, J. Oh, B.S. Yung, K. Schultheis, T.R.F. Smith, K.E. Broderick, Adipose tissue: A new target for electroporation-enhanced DNA vaccines, Gene Ther. 24 (12) (2017) 757–767, https://doi.org/10.1038/gt.2017.96.

[113] M. Dupuis, K. Denis-Mize, C. Woo, C. Goldbeck, M.J. Selby, M. Chen, G.R. Otten, J.B. Ulmer, J.J. Donnelly, G. Ott, D.M. McDonald, Distribution of DNA Vaccines Determines Their Immunogenicity After Intramuscular Injection in Mice, J. Immunol. 165 (5) (2000) 2850–2858, https://doi.org/10.4049/jimmunol.165.5.2850.

[114] M.A. Swartz, M.E. Fleury, Interstitial flow and its effects in soft tissues, Annu. Rev. Biomed. Eng. 9 (1) (2007) 229–256, https://doi.org/10.1146/annurev.bioeng.9.060906.151850.

[115] S. McGuire, D. Zaharoff, F. Yuan, Nonlinear dependence of hydraulic conductivity on tissue deformation during intratumoral infusion, Ann. Biomed. Eng. 34 (7) (2006) 1173–1181, https://doi.org/10.1007/s10439-006-9136-2.

[116] X.-Y. Zhang, J. Luck, M.W. Dewhirst, F. Yuan, Interstitial hydraulic conductivity in a fibrosarcoma, Am. J. Physiol. - Hear. Circ. Physiol. 279 (6) (2000) H2726–H2734, https://doi.org/10.1152/ajpheart.2000.279.6.H2726.

[117] H. Wiig, M.A. Swartz, Interstitial fluid and lymph formation and transport: Physiological regulation and roles in inflammation and cancer, Physiol. Rev. 92 (3) (2012) 1005–1060, https://doi.org/10.1152/physrev.00037.2011.

[118] P.A. Netti, D.A. Berk, M.A. Swartz, A.J. Grodzinsky, R.K. Jain, Role of extracellular matrix assembly in interstitial transport in solid tumors, Cancer Res. 60 (2000) 2497–2503.

[119] F. Xiao, C. Nicholson, J. Hrabe, S. Hrabětová, Diffusion of flexible random-coil dextran polymers measured in anisotropic brain extracellular space by integrative optical imaging, Biophys. J. 95 (3) (2008) 1382–1392, https://doi.org/10.1529/biophysj.107.124743.

[120] T. Stylianopoulos, B. Diop-Frimpong, L.L. Munn, R.K. Jain, Diffusion anisotropy in collagen gels and tumors: The effect of fiber network orientation, Biophys. J. 99 (10) (2010) 3119–3128, https://doi.org/10.1016/j.bpj.2010.08.065.

[121] H. Kim, H. Park, S.J. Lee, Effective method for drug injection into subcutaneous tissue, Sci. Rep. 7 (2017) 1–11, https://doi.org/10.1038/s41598-017-10110-w.

[122] G. Vandermeulen, E. Staes, M.L. Vanderhaeghen, M.F. Bureau, D. Scherman, V. Préat, Optimisation of intradermal DNA electrotransfer for immunisation, J. Control. Release. 124 (1-2) (2007) 81–87, https://doi.org/10.1016/j.jconrel.2007.08.010.

[123] A. Gothelf, F. Mahmood, F. Dagnaes-Hansen, J. Gehl, Efficacy of transgene expression in porcine skin as a function of electrode choice, Bioelectrochemistry. 82 (2) (2011) 95–102, https://doi.org/10.1016/j.bioelechem.2011.06.001.

[124] C.Y. Calvet, J. Thalmensi, C. Liard, E. Pliquet, T. Bestetti, T. Huet, P. Langlade-Demoyen, L.M. Mir, Optimization of a gene electrotransfer procedure for efficient intradermal immunization with an hTERT-based DNA vaccine in mice, Mol. Ther. - Methods Clin. Dev. 1 (2014) 14045, https://doi.org/10.1038/mtm.2014.45.

[125] T. Forjanič, D. Miklavčič, Numerical study of gene electrotransfer efficiency based on electroporation volume and electrophoretic movement of plasmid DNA, Biomed. Eng. Online. 17 (1) (2018), https://doi.org/10.1186/s12938-018-0515-3.

[126] L.C. Heller, M.J. Jaroszeski, D. Coppola, A.N. McCray, J. Hickey, R. Heller, Optimization of cutaneous electrically mediated plasmid DNA delivery using novel electrode, Gene Ther. 14 (3) (2007) 275–280, https://doi.org/10.1038/sj.gt.3302867.

[127] X. Ding, M.P. Stewart, A. Sharei, J.C. Weaver, R.S. Langer, K.F. Jensen, High-throughput nuclear delivery and rapid expression of DNA via mechanical and electrical cell-membrane disruption, Nat. Biomed. Eng. 1 (3) (2017), https://doi.org/10.1038/s41551-017-0039.

[128] T. Akerstrom, K. Vedel, J. Needham, P. Hojman, E. Kontou, Y. Hellsten, J.F.P. Wojtaszewski, Optimizing hyaluronidase dose and plasmid DNA delivery greatly improves gene electrotransfer efficiency in rat skeletal muscle, Biochem. Biophys. Reports. 4 (2015) 342–350, https://doi.org/10.1016/j.bbrep.2015.10.007.

[129] M. Manthorpe, F. Cornefert-Jensen, J. Hartikka, J. Felgner, A. Rundell, M. Margalith, V. Dwarki, Gene Therapy by Intramuscular Injection of Plasmid DNA: Studies on Firefly Luciferase Gene Expression in Mice, Hum. Gene Ther. 4 (4) (1993) 419–431, https://doi.org/10.1089/hum.1993.4.4-419.

[130] J.W. Henshaw, F. Yuan, Field distribution and DNA transport in solid tumors during electric field-mediated gene delivery, J. Pharm. Sci. 97 (2) (2008) 691–711, https://doi.org/10.1002/jps.21000.

[131] A. Zupanic, S. Corovic, D. Miklavcic, M. Pavlin, Numerical optimization of gene electrotransfer into muscle tissue, Biomed. Eng. Online. 9 (2010) 66, https://doi.org/10.1186/1475-925X-9-66.

[132] J. Grove, M. Marsh, The cell biology of receptor-mediated virus entry, J. Cell Biol. 195 (2011) 1071–1082, https://doi.org/10.1083/jcb.201108131.

[133] D.S. Dimitrov, Virus entry: Molecular mechanisms and biomedical applications, Nat. Rev. Microbiol. 2 (2) (2004) 109–122, https://doi.org/10.1038/nrmicro817.

[134] A. Srivastava, In vivo tissue-tropism of adeno-associated viral vectors, Curr. Opin. Virol. 21 (2016) 75–80, https://doi.org/10.1016/j.coviro.2016.08.003.

[135] G. McFadden, M.R. Mohamed, M.M. Rahman, E. Bartee, Cytokine determinants of viral tropism, Nat. Rev. Immunol. 9 (9) (2009) 645–655, https://doi.org/10.1038/nri2623.

[136] D. Miklavčič, N. Pavšelj, F.X. Hart, Electric Properties of Tissues, Wiley Encycl. Biomed. Eng., Am. Cancer Soc. (2006), https://doi.org/10.1002/9780471740360.ebs0403.

[137] S. Čorović, L.M. Mir, D. Miklavčič, In vivo muscle electroporation threshold determination: Realistic numerical models and in vivo experiments, J. Membr. Biol. 245 (9) (2012) 509–520, https://doi.org/10.1007/s00232-012-9432-8.

[138] D. Miklavcic, S. Corovic, G. Pucihar, N. Pavselj, Importance of tumour coverage by sufficiently high local electric field for effective electrochemotherapy, Eur. J. Cancer, Suppl. 4 (11) (2006) 45–51, https://doi.org/10.1016/j.ejcsup.2006.08.006.

[139] G. Serša, M. Čemažar, D. Šemrov, D. Miklavčič, Changing electrode orientation improves the efficacy of electrochemotherapy of solid tumors in mice, Bioelectrochemistry Bioenerg. 39 (1) (1996) 61–66, https://doi.org/10.1016/0302-4598(95)01866-2.

[140] J. Dermol-Černe, E. Pirc, D. Miklavčič, Mechanistic view of skin electroporation–models and dosimetry for successful applications: an expert review, Expert Opin. Drug Deliv. 17 (5) (2020) 689–704, https://doi.org/10.1080/17425247.2020.1745772.

[141] N. Pavšelj, V. Préat, D. Miklavčič, A numerical model of skin electropermeabilization based on in vivo experiments, Ann. Biomed. Eng. 35 (2007) 2138–2144, https://doi.org/10.1007/s10439-007-9378-7.

[142] N. Pavselj, D. Miklavcic, Numerical models of skin electropermeabilization taking into account conductivity changes and the presence of local transport regions, IEEE Trans. Plasma Sci. 36 (4) (2008) 1650–1658, https://doi.org/10.1109/TPS.2008.928715.

[143] M. Kranjc, B. Markelc, F. Bajd, M. Čemažar, I. Serša, T. Blagus, D. Miklavčič, In situ monitoring of electric field distribution in mouse tumor during electroporation, Radiology. 274 (1) (2015) 115–123, https://doi.org/10.1148/radiol.14140311.

[144] S. Corovic, I. Lackovic, P. Sustaric, T. Sustar, T. Rodic, D. Miklavcic, Modeling of electric field distribution in tissues during electroporation, Biomed. Eng. Online. 12 (2013) 1–27, https://doi.org/10.1186/1475-925X-12-16.

23

S. Sachdev, Tjaša Potočnik, L. Rems et al.

Bioelectrochemistry 144 (2022) 107994

[145] M. Kranjc, F. Bajd, I. Serša, D. Miklavčič, Magnetic resonance electrical impedance tomography for measuring electrical conductivity during electroporation, Physiol. Meas. 35 (6) (2014) 985–996, https://doi.org/10.1088/0967-3334/35/6/985.

[146] L.T. Muftuler, M.J. Hamamura, O. Birgul, O. Nalcioglu, In Vivo MRI Electrical Impedance Tomography (MREIT) of tumors, Technol. Cancer Res. Treat. 5 (2006) 381–387 (accessed October 5, 2021) https://europepmc.org/article/med/16866568.

[147] Y. Wang, Q.i. Shao, P.-F. Van de Moortele, E. Racila, J. Liu, J. Bischof, B. He, Mapping electrical properties heterogeneity of tumor using boundary informed electrical properties tomography (BIEPT) at 7T, Magn. Reson. Med. 81 (1) (2019) 393–409, https://doi.org/10.1002/mrm.27414.

[148] B. Kos, Treatment planning for electrochemotherapy and irreversible electroporation of deep-seated tumors, Handb. Electroporation, Springer, Cham (2017) 1001–1017, https://doi.org/10.1007/978-3-319-32886-7_2.

[149] J. Gehl, T.H. Sørensen, K. Nielsen, P. Raskmark, S.L. Nielsen, T. Skovsgaard, M. Mir, In vivo electroporation of skeletal muscle: Threshold, efficacy and relation to electric field distribution, Biochim. Biophys. Acta - Gen. Subj. 1428 (2-3) (1999) 233–240, https://doi.org/10.1016/S0304-4165(99)00094-X.

[150] D. Miklavčič, D. Šemrov, H. Mekid, L.M. Mir, A validated model of in vivo electric field distribution in tissues for electrochemotherapy and for DNA electrotransfer for gene therapy, Biochim. Biophys. Acta - Gen. Subj. 1523 (1) (2000) 73–83, https://doi.org/10.1016/S0304-4165(00)00101-X.

[151] D. Sel, D. Cukjati, D. Batiuskaite, T. Slivnik, L.M. Mir, D. Miklavcic, Sequential finite element model of tissue electropermeabilization, IEEE Trans. Biomed. Eng. 52 (5) (2005) 816–827, https://doi.org/10.1109/TBME.2005.845212.

[152] J. Dermol-Černe, T. Batista Napotnik, M. Reberšek, D. Miklavčič, Short microsecond pulses achieve homogeneous electroporation of elongated biological cells irrespective of their orientation in electric field, Sci. Rep. 10 (1) (2020), https://doi.org/10.1038/s41598-020-65830-3.

[153] S. Čorović, A. Županič, S. Kranjc, B. Al Sakere, A. Leroy-Willig, L.M. Mir, D. Miklavčič, The influence of skeletal muscle anisotropy on electroporation: In vivo study and numerical modeling, Med. Biol. Eng. Comput. 48 (7) (2010) 637–648, https://doi.org/10.1007/s11517-010-0614-1.

[154] P. Turjanski, N. Olaiz, F. Maglietti, S. Michinski, C. Suárez, F.V. Molina, G. Marshall, R. Rubinsky, The Role of pH Fronts in Reversible Electroporation, PLoS One. 6 (4) (2011) e17303, https://doi.org/10.1371/journal.pone.0017303.

[155] F. Maglietti, S. Michinski, N. Olaiz, M. Castro, C. Suárez, G. Marshall, M.R. Scarfi, The Role of Ph Fronts in Tissue Electroporation Based Treatments, PLoS One. 8 (11) (2013) e80167, https://doi.org/10.1371/journal.pone.0080167.

[156] N. Olaiz, E. Signori, F. Maglietti, A. Soba, C. Suárez, P. Turjanski, S. Michinski, G. Marshall, Tissue damage modeling in gene electrotransfer: The role of pH, Bioelectrochemistry. 100 (2014) 105–111, https://doi.org/10.1016/j.bioelechem.2014.05.001.

[157] M. Phillips, L. Rubinsky, A. Meir, N. Raju, B. Rubinsky, Combining Electrolysis and Electroporation for Tissue Ablation, Technol, Cancer Res. Treat. 14 (4) (2015) 395–410, https://doi.org/10.1177/1533034614560102.

[158] N. Klein, E. Guenther, F. Botea, M. Pautov, S. Dima, D. Tomescu, M. Popescu, A. Ivorra, M. Stehling, I. Popescu, M.R. Scarfi, The combination of electroporation and electrolysis (E2) employing different electrode arrays for ablation of large tissue volumes, PLoS One. 14 (8) (2019) e0221393, https://doi.org/10.1371/journal.pone.0221393.

[159] C.B. Arena, R.V. Davalos, Advances in Therapeutic Electroporation to Mitigate Muscle Contractions, J. Membr. Sci. Technol. 2 (2012) 1–3, https://doi.org/10.4172/2155-9589.1000E102.

[160] B. Mercadal, C.B. Arena, R.V. Davalos, A. Ivorra, Avoiding nerve stimulation in irreversible electroporation: a numerical modeling study, Phys. Med. Biol. 62 (20) (2017) 8060–8079, https://doi.org/10.1088/1361-6560/aa8c53.

[161] M. Wallace, B. Evans, S. Woods, R. Mogg, L. Zhang, A.C. Finnefrock, D. Rabussay, M. Fons, J. Mallee, D. Mehrotra, F. Schödel, L. Musey, Tolerability of Two Sequential Electroporation Treatments Using MedPulser DNA Delivery System (DDS) in Healthy Adults, Mol. Ther. 17 (5) (2009) 922–928, https://doi.org/10.1038/mt.2009.27.

[162] A. Županič, S. Ribarič, D. Miklavčič, Increasing the repetition frequency of electric pulse delivery reduces unpleasant sensations that occur in electrochemotherapy, Neoplasma. 54 (2007) 246–250.

[163] R. Fusco, E. Di Bernardo, V. D'Alessio, S. Salati, M. Cadossi, Reduction of muscle contraction and pain in electroporation-based treatments: An overview, World J. Clin. Oncol. 12 (5) (2021) 367–381, https://doi.org/10.5306/wjco.v12.i5.367.

[164] A. Steuer, A. Schmidt, P. Labohá, P. Babica, J.F. Kolb, Transient suppression of gap junctional intercellular communication after exposure to 100-nanosecond pulsed electric fields, Bioelectrochemistry. 112 (2016) 33–46, https://doi.org/10.1016/j.bioelechem.2016.07.003.

[165] B. Markelc, E. Bellard, G. Sersa, T. Jesenko, S. Pelofy, J. Teissié, R. Frangez, M.P. Rols, M. Cemazar, M. Golzio, Increased permeability of blood vessels after reversible electroporation is facilitated by alterations in endothelial cell-to-cell junctions, J. Control. Release. 276 (2018) 30–41, https://doi.org/10.1016/j.jconrel.2018.02.032.

[166] J.C. Weaver, R.A. Mintzer, Decreased bilayer stability due to transmembrane potentials, Phys. Lett. A. 86 (1) (1981) 57–59, https://doi.org/10.1016/0375-9601(81)90688-5.

[167] I.G. Abidor, V.B. Arakelyan, L.V. Chernomordik, Y.A. Chizmadzhev, V.F. Pastushenko, M.P. Tarasevich, Electric breakdown of bilayer lipid membranes. I. The main experimental facts and their qualitative

[168] T.D. Xie, L. Sun, T.Y. Tsong, Study of mechanisms of electric field-induced DNA transfection. I. DNA entry by surface binding and diffusion through membrane pores, Biophys. J. 58 (1) (1990) 13–19, https://doi.org/10.1016/S0006-3495(90)82349-3.

[169] H. Stopper, H. Jones, U. Zimmermann, Large scale transfection of mouse L-cells by electropermeabilization, BBA - Biomembr. 900 (1) (1987) 38–44, https://doi.org/10.1016/0005-2736(87)90275-6.

[170] D.S. Dimitrov, A.E. Sowers, Membrane electroporaton - fast molecular exchange by electroosmosis, BBA - Biomembr. 1022 (3) (1990) 381–392, https://doi.org/10.1016/0005-2736(90)90289-Z.

[171] T.-K. Wong, E. Neumann, Electric field mediated gene transfer, Biochem. Biophys. Res. Commun. 107 (2) (1982) 584–587, https://doi.org/10.1016/0006-291X(82)91531-5.

[172] E. Neumann, Membrane electroporation and direct gene transfer, Bioelectrochemistry Bioenerg. 28 (1-2) (1992) 247–267, https://doi.org/10.1016/0302-4598(92)80017-B.

[173] N. Eynard, S. Sixou, N. Duran, J. Teissie, Fast kinetics studies of Escherichia coli electrotransformation, Eur. J. Biochem. 209 (1) (1992) 431–436, https://doi.org/10.1111/j.1432-1033.1992.tb17306.x.

[174] E. Neumann, S. Kakorin, I. Tsoneva, B. Nikolova, T. Tomov, Calcium-mediated DNA adsorption to yeast cells and kinetics of cell transformation by electroporation, Biophys. J. 71 (2) (1996) 868–877, https://doi.org/10.1016/S0006-3495(96)79288-3.

[175] K. Schwister, B. Deuticke, Formation and properties of aqueous leaks induced in human erythrocytes by electrical breakdown, BBA - Biomembr. 816 (2) (1985) 332–348, https://doi.org/10.1016/0005-2736(85)90501-2.

[176] D.H. Mengistu, K. Bohinc, S. May, Binding of DNA to zwitterionic lipid layers mediated by divalent cations, J. Phys. Chem. B. 113 (36) (2009) 12277–12282, https://doi.org/10.1021/jp904986j.

[177] J.J. McManus, J.O. Rädler, K.A. Dawson, Does Calcium Turn a Zwitterionic Lipid Cationic?, J Phys. Chem. B. 107 (36) (2003) 9869–9875, https://doi.org/10.1021/jp034463d.

[178] A.Y. Antipina, A.A. Gurtovenko, Molecular-level insight into the interactions of DNA with phospholipid bilayers: Barriers and triggers, RSC Adv. 6 (43) (2016) 36425–36432, https://doi.org/10.1039/c6ra05607e.

[179] R.A. Böckmann, B.L. de Groot, S. Kakorin, E. Neumann, H. Grubmüller, Kinetics, statistics, and energetics of lipid membrane electroporation studied by molecular dynamics simulations, Biophys. J. 95 (4) (2008) 1837–1850, https://doi.org/10.1529/biophysj.108.129437.

[180] S. Haberl, D. Miklavčič, M. Pavlin, Effect of Mg ions on efficiency of gene electrotransfer and on cell electropermeabilization, Bioelectrochemistry. 79 (2) (2010) 265–271, https://doi.org/10.1016/j.bioelechem.2010.04.001.

[181] I. Koltover, K. Wagner, C.R. Safinya, DNA condensation in two dimensions, Proc. Natl. Acad. Sci. U. S. A. 97 (26) (2000) 14046–14051, https://doi.org/10.1073/pnas.97.26.14046.

[182] C. Herold, P. Schwille, E.P. Petrov, DNA condensation at freestanding cationic lipid bilayers, Phys. Rev. Lett. 104 (14) (2010), https://doi.org/10.1103/PhysRevLett.104.148102.

[183] A.G. Cherstvy, E.P. Petrov, Modeling DNA condensation on freestanding cationic lipid membranes, Phys. Chem. Chem. Phys. 16 (5) (2014) 2020–2037, https://doi.org/10.1039/C3CP53433B.

[184] B.J. Reynwar, G. Illya, V.A. Harmandaris, M.M. Müller, K. Kremer, M. Deserno, Aggregation and vesiculation of membrane proteins by curvature-mediated interactions, Nature. 447 (7143) (2007) 461–464, https://doi.org/10.1038/nature05840.

[185] I. Koltover, J.O. Rädler, C.R. Safinya, Membrane mediated attraction and ordered aggregation of colloidal particles bound to giant phospholipid vesicles, Phys. Rev. Lett. 82 (9) (1999) 1991–1994, https://doi.org/10.1103/PhysRevLett.82.1991.

[186] W. Krassowska, P.D. Filev, Modeling electroporation in a single cell, Biophys. J. 92 (2) (2007) 404–417, https://doi.org/10.1529/biophysj.106.094235.

[187] T. Portet, R. Dimova, A new method for measuring edge tensions and stability of lipid bilayers: Effect of membrane composition, Biophys. J. 99 (10) (2010) 3264–3273, https://doi.org/10.1016/j.bpj.2010.09.032.

[188] T. Portet, C. Favard, J. Teissié, D.S. Dean, M.P. Rols, Insights into the mechanisms of electromediated gene delivery and application to the loading of giant vesicles with negatively charged macromolecules, Soft Matter. 7 (2011) 3872–3881, https://doi.org/10.1039/c0sm01389g.

[189] D.L. Perrier, A. Vahid, V. Kathavi, L. Stam, L. Rems, Y. Mulla, A. Muralidharan, G.H. Koenderink, M.T. Kreutzer, P.E. Boukany, Response of an actin network in vesicles under electric pulses, Sci. Rep. 9 (1) (2019), https://doi.org/10.1038/s41598-019-44613-5.

[190] G. Saulis, R. Saulė, Size of the pores created by an electric pulse: Microsecond vs millisecond pulses, Biochim. Biophys. Acta - Biomembr., Elsevier 1818 (12) (2012) 3032–3039, https://doi.org/10.1016/j.bbamem.2012.06.018.

[191] A.T. Esser, K.C. Smith, T.R. Gowrishankar, Z. Vasilkoski, J.C. Weaver, Mechanisms for the intracellular manipulation of organelles by conventional electroporation, Biophys. J. 98 (2010) 2506–2514, https://doi.org/10.1016/j.bpj.2010.02.035.

[192] K.C. Smith, R.S. Son, T.R. Gowrishankar, J.C. Weaver, Emergence of a large pore subpopulation during electroporating pulses, Bioelectrochemistry. 100 (2014) 3–10, https://doi.org/10.1016/j.bioelechem.2013.10.009.

[193] R.S. Son, T.R. Gowrishankar, K.C. Smith, J.C. Weaver, Modeling a Conventional Electroporation Pulse Train: Decreased Pore Number, Cumulative Calcium

Transport and an Example of Electrosensitization, IEEE Trans. Biomed. Eng. 63 (3) (2016) 571–580, https://doi.org/10.1109/TBME.2015.2466234.

[194] R.M. Robertson, D.E. Smith, Self-diffusion of entangled linear and circular DNA molecules: Dependence on length and concentration, Macromolecules. 40 (2007) 3373–3377, https://doi.org/10.1021/ma070051h.

[195] M. Yu, W. Tan, H. Lin, A stochastic model for DNA translocation through an electropore, Biochim. Biophys. Acta - Biomembr. 1818 (11) (2012) 2494–2501, https://doi.org/10.1016/j.bbamem.2012.05.025.

[196] C. Rosazza, E. Phez, J.-M. Escoffre, L. Cézanne, A. Zumbusch, M.-P. Rols, Cholesterol implications in plasmid DNA electrotransfer: Evidence for the involvement of endocytotic pathways, Int. J. Pharm. 423 (1) (2012) 134–143, https://doi.org/10.1016/j.ijpharm.2011.05.024.

[197] L. Wang, S.E. Miller, F. Yuan, Ultrastructural analysis of vesicular transport in electrotransfection, Microsc. Microanal. 24 (5) (2018) 553–563, https://doi.org/10.1017/S143192761801509X.

[198] S. Kumari, S. MG, S. Mayor, Endocytosis unplugged: Multiple ways to enter the cell, Cell Res. 20 (3) (2010) 256–275, https://doi.org/10.1038/cr.2010.19.

[199] L.V. Chernomordik, A.V. Sokolov, V.G. Budker, Electrostimulated uptake of DNA by liposomes, BBA - Biomembr. 1024 (1) (1990) 179–183, https://doi.org/10.1016/0005-2736(90)90222-A.

[200] Y. Antov, A. Barbul, H. Mantsur, R. Korenstein, Electroendocytosis: Exposure of cells to pulsed low electric fields enhances adsorption and uptake of macromolecules, Biophys. J. 88 (3) (2005) 2206–2223, https://doi.org/10.1529/biophysj.104.051268.

[201] N. Ben-Dov, I. Rozman Grinberg, R. Korenstein, A.M. Delprato, Electroendocytosis Is Driven by the Binding of Electrochemically Produced Protons to the Cell's Surface, PLoS One. 7 (11) (2012) e50299, https://doi.org/10.1371/journal.pone.0050299.

[202] R. Lin, D.C. Chang, Y.-K. Lee, Single-cell electroendocytosis on a micro chip using in situ fluorescence microscopy, Biomed. Microdevices. 13 (6) (2011) 1063–1073, https://doi.org/10.1007/s10544-011-9576-9.

[203] T.Y. Tsong, Electroporation of cell membranes, Biophys. J. 60 (2) (1991) 297–306, https://doi.org/10.1016/S0006-3495(91)82054-9.

[204] H.N. Farrer, F.J.C. Rossotti, Proton-fluoride association in sodium perchlorate media, J. Inorg. Nucl. Chem. 26 (11) (1964) 1959–1965, https://doi.org/10.1016/0022-1902(64)80020-8.

[205] B. Sorre, A. Callan-Jones, J.-B. Manneville, P. Nassoy, J.-F. Joanny, J. Prost, B. Goud, P. Bassereau, Curvature-driven lipid sorting needs proximity to a demixing point and is aided by proteins, Proc. Natl. Acad. Sci. U. S. A. 106 (14) (2009) 5622–5626, https://doi.org/10.1073/pnas.0811243106.

[206] J.W. Murray, A.W. Wolkoff, Roles of the cytoskeleton and motor proteins in endocytic sorting, Adv. Drug Deliv. Rev. 55 (11) (2003) 1385–1403, https://doi.org/10.1016/j.addr.2003.07.008.

[207] C. Rosazza, J.-M. Escoffre, A. Zumbusch, M.-P. Rols, The actin cytoskeleton has an active role in the electrotransfer of plasmid DNA in mammalian cells, Mol. Ther. 19 (5) (2011) 913–921, https://doi.org/10.1038/mt.2010.303.

[208] D.A. Schafer, Regulating actin dynamics at membranes: A focus on dynamin, Traffic. 5 (2004) 463–469, https://doi.org/10.1111/j.1600-0854.2004.00199.x.

[209] A. Roux, G. Koster, M. Lenz, B. Sorre, J.-B. Manneville, P. Nassoy, P. Bassereau, Membrane curvature controls dynamin polymerization, Proc. Natl. Acad. Sci. U. S. A. 107 (9) (2010) 4141–4146, https://doi.org/10.1073/pnas.0913734107.

[210] S. Šatkauskas, M.F. Bureau, A. Mahfoudi, L.M. Mir, Slow accumulation of plasmid in muscle cells: Supporting evidence for a mechanism of DNA uptake by receptor-mediated endocytosis, Mol. Ther. 4 (4) (2001) 317–323, https://doi.org/10.1006/mthe.2001.0465.

[211] B. Markelc, E. Skvarca, T. Dolinsek, V.P. Kloboves, A. Coer, G. Sersa, M. Cemazar, Inhibitor of endocytosis impairs gene electrotransfer to mouse muscle in vivo, Bioelectrochemistry. 103 (2015) 111–119, https://doi.org/10.1016/j.bioelechem.2014.08.020.

[212] C. Faurie, E. Phez, M. Golzio, C. Vossen, J.-C. Lesbordes, C. Delteil, J. Teissié, M.-P. Rols, Effect of electric field vectoriality on electrically mediated gene delivery in mammalian cells, Biochim. Biophys. Acta - Biomembr. 1665 (1-2) (2004) 92–100, https://doi.org/10.1016/j.bbamem.2004.06.018.

[213] P.M. Graybill, R.V. Davalos, Cytoskeletal disruption after electroporation and its significance to pulsed electric field therapies, Cancers (Basel). 12 (5) (2020) 1132, https://doi.org/10.3390/cancers12051132.

[214] C. Kanthou, S. Kranjc, G. Sersa, G. Tozer, A. Zupanic, M. Cemazar, The endothelial cytoskeleton as a target of electroporation-based therapies, Mol. Cancer Ther. 5 (12) (2006) 3145–3152, https://doi.org/10.1158/1535-7163.MCT-06-0410.

[215] A. Steuer, K. Wende, P. Babica, J.F. Kolb, Elasticity and tumorigenic characteristics of cells in a monolayer after nanosecond pulsed electric field exposure, Eur. Biophys. J. 46 (6) (2017) 567–580, https://doi.org/10.1007/s00249-017-1205-y.

[216] H. Krassen, U. Pliquett, E. Neumann, Nonlinear current-voltage relationship of the plasma membrane of single CHO cells, Bioelectrochemistry. 70 (1) (2007) 71–77, https://doi.org/10.1016/j.bioelechem.2006.03.033.

[217] A.E. Sowers, The long-lived fusogenic state induced in erythrocyte ghosts by electric pulses is not laterally mobile, Biophys. J. 52 (6) (1987) 1015–1020, https://doi.org/10.1016/S0006-3495(87)83294-0.

[218] M.-P. Rols, J. Teissié, Experimental evidence for the involvement of the cytoskeleton in mammalian cell electropermeabilization, BBA - Biomembr. 1111 (1) (1992) 45–50, https://doi.org/10.1016/0005-2736(92)90272-N.

[219] G.L. Thompson, C. Roth, G. Tolstykh, M. Kuipers, B.L. Ibey, Disruption of the actin cortex contributes to susceptibility of mammalian cells to nanosecond

pulsed electric fields, Bioelectromagnetics. 35 (4) (2014) 262–272, https://doi.org/10.1002/bem.21845.

[220] M. Stacey, P. Fox, S. Buescher, J. Kolb, Nanosecond pulsed electric field induced cytoskeleton, nuclear membrane and telomere damage adversely impact cell survival, Bioelectrochemistry. 82 (2) (2011) 131–134, https://doi.org/10.1016/j.bioelechem.2011.06.002.

[221] A. Muralidharan, L. Rems, M.T. Kreutzer, P.E. Boukany, Actin networks regulate the cell membrane permeability during electroporation, Biochim. Biophys. Acta - Biomembr. 1863 (1) (2021) 183468, https://doi.org/10.1016/j.bbamem.2020.183468.

[222] H.B. Kim, S. Lee, J.H. Chung, S.N. Kim, C.K. Sung, K.Y. Baik, Effects of Actin Cytoskeleton Disruption on Electroporation In Vitro, Appl. Biochem. Biotechnol. 191 (4) (2020) 1545–1561, https://doi.org/10.1007/s12010-020-03271-4.

[223] D. Xiao, L. Tang, C. Zeng, J. Wang, X. Luo, C. Yao, C. Sun, Effect of actin cytoskeleton disruption on electric pulse-induced apoptosis and electroporation in tumour cells, Cell Biol. Int. 35 (2) (2011) 99–104, https://doi.org/10.1042/CBI20100464.

[224] G.L. Thompson, C. Roth, G. Tolstykh, M. Kuipers, B.L. Ibey, Role of cytoskeleton and elastic moduli in cellular response to nanosecond pulsed electric fields, in, Terahertz Ultrashort Electromagn. Pulses Biomed. Appl. (2013) 85850T, https://doi.org/10.1117/12.2005114.

[225] R. Dimova, K.A. Riske, Electrodeformation, electroporation, and electrofusion of giant unilamellar vesicles, in, Handb. Electroporation (2017) 235–252, https://doi.org/10.1007/978-3-319-32886-7_199.

[226] K.A. Riske, R. Dimova, Electro-deformation and poration of giant vesicles viewed with high temporal resolution, Biophys. J. 88 (2) (2005) 1143–1155, https://doi.org/10.1529/biophysj.104.050310.

[227] D.E. Chafai, V. Sulimenko, D. Havelka, L. Kubínová, P. Dráber, M. Cifra, Reversible and Irreversible Modulation of Tubulin Self-Assembly by Intense Nanosecond Pulsed Electric Fields, Adv. Mater. 31 (39) (2019) 1903636, https://doi.org/10.1002/adma.201903636.

[228] P. Marracino, D. Havelka, J. Průša, M. Liberti, J. Tuszynski, A.T. Ayoub, F. Apollonio, M. Cifra, Tubulin response to intense nanosecond-scale electric field in molecular dynamics simulation, Sci. Rep. 9 (1) (2019), https://doi.org/10.1038/s41598-019-46636-4.

[229] F.-C. Tsai, G.-H. Kuo, S.-W. Chang, P.-J. Tsai, Ca2+ signaling in cytoskeletal reorganization, cell migration, and cancer metastasis, Biomed Res. Int. 2015 (2015) 1–13, https://doi.org/10.1155/2015/409245.

[230] E.T. O'Brien, E.D. Salmon, H.P. Erickson, How calcium causes microtubule depolymerization, Cell Motil. Cytoskeleton. 36 (1997) 125–135, https://doi.org/10.1002/(SICI)1097-0169(1997)36:2<125::AID-CM3>3.0.CO;2-8.

[231] A. Görlach, K. Bertram, S. Hudecova, O. Krizanova, Calcium and ROS: A mutual interplay, Redox Biol. 6 (2015) 260–271, https://doi.org/10.1016/j.redox.2015.08.010.

[232] I. Semenov, S. Xiao, A.G. Pakhomov, Primary pathways of intracellular Ca2+ mobilization by nanosecond pulsed electric field, Biochim. Biophys. Acta - Biomembr. 1828 (3) (2013) 981–989, https://doi.org/10.1016/j.bbamem.2012.11.032.

[233] J.A. White, P.F. Blackmore, K.H. Schoenbach, S.J. Beebe, Stimulation of capacitative calcium entry in HL-60 cells by nanosecond pulsed electric fields, J. Biol. Chem. 279 (22) (2004) 22964–22972, https://doi.org/10.1074/jbc.M311135200.

[234] M.P. Rols, J. Teissié, Electropermeabilization of mammalian cells. Quantitative analysis of the phenomenon, Biophys. J. 58 (5) (1990) 1089–1098, https://doi.org/10.1016/S0006-3495(90)82451-6.

[235] T. Polajzer, T. Jarm, D. Miklavcic, Analysis of damage-associated molecular pattern molecules due to electroporation of cells in vitro, Radiol. Oncol. 54 (2020) 317–328, https://doi.org/10.2478/raon-2020-0047.

[236] W.E. Ford, W. Ren, P.F. Blackmore, K.H. Schoenbach, S.J. Beebe, Nanosecond pulsed electric fields stimulate apoptosis without release of pro-apoptotic factors from mitochondria in B16f10 melanoma, Arch. Biochem. Biophys. 497 (1-2) (2010) 82–89, https://doi.org/10.1016/j.abb.2010.03.008.

[237] I. Titushkin, M. Cho, Regulation of cell cytoskeleton and membrane mechanics by electric field: Role of linker proteins, Biophys. J. 96 (2) (2009) 717–728, https://doi.org/10.1016/j.bpj.2008.09.035.

[238] A.G. Pakhomov, S. Xiao, O.N. Pakhomova, I. Semenov, M.A. Kuipers, B.L. Ibey, Disassembly of actin structures by nanosecond pulsed electric field is a downstream effect of cell swelling, Bioelectrochemistry. 100 (2014) 88–95, https://doi.org/10.1016/j.bioelechem.2014.01.004.

[239] M.A. Rassokhin, A.G. Pakhomov, Electric field exposure triggers and guides formation of pseudopod-like blebs in U937 monocytes, J. Membr. Biol. 245 (9) (2012) 521–529, https://doi.org/10.1007/s00232-012-9433-7.

[240] L. Carr, S.M. Bardet, R.C. Burke, D. Arnaud-Cormos, P. Leveque, R.P. O'Connor, Calcium-independent disruption of microtubule dynamics by nanosecond pulsed electric fields in U87 human glioblastoma cells, Sci. Rep. 7 (1) (2017), https://doi.org/10.1038/srep41267.

[241] S. Li, N. Xiong, Y. Peng, K. Tang, H. Bai, X. Lv, Y. Jiang, X. Qin, H. Yang, C. Wu, P. Zhou, Y. Liu, Acidic pHe regulates cytoskeletal dynamics through conformational integrin β1 activation and promotes membrane protrusion, Biochim. Biophys. Acta - Mol. Basis Dis. 1864 (7) (2018) 2395–2408, https://doi.org/10.1016/j.bbadis.2018.04.019.

[242] L.C. Benov, P.A. Antonov, S.R. Ribarov, Oxidative damage of the membrane lipids after electroporation, Gen. Physiol. Biophys. (1994).

[243] B. Gabriel, J. Teissie, Generation of reactive-oxygen species induced by electropermeabilization of Chinese hamster ovary cells and their

25

119

consequence on cell viability, Eur. J. Biochem. 223 (1) (1994) 25–33, https://doi.org/10.1111/j.1432-1033.1994.tb18962.x.

[244] M. Maccarrone, M.R. Bladergroen, N. Rosato, A.F. Agro, Role of lipid peroxidation in electroporation-induced cell permeability, Biochem. Biophys. Res. Commun. 209 (2) (1995) 417–425, https://doi.org/10.1006/bbrc.1995.1519.

[245] Q. Xu, LP. Huff, M. Fujii, K.K. Griendling, Redox regulation of the actin cytoskeleton and its role in the vascular system, Free Radic. Biol. Med. 109 (2017) 84–107, https://doi.org/10.1016/j.freeradbiomed.2017.03.004.

[246] J. Suh, D. Wirtz, J. Hanes, Real-time intracellular transport of gene nanocarriers studied by multiple particle tracking, Biotechnol. Prog. 20 (2) (2004) 598–602, https://doi.org/10.1021/bp034251y.

[247] G.L. Wilson, B.S. Dean, G. Wang, D.A. Dean, Nuclear import of plasmid DNA in digitonin-permeabilized cells requires both cytoplasmic factors and specific DNA sequences, J. Biol. Chem. 274 (31) (1999) 22025–22032, https://doi.org/10.1074/jbc.274.31.22025.

[248] A. Coonrod, F.-Q. Li, M. Horwitz, On the mechanism of DNA transfection: Efficient gene transfer without viruses, Gene Ther. 4 (12) (1997) 1313–1321, https://doi.org/10.1038/sj.gt.3300536.

[249] A. El Ouahabi, M. Thiry, V. Pector, R. Fuks, J.M. Ruysschaert, M. Vandenbranden, The role of endosome destabilizing activity in the gene transfer process mediated by cationic lipids, FEBS Lett. 414 (1997) 187–192, https://doi.org/10.1016/S0014-5793(97)00973-3.

[250] H. Bai, G.M.S. Lester, L.C. Petishnok, D.A. Dean, Cytoplasmic transport and nuclear import of plasmid DNA, Biosci. Rep. 37 (2017), https://doi.org/10.1042/BSR20160616.

[251] E.E. Vaughan, R.C. Geiger, A.M. Miller, P.L. Loh-Marley, T. Suzuki, N. Miyata, D. A. Dean, Microtubule acetylation through HDAC6 inhibition results in increased transfection efficiency, Mol. Ther. 16 (11) (2008) 1841–1847, https://doi.org/10.1038/mt.2008.190.

[252] M. Stacey, J. Stickley, P. Fox, V. Statler, K. Schoenbach, S.J. Beebe, S. Buescher, Differential effects in cells exposed to ultra-short, high intensity electric fields: Cell survival, DNA damage, and cell cycle analysis, Mutat. Res. - Genet. Toxicol. Environ. Mutagen. 542 (1-2) (2003) 65–75, https://doi.org/10.1016/j.mrgentox.2003.08.006.

[253] W. Yang, Y.-H. Wu, D. Yin, H.P. Koeffler, D.E. Sawcer, P.T. Vernier, M.A. Gundersen, Differential sensitivities of malignant and normal skin cells to nanosecond pulsed electric fields, Technol. Cancer Res. Treat. 10 (3) (2011) 281–286, https://doi.org/10.7785/tcrt.2012.500204.

[254] J.W. Ivey, E.L. Latouche, M.B. Sano, J.H. Rossmeisl, R.V. Davalos, S.S. Verbridge, Targeted cellular ablation based on the morphology of malignant cells, Sci. Rep. 5 (1) (2015), https://doi.org/10.1038/srep17157.

[255] V.N. Pehlivanova, I.H. Tsoneva, R.D. Tzoneva, Multiple effects of electroporation on the adhesive behaviour of breast cancer cells and fibroblasts, Cancer Cell Int. 12 (1) (2012), https://doi.org/10.1186/1475-2867-12-9.

[256] R. Zhou, R.C. Geiger, D.A. Dean, Intracellular trafficking of nucleic acids, Expert Opin. Drug Deliv. 1 (1) (2004) 127–140, https://doi.org/10.1517/17425247.1.1.127.

[257] M.E. Dowty, P. Williams, G. Zhang, J.E. Hagstrom, J.A. Wolff, Plasmid DNA entry into postmitotic nuclei of primary rat myotubes, Proc. Natl. Acad. Sci. U. S. A. 92 (10) (1995) 4572–4576, https://doi.org/10.1073/pnas.92.10.4572.

[258] D.A. Dean, Nonviral gene transfer to skeletal, smooth, and cardiac muscle in living animals, Am. J. Physiol. - Cell Physiol. 289 (2) (2005) C233–C245, https://doi.org/10.1152/ajpcell.00613.2004.

[259] D.A. Dean, B.S. Dean, S. Muller, L.C. Smith, Sequence requirements for plasmid nuclear import, Exp. Cell Res. 253 (2) (1999) 713–722, https://doi.org/10.1006/excr.1999.4716.

[260] P. Blomberg, M. Eskandarpour, S. Xia, C. Sylvén, K.B. Islam, Electroporation in combination with a plasmid vector containing SV40 enhancer elements results in increased and persistent gene expression in mouse muscle, Biochem. Biophys. Res. Commun. 298 (4) (2002) 505–510, https://doi.org/10.1016/S0006-291X(02)02486-5.

[261] J.B. Martin, J.L. Young, J.N. Benoit, D.A. Dean, Gene transfer to intact mesenteric arteries by electroporation, J. Vasc. Res. 37 (2000) 372–380, https://doi.org/10.1159/000025753.

[262] J.L. Young, J.N. Benoit, D.A. Dean, Effect of a DNA nuclear targeting sequence on gene transfer and expression of plasmids in the intact vasculature, Gene Ther. 10 (17) (2003) 1465–1470, https://doi.org/10.1038/sj.gt.3302021.

[263] S. Guo, D.L. Jackson, N.I. Burcus, Y.J. Chen, S. Xiao, R. Heller, Gene electrotransfer enhanced by nanosecond pulsed electric fields, Mol. Ther. - Methods Clin. Dev. 1 (2014) 14043, https://doi.org/10.1038/mtm.2014.43.

[264] C. Ramos, D. Bonato, M. Winterhalter, T. Stegmann, J. Teissié, Spontaneous lipid vesicle fusion with electropermeabilized cells, FEBS Lett. 518 (2002) 135–138, https://doi.org/10.1016/S0014-5793(02)02676-5.

[265] D.L. Perrier, L. Rems, P.E. Boukany, Lipid vesicles in pulsed electric fields: Fundamental principles of the membrane response and its biomedical applications, Adv. Colloid Interface Sci. 249 (2017) 248–271, https://doi.org/10.1016/j.cis.2017.04.016.

[266] S. Chopra, P. Ruzgys, M. Maciulevičius, M. Jakutavičiūtė, S. Šatkauskas, Investigation of Plasmid DNA Delivery and Cell Viability Dynamics for Optimal Cell Electrotransfection In Vitro, Appl. Sci. 10 (2020) 6070, https://doi.org/10.3390/app10176070.

[267] Y.i. Han, X.-M. Liu, H. Liu, S.-C. Li, B.-C. Wu, L.-L. Ye, Q.-W. Wang, Z.-L. Chen, Cultivation of recombinant Chinese hamster ovary cells grown as suspended aggregates in stirred vessels, J. Biosci. Bioeng. 102 (5) (2006) 430–435, https://doi.org/10.1263/jbb.102.430.

[268] N.C. Stellwagen, C. Gelfi, P.G. Righetti, The free solution mobility of DNA, Biopolymers. 42 (1997) 687–703, https://doi.org/10.1002/(SICI)1097-0282(199711)42:6.

3   DISCUSSION AND CONCLUSIONS

3.1   DISCUSSION

Non-viral gene delivery methods hold great promises as they are assumed to be less toxic and safer in terms of gene delivery compared to viral vectors (Mingozzi and High, 2011). However, the success of any gene delivery method, either for *in vivo* delivery of genetic material or after gene transfer into the recipient cells *ex vivo*, depends greatly upon the efficiency of nucleic acid internalization by the target cells and, in the case of pDNA, reaching the cell nucleus in order to exert its therapeutic effect. Therefore, one of the biggest challenges hindering wider clinical success of non-viral gene delivery methods is improving gene delivery efficiency (Stewart et al., 2016).

Electroporation is one of the main non-viral methods for intracellular gene delivery where pulsed electric fields are used to transiently permeabilize the cell membrane allowing enhanced transmembrane transport (Sachdev et al., 2022). When GET is performed *ex vivo* usually limited number of cells is available, so the treatment needs to be as efficient as possible, meaning high transfection rate while preserving cell viability. When GET is performed *in vivo* the effect of tissue composition must be considered (Pérez-Herrero and Fernández-Medarde, 2021). Further, when using GET for DNA vaccination besides highly efficient, the treatment also needs to be patient friendly, without causing discomfort or even pain (Aycock et al., 2021; Cvetkoska et al., 2022).

The aim of the dissertation was to investigate parameters that influence GET efficiency with the goal of better understanding and improving GET efficiency. We explored the effect of extracellular environment on electroporation, cell survival, and GET, specifically slightly acidic extracellular pH which is present in tumors. Further, we investigated the effect of different pulse parameters, mainly pulse duration and polarity on GET. We tested the possibility of using short bipolar microsecond, and nanosecond pulses for GET since these pulses could possibly offer more patient friendly GET applications with decreased muscle contractions and could potentially increase cell survival (at least near electrodes) because of reduced electrochemical reactions during pulse delivery.

Experiments were performed using three cell lines namely, chines hamster ovary cells – CHO, murine C3H muscle myoblasts – C2C12, and human skin fibroblasts cell line – 1306. Cells were exposed to electric pulses either attached, growing in a monolayer through parallel platinum iridium wire electrodes or in suspension placed between stainless steel parallel plate electrodes or in commercial aluminum cuvettes. For pulse delivery two commercially available and two prototype pulse generators were used. Pulse protocols that represented longer monopolar pulses were 100 µs, 200 µs, 1 ms or 5 ms

long. HF-BP protocols consisted of symmetrical 2 µs long bipolar pulses and for nanosecond pulses durations of 200 ns and 500 ns were investigated.

Depending on the application, the efficiency of GET can be reported in different ways. Most often as percentage of transfected cells (referred as GET) which gives information about the percentage of cells which was successfully transfected among the cells that survived the treatment, most relevant in applications with cells which can rapidly divide. For applications where sensitive or rare cells are used it may be crucial that the majority of cells survive the treatment. In this case it is important that results of GET efficiency also include cell survival. GET efficiency representing percentage of transfected cells based on the number of cells that were exposed to electric pulses is referred as overall GET. Further, GET efficiency, if cells are transfected with fluorescent proteins, can be measured with median fluorescence intensity (MFI), representing the quantity of produced transfected protein. This is important in applications where the goal is the production of high levels of therapeutic proteins (Potočnik et al., 2022). In the dissertation we present results of GET *in vitro* using all three above-described ways of GET efficiency.

3.1.1 Slightly acidic pH_e (pH 6.5) can affect the process of electroporation: cell membrane permeabilization

Metabolism of tumor cells is changed in order to obtain the energy levels required for high proliferative rates which leads to alterations in pH_e and pH_i. Reversal of pH gradient across the cell membrane is one of the hallmarks of cancer. Alkaline pH_i helps avoid apoptosis, induces an increase in the proliferation of malignant cells through induction of G2/M transition and is directly related to the development of multiple drug resistance. Moreover, slightly acidic pH_e promotes invasion and metastasis, and increases multiple drug resistance, angiogenesis, and tumor immune escape (Pérez-Herrero and Fernández-Medarde, 2021).

Electric pulses trigger different processes in cells and on their membranes. Until now cell type and size, molecule which is delivered, duration and type of exposure, local membrane curvature, temperature, and osmotic pressure were reported to influence cell membrane permeabilization (Kotnik et al., 2019).

Also, characteristics of electroporation and recovery medium can influence the response of cells to applied electric field. Pulse parameters for efficient electroporation treatments are determined based on results obtained in *in vitro* experiments which are mostly performed in selected electroporation buffers (Potočnik et al., 2019). Electroporation medium composition can have a profound effect on electroporation effectiveness (Dermol et al., 2016). *In vitro* electroporation, ECT and GET experiments are usually performed in medium with neutral or slightly alkaline pH. Since the extracellular environment of

most tumors is slightly acidic, *in vivo* applications of electroporation are thus performed under slightly acidic conditions. With the aim of transferring the knowledge gained *in vitro* to *in vivo* treatments as effectively as possible, we investigated whether slightly acidic electroporation and recovery medium have any effect on cell membrane permeabilization (Potočnik et al., 2019).

We expected that slightly acidic pH_e can affect the process of electroporation, but we did not expect to detect differences in cell membrane permeabilization threshold. After electroporation in the slightly acidic (pH 6.5) medium we expected no differences in the cell membrane permeabilization compared to cells electroporated in growth medium.

The pH of the growth medium in experiments was lowered by the addition of HCl to pH 6.5. Our results show that electroporation and recovery medium pH had no effect on the permeabilization threshold of the CHO cell membrane. There was no significant difference between the uptake curves of propidium iodide (PI), a small membrane-impermeable molecule which fluorescence increases upon binding to nucleic acids inside the cytoplasm commonly used for detecting electroporation (Batista Napotnik and Miklavčič, 2018), between cells electroporated and recovered in medium of different pH. This implies that the induced transmembrane voltage and the accompanying processes of membrane defects formation are not affected by the acidity of electroporation or recovery medium (Potočnik et al., 2019).

According to our results of PI uptake measured by flow cytometry, we can confirm that slightly acidic (pH 6.5) electroporation and recovery medium pH have no effect on cell membrane permeabilization, as PI uptake was not different in all four combinations of electroporation and recovery medium pH used (Potočnik et al., 2019).

3.1.2 Slightly acidic pH_e (pH 6.5) can affect the process of electroporation: cell survival

Contrary to permeabilization, we expected that slightly acidic pH_e (pH 6.5) can affect the process of cell membrane resealing after electroporation. After electroporation and cell recovery in slightly acidic medium we expected improved survival of the cells after electroporation compared to cells electroporated and recovered in growth medium.

Cell membrane resealing is longer and more complex process compared to cell membrane permeabilization. Endocytosis and lysosomal trafficking, which are both a part of cell membrane repair mechanisms, can be altered by changing pH_e (Glunde et al., 2003; Ben-Dov and Korenstein, 2013).

Indeed, we observed differences in cell viability depending on the pH of electroporation and recovery medium. When cells were electroporated and recovered in slightly acidic

medium survival was significantly higher compared to cells electroporated and recovered in growth medium. Medium pH had small influence on cell viability if low or very high electric fields were applied. With fluorescence microscopy we observed that in growth medium less cells resealed their membranes within 5 min than in slightly acidic medium, which implies that in cells recovering in growth medium cell membrane resealing is slower (Potočnik et al., 2019).

In human mammary epithelial cells and breast cancer cells of different degrees of malignancy it was shown that pH_e values of pH 6.8 and pH 6.4 cause a significant displacement of lysosomes from the perinuclear region to the cell periphery. Additionally, higher number of lysosomes was observed in cells exposed to extracellular acidity (Glunde et al., 2003). High concentration of protons on cell surface also stimulates the formation of inward membrane invaginations and vesicles, accompanied by an enhanced uptake of macromolecules (Ben-Dov and Korenstein, 2012, 2013). Extracellular acidosis could in this way increase exocytosis of lysosomes and facilitate faster and more efficient cell membrane damage repair resulting in better cell survival in slightly acidic environment (Potočnik et al., 2019).

We observed characteristic changes in cell appearance under light microscope after electroporation with high electric field. Signs of cell damage which could lead to cell death, such as granulation, loss of cell membrane integrity and long-lasting membrane blebs were observed in cells exposed to electric pulses. The damage caused by electric field, especially the emergence of long-lasting huge membrane blebs, was more prominent in cells that were electroporated and recovered in growth medium compared to cells that were electroporated and left to recover in slightly acidic medium (Potočnik et al., 2019). Formation of blebs, which can be as big as the cell, was already reported as electric field induced cell damage (Tsong, 1991; Rassokhin and Pakhomov, 2012). Detailed mechanisms of bleb expansion and retraction are still unclear, but it was proposed that blebbing is a primary self-protection process for quick release of the stress inside cells which can prevent the sudden cell lysis (Rassokhin and Pakhomov, 2012).

We observed less blebs on the cells that were electroporated and left to recover in slightly acidic medium. Further, our results obtained with MTS assay showed higher survival of cells that were electroporated and recovered in slightly acidic medium (Potočnik et al., 2019). Previously it was shown that when cells are exposed to slightly acidic pH_e lysosomes rearrange from perinuclear region more to the periphery of the cell which could enable faster and/or more efficient cell membrane repair (Damaghi et al., 2015).

Based on our results where at lower electric fields applied, we observed only small differences in cell survival between slightly acidic and growth electroporation and recovery medium for standard ECT pulse protocol (ESOPE pulse protocol; 8 pulses,

100 µs, 1 Hz) the effect of slightly acidic pH_e present in tumors is most likely irrelevant. However, higher survival of cells that were electroporated and recovered in slightly acidic medium observed at higher electric fields imply that slightly acidic pH_e should be considered when applying IRE. Our results suggest that tissues which have slightly acidic pH_e such as tumors, might need pulses of higher amplitudes for IRE to successfully achieve ablation (Potočnik et al., 2019).

Based on the results, obtained in experiments performed in CHO cell line, we can confirm that there is a difference in cell membrane repair that depends on pH_e and that pH_e affects the characteristics of defects that form on cell membrane during and after electroporation. Our results suggest that slightly acidic pH_e (pH 6.5) allows more efficient repair of damage that is induced on cell membrane during electroporation with high pulse amplitudes. However, further studies including various cell lines are needed to confirm if our observations are general (Potočnik et al., 2019).

3.1.3 Slightly acidic pH_e (pH 6.5) is a factor affecting the efficiency of GET

Since slightly acidic pH_e affects cell survival after electroporation it could also affect efficiency of GET. We expect that in slightly acid (pH 6.5) medium *in vitro* GET will be less efficient because slightly acidic pH_e can decrease negative charge of pDNA and consequently its electrophoresis.

When electric pulses are delivered two opposing pH fronts spread from electrodes. On the anode side there is acid pH front and on cathode side there is alkaline (Turjanski et al., 2011). Previously only the effects of pH fronts that form between electrodes during pulse delivery on GET were studied, showing that pH fronts are the main reason for tissue damage near electrodes observed after GET (Olaiz et al., 2014). We analyzed only cells in the middle between the electrodes and observed that electroporation and recovery medium pH had effect on GET efficiency. Slightly acidic electroporation and recovery medium significantly decreased GET efficiency compared to growth electroporation and recovery medium (Potočnik et al., 2019).

The reason for lower GET efficiency could be that slightly acidic pH reduces net pDNA negative charge and decreases electrophoretic movement of pDNA which enables that pDNA establishes contact with cell membrane (Klenchin et al., 1991). This is supported also by lower GET efficiency of cells electroporated in slightly acidic and recovered in growth medium compared to cells electroporated and recovered in growth medium, and higher GET efficiency of cells electroporated in growth and recovered in slightly acidic medium compared to cells electroporated and recovered in slightly acidic medium (Potočnik et al., 2019).

Slightly acidic pH$_e$ also reduces endocytosis (Davoust et al., 1987) which is one of proposed mechanism of pDNA entry into cells during GET (Rosazza et al., 2016a, 2016b; Wang et al., 2018). We, however, did not observe any significant difference in GET efficiency between cells electroporated and recovered in growth medium and cells electroporated in growth and recovered in slightly acidic medium. GET efficiency was, however, higher with cells electroporated in slightly acidic and recovered in growth medium compared to cells electroporated and recovered in slightly acidic medium. Since no difference in GET efficiency between cells electroporated in growth and recovered in slightly acidic medium and cells electroporated in slightly acidic and recovered in growth medium was observed, we assume that slightly acidic pH effects are not limited to one but may affect several of the steps involved in GET. Although pH changes in the sample during pulse delivery depend on pulse parameters and may induce damage near the electrodes, our results show that away from the electrodes these effects are negligible, as no statistically significant difference in GET efficiency in the same pH combinations between three pulse protocols was observed. However, we tested only three pulse protocols out of a wide range of pulse protocols used in GET and only one plasmid size so more experiments with various pulse parameters and plasmids are needed to generalize our results (Potočnik et al., 2019).

In conclusion, according to our observations, slightly acidic pH$_e$ (pH 6.5) decreases GET efficiency. Our results suggest that slightly acidic pH$_e$ affects multiple steps of GET from pDNA and cell membrane complex formation to intracellular trafficking of pDNA (Potočnik et al., 2019). We can therefore confirm that slightly acidic pH$_e$ (pH 6.5) leads to lower GET efficiency.

3.1.4   GET with short micro and nanosecond pulses

Gene transfection by electroporation *in vitro* and *in vivo* is a well-established and efficient method with protocols that have been developed for decades and are widely used. Most often the use of a train of long millisecond monopolar pulses, few to several tens of millisecond is suggested, mainly because of importance of electrophoresis in pDNA and cell membrane complexes formation (Rosazza et al., 2016b). However, long monopolar pulses trigger muscle contractions which can cause discomfort or even pain (Mpendo et al., 2020). With expanding the use of GET from *in vitro* to *in vivo* the need to avoid pain and undesirable muscle contractions emerged. Further, it was recognized that electrochemical reactions, which accompany delivery of long pulses, could have negative effect on GET efficiency. In cell therapies, where cells are transfected *ex vivo*, usually the number of available cells is low, consequently it is important that most of the cells survive the treatment which further strengthens the need to reduce electrochemical reactions during the treatment (Potočnik et al., 2022).

3.1.4.1   pH and temperature changes during pulse delivery

We measured pH changes of overall cell suspension after pulse delivery because it was reported that when bipolar pulses are delivered electrochemical reactions are decreased (Kotnik et al., 2001; Chafai et al., 2015), and fewer metal ions are released from electrodes (Vižintin et al., 2020). Electric pulses delivery led to slight decrease in pH of cell suspension, but not large enough to affect cell membrane resealing dynamics (Potočnik et al., 2019). Drop in pH was stable during 5 min following pulse delivery in all pulse protocols tested except pulse protocol 8 × 5 ms where pH additionally decreased in the second minute after pulse delivery and remained constant then after. Significant drop in pH was observed after pulse protocol 8 × 5 ms compared to pH after delivery of pulse protocol 8 × 100 µs and pulse protocol HF-BP 1 (Potočnik et al., 2021). Already previously it was shown that longer pulses lead to more electrochemical reactions which cause changes in the chemical composition of electroporation medium and pH (Chafai et al., 2015). Our results suggest that larger pH changes must be occurring at anode side since the overall pH decreased after pulse delivery. Larger extension of the anodic pH front relative to the cathodic front was observed previously (Turjanski et al., 2011).

Electroporation medium composition can significantly affect temperature rise of the sample during pulse delivery. GET in our experiments was performed in recommended growth medium for each cell line because growth medium is more like *in vivo* extracellular fluid compared to other buffers used for GET. Growth medium is highly conductive which leads to high currents and increased electrochemical reactions during pulse delivery (Chafai et al., 2015). Additionally, high medium conductivity results in high currents leading to heating and temperature increase of the sample during pulse delivery. Temperature can affect cell membrane permeabilization and GET by influencing cell membrane fluidity (Kandušer et al., 2008; Donate et al., 2016). Final temperature of the electroporated cell samples measured during delivery of different pulse protocols to different cell lines in different growth media in our studies never exceeded 37 °C (which was the temperature at which sample was incubated after GET), meaning that temperature increase during pulse delivery should not have significant effect on GET efficiency (Potočnik et al., 2021, 2022). Although we are aware that like pH changes during pulse delivery also temperature changes are larger near electrodes, meaning that locally there could be some cells which were affected more significant by temperature changes.

3.1.4.2   pDNA concentration

During short pulse delivery there is a lack of electrophoresis which can in principle be compensated by higher pDNA concentration. It was already shown that with higher pDNA concentration successful GET can be achieved with shorter high voltage pulses where electrophoresis is weaker (Kandušer et al., 2009; Pavlin et al., 2010; Chopra et al., 2020). However, high concentration of pDNA can also have negative effect on cell

survival and in consequence on GET efficiency. Pathogen-associated molecular patterns that are associated with pDNA, such as unmethylated CpG motifs in pDNA can be recognized by TLR9 and induce an innate immune response in tissue which can lead to apoptosis activation (Michieletto et al., 2019; Harris and Elmer, 2021). Usually, *in vitro* experiments pDNA concentrations between 10 – 100 µg/ml are used (Markowicz et al., 2006; Pavlin and Kandušer, 2015; Yu et al., 2015; Zhang et al., 2018). In our experiments of GET with shorter pulses higher than usual pDNA concentrations were used, up to 500 µg/ml (Potočnik et al., 2021, 2022).

pDNA in cell suspension of CHO cells was not toxic even at the highest pDNA concentration, alone or in combination with applying any of the five pulse protocols tested as detected by MTS assay 24 h after GET (Potočnik et al., 2021). Contrary to our results on CHO cell line, in C2C12 myoblasts and 1306 fibroblasts we observed some decrease in cell survival with increasing pDNA concentration but not for all pulse protocols. Others also reported contradictory results of high pDNA concentrations effect on cell viability. Some studies reported that pDNA concentrations up to 1000 µg/ml did not decrease cell survival (Liew et al., 2013), while others reported that pDNA concentrations above 100 µg/ml already had negative effect on cell survival (Rols et al., 1992; Yao et al., 2009).

Our results of cell survival in C2C12 myoblasts and 1306 fibroblasts are comparable to those reported previously (Chopra et al., 2020), where authors observed decreased cell survival with pDNA concentrations higher than 400 µg/ml. However, the decrease in cell survival of C2C12 myoblasts and 1306 fibroblasts in our experiments was not high enough to cause drop in overall GET at 500 µg/ml of pDNA. These and our previous results in CHO cell line show that decrease in cell survival following GET with high pDNA concentration varies between cell lines. As observed by us and others (Lesueur et al., 2016), pDNA by itself, in the absence of pulse delivery, is not toxic to cells. High pDNA concentrations could trigger decrease in cell survival in different steps of GET. We have shown that higher pDNA concentration leads to larger pDNA aggregates formed on cell membrane (Potočnik et al., 2021) during pulse delivery which could slow down or obstruct cell membrane repair. Further, endosomal and/or cytoplasmic DNA sensors could be activated by high pDNA concentration in endosomes or cytoplasm which can induce programmed cell death (Zahid et al., 2020). Finally, cell death could be triggered by high number of pDNA copies in nucleus or by high number of transgenes produced (Semenova et al., 2019).

3.1.4.3   pDNA size

It has been reported that GET efficiency depends on the size of pDNA. We compared GET, MFI, cell survival, and overall GET with a 3.5 kb and a 4.7 kb pDNA. Both having CMV promoter and encoding GFP. In our experiments, we did not observe any difference in GET or cell survival between different pDNA sizes in C2C12 myoblasts and 1306

fibroblasts. Smaller pDNA led to higher overall GET only when using 8 x 100 µs pulse protocol in both cell lines. For other pulse protocols we did not observe increase in overall GET with smaller pDNA although, since we used the same concentration of pDNA (500 µg/ml), the copy number of smaller pDNA was 1.34 x higher compared to larger pDNA. Our results are contrary to observations by Novickij *et al.* (2020) where they report higher sub-microsecond high frequency GET with smaller pDNA. Improved GET efficiency with smaller pDNA was reported also by others (Molnar et al., 2004; Ribeiro et al., 2012). The difference in size of pDNA used in our study was only 25% which may be the reason why we did not observe increase in overall GET efficiency with smaller pDNA (Potočnik et al., 2022).

However, with smaller pDNA significantly higher MFI of GFP positive cells was observed in C2C12 myoblasts after GET with 200 ns, 500 ns and HF-BP pulses. Opposite, in 1306 fibroblasts higher MFI with smaller pDNA was observed after GET with 8 x 100 µs and 8 x 5 ms. Suggesting that in C2C12 myoblasts shorter pulses enabled more copies of smaller pDNA to reach the nucleus. With longer pulses MFI after GET with both pDNA sizes was comparable. The situation seems to be reversed in 1306 fibroblasts where longer pulses enabled more copies of smaller pDNA to reach the nucleus. This shows that besides cell line and pDNA size also pulse parameters affect the degree of transgene expression (Potočnik et al., 2022).

3.1.4.4   GET with high frequency bipolar pulses

Our aim was to achieve GET with HF-BP pulses. Presented results could potentially allow GET without pain and muscle contraction.

Usually, when applying the same on-time per treatment with HF-BP pulses higher electric field is required to achieve the same level of cell membrane permeabilization (Scuderi et al., 2019; Polajžer et al., 2020). This poses a problem as not only long duration, but also shorter pulses applied with high amplitude cause muscle contractions (Yao et al., 2017). We showed that with extended on time per treatment, either with increased pulse number in each burst or increased number of bursts we were able to achieve permeabilization and GET with HF-BP pulses at lower electric field compared to 8×100 µs pulses (Potočnik et al., 2021).

When changing the number of pulses in each burst, number of bursts and electric field amplitude we were able to achieve GET using HF-BP pulses. With HF-BP pulse protocols in CHO cells, C2C12 myoblasts, and 1306 fibroblasts we were able to achieve comparable GET efficiency to that of longer monopolar pulses but with higher pDNA concentration. Percent of GFP positive cells was increasing with increasing pDNA concentration. Increase was more pronounced when HF-BP pulse protocols were applied. Overall GET obtained by HF-BP pulse protocols was comparable to overall GET

obtained by long monopolar pulse protocols at the highest pDNA concentration, except for C2C12 myoblasts where overall GET efficiency with HF-BP protocol was lower compared to longer monopolar pulses (Potočnik et al., 2021, 2022).

Promoter of pDNA, pDNA copy number within the cell and the availability of cellular machinery for transcription and translation are among factors regulating protein expression following transfection. Fluorescence intensity of the cell is considered to be indicative of the number of pDNA copies inside the cell that have reached the cell nucleus and have been successfully transcribed and translated into fluorescent proteins (Cohen et al., 2009; Tsai et al., 2015). Our MFI results thus suggest that higher pDNA concentration can only partially compensate for the lack of electrophoresis with HF-BP pulses. MFI with the lowest and the highest pDNA concentration was significantly higher after GET with longer monopolar pulses (8×100 µs and 8×5 ms) compared to all three pulse protocols HF-BP in CHO cells. Although with the highest pDNA concentration we were able to achieve similar percent of transfected cells, the number of pDNA copies that were successfully transfected into cells was higher when longer monopolar pulses (8×100 µs and 8×5 ms) were used. This may suggest that in addition to cell membrane permeabilization and pDNA aggregates formation, electrophoresis is also involved in pDNA translocation across cell membrane (Potočnik et al., 2021). Similar results were observed for C2C12 myoblasts, but not for 1306 fibroblasts where MFI of GFP positive cells after GET with HF-BP pulses at the highest pDNA concentration was higher compared to MFI after 8×5 ms pulses and lower compared to 8×100 µs pulse protocol (Potočnik et al., 2022).

Formation of pDNA aggregates on the cell membrane revealed that increasing pDNA concentration also increases the fluorescence intensity of pDNA aggregates formed on cell membrane. Florescence intensity of pDNA aggregates also increased when longer pulses were applied (Potočnik et al., 2021).

No direct correlation between fluorescence intensity of pDNA aggregates formed on cell membrane and GET efficiency in CHO cells was observed. For example, fluorescence intensity of pDNA aggregates formed after HF-BP 2 pulse protocol with the highest pDNA concentration was almost 10 times lower compared to fluorescence intensity of pDNA aggregates formed after 8×5 ms protocol while no significant difference was observed in percent of GFP positive cells. Similar observations were reported previously (Haberl et al., 2013). The interaction of pDNA with the cell membrane is only one of the several steps involved in GET and barriers that pDNA must overcome in order to be expressed. Other factors such as pDNA stability in cytoplasm, its transport to perinuclear region and successful crossing of nuclear envelope are also crucial and contribute to differences in GET efficiency (Sachdev et al., 2022).

Based on the results of our study we can confirm that we can achieve successful GET with HF-BP pulses *in vitro,* however, at sufficiently high pDNA concentrations. GET efficiency also varies greatly between cell lines. The electric field chosen for GET with pulse protocols HF-BP was in the range of electric fields used for GET with longer monopolar pulses. GET efficiency increased with increasing pDNA concentration. However, with a focus on achieving GET efficiency comparable to that of longer monopolar pulses (8×100 µs and 8×5 ms pulses) five times higher pDNA concentration was needed for GET with HF-BP pulse protocols. Further optimization of HF-BP pulse protocols could reduce the need for high pDNA concentrations. Nevertheless, according to reports using similar HF-BP pulse protocols where even at double stimulating electric filed eightfold reduction in muscle contraction intensity was observed (Sano et al., 2015; Yao et al., 2017), we can conclude that our results potentially open completely new field of feasible GET applications – less painful and widely accepted GET applications, like nucleic acid-based vaccination. However, we are aware that achieving sufficiently high pDNA concentrations in tissue can be challenging (Potočnik et al., 2021).

3.1.4.5   GET with nanosecond pulses

Use of short pulses in GET remains poorly explored. We were the first showing that HF-BP can be used for GET (Potočnik et al., 2021) and there are only three papers reporting the use of nanosecond pulses for GET, although all at kHz and MHz pulse repetition rate (Ruzgys et al., 2018; Novickij et al., 2020, 2022). Our aim was with further exploring nanosecond range of pulse durations to also achieve GET with 200 ns and 500 ns pulses at lower pulse repetition rate.

In order to select protocols with which we would most likely achieve GET with nanosecond pulses we tested different pulse protocols by varying pulse duration, number, repetition frequency and amplitude of applied electric field. Similarly, as with HF-BP pulses also with 200 ns and 500 ns pulse increasing pDNA concentration led to significant increase in overall GET. This was especially evident in 1306 fibroblasts where at pDNA concentrations up to 100 µg/ml overall GET was higher with 8 x 100 µs, HF-BP and 8 x 5 ms pulses compared to 500 ns and 200 ns pulses, whereas at 500 µg/ml of pDNA there was no significant difference in overall GET between different pulse protocols (Potočnik et al., 2022).

Interestingly, this was not observed in C2C12 myoblasts where overall GET rose with increasing pDNA concentration for all pulse protocols. At the highest pDNA concentration (500 µg/ml) overall GET was however still significantly higher with longer pulse protocols (8 x 100 µs and 8 x 5 ms) where stronger electrophoresis is present compared to shorter pulse protocols (HF-BP, 500 ns and 200 ns) (Potočnik et al., 2022).

Difference in overall GET between the two cell lines (C2C12 myoblasts and 1306 fibroblasts) confirmed that efficiency of GET does not depend solely on parameters of applied pulses. GET is a multistep process including various intracellular mechanisms (e.g., cell membrane repair mechanism, DNA sensors activation, endocytic pathways, cytoskeleton organization) which can be different between different cell lines (Frandsen et al., 2016; Znidar et al., 2016).

In our experiments we achieved GET with nanosecond pulses in both cell lines, but overall GET was higher in 1306 fibroblasts than in C2C12 myoblasts. Difference in GET efficiency in different cell lines has been observed and reported previously (Bodwell et al., 1999; Čegovnik and Novaković, 2004; Smirnikhina et al., 2011), but the reasons for these differences are not well understood. Differences in GET efficiency could be the consequence of various biophysical factors and/or biological parameters (Tsong, 1991; Kotnik et al., 2019). Since we did not observe any differences in permeabilization the difference in GET efficiency is more likely the consequence of the difference in presence and degree of activity of cellular intrinsic mechanisms and pathways (Potočnik et al., 2022).

Also, MFI of GFP positive cells was higher in 1306 fibroblasts compared to C2C12 myoblasts. Suggesting that higher number of pDNA copies was transferred to 1306 fibroblasts during pulse delivery compared to C2C12 myoblasts. Production of proteins from transfected pDNA could be affected also by availability and degree of activity of cellular machinery for transcription and translation (Tsai et al., 2015). Based on this higher GET efficiency in 1306 fibroblasts could mean that the rate of pDNA transcription and translation into fluorescent protein is higher in 1306 fibroblasts compared to C2C12 myoblasts (Potočnik et al., 2022).

Further, we wanted to explore if there are any differences in time dynamics of pDNA expression after GET with different pulse parameters as this was often suggested. Our results show that the onset of GFP expression (both percentage of GFP positive cells and their MFI) are comparable for 200 ns, HF-BP, 8 x 100 μs and 8 x 5 ms pulse protocols. However, differences were observed in time dynamics of GFP expression between C2C12 myoblasts and 1306 fibroblasts. Similar curves for GET and MFI for all pulse durations in one cell line suggest that all pulse protocols triggered the same mechanisms responsible for pDNA translocation through cytoplasm to cell nucleus (Potočnik et al., 2022).

In C2C12 myoblasts maximum of GFP positive cells and their MFI reached peak soon after GET and then decreased fast, falling below 10% for all four pulse durations at day 6. Contrary, in 1306 fibroblasts there were no distinct peaks of maximum GFP positive cells and their MFI. Percentage of GFP positive cells was stable for longer period

compared to C2C12 myoblasts and then decreased slowly. On day 6 after GET with all pulse durations around half of the initial percentage of 1306 fibroblasts were still GFP positive. Differences in dynamics and duration of transgene expression after GET between cell lines have been observed previously (Chicaybam et al., 2017). Differences in curves of GET and MFI for all pulse protocols between different cell lines suggest that mechanisms of pDNA translocation through cytoplasm to cell nucleus and duration of transcription of pDNA are different in different cell lines (Potočnik et al., 2022).

The reason for lower percentage of GFP positive cells and their lower MFI with all pulse protocols in C2C12 myoblasts could also be higher number or degree of activation of DNA sensors in this cell line which could trigger pDNA degradation in a larger extent compared to 1306 fibroblasts. Endosomal DNA sensors could be activated during pDNA translocation to the nucleus with endocytic pathways, and cytoplasmic DNA sensors could be triggered by pDNA entering the cell cytoplasm through cell membrane defects formed during pulse delivery. Additionally, cytosolic DNA sensors might be triggered by pDNA released to cytoplasm after endosomal escape. It was shown that GET with pDNA can lead to upregulation of several proposed cytosolic DNA sensors in different tumor cell types (Znidar et al., 2016, 2018) and in C2C12 myoblasts (Semenova et al., 2019). Other reasons contributing to decrease in transgene expression over time in C2C12 myoblasts could be loss of the pDNA at each mitosis, de novo DNA methylation preventing pDNA transcription or pDNA degradation by endonucleases (Lesueur et al., 2016).

The observed differences in overall GET and MFI between the three cell lines studied could also be the consequence of variations in cell membrane composition (Rosazza et al., 2012), endocytic pathways specific for certain cell line or the degree of activation of endocytic pathways (Chang et al., 2014), as well as presence of cytosolic nucleases (Cervia et al., 2017).

Based on our results we can confirm that GET can be achieved with nanosecond pulses, but similar as for HF-BP pulses, at the expense of higher pDNA concentration.

3.1.5   Review of current understanding of GET

GET is currently in the clinical stage of investigations where it is being evaluated for its therapeutic benefits in different applications and for a wide variety of indications (Ginn et al., 2018). The understanding of how pDNA molecules, due to electric pulse delivery, overcame the barriers they encounter on their way to reach the nucleus, namely interstitium, cell membrane, cytoplasm, and nuclear envelope, is still not complete. The fact that a lot of mechanism which enable GET are still not (in detail) known hinders further and faster development and acceptance of GET clinical applications. Currently,

optimization of GET is predominantly done based on trial-and-error principle which is time consuming and not very efficient (Sachdev et al., 2022).

Based on this we prepared a review in which we summarized our current understanding of GET and critically discussed the mechanisms by which electric field can aid in overcoming these barriers. We also identified the gaps in knowledge that are hindering optimization of GET. The knowledge of how pDNA molecules interact and overcome the barriers during GET is scattered throughout vast amount of literature, which dates as far back as 1982 when the first report of *in vitro* GET was published (Neumann et al., 1982). We have identified the factors limiting the transport of pDNA through the barriers if the transport process is known, such as for the interstitium where achieving sufficiently high pDNA concentration still represents a significant challenge. Identifying and developing methods which can improve the distribution of pDNA and electric field in tissue and make the concentration of pDNA and electric field in the target tissue more homogenous, have tremendous potential in improving GET efficiency. We also identified gaps in the understanding of the transport process through the barriers where the transport process is still unknown, such as the cell membrane, the cytoplasm, and the nuclear envelope. At the cell membrane there is still the need to elucidate which is the dominant way of pDNA crossing the cell membrane, passage through defects in cell membrane or endocytosis of pDNA aggregates formed on cell membrane during pulse delivery. Further, there are several mechanisms proposed for transporting of pDNA through cytoplasm, such as endosomal vesicles or pDNA binding with adapter proteins, which interact with the cytoskeleton motor proteins. Similarly, there are several proposed mechanisms of how pDNA crosses nuclear envelope, such as DNA nuclear targeting sequences, fusion of endosomes bearing pDNA with endoplasmic reticulum and nuclear envelope-associated endosomes, however the (dominant) mechanism enabling pDNA passage across nuclear envelope is still not known. We hope that our review of the mechanisms of transport and addressing the transport limitations will enable further enhancement of GET efficiency *in vitro* as well as in *in vivo* across various cell types, tissue types and species (Sachdev et al., 2022).

3.2   CONCLUSIONS

With the aim of better understanding and optimizing GET we tested the effect of different parameters on GET efficiency. Since microenvironment in tumors where many applications of *in vivo* electroporation are performed is slightly acidic, we studied the effects of slightly acidic (pH 6.5) electroporation and recovery medium on cell membrane permeabilization, cell survival and GET. Further, in an attempt to enable more patient friendly applications of GET *in vivo* we strived to attain GET with short HF-BP and nanosecond pulses. Finally, current understanding of GET from a biophysical perspective and critical discussion of the mechanisms by which applied electric fields in electroporation can aid pDNA in overcoming the barriers encountered on the way to the nucleus *in vivo* was reviewed.

The conclusions from our work can be summarized as follows:

1. Slightly acidic (pH 6.5) electroporation medium does not affect permeabilization threshold. We did not observe any differences in permeabilization curves depending on the pH of electroporation and recovery medium.

2. The survival of cells is better if slightly acidic (pH 6.5) electroporation and recovery medium are used compared to survival of cells that were electroporated and recovered in growth medium. Our results imply that slightly acidic pH_e allows more efficient repair of damage that is induced on cell membrane during electroporation with high pulse amplitudes.

3. There is a difference in cell morphology between cells that were electroporated and left to recover in growth medium and cells that were electroporated and left to recover in slightly acidic (pH 6.5) medium. Cells electroporated and recovered in growth medium had more membrane blebs that formed faster, had larger diameter and were more stable than membrane blebs formed after electroporation and recovery of cells in slightly acidic medium. When cells were exposed to growth or slightly acidic medium without electroporation, we did not observe any differences in cell morphology.

4. Slightly acidic (pH 6.5) electroporation and recovery medium decrease GET. We obtained statistically significantly higher GET when cells were electroporated and recovered in growth medium compared to cells that were electroporated and recovered in slightly acidic medium.

5. GET can be achieved with HF-BP pulses. Overall GET obtained by HF-BP pulse protocols was comparable to overall GET obtained by longer monopolar pulse protocols.

6. Gene electrotransfer efficiency depends on plasmid concentration. With all pulse protocols percent of GFP positive cells increased with increasing pDNA concentration.

7. Decrease in cell survival after GET with high pDNA concentrations is cell line dependent. pDNA in cell suspension of CHO cells was not toxic even at the highest, pDNA concentration, alone or in combination with applying any of five pulse protocols. On the contrary, in C2C12 myoblasts and 1306 fibroblasts we observed some decrease in cell survival with increasing pDNA concentration but not for all pulse protocols.

8. Number of transferred plasmid copies is higher with longer monopolar pulses. Although we were able to achieve similar percent of GFP positive cell, the number of pDNA copies that were successfully transferred into cells, based on the measurement of MFI of GFP positive cells, is higher when longer monopolar pulses are used.

9. Size of pDNA aggregates formed on cell membrane depends on pDNA concentration and pulse duration. When applying longer pulses with higher pDNA concentration larger pDNA aggregates on cell membrane are formed.

10. There is no correlation between fluorescence intensity of pDNA aggregates and GET efficiency. With the highest pDNA concentration used, fluorescence intensity of pDNA aggregates formed after HF-BP pulses was almost 10 times lower compared to fluorescence intensity of pDNA aggregates formed after millisecond pulses while no significant difference was observed in percent of GFP positive cells.

11. GET can be achieved with nanosecond pulses. With 200 ns and 500 ns pulses at the highest pDNA concentration comparable overall GET in 1306 fibroblasts was achieved as with longer monopolar pulses.

12. GET efficiency largely varies between cell lines. In 1306 fibroblast comparable overall GET was achieved while in C2C12 myoblasts only around half as efficient overall GET was reached with 200 ns and 500 ns pulses when compared to longer monopolar pulses.

13. MFI of GFP positive cells depends on cell line and pulse parameters. MFI after all pulse protocols was much higher in 1306 fibroblasts compared to C2C12 myoblasts, also MFI was generally higher after GET with longer pulses compared to shorter HF-BP and nanosecond pulses.

14. In our experiments smaller pDNA did not significantly improve GET efficiency but it had effect on the degree of transgene expression. In C2C12 myoblasts MFI cells was significantly higher with smaller pDNA after GET with short HF-BP and nanosecond pulses, while in 1306 fibroblasts significantly higher MFI with smaller pDNA was observed with longer monopolar pulses.

15. We showed that time dynamics of transgene expression is comparable between millisecond, microsecond, HF-BP and nanosecond pulses but varies greatly between cell lines. In C2C12 myoblasts GET and MFI reached peak soon after GET and then decreased steadily till day 6 after GET. In 1306 fibroblasts GET and MFI reached

peak at later time and were more stable, with around half of initial cells still being GFP positive on day 6.

4   SUMMARY

4.1   SUMMARY

Gene transfection by electroporation (GET) is a nonviral method of nucleic acids delivery into cells based on electroporation phenomenon (Rosazza et al., 2016b; Sachdev et al., 2022). For effective pDNA delivery and expression several steps must be overcome, among which are: cell membrane permeabilization, pDNA cell membrane interaction, transfer of pDNA into the cell, intracellular trafficking of pDNA through cytoplasm and nuclear import of pDNA and its expression (Sachdev et al., 2022).

The aim of the dissertation was to investigate parameters that influence GET efficiency with the goal of better understanding and improving GET efficiency. We explored the effect of extracellular environment on electroporation, cell survival, and GET, specifically slightly acidic (pH 6.5) extracellular pH (pH$_e$), which is present in different tumors. Further, we investigated the effect of different pulse parameters, mainly pulse duration and polarity on GET. We tested short bipolar microsecond, and nanosecond pulses for GET, since these pulses could offer more patient friendly GET applications with reduced muscle contractions and could increase cell survival (at least near electrodes) because of reduced electrochemical reactions during pulse delivery. Experiments were performed in three cell lines. Cells were exposed to electric pulses either attached in monolayer or in suspension. For pulse delivery two commercially available and two prototype pulse generators were used. Pulse protocols that represented longer monopolar pulses were 100 µs, 200 µs, 1 ms or 5 ms. HF-BP protocols consisted of symmetrical 2 µs long bipolar pulses, and for nanosecond pulses durations of 200 ns and 500 ns were investigated. In all experiments cells were electroporated in growth medium, which approximates tissue extracellular fluid. GET efficiency was measured as percentage of GFP positive cells – GET, overall GET which also includes cell survival, and MFI of GFP positive cells which is indicative of how much transgene was produced (Potočnik et al., 2019, 2021, 2022).

Since many of current GET applications are in tumor cells where microenvironment is slightly acidic, we studied the effects of slightly acidic (pH 6.5) electroporation and recovery medium. We observed no difference in the permeabilization threshold at any electric field amplitude (0–1.4 kV/cm), of cells which were electroporated and allowed to recover in growth (pH 7.8) or slightly acidic (pH 6.5) medium. In contrast, statistically significant difference was observed in survival of cells which was 34% better when cells were electroporated and recovered in slightly acidic medium compared to cells that were electroporated and recovered in growth medium. It was previously shown that slightly acidic pH$_e$ causes a significant displacement of lysosomes from the perinuclear region to the cell periphery and higher number of lysosomes was observed in cells exposed to slightly acidic pH$_e$ (Glunde et al., 2003; Damaghi et al., 2015). High concentration of

140

protons on cell surface also stimulates the formation of inward membrane invaginations and vesicles, accompanied by an enhanced uptake of macromolecules (Ben-Dov et al., 2012; Ben-Dov and Korenstein, 2013). Slightly acidic pH_e could in this way increase exocytosis of lysosomes and facilitate faster and more efficient cell membrane damage repair resulting in better cell survival in slightly acidic environment. Our results indeed imply that slightly acidic pH_e (pH 6.5) allows more efficient repair of damage induced on cell membrane due to electroporation. Recovery after exposure to electric pulses was much better in slightly acidic medium than in growth medium. Cells electroporated and recovered in growth medium also had more membrane blebs that formed faster, had larger diameter and were more stable than membrane blebs formed after electroporation and recovery in slightly acidic medium (Potočnik et al., 2019). However, slightly acidic pH_e decreased GET. The lowest percentage of GFP positive cells was obtained when electroporation and recovery were done in slightly acidic medium. The reason for lower GET efficiency could be that slightly acidic pH_e reduces net pDNA negative charge and decreases electrophoretic movement of pDNA which enables that pDNA establishes contact with cell membrane (Klenchin et al., 1991). Slightly acidic pH_e also reduces endocytosis (Davoust et al., 1987) which is one of proposed mechanism of pDNA entry into cells during GET (Chang et al., 2014; Rosazza et al., 2016b; Wang et al., 2018).

During shorts pulse delivery there is a lack of electrophoresis which can in principle be compensated with higher pDNA concentration. In our experiments we tested different pDNA concentrations from $0 – 500$ µg/ml. In all pulse protocols (i.e. from 200 ns up to 5 ms pulse durations) and cell lines percent of GFP positive cells increased with increasing pDNA concentration. Also, overall GET increased with increasing pDNA concentration. With lower pDNA concentrations percent of GFP positive cells was higher with longer pulses, while with higher pDNA concentrations we achieved comparable GET efficiency also with shorter HF-BP and nanosecond pulses. However, high concentration of pDNA can have negative effect on cell survival. We observed that decrease in survival is cell line dependent, however, the decrease in cell survival in our experiments was not high enough to cause drop in overall GET. Additionally, although with shorter HF-BP and nanosecond pulses we were able to achieve comparable percentage of GFP positive cells their MFI was still lower compared to longer monopolar pulses (Potočnik et al., 2021, 2022).

Establishing contact between pDNA and cell membrane is an important step in GET. In analyzing fluorescence intensity of pDNA aggregates along cell perimeter following monopolar pulse protocols increased fluorescence intensity was observed only on one side of cell membrane, while after HF-BP protocol two peaks in fluorescence intensity were observed representing formation of pDNA aggregates on both poles of the cell facing the electrodes. No direct correlation between fluorescence intensity of pDNA aggregates formed on cell membrane and GET efficiency was however observed (Potočnik et al., 2021). Since pDNA size is reported to influence GET efficiency, we performed experiments using two different size pDNA. The difference in size of pDNA used in our study was only 25% which might be the reason why we did not observe

pronounced increase in overall GET efficiency with smaller pDNA (Potočnik et al., 2022). The time dynamics of pDNA expression was also monitored by measuring percentage of GFP positive cells and their MFI every 8 h for 6 days. Our results show that the dynamics of the onset of GFP expression are comparable for all pulse protocols tested (i.e. from 200 ns up to 5 ms pulse durations) but varies greatly between the cell lines. Differences in curves of GET and MFI for all pulse protocols between cell lines suggest that mechanisms of pDNA transport through the cytoplasm to cell nucleus and duration of transcription of pDNA are different in different cell lines (Potočnik et al., 2022).

Since there is still the lack of understanding and knowing the mechanism which enable GET, we reviewed our current understanding of GET and critically discussed the mechanisms by which electric field can aid in overcoming the barriers. We have identified the factors limiting the transport of pDNA through the barriers if the transport process is known, such as for the interstitium, where achieving sufficiently high pDNA concentration still represents a problem, suggesting that methods which can improve the distribution of pDNA and electric field and making the concentration of pDNA and electric field in the target tissue more homogenous, have tremendous potential in improving the efficiency of GET. At the cell membrane there is still a need to elucidate which is the dominant way of pDNA crossing the cell membrane, passage through defects in the cell membrane or endocytosis of pDNA aggregates formed on cell membrane during pulse delivery. Further, there are several mechanisms proposed for transport of pDNA through cytoplasm, and how pDNA crosses nuclear envelope, however the (dominant) mechanisms enabling pDNA passage to the nucleus are still unknown. We hope that this review will enable further improvement of GET efficiency *in vitro* as well as in *in vivo* across various cell types, tissue types and species (Sachdev et al., 2022).

4.2   POVZETEK

V doktorski nalogi smo preučevali pojav elektroporacije in nekatere biotehnološke ter medicinske aplikacije, ki na tem pojavu temeljijo. Elektroporacija je namreč ena od najuspešnejših metod za vnos različnih molekul v celice. Ko so celice izpostavljene električnemu polju zadostne amplitude in trajanja, pride do permeabilizacije celične membrane. Pri tem na celični membrani nastanejo poškodbe, skozi katere se lahko izmenjujejo ioni in molekule. Molekule, za katere je celica običajno neprepustna, lahko tako prehajajo preko celične membrane (Kotnik in sod., 2019). Na pojavu elektroporacije temelji tudi nevirusna metoda vnosa nukleinskih kislin v celice genska transfekcija z elektroporacijo (GET), poimenovana tudi genska elektrotransfekcija ali genski elektroprenos. Z GET lahko v celice vnašamo molekule DNK in RNK. V literaturi najpogosteje zasledimo vnos plazmidne DNK (pDNK) (Sachdev in sod., 2022). Za učinkovit vnos in izražanje pDNK mora biti izpolnjenih več pogojev, med katerimi so permeabilizacija celične membrane, stik pDNK s celično membrano, prenos pDNK v celico, znotrajcelični prenos pDNK v citoplazmi in prehod pDNK v jedro ter njeno izražanje (Rosazza in sod., 2016b; Sachdev in sod., 2022). Na uspešnost prenosa pDNK preko navedenih korakov vpliva več parametrov električnih pulzov in bioloških parametrov. Še vedno pa ne razumemo popolnoma kateri mehanizmi sodelujejo pri prenosu pDNK v posameznih korakih.

Da bi izboljšali razumevanje in učinkovitost GET, smo se v doktorski nalogi posvetili preučevanju vpliva parametrov, ki vplivajo na učinkovitost GET. Raziskovali smo vpliv zunajceličnega okolja na elektroporacijo, celično preživetje in GET, zlasti vpliv rahlo kislega (pH 6.5) zunajceličnega pH (pH_e), ki je prisoten v mnogih tumorjih. GET je v tumorjih namreč manj uspešna kot v drugih tkivih (Mir in sod., 1999; Cemazar in sod., 2009). Eden od razlogov je zagotovo kompaktna zunajcelična struktura, ki zmanjšuje mobilnost pDNK v celični okolici. Z razgraditvijo kompaktne zunajcelične strukture tumorskih celic lahko izboljšamo učinkovitost GET (Cemazar in sod., 2012). Aplikacije elektroporacije, kot so elektrokemoterapija (ECT), ireverzibilna elektroporacija (IRE) in GET, večinoma ciljajo tumorske celice, pri katerih je prisoten obrat gradienta pH preko celične membrane, ki nastane z znižanjem pH_e (Sharma in sod., 2015). Rahlo kisel pH_e vodi do premika lizosomov, ki so ključni pri celjenju poškodb na celični membrani, iz perinuklearne regije v bližino celične membrane (Glunde in sod., 2003). Na podlagi teh ugotovitev smo predvidevali, da rahlo kisel pH_e (pH 6.5) lahko vpliva na proces elektroporacije, predvsem na celjenje membrane po elektroporaciji.

Nadalje smo raziskali učinek nekaterih parametrov električnih pulzov, predvsem trajanja in polaritete, na uspešnost GET. Preizkusili smo, ali uspešno GET lahko dosežemo tudi z nizkofrekvenčnimi vlaki kratkih bipolarnih pulzov, ki si sledijo s frekvencami nekaj deset ali sto kHz (HF-BP), in monopolarnimi nanosekundnimi električnimi pulzi. Ti pulzi bi namreč lahko ponudili bolniku prijaznejšo in učinkovitejšo GET z zmanjšano mišično

kontrakcijo in izboljšanjem preživetja celic (vsaj v bližini elektrod) zaradi zmanjšanih elektrokemičnih reakcij med dovajanem pulzov. Preučili smo tudi, kako na uspešnost GET vpliva koncentracija pDNK ter opazovali časovno dinamiko izražanja transgena po GET z različnimi pulznimi protokoli.

Raziskave smo opravljali v okolju *in vitro*, na treh celičnih linijah, in sicer na ovarijskih celicah kitajskega hrčka – CHO, mišjih C3H mioblastih – C2C12 in celični liniji fibroblastov človeške kože – 1306. Celice smo izpostavili različnim protokolom električnih pulzov, bodisi pritrjene kot enoslojno celično kulturo preko vzporednih žičnatih elektrod iz platine in iridija, bodisi v suspenziji med vzporednima ploščatima elektrodama iz nerjavečega jekla ali v komercialnih kivetah z elektrodama iz aluminija. Električne pulze smo generirali z dvema komercialno dostopnima (Betatech Electro cell B10 in CellFX System) in dvema prototipnima generatorjema električnih pulzov. Pulzna protokola, ki sta predstavljala daljše monopolarne pulze, sta bila 8 x 100 μs in 8 x 5 ms. Pri obeh protokolih smo pulze dovedli s ponavljalno frekvenco 1 Hz. Protokoli HF-BP so bili sestavljeni iz vlakov simetričnih 2 μs dolgih bipolarnih pulzov in 2 μs trajajočo pavzo med obema fazama kot tudi pavzo med pulzi. Testirali smo 3 različne HF-BP pulzne protokole. V prvem smo dovedli 20 vlakov in v vsakem vlaku 216 pulzov, v drugem 50 vlakov s 50 pulzi in v tretjem 100 vlakov s 32 pulzi v vsakem vlaku. Vlaki so si sledili s ponavljalno frekvenco 1 Hz. Raziskali smo tudi uspešnost GET ob uporabi električnih pulzov, ki trajajo 200 ns in 500 ns. Dovedli smo 25, 100 ali 300 pulzov s ponavljalno frekvenco 10 Hz. Za vsak pulzni protokol in celično linijo smo testirali tudi različne amplitude električnega polja (8 x 5 ms: 0 – 1 kV/cm, 8 x 100 μs: 0 – 2 kV/cm, HF-BP: 0 – 2.5 kV/cm, 500 ns: 0 – 14 kV/cm, 200 ns: 0 – 19 kV/cm), da smo določili končno amplitudo električnega polja pri katerem je bila GET najuspešnejša. V vseh poskusih smo celice elektroporirali v rastnem mediju, ki je približek tkivne zunajcelične tekočine.

Za določitev permeabilizacije celične membrane z elektroporacijo smo uporabili propidijev jodid (PI). PI smo dodali celicam tik pred dovajanjem električnih pulzov za merjenje premeabilizacije celične membrane ali 5 minut po dovajanju električnih pulzov za spremljanje poteka popravljanja poškodb na celični membrani. Število celic, ki vsebujejo PI, smo določili s pretočno citometrijo ali fluorescenčno mikroskopijo. Za določanje presnovno aktivnih celic po elektroporaciji in GET smo uporabili test celičnega titra 96 AQueous One Solution Cell Proliferation Assay.

V poskusih GET smo uporabili plazmida pMAXGFP (3.5 kb) in pEGFP-N1 (4.7 kb). Oba plazmida nosita zapis za zeleni fluorescentni protein (GFP) pod kontrolo CMV promotorja. Testirali smo koncentracije 20, 40, 80, 100, 250 in 500 μg/ml pDNK. Učinkovitost GET smo merili s pretočno citometrijo in fluorescenčno mikroskopijo. Učinkovitost GET je bila izmerjena kot odstotek GFP pozitivnih celic, celokupna GET,

ki vključuje tudi celično preživetje, in mediana fluorescence (MFI) GFP pozitivnih celic, ki odraža koliko transgena je nastalo v celicah.

Spremljali smo tudi, ali obstajajo razlike v nastalih skupkih pDNK na celični membrani med različnimi pulznimi protokoli. pDNK smo označili z barvilom TOTO-1 in merili intenzivnosti fluorescence skupkov pDNK, ki nastanejo na celični membrani po dovajanju električnih pulzov. Da bi preverili, ali obstajajo razlike v časovni dinamiki izražanja GFP med različnimi pulznimi protokoli in celičnimi linijami v odstotku GFP pozitivnih celic in njihovi MFI, smo s pretočnim citometrom merili GET vsakih 8 ur 6 dni zapored.

Ker je mikrookolje pri nekaterih aplikacijah elektroporacije *in vivo* rahlo kislo, smo preučevali učinke rahlo kislega elektroporacijskega medija in medija v katerem so celice okrevale po elektroporaciji na permeabilizacijo celične membrane, celično preživetje in uspešnost GET. pH rastnega medija smo znižali do vrednosti 6,5 z dodatkom HCl. Elektroporacijo smo izvedli na celicah CHO z osmimi električnimi pulzi, ki so trajali 100 µs in so se ponavljali s frekvenco 1 Hz. Pri vseh uporabljenih amplitudah električnega polja (0–1,4 kV/cm) nismo opazili razlike v stopnji permeabilizacije med celicami, ki so bile elektroporirane in so okrevale v rastnem (pH 7,8) ali rahlo kislem (pH 6,5) mediju. To kaže, da kislost elektroporacijskega medija in medija v katerem celice okrevajo po elektroporaciji ne vpliva na vsiljeno transmembransko napetost in spremljajoče procese nastajanja membranskih poškodb med elektroporacijo (Potočnik in sod., 2019).

Opazili pa smo statistično pomembno razliko v preživetju celic, ki so bile izpostavljene amplitudam električnega polja, višjim od permeabilizacijskega praga. Preživetje celic CHO po elektroporaciji z 1,2 kV/cm, 1,8 kV/cm in 2,4 kV/cm je bilo boljše, če so bile celice elektroporirane in so okrevale v rahlo kislem mediju, kot preživetje celic, ki so bile elektroporirane in so okrevale v rastnem mediju. Največjo razliko smo opazili po elektroporaciji pri 1,8 kV/cm. Preživetje celic, ki so bile elektroporirane in so okrevale v rahlo kislem mediju, je bilo 34 % boljše od preživetja celic, ki so bile elektroporirane in so okrevale v rastnem mediju. pH medija je imel majhen vpliv na preživetje celic, če so bili dovedeni pulzi z nizko ali zelo visoko amplitudo. V predhodnih študijah so pokazali, da rahlo kisel pH_e povzroči premik lizosomov iz perinuklearne regije na celično periferijo. Poleg tega so v celicah, izpostavljenih rahlo kislemu pH_e, opazili večje število lizosomov (Glunde in sod., 2003; Damaghi in sod., 2015). Rahlo kisel pH_e bi lahko na ta način povečal eksocitozo lizosomov in omogočil hitrejše in učinkovitejše popravljanje poškodb celične membrane po elektroporaciji, kar bi posledično omogočilo boljše preživetje celic v kislem okolju (Potočnik in sod., 2019).

Nasprotno pa je rahlo kisel pH_e zmanjšal učinkovitost GET. Najnižji odstotek GFP pozitivnih celic je bil dosežen pri elektroporaciji in okrevanju celic v rahlo kislem mediju.

Zaradi kislega pH je zmanjšan neto negativni naboj pDNK. To pomeni manj učinkovito elektroforezo pDNK, ki prispeva k vzpostavitvi stika pDNK s celično membrano (Klenchin in sod., 1991), kar je lahko razlog za nižjo učinkovitost GET. To dodatno potrjuje tudi manjša učinkovitost GET pri celicah, ki so bile elektroporirane v rahlo kislem in so okrevale v rastnem mediju, v primerjavi s celicami, ki so bile elektroporirane in so okrevale v rastnem mediju, ter večja učinkovitost GET pri celicah, ki so bile elektroporirane v rastnem mediju in so okrevale v rahlo kislem mediju, v primerjavi s celicami, ki so bile elektroporirane in so okrevale v rahlo kislem mediju (Potočnik in sod., 2019). Kisli pH_e tudi zmanjša endocitozo (Davoust in sod., 1987), ki je eden od predlaganih mehanizmov vstopa pDNK v celice med GET (Chang in sod., 2014; Rosazza in sod., 2016b, 2016a; Wang in sod., 2018).

Opazili smo tudi razlike v morfologiji med celicami, ki so bile elektroporirane in so okrevale v rastnem mediju, in celicami, ki so bile elektroporirane in so okrevale v rahlo kislem mediju. Ko so bile celice zgolj izpostavljene rastnemu ali rahlo kislemu mediju, v njihovi morfologiji nismo opazili nobenih razlik. Celice, ki so bile elektroporirane in so okrevale v rastnem mediju so imele več membranskih mehurčkov, ki so nastali hitreje, so imeli večji premer in so bili prisotni dlje kot membranski mehurčki, ki so nastali po elektroporaciji in okrevanju celic v rahlo kislem mediju (Potočnik in sod., 2019).

Za spremljanje celjenja celične membrane po dovajanju električnih pulzov smo dodali PI celični suspenziji tik pred izpostavitvijo električnim pulzom ali 5 minut po aplikaciji električnih pulzov. Če je bil PI dodan pred izpostavitvijo električnim pulzom, rahlo kisel elektroporacijski in rahlo kisel medij za okrevanje celic nista pomembno vplivala na odstotek fluorescentnih celic, kar je skladno s permeabilizacijskimi krivuljami. Če so bile celice izpostavljene električnim pulzom in so okrevale v rastnem mediju, celice niso popravile poškodb na celični membrani v 5-minutnem časovnem intervalu po elektroporaciji. Okrevanje po izpostavljenosti električnim pulzom je bilo veliko hitrejše v rahlo kislem mediju kot v rastnem mediju, ne glede na to, ali je bila elektroporacija opravljena v rastnem ali rahlo kislem mediju. Naši rezultati kažejo, da rahlo kisel pH_e omogoča učinkovitejše popravilo poškodb, ki nastanejo na celični membrani med elektroporacijo z amplitudami eklektičnega polja, višjimi od permeabilizacijskega praga (Potočnik in sod., 2019).

Glede na ugotovitve Sweeney in sod. (2016), da lahko s pulznimi protokoli HF-BP dosežemo podoben delež permeabilizirane celične membrane, ki je tudi bolj simetrična, in nedavno uspešno doseženo GET s spreminjanjem ponavljalne frekvence nanosekundnih pulzov (Ruzgys in sod., 2018) smo predpostavljali, da lahko dosežemo uspešno GET tudi s krajšimi mikro in nanosekundnimi pulzi. Uporaba kratkih električnih pulzov bi tako lahko omogočila uspešno GET *in vivo* ob zmanjšanju neprijetnih občutkov bolečine in/ali mišične kontrakcije.

Da bi preučili uspešnost GET s HF-BP in nanosekundnimi pulzi smo spreminjali različne parametre pulzov. V protokolih s HF-BP smo spreminjali trajanje pulza, trajanje premora med pozitivno in negativno fazo bipolarnega pulza, število pulzov v posameznem vlaku, število vlakov, ki so se ponavljali s frekvenco 1 Hz, in amplitudo električnega polja. V protokolih z nanosekundnimi pulzi pa smo spreminjali trajanje pulza, število pulzov, frekvenco ponavljanja pulzov in amplitudo električnega polja (Potočnik in sod., 2021, 2022). Uspešnost GET s HF-BP in nanosekundnimi pulzi smo primerjali z uspešnostjo GET z uveljavljenimi protokoli električnih pulzov, tj. 8 x 5 ms in 8 x 100 µs, s ponavljalno frekvenco 1 Hz, ki smo jim spreminjali samo amplitudo električnega polja.

Elektroporacija s pulznim protokolom 8 x 5 ms je pri vseh celičnih linijah povzročila permeabilizacijo in zmanjšanje preživetja pri najnižji amplitudi električnega polja. Pulzna protokola HF-BP in 8 x 100 µs sta vodila do podobnega odstotka permeabiliziranih celic pri enakih amplitudah električnega polja. Če smo elektroporacijo izvedli z nanosekundnimi pulzi, smo za permeabilizacijo celične membrane morali uporabiti višje amplitude električnega polja. Prav tako je bila pri nanosekundnih pulzih potrebna višja amplituda električnega polja, da smo opazili zmanjšano preživetje celic v primerjavi s HF-BP, 8 x 100 µs in 8 x 5 ms pulznimi protokoli (Potočnik in sod., 2021, 2022).

Presečišče permeabilizacijske in preživitvene krivulje celic določa amplitudo električnega polja, pri kateri je največji delež živih celic permeabiliziran. Ker amplituda električnega polja, ki zagotavlja optimalno permeabilizacijo s PI, ni nujno optimalna za privzem pDNK pri GET, smo izvedli GET s tremi različnimi amplitudami električnega polja v območju od nekoliko pod do nekoliko nad presečiščem permeabilizacijske in preživitvene krivulje. Tako smo določili amplitudo električnega polja, pri kateri je GET najboljša. Pri vseh pulznih protokolih smo opazili majhne razlike v optimalni amplitudi električnega polja za GET med celičnimi linijami (Potočnik in sod., 2021, 2022).

Pomanjkanje elektroforeze med dovajanjem kratkih pulzov bi lahko nadomestili z višjo koncentracijo pDNK. V naših poskusih smo testirali različne koncentracije pDNK; od 0 – 500 µg/ml. V vseh pulznih protokolih in pri vseh celičnih linijah se je odstotek GFP pozitivnih celic povečal z naraščajočo koncentracijo pDNK. Pri celični liniji CHO in fibroblastih 1306 povečanje koncentracije pDNK nad 100 µg/ml, če sta bila uporabljena pulzna protokola 8 x 100 µs ali 8 x 5 ms, skoraj ni povzročilo povečanja odstotka GFP pozitivnih celic. V nasprotju se je v poskusih z mioblasti C2C12 odstotek GFP pozitivnih celic povečal z višjimi koncentracijami pDNK z vsemi pulznimi protokoli. Pri nižjih koncentracijah pDNK (20-100 µg/ml) je bil odstotek GFP pozitivnih celic višji pri daljših pulzih – 8 x 100 µs in 8 x 5 ms, pri višjih koncentracijah pDNK (250-500 µg/ml) pa smo dosegli primerljivo GET tudi s HF-BP in nanosekundnimi pulzi (Potočnik in sod., 2021, 2022).

Visoka koncentracija pDNK ima lahko negativen učinek na celično preživetje in posledično na učinkovitost GET. Naši rezultati preživetja mioblastov C2C12 in fibroblastov 1306 so podobni tistim, o katerih so poročali Chopra in sod. (2020), kjer so avtorji opazili zmanjšano preživetje CHO celic s koncentracijami pDNK višjimi od 400 µg/ml. Vendar zmanjšanje celičnega preživetja mioblastov C2C12 in fibroblastov 1306 v naših poskusih ni povzročilo zmanjšanja celokupne GET pri 500 µg/ml pDNK. Tudi GET s koncentracijami pDNK do 500 µg/ml na celični liniji CHO ni vplivala na preživetje (Potočnik in sod., 2021). Naši rezultati kažejo, da je zmanjšanje preživetja celic po GET z visoko koncentracijo (500 µg/ml) pDNK odvisno od celične linije (Potočnik in sod., 2021, 2022).

Za vsak poskus smo zbrali tudi meritve MFI GFP pozitivnih celic na pretočnem citometru. MFI celic nakazuje, koliko kopij pDNK je bilo uspešno prepisanih in prevedenih v fluorescentni protein. MFI GFP pozitivnih celic se je med različnimi celičnimi linijami razlikovala. Pri vseh celičnih linijah in pulznih protokolih se je MFI GFP pozitivnih celic povečala z naraščajočo koncentracijo pDNK. Čeprav smo s HF-BP in nanosekundnimi pulzi uspeli doseči primerljiv odstotek GFP pozitivnih celic, je bila njihova MFI nižja v primerjavi z MFI GFP pozitivnih celic, ki so bile izpostavljene daljšim monopolarnim pulzom (8x 100 µs in 8 x 5 ms) kar kaže na pomembno vlogo elektroforeze tudi pri prehodu pDNK preko celične membrane (Potočnik in sod., 2021, 2022).

Tudi celokupna GET je naraščala z naraščajočo koncentracijo pDNK pri vseh pulznih protokolih in vseh celičnih linijah. Najvišja celokupna GET (40 %) je bila pri celični liniji CHO dosežena s pulznim protokolom 8 x 5 ms. Celokupna GET s pulznim protokolom 8 x 100 µs in pulznimi protokoli HF-BP z najvišjo koncentracijo pDNK (500 µg/ml) ni bila statistično pomembno različna (28 % v primerjavi s 32 %, 34 % in 25 %). Pri mioblastih C2C12 je bil najvišja celokupna GET, s 500 µg/ml pDNK, dosežena s pulznima protokoloma 8 x 5 ms (34 %) in 8 x 100 µs (30 %). Sledili so pulzni protokoli HF-BP (18 %), 500 ns (12 %) in 200 ns (12 %). Pri fibroblastih 1306 smo dosegli najvišjo celokupno GET s pulznim protokolom 8 x 100 µs (32 % pri 500 µg/ml pDNK) ne glede na uporabljeno koncentracijo pDNK. Zanimivo je, da smo z najvišjo koncentracijo pDNK, z uporabo pulznega protokola 8 x 5 ms dosegli najnižjo celokupno GET (14%), celo nižjo kot z uporabo nanosekundnih (500 ns: 25 %, 200 ns: 27 %) in HF-BP pulznih protokolov (21%) (Potočnik in sod., 2021, 2022).

Interakcijo pDNK s celično membrano smo z fluorescenčno označeno pDNK opazovali pri GET s pulznimi protokoli 8 x 100 µs, 8 x 5 ms in HF-BP pri celični liniji CHO. Za vsak pulzni protokol smo testirali najnižjo in najvišjo koncentracijo pDNK, 20 µg/ml oziroma 500 µg/ml. V odsotnosti dovajanja pulzov nismo opazili povečane intenzivnosti

fluorescence na celični membrani. Pri analizi intenzivnosti fluorescence vzdolž celičnega oboda po GET s pulznima protokoloma 8 x 100 µs in 8 x 5 ms smo povečano intenzivnost fluorescence opazili samo na eni strani celične membrane, saj so nastali skupki pDNK le na delu celične membrane, ki je bil obrnjen proti katodi. Pri analizi intenzivnosti fluorescence vzdolž celičnega oboda po GET s pulznim protokolom HF-BP pa smo opazili dva, sicer manj izrazita, vrha intenzivnosti fluorescence, ki predstavljata skupke pDNK na obeh polih celice obrnjenih proti elektrodam. Analiza fluorescence skupkov pDNK na celični membrani je pokazala, da povečanje koncentracije pDNK poveča tudi intenzivnost fluorescence skupkov pDNK, ki nastanejo na celični membrani. Intenzivnost fluorescence skupkov pDNK je bila večja ob uporabi daljših pulzov (Potočnik in sod., 2021). Nismo pa opazili neposredne korelacije med intenzivnostjo fluorescence skupkov pDNK, nastalih na celični membrani, in odstotkom GFP pozitivnih celic. Intenzivnost fluorescence skupkov pDNK, nastalih po pulznem protokolu HF-BP z najvišjo koncentracijo pDNK, je bila skoraj 10-krat nižja v primerjavi z intenzivnostjo fluorescence skupkov pDNK, nastalih po pulznem protokolu 8 × 5 ms, medtem ko je bil odstotek GFP pozitivnih celic primerljiv med obema pulznima protokoloma. O podobnih opažanjih so poročali že prej (Haberl in sod., 2013). Interakcija pDNK s celično membrano je le eden od več korakov in ovir, ki jih mora pDNK premagati, da se lahko izrazi. Drugi dejavniki, kot so stabilnost pDNK v citoplazmi, njen transport v perinuklearno regijo in uspešno prečkanje jedrne ovojnice, so prav tako ključni in prispevajo k razlikam v učinkovitosti GET (Sachdev in sod., 2022).

Ker naj bi velikost pDNK vplivala na učinkovitost GET, smo naredili poskuse z uporabo dveh različnih velikosti pDNK, pri čemer smo primerjali 3,5 kb plazmid pmaxGFP in 4,7 kb plazmid pEGFP-N1, ki nosita zapis za GFP pod nadzorom promotorja CMV. Koncentracija obeh plazmidov v vseh poskusih je bila 500 µg/ml, kar pomeni, da je bilo število kopij manjše pDNK 1,34 x višje. V mioblastih C2C12 je bila z manjšo pDNK opažena znatno višja celokupna GET samo za pulzni protokol 8 x 100 µs. Celokupna GET s pulznimi protokoli 200 ns, 500 ns in HF-BP je bila primerljiva pri obeh plazmidih. Zanimivo je, da je bila celokupna GET z 8 x 5 ms nižja z manjšo pDNK v primerjavi z večjo pDNK. Podobne rezultate smo dobili tudi pri fibroblastih 1306. Znatno višjo celokupno GET z manjšo pDNK smo dosegli le s pulznim protokolom 8 x 100 µs. S pulznimi protokoli 200 ns, 500 ns, HF-BP in 8 x 5 ms smo opazili primerljivo celokupno GET pri obeh velikostih pDNK. Razlika v velikosti pDNK, uporabljeni v naši raziskavi, je bila le 25 %, kar je lahko razlog, da nismo opazili izrazitega povečanja celokupne GET z manjšo pDNK (Potočnik in sod., 2022). Pri primerjavi MFI GFP pozitivnih celic vseh pulznih protokolov med različnimi velikostmi pDNK smo opazili izrazito razliko med obema celičnima linijama. V mioblastih C2C12 je bila MFI GFP pozitivnih celic statistično značilno višja z manjšo pDNK (pmaxGFP) po GET s pulznimi protokoli 200 ns, 500 ns in HF-BP, medtem ko je bila MFI pri fibroblastih 1306 statistično značilno višja z manjšo pDNK po pulznih protokolih 8 x 100 µs in 8 x 5 ms. To kaže, da poleg

celične linije in velikosti pDNK na stopnjo izražanja transgena vplivajo tudi parametri električnih pulzov (Potočnik in sod., 2022).

Časovno dinamiko izražanja pDNK smo spremljali pri mioblastih C2C12 in fibroblastih 1306. Odstotek GFP pozitivnih celic in njihovo MFI smo merili vsakih 8 ur 6 dni. Naši rezultati kažejo, da je dinamika začetka ekspresije GFP (tako odstotek GFP pozitivnih celic kot njihova MFI) primerljiva za vse testirane pulzne protokole (tj. od 200 ns do 5 ms trajanja pulza), vendar se močno razlikuje med obema celičnima linijama (Potočnik in sod., 2022).

V mioblastih C2C12 se je odstotek GFP pozitivnih celic pri vseh pulznih protokolih s časom povečeval in je dosegel maksimum 32 ur po GET. Največji odstotek GFP pozitivnih celic je bil dosežen s pulznim protokolom 8 x 100 µs (46,2 %), sledili pa so pulzni protokoli HF-BP (31,9 %), 8 x 5 ms (17,8 %) in 25 x 200 ns (6,9 %). Po 32 urah je odstotek GFP pozitivnih celic pričel upadati in se po 144 urah (tj. 6 dneh) zmanjšal pod 10 % pri vseh pulznih protokolih. Podobno, a časovno zamaknjeno dinamiko smo opazili tudi pri MFI GFP pozitivnih mioblastov C2C12. Po GET s pulznima protokoloma 8 x 100 µs in HF-BP smo največjo MFI zaznali po 24 urah, nato pa se je s časom zmanjševala. Zanimivo je, da smo po GET s pulznima protokoloma 8 x 5 ms in 25 x 200 ns največjo MFI izmerili že po osmih urah, nato pa je upadala (Potočnik in sod., 2022).

V nasprotju z mioblasti C2C12 pri fibroblastih 1306 pri vseh testiranih pulznih protokolih nismo zaznali izrazitega vrha v odstotku GFP pozitivnih celic v odvisnosti od časa. Odstotek GFP pozitivnih celic je bil visok med 8 in 64 urami po GET s pulznima protokoloma 8 x 5 ms in 25 x 200 ns, med 24 in 104 urami po GET s pulznim protokolom 8 x 100 µs in med 40 in 112 urami po GET s HF-BP. Največji odstotek GFP pozitivnih celic je bil dosežen s pulznim protokolom 8 x 100 µs (pri 48 urah, 55,2 %), sledil je HF-BP (pri 80 urah, 50,8 %), 25 x 200 ns (pri 40 urah, 29,2 %) in pulzni protokol 8 x 5 ms (pri 40 h, 24,3 %). Zanimivo je, da je bil večji odstotek GFP pozitivnih celic dosežen s pulznim protokolom 25 x 200 ns kot s pulznim protokolom 8 x 5 ms. Ko je odstotek GFP pozitivnih celic dosegel vrh, se je pri večini pulznih protokolov počasi manjšal, razen pri pulznem protokolu HF-BP, kjer je ostal na isti ravni ves čas opazovanja. Tako smo šesti dan (tj. 144 h) po GET s pulznim protokolom 8 x 100 µs zaznali 31,1 % GFP pozitivnih celic, po GET s pulznim protokolom HF-BP 47,0 % GFP pozitivnih celic, po GET s pulznim protokolom 25 x 200 ns 11,3 % GFP pozitivnih celic in po GET s pulznim protokolom 8 x 5 ms 9,5 % GFP pozitivnih celic. Široke in neizrazite vrhove smo opazili tudi pri MFI v odvisnosti od časa pri vseh pulznih protokolih, ki smo jih uporabili za GET na fibroblastih 1306. MFI je dosegla vrh pozneje kot največji odstotek GFP pozitivnih celic, med 24 in 104 urami po GET s pulznim protokolom 25 x 200 ns, med 40 in 104 urami po GET s pulznima protokoloma 8 x 100 µs in 8 x 5 ms ter med 32 in 72 ur po GET s pulznim protokolom HF-BP. Primerljiva MFI je bila opažena pri pulznih

protokolih 8 x 5 ms, 8 x 100 µs in HF-BP, in je bila višja v primerjavi s pulznim protokolom 25 x 200 ns. Razlike v časovni odvisnosti odstotka GFP pozitivnih celic in MFI med celičnima linijama kažejo, da so mehanizmi prenosa pDNK skozi citoplazmo v celično jedro in trajanje prepisovanja pDNK različni v različnih celičnih linijah (Potočnik in sod., 2022).

Razlog za nižji odstotek GFP pozitivnih celic in njihovo nižjo MFI, ki smo jo zaznali pri vseh uporabljenih pulznih protokolih v mioblastih C2C12, bi lahko bilo večje število ali stopnja aktivacije senzorjev DNK pri tej celični liniji, kar bi lahko v večji meri sprožilo razgradnjo pDNK v primerjavi s fibroblasti 1306. Endosomski senzorji DNK bi se lahko aktivirali med prenosom pDNK v jedro z endocitozo, citoplazemske senzorje DNK pa bi lahko aktivirala pDNK, ki vstopi v celično citoplazmo skozi poškodovano celično membrano do katere pride med dovajanjem pulzov. Poleg tega lahko citoplazemske senzorje DNK sproži pDNK, ki se sprosti v citoplazmo celice po endosomskem pobegu. Pokazano je bilo, da lahko GET s pDNK povzroči povečano aktivnost več citoplazemskih senzorjev DNK v različnih tipih tumorskih celic (Znidar in sod., 2016, 2018) in v mioblastih C2C12 (Semenova in sod., 2019). Drugi razlogi, ki prispevajo k manjšemu izražanju transgena skozi čas v mioblastih C2C12, bi lahko bili izguba pDNK pri vsaki mitozi, de novo metilacija DNK, ki preprečuje transkripcijo pDNK, ali razgradnja pDNK z endonukleazami (Lesueur in sod., 2016).

Opažene razlike v celokupni GET in MFI med tremi proučevanimi celičnimi linijami so lahko tudi posledica razlik v sestavi celične membrane (Rosazza in sod., 2012), endocitotskih poteh, specifičnih za določeno celično linijo, ali stopnji aktivacije endocitotskih poti (Chang in sod., 2014), kot tudi prisotnosti citoplazemskih nukleaz (Cervia in sod., 2017).

Ker naj bi bile med uporabo krajših bipolarnih pulzov elektrokemijske reakcije manj izrazite kot med uporabo daljših monopolarnih pulzov, smo merili pH po dovajanju električnih pulzov med elektrodama, v sredini 4 mm kivet. Meritev smo izvajali 5 min pri temperaturi 37 ºC. Po dovajanju pulzov smo dodali tudi telečji serum in premešali celice s pipetiranjem, kot pri GET protokolu, zato so bile lokalne spremembe pH v kiveti zamegljene. Elektroporacija je statistično pomembno znižala pH celotnega vzorca celic CHO. pH se je pri vseh testiranih pulznih protokolih prvo minuto po GET znižal za 0,17– 0,27 in ostal konstantno nižji vseh 5 minut. Po GET s pulznim protokolom 8 x 5 ms pa se je pH dodatno znižal za 0,11 v drugi minuti po dovajanju pulzov in nato ostal nespremenjen. Pri primerjavi sprememb pH v 5 minutah po GET z različnih pulznimi protokoli smo opazili statistično značilno razliko drugo, tretjo, četrto in peto minuto po GET med pulznim protokolom 8 x 5 ms in pulznima protokoloma 8 x 100 µs in HF-BP. Na vsaki časovni točki je bil pH po GET s pulznim protokolom 8 x 5 ms bistveno nižji v primerjavi s pH po GET s pulznim protokolom 8 x 100 µs ali pulznim protokolom HF-

BP. Kljub temu, da je bilo zmanjšanje statistično značilno, opažen padec pH ni bil velik. Najnižje izmerjene vrednosti pH so bile še vedno nad 7,2. Že prej je bilo dokazano, da daljši pulzi vodijo do intenzivnejših elektrokemičnih reakcij, ki povzročajo spremembe v kemični sestavi elektroporacijskega medija in spremembe pH (Chafai in sod., 2015). Naši rezultati kažejo, da se večje spremembe pH dogajajo ob anodi, saj se je skupni pH zmanjšal po dovajanju pulzov. Večje spremembe pH ob anodi so opazili tudi drugi raziskovalci (Turjanski in sod., 2011).

Med dovajanjem električnih pulzov se poveča temperatura celičnega vzorca. Povečanje temperature je odvisno od sestave medija, v katerem so celice izpostavljene električnim pulzom. V naših poskusih je bila GET narejena v priporočenem rastnem mediju za vsako celično linijo, ker je rastni medij bolj podoben zunajcelični tekočini *in vivo* v primerjavi z drugimi mediji, ki se uporabljajo za GET. Rastni medij ima veliko specifično električno prevodnost, kar vodi do visokih tokov in povečanih elektrokemičnih reakcij med dovajanjem pulzov (Chafai in sod., 2015) ter do segrevanja in povišanja temperature vzorca. Od temperature je odvisna fluidnost celične membrane (Donate in sod., 2016), ki vpliva na permeabilizacijo celične membrane in GET. Končna temperatura vzorcev elektroporiranih celic, izmerjena med dovajanjem različnih pulznih protokolov različnim celičnim linijam v različnih rastnih medijih v naših poskusih, ni bila nikoli višja od 37 °C (kar je bila temperatura, pri kateri je bil vzorec inkubiran po GET), kar pomeni, da dvig temperature med dovajanjem pulzov ne bi smel vplivati na učinkovitost GET. Zavedamo se, da so, podobno kot spremembe pH med dovajanjem pulzov, tudi temperaturne spremembe večje v bližini elektrod, kar pomeni, da bi temperaturne spremembe lokalno lahko vplivale na permeabilizacijo in preživetje nekaterih celic (Potočnik in sod., 2021, 2022).

Zaradi pomanjkanja razumevanja in poznavanja vseh mehanizmov, ki omogočajo GET, smo pripravili pregled, v katerem smo zbrali naše trenutno razumevanje GET in kritično razpravljali o mehanizmih, s katerimi lahko električno polje pripomore k transportu pDNK do celičnega jedra. Identificirali smo tudi vrzeli v znanju, ki ovirajo optimizacijo GET. Znanje o tem, kako molekule pDNK premagujejo ovire med GET, je razpršeno po literaturi, ki sega v leto 1982 s prvim poročilom o *in vitro* GET (Neumann in sod., 1982). Zagotavljanje dovolj visoke koncentracije pDNK v medceličnini v tkivu še vedno predstavlja izziv. Metode, ki lahko izboljšajo porazdelitev pDNK in električnega polja ter omogočijo bolj homogeno koncentracijo pDNK in električnega polja v ciljnem tkivu, imajo tako velik potencial za izboljšanje učinkovitosti GET. Ugotovili smo tudi pomanjkanje razumevanja transportnega procesa skozi ovire, kjer transportni proces še ni znan, kot so celična membrana, citoplazma in jedrna ovojnica. Še vedno ni jasno kateri je prevladujoči način prehajanja pDNK skozi celično membrano, prehod skozi poškodbe celične membrane ali endocitoza skupkov pDNK, ki nastanejo na celični membrani med dovajanjem pulzov. Poleg tega je predlaganih več mehanizmov za prenos pDNK skozi

citoplazmo, kot so endosomski vezikli ali vezava pDNK s povezovalnimi proteini, ki se preko motoričnih proteinov povezujejo s citoskeletom. Podobno obstaja več predlaganih mehanizmov kako pDNK prečka jedrno ovojnico. Med njimi so zaporedja, ki ciljajo na jedrno DNK, zlitje endosomov, ki nosijo pDNK, z endoplazemskim retikulumom in endosomi, povezanimi z jedrno ovojnico, vendar je (prevladujoči) mehanizem, ki omogoča prehod pDNK do celičnega jedra, še vedno neznan. Upamo, da bo zbrano znanje o mehanizmih prenosa pDNK v celico med GET v preglednem članku omogočilo hitrejše izboljšanje učinkovitosti GET *in vitro* kot tudi *in vivo* v različnih tipih celic, tkiv in bioloških vrstah (Sachdev in sod., 2022).

5   REFERENCES

Algazi A.P., Twitty C.G., Tsai K.K., Le M., Pierce R., Browning E., Hermiz R., Canton
   D.A., Bannavong D., Oglesby A., Francisco M., Fong L., Pittet M.J., Arlauckas
   S.P., Garris C., Levine L.P., Bifulco C., Ballesteros-Merino C., Bhatia S.,
   Gargosky S., Andtbacka R.H.I., Fox B.A., Rosenblum M.D., Daud A.I. 2020.
   Phase II Trial of IL-12 Plasmid Transfection and PD-1 Blockade in
   Immunologically Quiescent Melanoma. Clinical Cancer Research, 26: 2827–2837

Alzubi J., Lock D., Rhiel M., Schmitz S., Wild S., Mussolino C., Hildenbeutel M.,
   Brandes C., Rositzka J., Lennartz S., Haas S.A., Chmielewski K.O., Schaser T.,
   Kaiser A., Cathomen T., Cornu T.I. 2021. Automated generation of gene-edited
   CAR T cells at clinical scale. Molecular Therapy - Methods and Clinical
   Development, 20: 379–388

Antipina A.Y., Gurtovenko A.A. 2016. Molecular-level insight into the interactions of
   DNA with phospholipid bilayers: Barriers and triggers. RSC Advances, 6: 36425–
   36432

Antov Y., Barbul A., Mantsur H., Korenstein R. 2005. Electroendocytosis: Exposure of
   cells to pulsed low electric fields enhances adsorption and uptake of
   macromolecules. Biophysical Journal, 88: 2206–2223

Arena C.B., Sano M.B., Rylander M.N., Davalos R. V. 2011. Theoretical considerations
   of tissue electroporation with high-frequency bipolar pulses. IEEE Transactions on
   Biomedical Engineering, 58: 1474–1482

Aycock K.N., Zhao Y., Lorenzo M.F., Davalos R. V. 2021. A Theoretical Argument for
   Extended Interpulse Delays in Therapeutic High-Frequency Irreversible
   Electroporation Treatments. IEEE Transactions on Biomedical Engineering, 68:
   1999–2010

Badding M.A., Lapek J.D., Friedman A.E., Dean D.A. 2013. Proteomic and functional
   analyses of protein-DNA complexes during gene transfer. Molecular Therapy, 21:
   775–785

Batista Napotnik T., Reberšek M., Vernier P.T., Mali B., Miklavčič D. 2016. Effects of
   high voltage nanosecond electric pulses on eucaryotic cells (in vitro): A systematic
   review. Bioelectrochemistry, 110: 1–12

Batista Napotnik T., Miklavčič D. 2018. In vitro electroporation detection methods –
   An overview., Bioelectrochemistry, 120: 166-182

Batista Napotnik T., Polajžer T., Miklavčič D. 2021. Cell death due to electroporation –
   A review. Bioelectrochemistry, 141, 107871,
   doi.org/10.1016/j.bioelechem.2021.107871: 18 p.

Ben-Dov N., Korenstein R. 2012. Enhancement of cell membrane invaginations,
   vesiculation and uptake of macromolecules by protonation of the cell surface.
   PLoS ONE, 7: e3520, doi.org/10.1371/journal.pone.0035204: 16 p.

Ben-Dov N., Rozman Grinberg I., Korenstein R. 2012. Electroendocytosis Is Driven by
   the Binding of Electrochemically Produced Protons to the Cell's Surface. PLoS
   ONE, 7: e50299, doi.org/10.1371/journal.pone.0050299: 8 p.

Ben-Dov N., Korenstein R. 2013. Proton-induced endocytosis is dependent on cell
   membrane fluidity, lipid-phase order and the membrane resting potential.
   Biochimica et Biophysica Acta – Biomembranes, 1828: 2672–2681

Bhatia S., Longino N. V., Miller N.J., Kulikauskas R., Iyer J.G., Ibrani D., Blom A.,

Byrd D.R., Parvathaneni U., Twitty C.G., Campbell J.S., Le M.H., Gargosky S., Pierce R.H., Heller R., Daud A.I., Nghiem P. 2020. Intratumoral delivery of plasmid IL12 via electroporation leads to regression of injected and noninjected tumors in Merkel cell carcinoma. Clinical Cancer Research, 26: 598–607

Bodwel J., Swift F., Richardson J. 1999. Long duration electroporation for achieving high level expression of glucocorticoid receptors in mammalian cell lines. Journal of Steroid Biochemistry and Molecular Biology, 68: 77–82

Bohloli M., Atashi A., Soleimani M., Kaviani S., Anbarlou A. 2016. Investigating Effects of Acidic pH on Proliferation, Invasion and Drug-Induced Apoptosis in Lymphoblastic Leukemia. Cancer Microenvironment, 9: 119–126

Brunner S., Fürtbauer E., Sauer T., Kursa M., Wagner E. 2002. Overcoming the nuclear barrier: Cell cycle independent nonviral gene transfer with linear polyethylenimine or electroporation. Molecular Therapy, 5: 80–86

Bumke M.A., Neri D., Elia G. 2003. Modulation of gene expression by extracellular pH variations in human fibroblasts: A transcriptomic and proteomic study. Proteomics, 3: 675–688

Campana L.G., Edhemovic I., Soden D., Perrone A.M., Scarpa M., Campanacci L., Cemazar M., Valpione S., Miklavčič D., Mocellin S., Sieni E., Sersa G. 2019. Electrochemotherapy – Emerging applications technical advances, new indications, combined approaches, and multi-institutional collaboration., European Journal of Surgical Oncology, 45, 2: 92-102

Castro-Gomes T., Corrotte M., Tam C., Andrews N.W. 2016. Plasma membrane repair is regulated extracellularly by proteases released from lysosomes. PLoS ONE, 11, 3: e0152583, doi.org/10.1371/journal.pone.0152583: 26 p.

Čegovnik U., Novaković S. 2004. Setting optimal parameters for in vitro electrotransfection of B16F1, SA1, LPB, SCK, L929 and CHO cells using predefined exponentially decaying electric pulses. Bioelectrochemistry, 62: 73–82

Čemažar M., Jarm T., Miklavčič D., Lebar A.M., Ihan A., Kopitar N.A., Serša G. 1998. Effect of electric-field intensity on electropermeabilization and electrosensitivity of various tumor-cell lines in vitro. Electro- and Magnetobiology, 17: 263–272

Čemažar M., Golzio M., Serša G., Hojman P., Kranjc S., Mesojednik S., Rols M.P., Teissie J. 2009. Control by pulse parameters of DNA electrotransfer into solid tumors in mice. Gene Therapy, 16: 635–644

Čemažar M., Golzio M., Serša G., Escoffre J.M., Coer A., Vidic S., Teissie J. 2012. Hyaluronidase and collagenase increase the transfection efficiency of gene electrotransfer in various murine tumors. Human Gene Therapy, 23: 128–137

Cervia L.D., Chang C.C., Wang L., Yuan F. 2017. Distinct effects of endosomal escape and inhibition of endosomal trafficking on gene delivery via electrotransfection. PLoS ONE, 12, 2: e0171699, doi.org/10.1371/journal.pone.0171699: 18 p.

Cervia L.D., Yuan F. 2018. Current Progress in Electrotransfection as a Nonviral Method for Gene Delivery., Molecular Pharmaceutics, 15, 9: 3617–3624

Cervia L.D., Chang C.C., Wang L., Mao M., Yuan F. 2018. Enhancing Electrotransfection Efficiency through Improvement in Nuclear Entry of Plasmid DNA. Molecular Therapy - Nucleic Acids, 11: 263–271

Chafai D.E., Mehle A., Tilmatine A., Maouche B., Miklavčič D. 2015. Assessment of the electrochemical effects of pulsed electric fields in a biological cell suspension. Bioelectrochemistry, 106: 249–257

Chang A.Y., Liu X., Tian H., Hua L., Yang Z., Wang S. 2020. Microfluidic Electroporation Coupling Pulses of Nanoseconds and Milliseconds to Facilitate Rapid Uptake and Enhanced Expression of DNA in Cell Therapy. Scientific Reports, 10: 1–10

Chang C.C., Wu M., Yuan F. 2014. Role of specific endocytic pathways in electrotransfection of cells. Molecular Therapy - Methods and Clinical Development, 1: 14058, doi.org/10.1038/mtm.2014.58: 8 p.

Chaumet A., Wright G.D., Seet S.H., Tham K.M., Gounko N. V., Bard F. 2015. Nuclear envelope-associated endosomes deliver surface proteins to the nucleus. Nature Communications, 6; 8218, doi.org/10.1038/ncomms9218: 9 p.

Chernomordik L. V., Sokolov A. V., Budker V.G. 1990. Electrostimulated uptake of DNA by liposomes. BBA – Biomembranes, 1024: 179–183

Chicaybam L., Barcelos C., Peixoto B., Carneiro M., Limia C.G., Redondo P., Lira C., Paraguassú-Braga F., Vasconcelos Z.F.M. De Barros L., Bonamino M.H. 2017. An Efficient Electroporation Protocol for the Genetic Modification of Mammalian Cells. Frontiers in Bioengineering and Biotechnology, 4: 99, doi.org/10.3389/fbioe.2016.00099: 13 p.

Chong Z.X., Yeap S.K., Ho W.Y. 2021. Transfection types, methods and strategies: A technical review. PeerJ, 9: e11165, doi.org/10.7717/peerj.11165: 13 p.

Chopinet L., Wasungu L., Rols M.P. 2012. First explanations for differences in electrotransfection efficiency in vitro and in vivo using spheroid model. International Journal of Pharmaceutics, 423, 1: 7–15

Chopinet L., Batista-Napotnik T., Montigny A., Rebersek M., Teissié J., Rols M.P., Miklavčič D. 2013. Nanosecond electric pulse effects on gene expression. Journal of Membrane Biology, 246: 851–859

Chopra S., Ruzgys P., Maciulevičius M., Jakutavičiute M., Šatka S. 2020. Investigation of plasmid DNA delivery and cell viability dynamics for optimal cell electrotransfection in vitro. Applied Sciences (Switzerland), 10, 17: 6070, doi.org/10.3390/app10176070: 11 p.

Cohen R.N., Van der Aa M.A.E.M., Macaraeg N., Lee A.P., Szoka F.C. 2009. Quantification of plasmid DNA copies in the nucleus after lipoplex and polyplex transfection. Journal of Controlled Release, 135: 166–174

Cooper S.T., McNeil P.L. 2015. Membrane repair: Mechanisms and pathophysiology. Physiological Reviews, 95: 1205–1240

Crowther M., Brown N.J., Bishop E.T., Lewis C.E. 2001. Microenvironmental influence on macrophage regulation of angiogenesis in wounds and malignant tumors. Journal of Leukocyte Biology, 70: 478–490

Cvetkoska A., Maček-Lebar A., Trdina P., Miklavčič D., Reberšek M. 2022. Muscle contractions and pain sensation accompanying high-frequency electroporation pulses. Scientific Reports, 12: 1–15

Damaghi M., Tafreshi N.K., Lloyd M.C., Sprung R., Estrella V., Wojtkowiak J.W., Morse D.L., Koomen J.M., Bui M.M., Gatenby R.A., Gillies R.J. 2015. Chronic acidosis in the tumour microenvironment selects for overexpression of LAMP2 in the plasma membrane. Nature Communications, 6, 16: 1–13

Dauty E., Verkman A.S. 2005. Actin cytoskeleton as the principal determinant of size-dependent DNA mobility in cytoplasm: A new barrier for non-viral gene delivery. Journal of Biological Chemistry, 280: 7823–7828

Davalos R. V., Mir L.M., Rubinsky B. 2005. Tissue ablation with irreversible electroporation. Annals of Biomedical Engineering, 33: 223–231

Davoust J., Gruenberg J., Howell K.E. 1987. Two threshold values of low pH block endocytosis at different stages. The EMBO Journal, 6: 3601–3609

Dermol J., Pakhomova O.N., Pakhomov A.G., Miklavčič D. 2016. Cell electrosensitization exists only in certain electroporation buffers. PLoS ONE, 11, 7: : e0159434, doi.org/10.1371/journal.pone.0159434: 19 p.

Dinchuk J.E., Kelley K.A., Callahan G.N. 1992. Flow cytometric analysis of transport activity in lymphocytes electroporated with a fluorescent organic anion dye. Journal of Immunological Methods, 155: 257–265

Donate A., Bulysheva A., Edelblute C., Jung D., A. Malik M., Guo S., Burcus N., Schoenbach K., Heller R. 2016. Thermal Assisted In Vivo Gene Electrotransfer. Current Gene Therapy, 16: 83–89

Duggan S.P., Gallagher W.M., Fox E.J.P., Abdel-Latif M.M., Reynolds J. V., Kelleher D. 2006. Low pH induces co-ordinate regulation of gene expression in oesophageal cells. Carcinogenesis, 27: 319–327

El Ouahabi A., Thiry M., Pector V., Fuks R., Ruysschaert J.M., Vandenbranden M. 1997. The role of endosome destabilizing activity in the gene transfer process mediated by cationic lipids. FEBS Letters, 414: 187–192

Elouahabi A., Ruysschaert J.M. 2005. Formation and intracellular trafficking of lipoplexes and polyplexes., Molecular Therapy, 11, 3: 336-347

Fajrial A.K., He Q.Q., Wirusanti N.I., Slansky J.E., Ding X. 2020. A review of emerging physical transfection methods for CRISPR/Cas9-mediated gene editing, Theranostics, 10, 12: 5532-5549

Faroja M., Ahmed M., Appelbaum L., Ben-David E., Moussa M., Sosna J., Nissenbaum I., Nahum Goldberg S. 2013. Irreversible electroporation ablation: Is all the damage nonthermal?, Radiology, 266: 462–470

Farrer H.N., Rossotti F.J.C. 1964. Proton-fluoride association in sodium perchlorate media., Journal of Inorganic and Nuclear Chemistry, 26, 11: 1959-1965

Faurie C., Phez E., Golzio M., Vossen C., Lesbordes J.C., Delteil C., Teissié J., Rols M.P. 2004. Effect of electric field vectoriality on electrically mediated gene delivery in mammalian cells. Biochimica et Biophysica Acta – Biomembranes, 1665: 92–100

Faurie C., Rebersek M., Golzio M., Kanduser M., Escoffre J.M., Pavlin M., Teissie J., Miklavčič D., Rols M.P. 2010. Electro-mediated gene transfer and expression are controlled by the life-time of DNA/membrane complex formation. Journal of Gene Medicine, 12: 117–125

Folegatti P.M., Bittaye M., Flaxman A., Lopez F.R., Bellamy D., Kupke A., Mair C., Makinson, R., Sheridan, J., Rohde, C., Halwe, S., Jeong, Y., Park, Y.S., Kim, J.O., Song M., Boyd A., Tran N., Silman D., Poulton I., Datoo M., Marshall J., Themistocleous Y., Lawrie A., Roberts R., Berrie E., Becker S., Lambe T., Hill A., Ewer K., Gilbert S. 2020. Safety and immunogenicity of a candidate Middle East respiratory syndrome coronavirus viral-vectored vaccine: a dose-escalation, open-label, non-randomised, uncontrolled, phase 1 trial. The Lancet Infectious Diseases, 20: 816–826

Ford W.E., Ren W., Blackmore P.F., Schoenbach K.H., Beebe S.J. 2010. Nanosecond pulsed electric fields stimulate apoptosis without release of pro-apoptotic factors

from mitochondria in B16f10 melanoma. Archives of Biochemistry and Biophysics, 497: 82–89

Frandsen S.K., McNeil A.K., Novak I., McNeil P.L., Gehl J. 2016. Difference in Membrane Repair Capacity Between Cancer Cell Lines and a Normal Cell Line. Journal of Membrane Biology, 249: 569–576

Geboers B., Scheffer H.J., Graybill P.M., Ruarus A.H., Nieuwenhuizen S., Puijk R.S., Van Den Tol P.M., Davalos R. V., Rubinsky B., De Gruijl T.D., Miklavčič D., Meijerink M.R. 2020. High-voltage electrical pulses in oncology: Irreversible electroporation, electrochemotherapy, gene electrotransfer, electrofusion, and electroimmunotherapy, Radiology. Radiological Society of North America (RSNA), 295, 2: 254–272

Gehl J., Mir L.M. 1999. Determination of optimal parameters for in vivo gene transfer by electroporation, using a rapid in vivo test for cell permeabilization. Biochemical and Biophysical Research Communications, 261: 377–380

Ginn S.L., Amaya A.K., Alexander I.E., Edelstein M., Abedi M.R. 2018. Gene therapy clinical trials worldwide to 2017: An update, Journal of Gene Medicine, 20: e3015, doi.org/10.1002/jgm.3015: 16 p.

Glunde K., Guggino S.E., Solaiyappan M., Pathak A.P., Ichikawa Y., Bhujwalla Z.M. 2003. Extracellular Acidification Alters Lysosomal Trafficking in Human Breast Cancer Cells. Neoplasia, 5: 533–545

Golberg A., Sack M., Teissie J., Pataro G., Pliquett U., Saulis G., Stefan T., Miklavčič D., Vorobiev E., Frey W. 2016. Energy-efficient biomass processing with pulsed electric fields for bioeconomy and sustainable development., Biotechnology for Biofuels, 9: 94, doi.org/10.1186/s13068-016-0508-z: 22 p.

Golzio M., Teissié J., Rols M.P. 2002a. Direct visualization at the single-cell level of electrically mediated gene delivery. Proceedings of the National Academy of Sciences of the United States of America, 99: 1292–1297

Golzio M., Teissié J., Rols M.P. 2002b. Cell synchronization effect on mammalian cell permeabilization and gene delivery by electric field. Biochimica et Biophysica Acta – Biomembranes, 1563: 23–28

Guo S., Jackson D.L., Burcus N.I., Chen Y.J., Xiao S., Heller R. 2014. Gene electrotransfer enhanced by nanosecond pulsed electric fields. Molecular Therapy - Methods and Clinical Development, 1: 14043, doi.org/10.1038/mtm.2014.43: 8 p.

Haberl S., Kandušer M., Flisar K., Hodžić D., Bregar V.B., Miklavčič D., Escoffre J.M., Rols M.P., Pavlin M. 2013. Effect of different parameters used for in vitro gene electrotransfer on gene expression efficiency, cell viability and visualization of plasmid DNA at the membrane level. Journal of Gene Medicine, 15: 169–181

Harris E., Elmer J.J. 2021. Optimization of electroporation and other non-viral gene delivery strategies for T cells. Biotechnology Progress, 37: e3066, doi.org/10.1002/btpr.3066: 8 p.

Heller C., Heller L.R. 2010. Electroporation Gene Therapy Preclinical and Clinical Trials for Melanoma. Current Gene Therapy, 10: 312–317

Heller R., Jaroszeski M., Atkin A., Moradpour D., Gilbert R., Wands J., Nicolau C. 1996. In vivo gene electroinjection and expression in rat liver. FEBS Letters, 389: 225–228

Heller R., Heller L.C. 2015. Gene Electrotransfer Clinical Trials. Advances in Genetics, 89: 235–262

Kandušer M., Šentjurc M., Miklavčič D. 2008. The temperature effect during pulse application on cell membrane fluidity and permeabilization. Bioelectrochemistry, 74: 52–57

Kandušer M., Miklavčič D., Pavlin M. 2009. Mechanisms involved in gene electrotransfer using high- and low-voltage pulses - An in vitro study. Bioelectrochemistry, 74: 265–271

Klein N., Guenther E., Botea F., Pautov M., Dima S., Tomescu D., Popescu M., Ivorra A., Stehling M., Popescu I. 2019. The combination of electroporation and electrolysis (E2) employing different electrode arrays for ablation of large tissue volumes. PLoS ONE, 14, 8: : e0221393, doi.org/10.1371/journal.pone.0221393: 13 p.

Klenchin V.A., Sukharev S.I., Serov S.M., Chernomordik L. V., Chizmadzhev Y. A. 1991. Electrically induced DNA uptake by cells is a fast process involving DNA electrophoresis. Biophysical Journal, 60: 804–811

Kotnik T., Miklavčič D., Mir L.M. 2001. Cell membrane electropermeabilization by symmetrical bipolar rectangular pulses: Part II. Reduced electrolytic contamination. Bioelectrochemistry, 54, 1: 91–95

Kotnik T., Rems L., Tarek M., Miklavčič D. 2019. Membrane Electroporation and Electropermeabilization: Mechanisms and Models., Annual Review of Biophysics, 48: 63-91

Kumari S., Mg S., Mayor S. 2010. Endocytosis unplugged: Multiple ways to enter the cell., Cell Research, 20: 256-275

Lacković I., Magjarević R., Miklavčič D. 2009. Three-dimensional finite-element analysis of joule heating in electrochemotherapy and in vivo gene electrotransfer. IEEE Transactions on Dielectrics and Electrical Insulation, 16: 1338–1347

Lambricht L., Lopes A., Kos S., Serša G., Préat V., Vandermeulen G. 2016. Clinical potential of electroporation for gene therapy and DNA vaccine delivery. Expert Opinion on Drug Delivery, 13: 295–310

Lechardeur D., Sohn K.J., Haardt M., Joshi P.B., Monck M., Graham R.W., Beatty B., Squire J., O'Brodovich H., Lukacs G.L. 1999. Metabolic instability of plasmid DNA in the cytosol: A potential barrier to gene transfer. Gene Therapy, 6: 482–497

Lesueur L.L., Mir L.M., André F.M. 2016. Overcoming the Specific Toxicity of Large Plasmids Electrotransfer in Primary Cells In Vitro. Molecular Therapy - Nucleic Acids. 5: e291, doi.org/10.1038/mtna.2016.4: 10 p.

Li Y., Wu, M., Zhao D., Wei Z., Zhong W., Wang X., Liang Z., Li Z. 2015. Electroporation on microchips: The harmful effects of pH changes and scaling down. Scientific Reports, 5: 17817, doi.org/10.1038/srep17817: 11 p.

Liew A., André F.M., Lesueur L.L., De Ménorval M.A., O'Brien T., Mir L.M. 2013. Robust, efficient, and practical electrogene transfer method for human mesenchymal stem cells using square electric pulses. Human Gene Therapy Methods, 24: 289–297

Lukacs G.L., Haggie P., Seksek O., Lechardeur D., Freedman N., Verkman A.S. 2000. Size-dependent DNA mobility in cytoplasm and nucleus. Journal of Biological Chemistry, 275: 1625–1629

Maglietti F., Michinski S., Olaiz N., Castro M., Suárez C., Marshall G. 2013. The role of Ph fronts in tissue electroporation based treatments. PLoS ONE, 8, 11: e80167, doi.org/10.1371/journal.pone.0080167: 8 p.

Mahnič-Kalamiza S., Vorobiev E., Miklavčič D. 2014. Electroporation in Food
   Processing and Biorefinery. Journal of Membrane Biology, 247: 1279–1304

Mahnič-Kalamiza S., Miklavčič D. 2020. Scratching the electrode surface: Insights into
   a high-voltage pulsed-field application from in vitro & in silico studies in
   indifferent fluid. Electrochimica Acta, 363: 137187,
   doi.org/10.1016/j.electacta.2020.137187: 15 p.

Mali B., Jarm T., Snoj M., Serša G., Miklavčič D. 2013. Antitumor effectiveness of
   electrochemotherapy: A systematic review and meta-analysis., European Journal of
   Surgical Oncology, 39, 1: 4–16

Mandal K. 2020. Review of PIP2 in cellular signaling, functions and diseases.
   International Journal of Molecular Sciences, 21: 1–20

Maor E., Sugrue A., Witt C., Vaidya V.R., DeSimone C. V., Asirvatham S.J., Kapa S.
   2019. Pulsed electric fields for cardiac ablation and beyond: A state-of-the-art
   review. Heart Rhythm, 16: 1112–1120

Markel, B., Skvarča E., Dolinšek T., Kloboves V.P., Coer A., Serša, G., Čemazar, M.
   2015. Inhibitor of endocytosis impairs gene electrotransfer to mouse muscle in
   vivo. Bioelectrochemistry, 103: 111–119

Markowicz S., Niedzielska J., Kruszewski M., Ołdak T., Gajkowska A., Machaj E.K.,
   Kurzak H., Pojda Z. 2006. Nonviral transfection of human umbilical cord blood
   dendritic cells is feasible, but the yield of dendritic cells with transgene expression
   limits the application of this method in cancer immunotherapy. Acta Biochimica
   Polonica, 53: 203–211

Maucksch C., Bohla A., Hoffmann F., Schleef M., Aneja M.K., Elfinger M., Hartl D.,
   Rudolph C. 2009. Transgene expression of transfected supercoiled plasmid DNA
   concatemers in mammalian cells. The Journal of Gene Medicine, 11: 444–453

Meglič Haberel S., Kotnik T. 2017. V: Electroporation-based applications in
   biotechnology. Handbook of Electroporation. Miklavčič D. (ur.). Cham,
   Switzerland, Springer International Publishing: 2153–2169

Mercadal B., Arena C.B., Davalos R. V., Ivorra A. 2017. Avoiding nerve stimulation in
   irreversible electroporation: A numerical modeling study. Physics in Medicine and
   Biology, 62: 8060–8079

Michieletto D., Lusic M., Marenduzzo D., Orlandini E. 2019. Physical principles of
   retroviral integration in the human genome. Nature Communications, 10: 1–11

Miklavčič D., Snoj M., Zupanič A., Kos B., Čemažar M., Kropivnik M., Bracko M.,
   Pečnik T., Gadzijev E., Serša G. 2010. Towards treatment planning and treatment
   of deep-seated solid tumors by electrochemotherapy. Biomedical Engineering
   Online, 9: 10, doi.org/10.1186/1475-925X-9-10: 12 p.

Mingozzi F., High K.A. 2011. Immune Responses to AAV in Clinical Trials. Current
   Gene Therapy, 11: 321–330

Mir L.M., Banoun H., Paoletti C. 1988. Introduction of definite amounts of
   nonpermeant molecules into living cells after electropermeabilization: Direct
   access to the cytosol. Experimental Cell Research, 175: 15–25

Mir L.M., Bureau M.F., Gehl J., Rangara R., Rouy D., Caillaud J.M., Delaere P.,
   Branellec D., Schwartz B., Scherman D. 1999. High-efficiency gene transfer into
   skeletal muscle mediated by electric pulses. Proceedings of the National Academy
   of Sciences of the United States of America, 96: 4262–4267

Molnar M.J., Gilbert R., Lu Y., Liu A.B., Guo A., Larochelle N., Lochmuller H., Petrof

B.J., Nalbantoglu J., Karpati G. 2004. Factors influencing the efficacy, longevity, and safety of electroporation-assisted plasmid-based gene transfer into mouse muscles. Molecular Therapy, 10: 447–455

Morrow M.P., Kraynyak K.A., Sylvester A.J., Shen X., Amante D., Sakata L., Parker L., Yan J., Boyer J., Roh C., Humeau L., Khan A.S., Broderick K., Marcozzi-Pierce K., Giffear M., Lee J., Trimble C.L., Kim J.J., Sardesai N.Y., Weiner D.B., Bagarazzi M.L. 2016. Augmentation of cellular and humoral immune responses to HPV16 and HPV18 E6 and E7 antigens by VGX-3100. Molecular Therapy – Oncolytics, 3: 16025, doi.org/10.1038/mto.2016.25: 11 p.

Mpendo J., Mutua G., Nanvubya A., Anzala O., Nyombayire J., Karita E., Dally L., Hannaman D., Price M., Fast P.E., Priddy F., Gelderblom H.C., Hills N.K. 2020. Acceptability and tolerability of repeated intramuscular electroporation of Multi-antigenic HIV (HIVMAG) DNA vaccine among healthy African participants in a phase 1 randomized controlled trial. PLOS ONE, 15: e0233151, doi.org/10.1371/journal.pone.0233151: 14 p.

Murray J.W., Wolkoff A.W. 2003. Roles of the cytoskeleton and motor proteins in endocytic sorting. Advanced Drug Delivery Reviews, 55: 1385–1403

Neumann E., Schaefer-Ridder M., Wang Y., Hofschneider P.H. 1982. Gene transfer into mouse lyoma cells by electroporation in high electric fields. The EMBO Journal, 1: 841–845

Novickij V., Balevičiūtė A., Ruzgys P., Šatkauskas S., Novickij J., Zinkevičienė A., Girkontaitė I. 2020. Sub-microsecond electrotransfection using new modality of high frequency electroporation. Bioelectrochemistry, 136: 107594, doi.org/10.1016/j.bioelechem.2020.107594: 8 p.

Novickij V., Balevičiute A., Malysko V., Želvys A., Radzevičiute E., Kos B., Zinkeviciene A., Miklavčič D., Novickij J., Girkontaite I. 2022. Effects of Time Delay between Unipolar Pulses in High Frequency Nano-Electrochemotherapy. IEEE Transactions on Biomedical Engineering, 69: 1726–1732

Olaiz N., Signori E., Maglietti F., Soba A., Suárez C., Turjanski P., Michinski S., Marshall, G. 2014. Tissue damage modeling in gene electrotransfer: The role of pH. Bioelectrochemistry, 100: 105–111

Pavlin M., Flisar K., Kandušer M. 2010. The role of electrophoresis in gene electrotransfer. Journal of Membrane Biology, 236: 75–79

Pavlin M., Kandušer M. 2015. New Insights into the Mechanisms of Gene Electrotransfer - Experimental and Theoretical Analysis. Scientific Reports, 5: 9132, doi.org/10.1038/srep09132: 11 p.

Pérez-Herrero E., Fernández-Medarde A. 2021. The reversed intra- and extracellular pH in tumors as a unified strategy to chemotherapeutic delivery using targeted nanocarriers. Acta Pharmaceutica Sinica B, 11: 2243–2264

Phillips M., Rubinsky L., Meir A., Raju N., Rubinsky B. 2015. Combining electrolysis and electroporation for tissue ablation. Technology in Cancer Research and Treatment, 14: 395–410

Polajžer T., Dermol-Černe J., Reberšek M., O'Connor R., Miklavčič D. 2020. Cancellation effect is present in high-frequency reversible and irreversible electroporation. Bioelectrochemistry, 132: 107442, doi.org/10.1016/j.bioelechem.2019.107442: 11 p.

Potočnik T., Miklavčič D., Maček Lebar A. 2019. Effect of electroporation and

recovery medium pH on cell membrane permeabilization, cell survival and gene transfer efficiency in vitro. Bioelectrochemistry, 130: 107342, doi.org/10.1016/j.bioelechem.2019.107342: 11 p.

Potočnik T., Miklavčič, D., Maček Lebar A. 2021. Gene transfer by electroporation with high frequency bipolar pulses in vitro. Bioelectrochemistry, 140: 107803, doi.org/10.1016/j.bioelechem.2021.107803: 13 p.

Potočnik T., Sachdev S., Polajžer T., Lebar A.M., Miklavčič D. 2022. Efficient Gene Transfection by Electroporation—In Vitro and In Silico Study of Pulse Parameters. Applied Sciences, 12, 16: 8237, doi.org/10.3390/app12168237: 50 p.

Qualmann B., Kessels M.M. 2002. Endocytosis and the cytoskeleton. International Review of Cytology, 220: 93–144

Rassokhin M.A., Pakhomov A.G. 2012. Electric field exposure triggers and guides formation of pseudopod-like blebs in U937 monocytes. Journal of Membrane Biology, 245: 521–529

Reddy A., Caler E. V., Andrews N.W. 2001. Plasma membrane repair is mediated by Ca2+-regulated exocytosis of lysosomes. Cell, 106: 157–169

Reddy V.Y., Neuzil P., Koruth J.S., Petru J., Funosako M., Cochet H., Sediva L., Chovanec M., Dukkipati S.R., Jais P. 2019. Pulsed Field Ablation for Pulmonary Vein Isolation in Atrial Fibrillation. Journal of the American College of Cardiology, 74: 315–326

Rems L., Tarek M., Casciola M., Miklavčič D. 2016. Properties of lipid electropores II: Comparison of continuum-level modeling of pore conductance to molecular dynamics simulations. Bioelectrochemistry, 112: 112–124

Rennick J.J., Johnston A.P.R., Parton R.G. 2021. Key principles and methods for studying the endocytosis of biological and nanoparticle therapeutics. Nature Nanotechnology, 16: 266–276

Ribeiro S., Mairhofer J., Madeira C., Diogo M.M., Lobato Da Silva C., Monteiro G., Grabherr R., Cabral J.M. 2012. Plasmid DNA size does affect nonviral gene delivery efficiency in stem cells. Cellular Reprogramming, 14: 130–137

Robertson R.M., Smith D.E. 2007. Self-diffusion of entangled linear and circular DNA molecules: Dependence on length and concentration. Macromolecules, 40: 3373–3377

Rols M. P., Coulet D., Teissie J. 1992. Highly efficient transfection of mammalian cells by electric field pulses: Application to large volumes of cell culture by using a flow system. European Journal of Biochemistry, 206: 115–121

Rols M.P., Delteil C., Golzio M., Dumond P., Gros S., Teissie J. 1998. In vivo electrically mediated protein and gene transfer in murine melanoma. Nature Biotechnology, 16: 168–171

Rosazza C., Escoffre J.M., Zumbusch A., Rols M.P. 2011. The actin cytoskeleton has an active role in the electrotransfer of plasmid DNA in mammalian cells. Molecular Therapy, 19: 913–921

Rosazza C., Phez E., Escoffre J.M., Cézanne L., Zumbusch A., Rols M.P. 2012. Cholesterol implications in plasmid DNA electrotransfer: Evidence for the involvement of endocytotic pathways. International Journal of Pharmaceutics, 1: 134–143

Rosazza C., Buntz A., Rieß T., Wöll D., Zumbusch A., Rols M.P. 2013. Intracellular tracking of single-plasmid DNA particles after delivery by electroporation.

Molecular Therapy, 21: 2217–2226

Rosazza C., Deschout H., Buntz A., Braeckmans K., Rols M.P., Zumbusch A. 2016a. Endocytosis and Endosomal Trafficking of DNA After Gene Electrotransfer In Vitro. Molecular Therapy - Nucleic Acids, 5: e286, doi.org/10.1038/mtna.2015.59: 11 p.

Rosazza C., Haberl Meglič S., Zumbusch A., Rols M.-P., Miklavčič D. 2016b. Gene Electrotransfer: A Mechanistic Perspective. Current Gene Therapy, 16: 98–129

Roux A., Koster G., Lenz M., Sorre B., Manneville J.B., Nassoy P., Bassereau P. 2010. Membrane curvature controls dynamin polymerization. Proceedings of the National Academy of Sciences of the United States of America, 107: 4141–4146

Ruzgys P., Novickij V., Novickij J., Šatkauskas S. 2018. Nanosecond range electric pulse application as a non-viral gene delivery method: proof of concept. Scientific Reports, 8: 15502, doi.org/10.1038/s41598-018-33912-y: 8 p.

Sachdev S., Feijoo Moreira S., Keehnen Y., Rems L., Kreutzer M.T., Boukany P.E. 2020. DNA-membrane complex formation during electroporation is DNA size-dependent. Biochimica et Biophysica Acta – Biomembranes, 1862, 2: 183089, doi.org/10.1016/j.bbamem.2019.183089: 7 p.

Sachdev S., Potočnik T., Rems L., Miklavčič D. 2022. Revisiting the role of pulsed electric fields in overcoming the barriers to in vivo gene electrotransfer. Bioelectrochemistry, 144: 107994, doi.org/10.1016/j.bioelechem.2021.107994: 26 p.

Sæbøe-Larssen S., Fossberg E., Gaudernack G. 2002. mRNA-based electrotransfection of human dendritic cells and induction of cytotoxic T lymphocyte responses against the telomerase catalytic subunit (hTERT). Journal of Immunological Methods, 259: 191–203

Sano M.B., Arena C.B., Bittleman K.R., Dewitt M.R., Cho H.J., Szot C.S., Saur D., Cissell J.M., Robertson J., Lee Y.W., Davalos R. V. 2015. Bursts of Bipolar Microsecond Pulses Inhibit Tumor Growth. Scientific Reports, 5: 14999, doi.org/10.1038/srep14999: 13 p.

Sano M.B., Fan R.E., Cheng K., Saenz Y., Sonn G.A., Hwang G.L., Xing L. 2018. Reduction of Muscle Contractions during Irreversible Electroporation Therapy Using High-Frequency Bursts of Alternating Polarity Pulses: A Laboratory Investigation in an Ex Vivo Swine Model. Journal of Vascular and Interventional Radiology, 29: 893-898.e4, doi.org/10.1016/j.jvir.2017.12.019: 10 p.

Šatkauskas S., Bureau M.F., Mahfoudi A., Mir L.M. 2001. Slow accumulation of plasmid in muscle cells: Supporting evidence for a mechanism of DNA uptake by receptor-mediated endocytosis. Molecular Therapy, 4: 317–323

Šatkauskas,S., Bureau M.F., Puc M., Mahfoudi A., Scherman D., Miklavčič D., Mir L.M. 2002. Mechanisms of in vivo DNA electrotransfer: Respective contribution of cell electropermeabilization and DNA electrophoresis. Molecular Therapy, 5: 133–140

Šatkauskas S., André F., Bureau M.F., Scherman D., Miklavčič D., Mir, L.M. 2005. Electrophoretic component of electric pulses determines the efficacy of in vivo DNA electrotransfer. Human Gene Therapy, 16: 1194–1201

Saulis G., Lape R., Pranevičiute R., Mickevičius D. 2005. Changes of the solution pH due to exposure by high-voltage electric pulses. Bioelectrochemistry, 67: 101–108

Sayed N., Allawadhi P., Khurana A., Singh V., Navik U., Pasumarthi S.K., Khurana I.,

Banothu A.K., Weiskirchen R., Bharani K.K. 2022. Gene therapy: Comprehensive overview and therapeutic applications. Life Sciences, 294: 120375, doi.org/10.1016/j.lfs.2022.120375: 21 p.

Schafer D.A. 2004. Regulating actin dynamics at membranes: A focus on dynamin., Traffic, 5, 7: 463-469

Scheffer H.J., Nielsen K., De Jong M.C., Van Tilborg A.A.J.M., Vieveen J.M., Bouwman A., Meijer S., Van Kuijk C., Van Den Tol P., Meijerink M.R. 2014. Irreversible electroporation for nonthermal tumor ablation in the clinical setting: A systematic review of safety and efficacy., Journal of Vascular and Interventional Radiology, 25, 7: 997-1011

Scuderi M., Reberšek M., Miklavčič D., Dermol-Černe J. 2019. The use of high-frequency short bipolar pulses in cisplatin electrochemotherapy in vitro. Radiology and Oncology, 53: 194–205

Semenova N., Bošnjak M., Markelc B., Žnidar K., Čemažar M., Heller L. 2019. Multiple cytosolic DNA sensors bind plasmid DNA after transfection. Nucleic Acids Research, 47: 10235–10246

Sharma M., Astekar M., Soi S., Manjunatha B., Shetty D., Radhakrishnan R. 2015. pH Gradient Reversal: An Emerging Hallmark of Cancers. Recent Patents on Anti-Cancer Drug Discovery, 10: 244–258

Shearer L.J., Petersen N.O. 2019. Distribution and Co-localization of endosome markers in cells. Heliyon, 5: e02375, doi.org/10.1016/j.heliyon.2019.e02375: 8 p.

Singh A.K., McGuirk J.P. 2020. CAR T cells: continuation in a revolution of immunotherapy, The Lancet Oncology, 21, 3: e168-e178, doi.org/10.1016/S1470-2045(19)30823-X: 11 p.

Smirnikhina S.A., Lavrov A. V., Bochkov N.P. 2011. Dynamics of elimination of plasmids and expression of VEGF121 gene transfected into human mesenchymal stem cells by different methods. Bulletin of Experimental Biology and Medicine, 151: 121–125.

Sokołowska E., Błachnio-Zabielska A.U. 2019. A critical review of electroporation as a plasmid delivery system in mouse skeletal muscle. International Journal of Molecular Sciences, 20, 11: 2776, doi.org/10.3390/ijms20112776: 21 p.

Sorre B., Callan-Jones A., Manneville J.B., Nassoy P., Joanny J.F., Prost J., Goud B., Bassereau P. 2009. Curvature-driven lipid sorting needs proximity to a demixing point and is aided by proteins. Proceedings of the National Academy of Sciences of the United States of America, 106: 5622–5626

Spiller D.G., Giles R. V., Grzybowski J., Tidd D.M., Clark R.E. 1998. Improving the intracellular delivery and molecular efficacy of antisense oligonucleotides in chronic myeloid leukemia cells: A comparison of Streptolysin-O permeabilization, electroporation, and lipophilic conjugation. Blood, 91: 4738–4746

Stewart M.P., Sharei A., Ding X., Sahay G., Langer R., Jensen K.F. 2016. In vitro and ex vivo strategies for intracellular delivery. Nature, 538: 183–192

Stubbs M., McSheehy P.M.J., Griffiths J.R., Bashford C.L. 2000. Causes and consequences of tumour acidity and implications for treatment. Molecular Medicine Today, 6: 15–19

Sugrue A., Maor E., Ivorra A., Vaidya V., Witt C., Kapa S., Asirvatham S. 2018. Irreversible electroporation for the treatment of cardiac arrhythmias., Expert Review of Cardiovascular Therapy, 16, 5: 349-360

Sukharev S.I., Klenchin V.A., Serov S.M., Chernomordik L. V., Chizmadzhev Y.A. 1992. Electroporation and electrophoretic DNA transfer into cells. The effect of DNA interaction with electropores. Biophysical Journal, 63: 1320–1327

Sweeney D.C., Reberšek M., Dermol J., Rems L., Miklavčič D., Davalos R. V. 2016. Quantification of cell membrane permeability induced by monopolar and high-frequency bipolar bursts of electrical pulses. Biochimica et Biophysica Acta – Biomembranes, 1858: 2689–2698

Tarek M. 2005. Membrane electroporation: A molecular dynamics simulation. Biophysical Journal, 88: 4045–4053

Tekle E., Astumian R.D., Chock P.B. 1991. Electroporation by using bipolar oscillating electric field: An improved method for DNA transfection of NIH 3T3 cells. Proceedings of the National Academy of Sciences of the United States of America, 88: 4230–4234

Thompson G.L., Roth C.C., Kuipers M.A., Tolstykh G.P., Beier H.T., Ibey B.L. 2016. Permeabilization of the nuclear envelope following nanosecond pulsed electric field exposure. Biochemical and Biophysical Research Communications, 470: 35–40

Topol E.J. 2021. Messenger RNA vaccines against SARS-CoV-2. Cell, 184, 6: 1401, doi.org/10.1016/j.cell.2020.12.039: 2 p.

Tsai Y.C., Tsai T.H., Chang C.P., Chen S.F., Lee Y.M., Shyue S.K. 2015. Linear correlation between average fluorescence intensity of green fluorescent protein and the multiplicity of infection of recombinant adenovirus. Journal of Biomedical Science, 22: 31, doi.org/10.1186/s12929-015-0137-z: 9 p.

Tsong T.Y. 1991. Electroporation of cell membranes., Biophysical Journal, 60, 2: 297-306

Turjanski P., Olaiz N., Maglietti F., Michinski S., Suárez C., Molina F.V., Marshall G. 2011. The role of pH fronts in reversible electroporation. PLoS ONE, 6, 4: e17303, doi.org/10.1371/journal.pone.0017303: 7 p.

Utvik J.K., Nja A., Gundersen K. 1999. DNA injection into single cells of intact mice. Human Gene Therapy, 10: 291–300

Vasan S., Hurley A., Schlesinger S.J., Hannaman D., Gardiner D.F., Dugin D.P., Boente-Carrera M., Vittorino R., Caskey M., Andersen J., Huang Y., Cox, J.H., Tarragona-Fiol T., Gill D.K., Cheeseman H., Clark L., Dally L., Smith C., Schmidt C., Park H.H., Kopycinski J.T., Gilmour J., Fast P., Bernard R., Ho D.D. 2011. In vivo electroporation enhances the immunogenicity of an HIV-1 DNA vaccine candidate in healthy volunteers. PLoS ONE, 6, 5: e19252, doi.org/10.1371/journal.pone.0019252: 10 p.

Vaughan E.E., Dean D.A. 2006. Intracellular trafficking of plasmids during transfection is mediated by microtubules. Molecular Therap 13: 422–428

Verspohl E.J., Kaiserling-Buddemeier I., Wienecke A. 1997. Introducing specific antibodies into electropermeabilized cells is a valuable tool for eliminating specific cell functions. Cell Biochemistry and Function, 15: 127–134

Vižintin A., Vidmar J., Ščančar J., Miklavčič D. 2020. Effect of interphase and interpulse delay in high-frequency irreversible electroporation pulses on cell survival, membrane permeabilization and electrode material release. Bioelectrochemistry, 134: 107523, doi.org/10.1016/j.bioelechem.2020.107523: 14 p.

Vižintin A., Marković S., Ščančar J., Miklavčič D. 2021. Electroporation with nanosecond pulses and bleomycin or cisplatin results in efficient cell kill and low metal release from electrodes. Bioelectrochemistry, 140: 107798, doi.org/10.1016/j.bioelechem.2021.107798: 12 p.

Wang L., Miller S.E., Yuan F. 2018. Ultrastructural analysis of vesicular transport in electrotransfection. Microscopy and Microanalysis, 24: 553–563

Williams R. 2007. PIP2 in endocytosis. Journal of Cell Biology, 177: 185–185

Wilson J.M., Flotte T.R. 2020. Moving Forward after Two Deaths in a Gene Therapy Trial of Myotubular Myopathy. Human Gene Therapy, 31: 695–696

Wu M., Yuan F. 2011. Membrane binding of plasmid DNA and endocytic pathways are involved in electrotransfection of mammalian cells. PLoS ONE, 6, 6: e20923, doi.org/10.1371/journal.pone.0020923: 9 p.

Yao S., Rana S., Liu D., Wise G.E. 2009. Electroporation optimization to deliver plasmid DNA into dental follicle cells. Biotechnology Journal, 4: 1488–1496

Yao C., Dong S., Zhao Y., Lv Y., Liu H., Gong L., Ma J., Wang H., Sun Y. 2017. Bipolar Microsecond Pulses and Insulated Needle Electrodes for Reducing Muscle Contractions during Irreversible Electroporation. IEEE Transactions on Biomedical Engineering, 64: 2924–2937

Yarmush M.L., Golberg A., Serša G., Kotnik T., Miklavčič D. 2014. Electroporation-based technologies for medicine: Principles, applications, and challenges. Annual Review of Biomedical Engineering, 16: 295–320

Yin H., Kanasty R.L., Eltoukhy A.A., Vegas A.J., Dorkin J.R., Anderson D.G. 2014. Non-viral vectors for gene-based therapy, Nature Reviews Genetics, 15: 541–555

Young J.L., Dean D.A. 2015. Electroporation-Mediated Gene Delivery. Advances in Genetics, 89: 49–88

Yu L., Reynaud F., Falk J., Spencer A., Ding Y. Di, Baumlé V., Lu R., Castellani V., Yuan C., Rudkin B.B. 2015. Highly efficient method for gene delivery into mouse dorsal root ganglia neurons. Frontiers in Molecular Neuroscience, 8: 2 doi.org/10.3389/fnmol.2015.00002: 9 p.

Zahid A., Ismail H., Li B., Jin T. 2020. Molecular and Structural Basis of DNA Sensors in Antiviral Innate Immunity. Frontiers in Immunology, 11: 613039, doi.org/10.3389/fimmu.2020.613039: 15 p.

Zhang Z., Qiu S., Zhang X., Chen W. 2018. Optimized DNA electroporation for primary human T cell engineering. BMC Biotechnology, 18: 4, doi.org/10.1186/s12896-018-0419-0: 9 p.

Zhao Z., Anselmo A.C., Mitragotri S. 2022. Viral vector-based gene therapies in the clinic. Bioengineering and Translational Medicine, 7, 1: e10258, doi.org/10.1002/btm2.10258: 20 p.

Zhen Y., Radulovic M., Vietri M., Stenmark H. 2021. Sealing holes in cellular membranes. The EMBO Journal, 40: e106922, doi.org/10.15252/embj.2020106922: 13 p.

Zheng T., Jaattela M., Liu B. 2020. pH gradient reversal fuels cancer progression. International Journal of Biochemistry and Cell Biology, 125: 105796, doi.org/10.1016/j.biocel.2020.105796: 23 p.

Znidar K., Bošnjak M., Čemažar M., Heller L.C. 2016. Cytosolic DNA Sensor Upregulation Accompanies DNA Electrotransfer in B16.F10 Melanoma Cells. Molecular Therapy - Nucleic Acids, 5: e322, doi.org/10.1038/mtna.2016.34: 11 p.

Znidar K., Bošnjak M., Semenova N., Pakhomova O., Heller L., Čemažar M. 2018. Tumor cell death after electrotransfer of plasmid DNA is associated with cytosolic DNA sensor upregulation. Oncotarget, 9: 18665–18681

Zorec B., Pavšelj N. 2013. Active enhancement methods for intra-and transdermal drug delivery: a review. Slovenian Medical Journal, Zdravniski Vestnik, 82: 339–356

ACKNOWLEDGEMENTS

First, I would like to thank my supervisor Doc. Dr. Alenka Maček Lebar for her continuous support, guidance, and encouragement during my PhD study. I would also like to thank Prof. Dr. Damijan Miklavčič for his support, motivation, and immense knowledge, and last but not least for the opportunity to enroll in PhD study and to work on many interesting projects.

I would like to thank the commission for assessment and defense: Prof. Dr. Marko Kreft, Prof. Dr. Tadej Kotnik and Research Director Marie-Pierre Rols for reviewing the doctoral dissertation and constructive comments and advice.

I am deeply grateful for my colleagues and ex-colleagues at the Laboratory of Biocybernetics at the Faculty of Electrical Engineering. Special thanks to Aleksandra, Žana, Tamara and Lea for interesting discussions and many laughs during our coffee and lunch breaks.

I am sincerely grateful to my family for always being there for me, encouraging me and believing in me. Special thank goes to my sister Anja. Thank you for believing in me and remembering me that I can. Thanks also to all my friends who always cheered me up.

ANNEXES

ANNEX A: Permission by Elsevier to use published articles in printed and online version of dissertation for articles Potočnik et al. (2019), Potočnik et al. (2021) and Sachdev et al. (2022).

ELSEVIER

Home > About > Policies > Copyright > **Permissions**

Permissions

As a general rule, permission should be sought from the rights holder to reproduce any substantial part of a copyrighted work. This includes any text, illustrations, charts, tables, photographs, or other material from previously published sources. Obtaining permission to re-use content published by Elsevier is simple. Follow the guide below for a quick and easy route to permission.

Permission guidelines   ScienceDirect content   ClinicalKey content   Tutorial videos   Help and support

Permission guidelines
For further guidelines about obtaining permission, please review our Frequently Asked Questions below:

When is permission required? +

When is permission not required? +

From whom do I need permission? +

How do I obtain permission to use photographs or illustrations? +

Do I need to obtain permission to use material posted on a website such as Blogs/Google Images/e-commerce websites? +

What rights does Elsevier require when requesting permission? +

How do I obtain permission from another publisher? +

What is RightsLink? +

What should I do if I am not able to locate the copyright owner? +

Can I obtain permission from a Reproduction Rights Organization (RRO)? +

ELSEVIER

About Elsevier   Products & Solutions   Services   Shop & Discover   Search 🔍   ⑦ 🛒 👤

Permission guidelines   ScienceDirect content   ClinicalKey content   Tutorial videos   Help and support

Can I obtain permission from a Reproduction Rights Organization (RRO)? +

Is Elsevier an STM signatory publisher? +

Do I need to request permission to re-use work from another STM publisher? +

Do I need to request permission to text mine Elsevier content? +

Can I include/use my article in my thesis/dissertation? +

Which uses of a work does Elsevier view as a form of 'prior publication'? +

How do I obtain permission to use Elsevier journal material such as figures, tables, or text excerpts, if the request falls within the STM permissions guidelines? +

How do I obtain permission to use Elsevier journal material such as figures, tables, or text excerpts, if the amount of material I wish to use does not fall within the free limits set out in the STM permissions guidelines? +

How do I obtain permission to use Elsevier Book material such as figures, tables, or text excerpts? +

How do I obtain permission to use Elsevier material that is NOT on ScienceDirect or Clinical Key? +

Can I use material from my Elsevier journal article within my thesis/dissertation? –

As an Elsevier journal author, you have the right to include the article in a thesis or dissertation (provided that this is not to be published commercially) whether in full or in part, subject to proper acknowledgment; see the Copyright page for more information. No written permission from Elsevier is necessary.

This right extends to the posting of your thesis to your university's repository provided that if you include the published journal article, it is embedded in your thesis and not separately downloadable.

Can I modify a figure when I have received permission to use it? +

ANNEX B: Permission by MDPI to use published article in printed and online version of dissertation for article Potočnik et al. (2022).

MDPI Open Access Information and Policy

All articles published by MDPI are made immediately available worldwide under an open access license. This means:

- everyone has free and unlimited access to the full-text of *all* articles published in MDPI journals;
- everyone is free to re-use the published material if proper accreditation/citation of the original publication is given;
- open access publication is supported by the authors' institutes or research funding agencies by payment of a comparatively low Article Processing Charge (APC) for accepted articles.

Permissions

No special permission is required to reuse all or part of article published by MDPI, including figures and tables. For articles published under an open access Creative Common CC BY license, any part of the article may be reused without permission provided that the original article is clearly cited. Reuse of an article does not imply endorsement by the authors or MDPI.

External Open Access Resources

Those who are new to the concept of open access might find the following websites or the *Open Access Explained!* video informative:

- Wikipedia article on Open Access
- Open Access Network